LUND UNIVERSITY

Failure Monitoring and Asset Condition Assessment in Water Supply Systems

Misiunas, Dalius

2005

Failure Monitoring and Asset Condition Assessment in Water Supply Systems

Dalius Misiunas

LUND UNIVERSITY

Doctoral Dissertation in Industrial Automation
Department of
Industrial Electrical Engineering and Automation

Department of
Industrial Electrical Engineering and Automation
Lund University
Box 118
SE-221 00 LUND
SWEDEN

http://www.iea.lth.se

ISBN 91-88934-40-3
CODEN:LUTEDX/(TEIE-1048)/1-349/(2005)

Printed in Sweden by Media-Tryck
Lund University
Lund, 2005

Mano Tėvams

Abstract

In this thesis, different aspects of failure management in urban water supply systems are discussed. As assets are getting older, the number of pipe failures is increasing. Therefore, an efficient failure management strategy becomes important. Two types of failure management strategies can be applied: proactive asset condition assessment to prevent a failure and reactive failure detection and location to minimize the reaction time and losses associated with a failure. Currently available condition assessment techniques cannot be extensively applied in water supply systems due to high cost and slow speed of inspection. Existing failure detection and location approaches do not allow for quick reaction to failures. Thus, there is a need for systematic inspection and monitoring techniques. Automatic failure monitoring and systematic asset condition assessment methods are presented in this thesis.

Due to the different topology and hydraulic characteristics of the transmission (pipelines) and distribution (network) components of a water supply system, separate failure detection and location techniques are proposed. For both pipeline and network cases, two types of failures are considered - sudden pipe ruptures and breaks that develop over a longer period of time. For the pipeline case, a periodical leak diagnosis system based on transient response difference monitoring, is presented together with a burst monitoring, detection and location system, which is designed for rapid reaction to sudden pipeline ruptures. A single continuous pressure monitoring station is sufficient to detect and locate a failure along the whole length of a pipeline. Proposed systems have been validated in laboratory and field conditions.

For the network case, two continuous failure monitoring approaches are developed, which are based on steady-state (first method) and unsteady-state

(second method) analysis. Continuous monitoring of the pressure is performed at a number of locations within the network. The steady-state analysis technique is verified using simulations and the unsteady-state analysis approach has been successfully tested on a real water distribution network. The optimal placement of pressure monitoring stations, limits of burst sizes that will be detected, uncertainty of the results and implementation aspects are discussed for both approaches. The methods presented can significantly reduce the required time for pipe failure detection and location.

A transient-analysis-based low-cost, long-range nondestructive pipe condition assessment technique is presented that can be used as a proactive failure management tool and for rehabilitation planning in water transmission pipelines. A comparative evaluation of different pipeline sections can be made and critical sections with a high degree of deterioration can be identified. The approach has been validated on a real pipeline. Finally, a transient-based methodology is presented, which is designed to test the seal quality of inline valves that are used to isolate pipe failures. The method has been successfully tested on large diameter valves of transmission pipelines and can be applied in a network situation.

The techniques presented in this thesis contribute to different points in the pipe asset management cycle and can improve reliability, availability, safety and efficiency of the urban water supply.

Preface

The work presented in this thesis was carried out through the course of the PhD studies at the Department of Industrial Electrical Engineering and Automation (IEA), Lund University, Sweden. Part of the time was spent at the Centre for Applied Modelling in Water Engineering, School of Civil and Environmental Engineering, the University of Adelaide, Australia. The research project was initiated in 2001 under the title "Integrated information and operation systems in urban water infrastructure". Results from the first part of the project were summarised in a Licentiate thesis "Burst detection and location in pipelines and pipe networks – with application in water distribution systems" published in 2003. Most of the material of this thesis has been published in several international journal and conference papers.

The topic of this thesis is failure monitoring and asset condition assessment in water supply systems. The main focus of the work was on the development of systematic approaches for effective failure management, including proactive techniques for preventing failures and reactive methods for minimising the consequences of failures. Presented methods were derived using knowledge from different research fields, such as automation, hydraulics, mechanics, statistics and mathematical modelling.

The structure of the thesis is chosen so that each of the derived techniques is presented in an individual chapter, which can be read separately.

Acknowledgements

First of all, I would like to express my most sincere gratitude to my supervisor Professor Gustaf Olsson, who has given me the opportunity to undertake this work. His optimism and ability to put things into perspective have been a great source of inspiration. I also want to thank Gustaf for his trust and encouragement.

The Department of Industrial Electrical Engineering and Automation (IEA) is a great place to work at. I want to thank all of the people at the Department for contributing to a good working environment. I would especially like to thank Dr. Inés Romero for being a great friend, Dr. Christian Rosén for help with LaTeX code, Associate Professor Ulf Jeppsson for proof-reading the manuscript, Dr. Gunnar Lindstedt for solving computer problems, Anita Borné and Christina Rentschler for doing the paper work and Carina Lindström and Getachew Darge for their help with practical things.

Fourteen months spent at the Centre for Applied Modelling in Water Engineering, School of Civil and Environmental Engineering, the University of Adelaide, Australia were both interesting and fruitful. I would like to thank Associate Professor Angus Simpson and Associate Professor Martin Lambert for their help, guidance, valuable opinions and inspiration. It has been a great pleasure to be a part of the "transient" group. Dr. John Vítkovský has been a great teacher and colleague, his clear answers and critical views were highly appreciated. I also want to thank all the people at the School of Civil and Environmental Engineering for creating a warm and friendly atmosphere.

The following persons have contributed to the experimental work described

in this thesis: Greg Milsom, Jim Braendler (Assets Management, SA Water, Adelaide, Australia), Neil Kleinig (Morgan area District Manager, SA Water, Australia), SA Water operation personnel at Morgan, Dr. John Nixon (Senior Research Scientist, United Water International Pty Ltd, Adelaide, Australia), Mr. Roger Duthie (Water Operation Coordinator, United Water International Pty Ltd, Adelaide, Australia), Bruce Lucas, Daniel Trezise, Ian Cates, Gregory Atkins, Jeffrey Hiorns (School of Civil and Environmental Engineering instrumentation/laboratory staff, the University of Adelaide, Australia), Mark Stephens, Dr. Pedro Lee, Young-il Kim, Aaron Zecchin and Nicole Arbon (School or Civil and Environmental Engineering, the University of Adelaide, Australia).

I also wish to thank all of my friends who have been with me through this time - my “family” here in Lund, my mates down under and those who beared with me since school. I was lucky to meet them one day and I am very happy to still keep in touch, even if some of them are on the other side of the world. Without friends it would have been hard to survive through bad weather or approaching deadlines. I am grateful for all the happy moments we have had together.

I want to thank Greer for being a special person in my life. Her support, inspiration, friendship and love made the journey towards this goal much easier.

Finally, I would like to thank my parents Argirdas and Dalia and my brother Linas for their love and understanding. Although being far away, they have always been my greatest supporters.

Lund, November 3, 2005
Dalius Misiunas

This work was partially supported by VINNOVA, Per Westling Fund, The Royal Swedish Academy of Sciences, Kungliga Fysiografiska Sällskapet i Lund and J. Gust. Richert Foundation. Their support is gratefully acknowledged.

Nomenclature and abbreviations

A	Cross-sectional pipe area
a	Wave speed
B	Pipe characteristic impedance
C_1	Coefficient describing dispersion of the wave front
C_2	Coefficient that compensates for neglect of frictional effects
C_dA_0	Lumped burst orifice coefficient
C_d	Orifice discharge coefficient
D	Pipe diameter
D_L	Diameter of leak orifice
E	Young's modulus of elasticity of conduit walls
e	Error term (or pipe wall thickness)
f	Friction factor
g	Gravitational constant
H	Hydraulic head
h	CUSUM threshold parameter
H_0	Initial head in pipeline
K	Valve resistance coefficient

L	Pipeline length
N	Number of nodes in network
OF	Objective function
P	Wave reflection coefficient
Pr	Probability
Q	Volumetric flow rate
R	Pipe resistance coefficient
Re	Reynolds number
S_t	CUSUM variable
T	Wave transmission coefficient
t	Time
V	Mean velocity of flow
VB	Volume balance
w	Weighting factor
X	Distance
y_t	RLS filter measured input signal
Z	Sampling design
β	Threshold value used when calculating the performance criteria of a sampling design
ΔH	Head change due to burst
ΔH_L	Magnitude of reflection from leak
ΔH_R	Magnitude of reflected transient wave
ΔH_T	Magnitude of transmitted transient wave

ΔH_W	Magnitude of generated transient wave
Δt	Time difference
Δx	Length of computational unit
ϵ_t	RLS filter prediction error
η	Performance indicator
λ	RLS filter forgetting factor
ν	CUSUM drift parameter
∂	Partial derivative
ϕ	Parameter in wave speed equation depending on pipe anchoring
ρ	Fluid density
τ	Wave travel time
θ_t	RLS filter output signal
AC	Asbestos cement
ANN	Artificial neural network
CCTV	Closed-circuit television
CPM	Computational pipeline monitoring
CUSUM	Cumulative sum
DICL	Ductile iron concrete-lined
DMA	District metering area
EKF	Extended Kalman filter
FDR	Frequency domain response
FPAV	Fire plug air valve

GA	Genetic algorithm
GIS	Geographic information system
GPR	Ground penetrating radar
ITA	Inverse transient analysis
LRM	Leak reflection method
MOC	Method of characteristics
MSCL	Mild steel concrete-lined
NDE	Nondestructive evaluation
NDT	Nondestructive testing
PPA	Pressure point analysis
RLS	Recursive least squares
RTTM	Real-time transient model
SCADA	Supervisory control and data acquisition
SCC	Stress corrosion crack
SPLD	Statistical pipeline leak detection
SPRT	Sequential probability ratio test
TDR	Time domain reflectometry
UFW	Unaccounted for water
WFP	Water filtration plant
WLS	Weighted least squares
WSS	Water supply system

Contents

Chapter 1

Introduction

This chapter gives an overview of the work presented in this thesis. The motivation and objectives for the work are presented together with a brief summary of main contributions, the outline of this thesis and the list of publications that are part of this work.

1.1 Motivation

The present state of the urban water supply infrastructure is a result of hundreds of years of development and large investments. The size, cost and complexity of today's water supply systems prevent radical changes. The environmental concerns over the last few decades, together with increased awareness of customers, have placed pressure on water utilities to improve water services. This pressure is supported by the rapid development of advanced technologies in instrumentation, control and computer applications. Although considerable efforts have been made to advance the operation of water systems, water supply still remains one of the most stagnant parts in the urban infrastructure system.

Water is a precious resource and is essential for human existence. Therefore a special concern has been expressed by policy makers with emphasis on the conservation of natural resources. New legislation has raised higher

demands for the efficiency of water supply in many countries. Moreover, there are indications that water policies will become even stricter in the near future. This situation forces water utilities to look for new ways to improve the condition and operation of the existing water supply systems.

Reliability, availability, safety and efficiency can be identified as key parameters describing the performance of the water supply service. Reliability is the probability that the system will operate correctly, availability is the probability that the system will be operational, safety is the absence of hazardous consequences for the users and the environment and efficiency is related to the level of losses.

1.2 Objectives

This research project was initiated with a very broad objective – to improve the operation of urban water supply by utilising available resources and technology. During the initial stage, a number of problems that were of greatest concern from the water industry's point of view were identified (Misiunas; 2001a,b,c,d). As a result, the following main objective was formulated:

> to develop techniques that would utilise available measurement, data analysis, modelling and optimisation methods to reduce the risk of failure, minimize losses associated with the failure and improve the reliability, availability, safety and efficiency of the urban water supply service.

Additionally, the following priorities were set:

systematic, real-time and automated approaches;

pipeline and pipe network applications;

laboratory and/or field validation.

1.3 Contributions

The conclusions and contribution of the thesis are presented in Chapter 13. A brief summary of the main results is given here (in order of appearance in the thesis):

- pipe deterioration and failure process is analysed and both proactive and reactive pipe failure management strategies are discussed. A review of the existing techniques for proactive condition assessment and reactive failure detection and location is presented;

- an algorithm for automatic periodical pipeline leak diagnosis based on the transient response difference monitoring is presented together with validation results from the field;

- an automatic pipeline burst monitoring, detection and location approach based on continuous monitoring of pressure and hydraulic transient analysis is presented along with validation from laboratory and field experiments;

- an automatic network failure monitoring, detection and location technique based on steady-state analysis is presented and validated using simulations;

- an automatic network burst monitoring, detection and location technique based on unsteady-state analysis is presented together with field validation results;

- a nondestructive evaluation (NDE) approach for pipeline condition assessment based on hydraulic transient analysis and its validation in the field are presented;

- an approach for testing the seal quality of inline stop valves is derived and validated in the laboratory and in the field.

1.4 Outline of the thesis

Part I of this thesis gives an overview of the pipe asset deterioration, failure and management in water supply systems. Chapter 2 discusses the structure of urban water supply, existing pipe assets, pipe failure types, causes, management cycle and associated costs. Reviews of existing pipe condition assessment techniques and pipe failure detection and location methods are presented in Chapters 3 and 4, respectively.

Part II of this thesis describes two techniques for *pipeline* failure management. The first method (Chapter 5) is used for periodical leak diagnosis and is based on hydraulic transient response difference monitoring. The second approach (Chapter 6) is a pipeline burst monitoring system based on the continuous monitoring of the pressure. Chapter 7 discusses the performance, application and implementation of the proposed techniques.

Part III of this thesis describes two techniques for failure monitoring, detection and location in *pipe networks*. The first method (Chapter 8) is based on steady-state analysis of the network and the second approach (Chapter 9), is based on unsteady-state analysis of the network. Chapter 10 discusses the performance, application and implementation of the proposed techniques.

Part IV of this thesis presents two techniques for asset condition assessment. A hydraulic-transient-analysis-based approach for a long range and low cost non-intrusive pipeline condition assessment is presented in Chapter 11. In Chapter 12, a method is presented for fast, non-intrusive testing of inline valves.

Part V of this thesis presents a summary of all results and suggestions for future work are made. This part also contains some personal recommendations.

Part VI contains five appendices: laboratory and field testing is discussed in Appendix A; Appendix B describes fluid transient modelling; pressure wave transmission and reflection coefficients are derived in Appendix C; calculation of burst and leak sizes are shown in Appendices D and E, respectively.

1.5 Publications

Theses

Misiunas, D. (2003). *Burst Detection and Location in Pipelines and Pipe Networks – with Applications in Water Distribution Systems.* Licentiate thesis (ISBN 91-88934-30-6), Lund University, Lund, Sweden.

International journal publications

Misiunas, D., Vitkovský, J., Olsson, G., Simpson, A. R. and Lambert, M. F. (2005). Pipeline break detection using the transient monitoring. *Journal of Water Resources Planning and Management*, ASCE, 131(4), 316-325.

Misiunas, D., Vitkovský, J., Olsson, G., Simpson A. and Lambert, M. (2005). Failure monitoring in water distribution networks. *Water Science and Technology* (accepted).

International conference publications (peer review)

Misiunas, D., Vítkovský, J., Olsson, G., Simpson, A. and Lambert, M. (2003). Pipeline burst detection and location using a continuous monitoring technique. *Proc. International Conference on Advances in Water Supply Management, CCWI*, Imperial College, London, UK, September 15-17, 2003, pp. 89-96.

Misiunas, D., Vítkovský, J., Olsson, G., Simpson, A. and Lambert, M. (2004). Burst detection and location in pipe networks using a continuous monitoring technique. *Proc.* 9^{th} *International Conference Pressure Surges*, Chester, UK, March 24-26, 2004, pp. 225-238.

Misiunas, D., Lambert, M., Simpson A. and Olsson, G. (2005). Burst detection and location in water distribution networks. *Proc.* 3^{rd} *International Conference on Efficient Use and Management of Water*, Santiago, Chile, March 15-17, 2005, pp. 464-471.

Misiunas, D., Lambert, M., Simpson A. and Olsson, G. (2005). Burst detection and location in water transmission pipelines. *Proc. World Water and Environmental Resources Congress, ASCE*, Anchorage, Alaska, USA, May 15-19, 2005.

Misiunas, D., Vitkovský, J., Olsson, G., Simpson A. and Lambert, M. (2005). Failure monitoring in water distribution networks. *Proc.* 2^{nd} *IWA Conference on Instrumentation, Control and Automation*, Busan, Korea, May 29 - June 2, 2005, pp. 631-639.

Misiunas, D., Simpson, A., Lambert, M. and Olsson, G. (2005). Hydraulic transients for diagnosis of inline valves in water transmission pipelines. *Proc. International Conference on Water Management for the* 21^{st} *Century, CCWI*, Exeter, UK, September 5-7, 2005, pp. 293-298.

Misiunas, D., Lambert, M., Simpson, A. and Olsson, G. (2005). Condition assessment of water transmission pipelines using hydraulic transients. *Proc. International Conference on Water Management for the* 21^{st} *Century, CCWI*, Exeter, UK, September 5-7, 2005, pp. 269-274.

Technical reports

Misiunas, D. (2001). Drinking water quality. Literature study on water distribution systems, *Technical report TEIE-7169*, Dept. of Industrial Electrical Engineering and Automation, Lund University, Lund, Sweden.

Misiunas, D. (2001). Dynamic behavior of a pump/pipeline system. Literature study on water distribution systems, *Technical report TEIE-7166*, Dept. of Industrial Electrical Engineering and Automation, Lund University, Lund, Sweden.

Misiunas, D. (2001). Leakage control. Literature study on water distribution systems, *Technical report TEIE-7167*, Dept. of Industrial Electrical Engineering and Automation, Lund University, Lund, Sweden.

Misiunas, D. (2001). Water storage. Literature study on water distribution systems, *Technical report TEIE-7168*, Dept. of Industrial Electrical Engineering and Automation, Lund University, Lund, Sweden.

Misiunas, D. (2002). Integrated information and operation systems in urban water infrastructure – leakage control, *Technical report TEIE-7172*, Dept. of Industrial Electrical Engineering and Automation, Lund University, Lund, Sweden.

Part I

Problem overview

Summary: *The urban water supply is a large and complex infrastructure that has been expanded and developed during the last century. While getting older, water supply assets, primarily pipes, are exposed to the deterioration process and consecutive pipe failure. The increased number of pipe failures has raised the need for water utilities to look for efficient proactive and reactive pipe failure management strategies.*

Part I of this thesis gives an overview of the pipe asset deterioration, failure and management in water supply systems. Chapter 2 discusses the structure of urban water supply, existing pipe assets, pipe failure types, causes, management cycle and associated costs. Reviews of existing pipe condition assessment techniques and pipe failure detection and location methods are presented in Chapters 3 and 4, respectively.

Chapter 2

Pipe deterioration, failure and management in water supply systems

The main focus of this chapter is the deterioration and failure of pipe assets in urban water supply systems (WSS). A sequential process of pipe deterioration is discussed. Pipe failure (partial or complete) is a part of the deterioration process. Different failure mechanisms and causes are outlined. A brief overview of existing deterioration modelling and failure prediction techniques is given. Costs associated with the failure are analysed. The failure management cycle is presented by introducing proactive and reactive actions. Finally, the cost-benefit analysis of failure management is discussed.

2.1 Structure of the water supply system

Although the size and complexity of drinking water supply systems may vary dramatically, they all have the same basic purpose – to deliver water from the source (or treatment facility) to the customer. The objectives of an urban water system are to provide safe, potable water for domestic use, adequate quantity of water at sufficient pressure for fire protection and water for industrial use. Sources for municipal supplies are wells, rivers, lakes

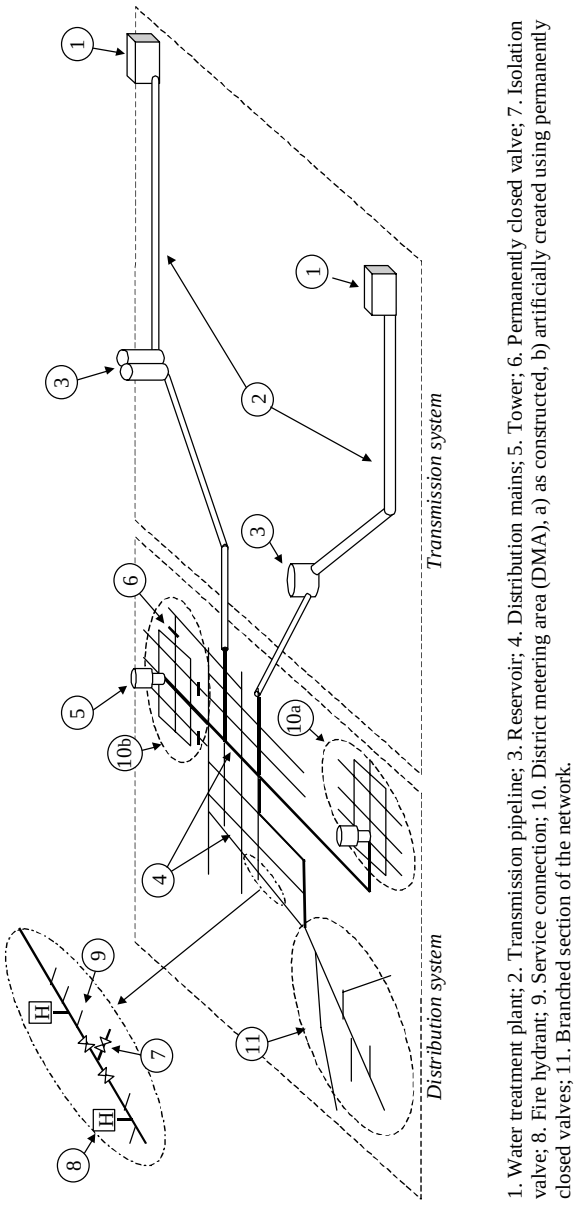

Figure 2.1: Structure of a water supply system

and reservoirs. About two thirds of the water for public supplies around the world comes from surface-water sources. Often groundwater is of adequate quality to preclude treatment other than chlorination and fluoridation. The structure of a water supply system is illustrated in Figure 2.1. The whole system can be divided into two major parts - the transmission system and the distribution system.

Transmission system

A transmission system consists of components that are designed to convey large amounts of water over great distances, typically between major facilities within the system. The common example of a transmission system is a treatment facility and storage reservoirs setup as shown in Figure 2.1. Water transmission pipelines usually have diameters above 300 mm and can be built underground as well as aboveground. The length of pipelines can vary significantly. In some areas the water has to be transported over a distance of several hundreds of kilometers. The typical elements of transmission pipelines are inline stop valves, fire plug air valves (FPAV), scour valves and manholes. Pumps may be used to transport the water from one facility to another (treatment plant to reservoir or reservoir to reservoir). To minimise the cost of operation, the pumping is performed during the time when the energy costs are lower, i.e. off-peak electricity use hours. The flow rate in the transmission pipeline during the pumping is quite high and the water is often stagnant during the rest of the time. Individual customers are usually not served directly from transmission mains. In some cases, distribution mains can be connected at some points along the length of the transmission pipeline.

Distribution system

The water transported in transmission pipelines to the residential areas is distributed through the water distribution system. Generally, a distribution system has a complex topology and contains a large number of elements. Two types of pipes are found in the distribution system - distribution mains and service connections. Distribution mains are an intermediate step towards

delivering water to the end customers and are smaller in diameter than transmission mains. Typically, distribution mains follow the general topology and alignment of the city streets. Pipes can be interconnected by junctions and form loops. Typically, the urban distribution system is a combination of looped and branched topologies as shown in Figure 2.1. Figure 2.1 also shows a closer view of the parts of the water distribution system at the street level. Generally, every single branch in the distribution network has a stop valve at each end. Valves are installed for the purpose of isolation in case of a failure event or during maintenance work. They can also be used to reroute flows in the network: In some cases valves are closed permanently to establish pressure zones within the network or to form district metering areas (DMAs) as shown in Figure 2.1 (10b). A fire hydrant connector point is another common element in both transmission and distribution parts of the water supply system. The regulations regarding the density of fire hydrants in a distribution network can vary between countries, but in general, fire hydrants are likely to be installed every 100 m. Elbows, tees, crosses, and numerous other fittings are used to connect and redirect sections of pipes. Along with isolation valves, various control valves (pressure-reducing, pressure-sustaining, etc.) are installed in the system. Finally, the network may contain pumps, air-release devices, water hammer control devices and other operational and maintenance installations. Services, also called service lines, are the smallest pipes in the supply system and transmit the water from the distribution mains to the customers. Usually, service pipes have smaller diameter than distribution mains and run from the street to the property. Households, businesses and industries have their own internal plumbing systems to transport water to sinks, washing machines, and so forth.

System configuration

As showed in Figure 2.1, water distribution systems can have either looped or branched structures. As the name suggests, in a looped system there might be several different paths that the water can follow to get from the source to a particular customer. In a branched system, also called a tree system, the water has only one possible path from the source to a customer. Looped systems are generally more desirable than branched systems because, coupled with sufficient valving, they can provide an additional level of reliability (Khomsi

et al.; 1996). When shutdowns occur due to failure or planned repairs, loops allow consumers to benefit from the reduced service rather than having no water supply at all, which would be the case in the branched network. Another advantage of a looped configuration is that, because there is more than one path for water to reach the user, the velocities will be lower, and system capacity greater. However, the installation cost for a looped system is higher than for a branched system. Thus, most of water supply systems are complex combinations of loops and branches, compromising between redundancy (looped) and cost savings (branched). As already mentioned earlier in this section, in some cases the topology of the distribution system may be changed after construction by permanently closing inline stop valves and forming pressure zones or district metering areas (DMAs).

2.2 Pipe assets

Pipes, valves, pumps, reservoirs and all other components of a water supply system constitute a water supply asset. Pipes are one of the principal assets. As described in a previous section, there are three main types of pipes in the water supply system – transmission mains, distribution mains and services.

Pipe materials

Historically, a variety of materials and technologies have been used in the production of water supply pipes. The material of a particular pipe depends on the year of installation and the diameter. For large transmission pipelines (with diameters over 300 mm) steel, mild steel cement-lined (MSCL) or prestressed concrete cylinder pipes (PCCP) are typically used. Older water distribution mains are typically made of cast iron or asbestos cement, while mainly ductile iron and poly-vinyl chloride (PVC) are used for newer mains. The distribution of pipe materials in existing systems varies between countries and even towns. Pipe material distribution statistics for different countries can be found in the literature. Pipe material data from 500 water companies around Germany was presented in Weimer (2001). Pelletier et al. (2003) reviewed data from three Canadian municipalities.

Babovic et al. (2002) showed data from Copenhagen city (Denmark) water supply. In NRC (1995), a pipe material survey from 21 Canadian cities was made. Unwin et al. (2003) showed the pipe material data from UK water service provider. Finally, Rajani and Kleiner (2004) presented a summary of the pipe material distribution from 13 European countries. The data from different countries shows that, on an average, cast iron is the dominating pipe material. Depending on the country, 40-60% of pipes are produced from cast iron. The second most widely used material is ductile iron with 25-30% of the whole system. Cast iron and ductile iron are followed by asbestos cement and plastic, each of which, depending on the country, can constitute 10-30% of the network. However, it has to be noted that the distribution of pipe metrials is likely to change in the future due to the current extensive use of plastic pipes. The most common materials of service connection pipes are steel, plastic and lead. As shown in Weimer (2001), 43% of services in Germany are plastic, 36% are made out of steel and lead constitutes 8% of the service pipes.

Pipe age

The first urban water supply systems were built more than five hundred years ago. A large portion of originally constructed pipes are still in operation today. Building urban water supply infrastructure required large investments and therefore the existing systems cannot be changed or upgraded over a short period of time. The age of pipes can usually be estimated from their material type. The oldest component of networks is cast iron installations that can go back as far as 1500. The average age of cast iron pipes that are present in existing systems is around 50 years. No cast iron pipes were installed after 1970. Steel, ductile iron, asbestos cement and concrete pipes were introduced to urban water supply systems around 50 years ago. Finally, plastic materials have been popular since the 1970s and constitute a large proportion of current installations. Overall, considering the distribution of pipe material that was discussed earlier in this section, the average age of water supply pipes in developed countries can be estimated to be around 50 years. It is logical to expect that the condition of the water infrastructure has been affected by deterioration processes ever since the initial installation.

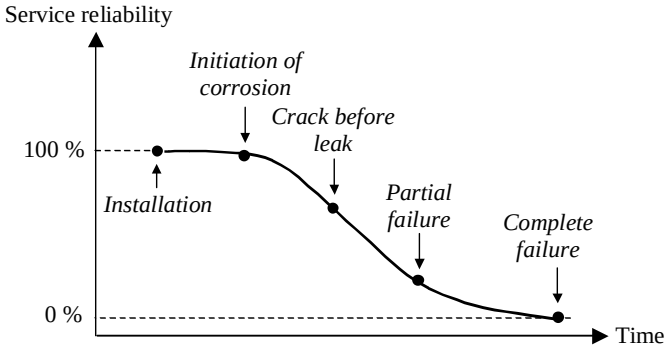

Figure 2.2: Pipe failure development

2.3 Pipe deterioration process

Pipe failure can be described as a multi-step process as shown in Figure 2.2. The following steps can be identified:

1. *Installation*. The new intact pipe is installed.
2. *Initiation of corrosion*. After the pipe has been in operation for some time, the corrosion processes start on the interior or exterior (or both) surface of the pipe.
3. *Crack before leak*. Cracks, corrosion pits and graphitisation are typical products of the corrosion process. In some cases cracks can be initiated by mechanical stress.
4. *Partial failure*. Eventually, developing corrosion pits and cracks reduce the residual strength of the pipe wall below the internal or external stresses and the pipe wall breaks. As a consequence, the leak or burst will be initiated depending on the size of the break. In some cases the size of the failure is not big enough to be readily detected.
5. *Complete failure*. The complete failure of the pipe can be caused by a crack, corrosion pit, already existing leak/burst or a third party interference. Such a failure is usually followed by water appearing on the ground surface or a considerable change in the hydraulic balance of the system.

Not all pipes will have a failure sequence as shown in Figure 2.2. Wang and Atrens (2004) have shown that stress corrosion cracks (SCC) are likely to be active cracks, i.e. develop with time. In Makar (2000); Makar et al. (2001) the evidence of a multi-event cracking is presented, indicating that there can be a substantial time interval between the initial and subsequent cracks. According to Saegrov et al. (1999), the temporal development of the failure is influenced by the material of the pipe. Steel and ductile iron pipes are likely to leak before they break. Cast iron and larger diameter prestressed concrete pipes typically break before they leak. Plastic and PVC pipes can do either, depending on the installation and operational conditions. The deterioration mechanisms in plastic pipes are not well known since they are likely to be slower and plastic pipes have been in use only for the last 30–40 years.

The time intervals between the different steps in the pipe deterioration process can vary considerably. As an example, in Atkinson et al. (2002) it was shown that, for small cast iron pipes (diameter less than 100 mm), the critical pit depth that corresponds to the situation when service stress exceeds the residual strength of the material is approximately equal to 30% of the pipe wall thickness. The history of the failure development is likely to be specific for a particular pipe and is extremely difficult to predict. The situation becomes even more complicated when failures caused by the third party interference or other external forces are considered.

2.4 Pipe failure

Pipe failure occurs when the pipe cannot contain the fluid internally within the pipe–either the strength is too low (from wrong material selection, fatigue, stress corrosion, etc.) or the stress is too high (overloads, loss of wall thickness etc.) resulting in an interference zone between loads and strengths. Generally, pipe failures can be classified by type and by size.

Causes of failure

Kleiner et al. (2001) has classified the deterioration of pipes into two categories. The first one is structural deterioration, which diminishes the pipe's

structural resiliency and its ability to withstand the various types of stress imposed upon it. The second one is deterioration of the inner surface of the pipe resulting in diminished hydraulic capacity, degradation of water quality and reduced structural resiliency in cases of severe internal corrosion. Pipe breakage, with exception of situations when it is caused by a third party interference, is likely to occur when the environmental and operational stresses act upon pipes whose structural integrity has been compromised by corrosion, degradation, inadequate installation or manufacturing defects.

Corrosion. It is widely accepted (Makar et al.; 2001; Rajani and Kleiner; 2001) that the predominant deterioration mechanism on the exterior of cast and ductile iron pipes is electro-chemical corrosion with the damage occurring in the form of corrosion pits. The damage to gray cast iron is often identified by the presence of graphitisation - a result of iron being leached away by corrosion. Either form of metal loss represents a corrosion pit that will grow with time and eventually lead to a pipe break. The physical environment of the pipe has a significant impact on the deterioration rate. Severe internal corrosion may also impact pipe structure deterioration. Plastic pipe materials also may suffer from chemical degradation. Asbestos cement and concrete pipes are subject to deterioration due to various chemical processes that either leach out the cement material or penetrate the concrete to form products that weaken the cement matrix.

Excessive forces. Quite often a pipe failure is caused by a combination of some form of damage or manufacturing flaw and applied external forces. External forces can be induced by a number of different sources, such as pipe-soil interaction, traffic or climate (Rajani and Tesfamariam; 2004; Hudak et al.; 1998). In some cases, the external load might be applied at a significant distance from the failure location. Rajani and Kleiner (2001) have identified two main types of mechanical stresses that may contribute to the failure of a pipe - longitudinal and transverse. Longitudinal stress can be caused by: (1) thermal contraction due to low temperature of the water in the pipe and the pipe surroundings, (2) bending stress due to soil differential movement or large voids in the bedding near the pipe (as a result of leaks), (3) inadequate trench and bedding practices, (4) third party interference. Transverse stress can be caused by: (1) hoop stress due to pressure in the pipe, (2) ring stress due to soil loading, (3) ring stress due to other external loading, i.e. traffic,

and (4) ring loads caused by freezing moisture expansion in the surrounding soil.

Production flaws. Porosity is one of the most common manufacturing defects in cast iron pipes. Inclusions result in a discontinuity of the pipe material and may act as crack formers. The variation in a pipe wall thickness may lead to a situation where a part of the pipe wall might no longer have a sufficient wall thickness for expected maximum pressures. Yet another manufacturing flaw is the presence of iron phosphide structures throughout the pipe metal. Phosphorus is added to reduce the production costs. However, the iron phosphide compound is brittle and weakens the pipe.

Human error. Starting with an incorrect design, there are several practices during and after the construction that can contribute to the failure of the pipe. Poor transportation, movement and installation techniques can promote corrosion followed by the failure of the pipe. Accidentally removed coating exposes the pipe to extensive corrosion. Another possible cause of the failure is a third party damage. The most frequent example is during an excavation.

Failure mechanisms

Pipe breakage type describes the actual manner in which pipe breaks. The failure mechanism varies depending on the material and the diameter of a pipe. Pipe breakage types have been classified by O'day (1982) into three main categories:

Circumferential cracking. Circumferential cracking (Figure 2.3) is typically caused by bending forces applied to the pipe. Bending stress is often the result of soil movement, thermal contraction or third party interference. Circumferential cracking is the most common failure mode for smaller diameter cast iron pipes. In Hu and Hubble (2005) statistics of asbestos cement water main breaks from the city of Regina in Canada were presented. Circumferential breaks were shown to be the predominant failure mode comprising 90.9% of all pipe failures. It was also demonstrated that the failure rate was decreasing with increasing pipe diameter.

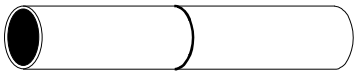

Figure 2.3: Circumferential cracking

Longitudinal cracking. Longitudinal cracking (Figure 2.4) is more common in large diameter pipes. It can be caused by a number of different types of loading, such as internal water pressure and ring stress created by the soil cover load, external load or thermal changes. An initial small crack can expand along the length of the pipeline. In some cases, two cracks on opposite sides of the pipe are initiated, resulting in a complete detachment of the section of the pipe that may be as long as the pipe segment itself.

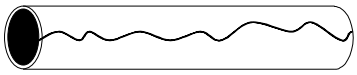

Figure 2.4: Longitudinal cracking

Bell splitting. Bell splitting (Figure 2.5) is most common in small diameter cast iron pipes. The main reason for bell splitting is the sealing of the joints. Originally, the joints were sealed using lead. In the 1930s and 1940s the lead was substituted by leadite which, as a non-metallic compound, has a different thermal expansion coefficient than lead. This, at low temperatures, can cause bell splitting.

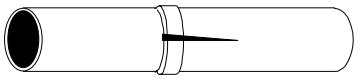

Figure 2.5: Bell splitting

In addition to the three breakage types described above Makar et al. (2001) introduced the following failure modes:

Corrosion pitting and blow-out holes. It is widely accepted that corrosion is an important factor that plays a major role in the pipe failure process. A corrosion pit (Figure 2.6a) reduces the thickness and mechanical resistance of the pipe wall. When the wall is thinned to a certain point, the internal

pressure blows out a hole (Figure 2.6b). The size of the hole depends on the distribution of corrosion and the pressure in the pipe. In some cases a blow-out hole can be fairly large.

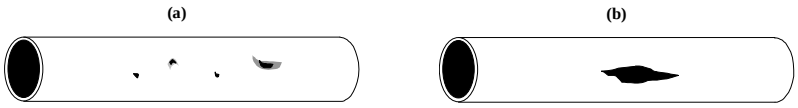

Figure 2.6: (a) corrosion pitting and (b) blow-out hole

Bell shearing. Large diameter pipes are not likely to suffer from a circumferential failure. Instead, large diameter gray cast iron pipes fail by having a section of a bell shear off as shown in Figure 2.7. The simple compressive loading is likely to cause a longitudinal crack that propagates along the length of the pipeline. Bending, however, often results in the occurrence of bell shearing.

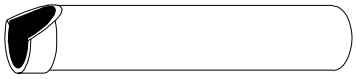

Figure 2.7: Bell shearing

Spiral cracking. Spiral cracking (Figure 2.8) is a rather unique failure mode that sometimes occurs in medium diameter pipes. The initially circumferential crack propagates along the length of the pipe in a spiral fashion. Historically, this type of failure is associated with pressure surges, but it can also be related to a combination of bending force and internal pressure.

Figure 2.8: Spiral cracking

Part of the system	Total (%)	Background leakage (%)	Bursts	
			reported (%)	unreported (%)
Transmission	6	98	2	0
Distribution	24	64	5	31
Service	70	50	7	43
Overall	100	56	6	38

Table 2.1: Loss distribution for a sample area (Lambert; 1994)

Failure classification

The most common practice is to classify pipe failures into two main categories - leaks and bursts. It is hard to clearly define what factors that should be used when attributing a particular pipe failure to one of those two categories. According to the International Water Association (IWA) guidelines (EUREAU; 2001; Lambert and Hirner; 2000), real losses in water distribution systems can be divided into background leakage, reported bursts and unreported bursts. All points of loss that have a flow rate below a certain threshold value are categorised as background leakage. In practice, this category includes all the leaks from fittings (air valves, hydrants, taps, etc.). If the flow rate of the leak exceeds the threshold value, it is classified as a burst. Bursts are further divided into two categories - reported bursts and unreported bursts. Typically, failures that result in the appearance of water on the ground surface are reported and therefore can be referred to as reported bursts. Depending on the environment of the pipe, in some cases even a large discharge does not surface and therefore will not be reported. Such failures are referred to as unreported bursts and are running until they are detected during an active leakage control campaign. The background leakage is usually quantified for the whole (or part) of the network collectively, whereas bursts, both reported and unreported, are quantified individually.

In Lambert (1994) an example distribution of water losses caused by different types of failures in all parts of the supply system is presented. To distinguish between background leakage and bursts, an arbitrary flow rate value of 500 L/h or 0.129 L/s was used. Table 2.1 presents results from the examined supply area with a population of $90\,000$ with $41\,500$ properties, 50

Part of the system	Flow rate* M^3/d	Average duration of the burst**	
		Reported burst	Unreported burst
Transmission	150	1 day	n/a
Distribution	50	1.1 day	12 days
Service	25	16 days	267 days

* Average night pressure of 40 m was assumed
** Includes detection, location and repair

Table 2.2: Parameters of different bursts (Lambert; 1994)

km of transmission mains, 907 km of distribution mains and an average night pressure of about 70 m. In the same paper, provisional average flow rates for different types of bursts are suggested. Average durations of different types of bursts are given. All the information is summarised in Table 2.2.

In some cases when reactive pipe failure management is considered, different definitions of leak and burst can be used. In that context, leaks often include all failures that are present in the system at the moment of inspection, whereas bursts are considered as discrete events. Such a classification disregards the size of the flow rate and therefore even failures with a large discharge are still referred to as leaks. It is common to consider that the burst is a result of a sudden fracture of a pipe.

Classification of failures exists in other industries. In Fleming and Lydell (2004) the grouping of failure modes in nuclear power plant piping systems with respect to the size is presented. Four main failure types are identified: crack/wall thinning, pinhole leaks ($q_L < 0.063$ L/s), leaks ($0.063 < q_L < 3.155$ L/s), and ruptures ($q_L > 3.155$ L/s). The classification of leaks in gas pipelines is discussed in Huebler (2000). According to the practice of gas pipeline operation utilities, leaks are classified as to the urgency of repair based on the potential danger they present. Typically, leaks are classified in three groups: those that need repair in 24 to 48 hrs., those to be repaired within 30 days and those that do not need immediate repair but are monitored annually. Some utilities subdivide the second category of leaks into those that should be repaired in 5 to 10 days and those that should be re-inspected within 3 to 4 months.

Source	Breaks/100 km/year				
	Cast iron	Ductile iron	Steel	AC	PVC
NRC (1995)	36	9.5	n/a	5.7	0.7
Pelletier et al. (2003)	55	20	n/a	n/a	2
Weimer (2001)	27	3	33	n/a	4

AC - asbestos cement, PVC - polyvinyl chloride

Table 2.3: Pipe break frequency for different materials

Frequency of the failure

Several factors have been indicated in the literature to have an influence on the frequency of pipe breaks. Pipe age, material and diameter are the main factors that influence the frequency of pipe breaks in the supply system. Soil parameters, climate changes, pressure in the system and the type of environment of the pipe have also been shown to affect the rate of pipe failure. One of the common indicators used to quantify the frequency of pipe failures for a particular system is the annual number of breaks per hundred kilometers of pipe (# of breaks/100 km/year). In Table 2.3, pipe break frequencies presented in three different studies are shown.

Table 2.3 clearly indicates that the majority of breaks occur in cast iron pipes. In most of the water supply systems, cast iron pipes are the oldest pipes, often installed more that 50 years ago. Many studies have also indicated the increase of the pipe failure frequency with time. As a conclusion, pipe age can be referred to as the predominant cause of pipe failure. Thus, the number of incidents in urban water supply systems is likely to be continuously increasing in the future as systems grow older.

Consequences of a failure

Losses associated with a pipe failure can be divided into three main categories in a similar manner as suggested by Makar and Kleiner (2000):

1. Direct costs
    - repair cost that depends on the parameters of the pipe and failure as well as the location of the failure;
    - cost of lost water that depends on the severity of the failure, the isolation time, the size of the pipe and the production cost of water;
    - cost of damage to the surrounding infrastructure and property (flooding, road collapse, structural damage, etc.) that depends on the severity and location of the failure as well as the time of isolation;
    - liabilities (injury, accident, etc.) that depend on the severity and location of the failure.
2. Indirect costs
    - costs of supply interruption (loss of business due to the water outage) that depend on the isolation time of the failure;
    - cost of potentially increased deterioration rate of affected surrounding infrastructure and property;
    - cost of a decreased fire-fighting capacity, both due to water outage and insufficient hydraulic capacity.
3. Social costs
    - cost of water quality degradation due to contaminant intrusion caused by de-pressurising;
    - cost of decrease in public trust and quality of water supply that depends on the location and isolation time of the failure;
    - cost of disruption of the traffic and business that depends on the location and isolation time of the failure;
    - cost of disruption of the water supply to special facilities (hospitals, schools, etc.) that depends on the location and isolation time of the failure.

Figure 2.9 shows the component of the real cost of the pipe failure as a function of the time after the failure. The total cost associated with the pipe

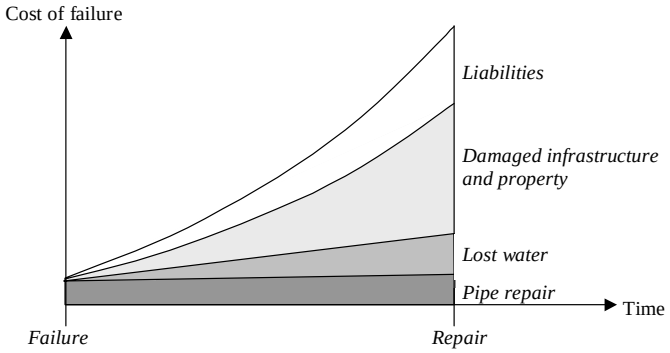

Figure 2.9: Losses associated with failure

failure depends on the severity and duration of the event and can reach a fairly high value. As an example, if a small leak is considered, the real costs for some time after the leak has occurred will be approximately equal to the sum of the repair cost and the cost of water that is lost. However, if the leak remains undetected for a longer time, it can cause damage to surroundings (especially if the size of the leak is increasing with time). Thus, another two components, i.e. damage to the surrounding infrastructure and property and liabilities, will be contributing to the real cost of the leak. If the example of a larger burst is considered, the real cost of the failure will include all components and will be increasing rapidly after the failure as shown in Figure 2.9. Generally, if the failure is not detected and located soon after it occurs, the damage to the surrounding infrastructure or property and liabilities are likely to be the major contributors to the overall cost of the pipe failure. Furthermore, the total cost of the pipe failure is expected to be increasing exponentially if failure management action is considerably delayed.

2.5 Failure management cycle

Since pipe failure has become quite a common event in the urban water supply systems, failure management is a part of the everyday operation of pipelines and pipe networks. However, the number of pipe failure management

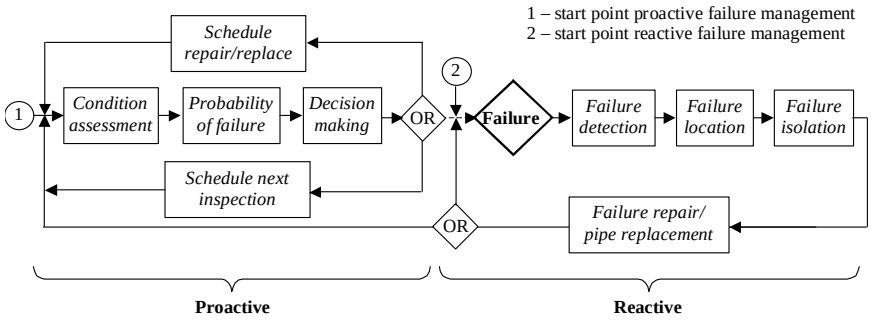

Figure 2.10: The pipe failure management cycle

techniques that are currently practiced by the water industry is not very large. On the contrary, a whole range of methodologies have been described in the literature, indicating the clear interest in such tools. Depending on the timing of failure management activities with respect to the failure itself, two types of pipe failure management strategies can be defined: proactive failure management, when the pipe repair/replacement decisions are made prior to the failure event to prevent the failure, and reactive failure management, when the repair/replacement is performed only after the failure has occurred. In Makar and Kleiner (2000), the pipe management cycle is described with the focus on the proactive part. A similar pipe failure management cycle can be defined including both proactive and reactive parts as shown in Figure 2.10.

Proactive failure management. In proactive failure management, the sequence starts at point 1 in Figure 2.10. Condition assessment is a proactive technique that is used to evaluate the current state of the pipe. The results obtained from condition assessment are then used to estimate the probability of failure or the residual lifetime of the pipe. The condition assessment will be discussed in more detail in Chapter 3 and a new condition assessment technique will be presented in Part IV of this thesis. Depending on the estimated risk of failure, the decision is made whether the pipe needs to be repaired/replaced/rehabilitated. The rehabilitation time can be scheduled in the short or the long term. Alternatively, the time for the next inspection (condition assessment) is set. Proactive failure management is a part of an overall asset rehabilitation planning strategy. One of the main challenges in the process of the rehabilitation planning is understanding the process of

pipe deterioration. Ideally, if the proactive failure management is efficient, all pipe incidents should be prevented. However, in case a failure occurs in a pipe, reactive measures have to be taken.

Reactive failure management. If the proactive pipe failure management is not implemented, a reactive management scheme has to be executed starting from point 2 in Figure 2.10. As already mentioned, the reactive part of the failure management cycle is also necessary when the proactive management fails to prevent the failure. As a first step in the reactive management sequence, the failure has to be detected. After that, the actual location of the failure has to be identified and the damaged section of the pipeline/network has to be isolated. The repair of the failure or replacement of the broken pipe is the last step in the reactive management sequence. After the repair or replacement, the pipe management routine returns to the initial point. A review of reactive failure management techniques is presented in Chapter 4. Automatic failure monitoring, detection and location techniques make up the major part of the contributions in this thesis and are described in Parts II and III.

2.6 Pipe rehabilitation planning

With water supply systems getting older, pipe rehabilitation planning is being given more and more attention both from the water industry and from the research community. The main objective of rehabilitation planning is to ensure the required performance of the system and maximise the economic efficiency of the operation. There are three major performance indicators that have to be considered:

- hydraulic performance;
- water quality;
- reliability of the service.

A large number of rehabilitation strategies have been described in the literature (Saegrov et al.; 1999; Babovic et al.; 2002; Engelhardt et al.; 2000, 2002; Davis; 2000; Lei and Saegrov; 1998) including those that are ready-to-use

(Saegrov and Schilling; 2004; Hadzilacos et al.; 2000; Luong and Fujiwara; 2002; Luong and Nagarur; 2005; Kleiner; 2001). Since rehabilitation is not the main focus of the work presented in this thesis, no review of available rehabilitation strategies will be made. Such a review can be found in Engelhardt et al. (2000). Most of the existing rehabilitation planning methods require an understanding of the pipe deterioration process. Pipe deterioration modelling (asset modelling) can be classified into two groups - physical and statistical. In Babovic et al. (2002), a third group of models was identified that represents an integrated approach based on the data mining techniques and hydroinformatics.

Physical pipe deterioration models

Physical/mechanical models are built to analyse the loads that are imposed on the pipe and the structural resistance of the pipe in order to predict the failure. Numerous components have to be considered, such as external loads, deterioration rates and material properties. In Rajani and Kleiner (2001), a comprehensive review of physical models describing the structural performance of pipes is presented. Some of the models describe only one component that affects the deterioration of pipes (pipe-soil interaction, structural resistance, corrosion status, frost load) while others try to model the whole range of factors.

Two main groups of models have been identified - deterministic and probabilistic. Deterministic models aim to predict the corrosion pit growth to estimate the remaining wall thickness and, consequentially, the service life of the pipe. Probabilistic models are designed to calculate the probability of the survival of the pipe over a certain period of time, predict the remaining life time or estimate the probability of failure. The main difference between the probabilistic and deterministic models is that probabilistic models incorporate na uncertainty component which is ignored in the deterministic models. The type of data that is required for different methods is similar and includes pipe age, soil parameters, wall thickness and current depth of corrosion pits. The corrosion pit measurement can be acquired indirectly using the nondestructive testing (NDT) techniques or directly by examining exhumed pipe samples.

Statistical pipe deterioration models

The data required to build physical pipe deterioration models is often not available and its collection has a significant cost. As an alternative to physical modelling, statistical models have been proposed to explain, quantify and predict pipe breakage or structural pipe failures. A review of statistical models that can be found in the literature is presented in Kleiner and Rajani (2001). Most of the available statistical models use the historical data of pipe failure to predict the future trends. These models can be classified into deterministic and probabilistic categories. Deterministic models use two or three parameter equations to derive breakage patterns, based on pipe age and breakage history. The division of pipes into groups with homogeneous properties (operational, environmental and pipe type) is often used, which requires efficient grouping schemes to be available. Probabilistic models are used to estimate pipe life expectancy or failure probability. Statistical models do not require any condition assessment information.

Hydroinformatics

Hydrinformatics is the discipline that provides a framework for development and application of advanced innovative techniques for water distribution network management. Savic et al. (1997) indicated that two major tools particularly suitable for water industry applications are geographic information systems (GIS) and data mining techniques, such as artificial neural networks (ANNs) and genetic algorithms (GAs). The main purpose of GIS is to collect, store and manage the accurate and comprehensive network data (Lang; 1992; Bell; 1993). Data mining (Savic and Walters; 1999; Babovic et al.; 2002), also referred to as knowledge discovery in databases, data harvesting, data archeology, functional dependency analysis, knowledge extraction and data pattern analysis, is the automated way to analyse large volumes of data to identify trends and patterns that are important for operation, maintenance and rehabilitation of water supply system. With advanced SCADA (supervisory control and data acquisition) systems and large asset, customer and maintenance databases, water utilities are facing the challenge of efficiently extracting useful information from data. Data mining techniques can be used

for different purposes. ANNs can be used for demand forecasting (Bougadis et al.; 2005) and for scanning large amounts of data (both operational variables and historical records) to identify a failure event (Mounce et al.; 2003) or to estimate failure patterns. GAs can be utilized for optimisation of system design (Simpson et al.; 1994; Savic et al.; 1997), operational decisions (Mackle et al.; 1995; Beckwith and Wong; 1995; Barán et al.; 2005) and maintenance plans (Savic et al.; 1995a,b; Halhal and Savic; 1999).

Application in water supply systems

The selection of the appropriate rehabilitation/proactive failure management technique depends on the cost-benefit ratio. The cost is represented by inspection costs and the benefit is proportional to the losses associated with a failure. It is clear that comprehensive physical pipe deterioration models can lead to a robust and reliable prediction of pipe failures. However, the cost of acquiring pipe condition information that is necessary for the model depends on the length of the pipe that has to be examined. Physical models can be applied on asset-to-asset basis while statistical models allow failure prediction on a larger scale. Thus, due to different topology, condition assessment and failure costs, proactive failure management is approached in different ways in transmission and distribution systems.

Transmission pipelines. The cost of building physical models can be justified for the large transmission pipelines where the consequences of the failure can be very expensive. There is a number of different nondestructive evaluation techniques that can be applied to obtain the necessary parameters for physical pipe deterioration models. Available approaches are reviewed in Chapter 3. In some cases, such as oil or gas pipelines, the prevention of the failure is critical and therefore all pipes are inspected using nondestructive techniques on a periodical basis. However, due to budget constraints, not all pipelines in a water supply system can be monitored and therefore the challenge of prioritisation of pipes for analysis becomes an additional difficulty in the management cycle.

The choice of pipes for inspection can be based on two criteria (Makar and Kleiner; 2000). The first one is the risk associated with the failure of the pipe.

Pipes that are supplying hospitals or schools or pipes that are installed close to highways or other strategic infrastructure should be prioritised for inspection. The second criteria is the pipe condition assessed by the pipe operator. Such condition assessment is often based on experience. Kleiner (2001) also indicated expert opinion to be an important resource in the inspection planning (and rehabilitation) process. Statistical or data mining methods could also be utilised in the procedure of inspection planning.

Distribution mains. In distribution systems, mainly due to the size (total length of mains), using statistical pipe deterioration models is probably the only currently feasible option. The application of currently available nondestructive evaluation techniques is infeasible. To cover the whole network, the rehabilitation planning has to be focused on groups of pipes and not on individual assets. Thus, as stated in Makar and Kleiner (2000), pipe break history-based statistical rehabilitation planning approaches are more likely to be classified as pipe failure management techniques rather than failure prevention measures. The efficiency of rehabilitation planning depends on the quality and quantity of available data. Ideally, pipe material, size, age, type of bedding, soil characteristics, operating pressures, water temperatures, time, place and type of historical breaks should be available. However, in many cases, only partial sets of data exist. Further development of nondestructive evaluation techniques with a potential for cost reduction and extension of their operational range may allow the use of physical models for distribution mains in the future.

2.7 Cost of failure management

The cost of pipe failure management is highly dependent on the type of techniques and practices that are used. The whole range of approaches starting with inexpensive visual inspection and ending with video surveillance and other advanced technologies is available. The choice of the failure management technique depends on which stage of the pipe deterioration process it is applied. Generally, the earlier stage of the pipe deterioration is considered, the more complex and expensive the inspection technique has to be applied. Figure 2.11 shows the inspection cost as a function of the application time. The cost of the inspection is high in the early stage of the pipe deterioration

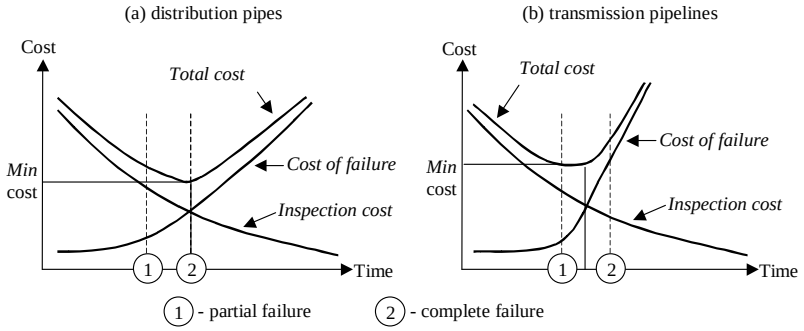

Figure 2.11: Variation of inspection and failure costs during the deterioration process

process and decreases considerably after the partial or complete failure of the pipe has occurred.

The cost is often the limiting factor when in comes to selection of failure management strategies. Water supply utilities do not usually have a budget that would allow large investment and therefore less advanced techniques are chosen. to the contrary, any oil or gas pipeline has one or more continuously operating failure monitoring systems. The installation of the corresponding amount of instrumentation in the water supply system is practically infeasible. Thus, the water industry is forced to search for less expensive options that are likely to have a lower performance standard. The application of failure management techniques can be approached from an economical perspective where the inspection cost is compared to the cost associated with the failure as shown in Figure 2.11. The losses associated with the failure are changing in the opposite manner to the inspection costs. The later the stage of the deterioration process, the larger the losses are. If the pipe is intact, the risk associated with the failure is the only component of the failure cost. Once the partial failure has occurred, the losses increase with time, since the water is lost and the surrounding infrastructure and property is being damaged. Furthermore, once the pipe has failed completely, the increase in the cost of failure becomes larger due to the interruption/degradation of the water supply service. The total cost of pipe management is equal to the sum of the cost of inspection and the cost of failure. Economically, the optimal time for pipe inspection corresponds to the point where the total cost is

minimal (intersection of the curves). The cost of the inspection at that stage will be equal to the losses caused by the failure. Failure management prior to that point in time cannot be financially justified and delay of the inspection beyond the time corresponding to the minimal cost will result in higher losses.

The actual shape of curves in Figure 2.11 and, consequently, the minimal pipe management cost depends on the particular situation. In general, Figure 2.11a can be applied for distribution networks and Figure 2.11b can be used for transmission pipelines. The consequences of a failure (both partial and complete) in the large transmission mains can be quite expensive and therefore the cost of failure increases faster than in the case of the distribution network. Still, due to the relatively low cost of water and the fairly high cost of currently available proactive failure management techniques along with restrictions on the budget of water utilities, only reactive failure management can be economically justified in water supply systems. To the contrary, in the oil and gas industries, where the cost of failure is extremely high, failure management measures are taken at an early stage of the pipe deterioration process.

Despite the current situation, the overall goal of the water industry is to increase the efficiency and reliability of its service. Rapid development of other parts in the urban infrastructure has increased the pressure on water utilities from both policy makers and the public. To achieve the improvement of the service, the necessary measures have to be taken as early as possible in the pipe deterioration process. The main objective is to reduce the cost of failure even if the optimal (minimum cost) point is not reached. There are two possible ways of reducing the losses associated with the failure: (1) reduce the reaction time to the failure, i.e. the time it takes to detect, locate and isolate the failure, and (2) systematically introduce proactive failure management by reducing the cost of existing nondestructive testing techniques and developing new low-cost approaches.

Chapter 3

Review of pipe condition assessment techniques

There are two main approaches for assessing the condition of a pipe. The first approach is direct inspection and monitoring, also called non-destructive testing (NDT). The second condition assessment approach is based on using indirect indicators, such as soil properties and historical pipe breakage rates. In this chapter, available non-destructive evaluation techniques are reviewed.

3.1 Nondestructive testing and evaluation

Nondestructive testing is the type of testing that allows detecting and evaluating of defects in materials without disturbing the specimen's structural or surface integrity. The history of NDT started with studies of ultrasonic waves and their application for detecting flaws in metal objects (Sokolov; 1935). In the 1950s, ultrasonics were applied for manufacturing flaw testing in pipes. Later on, the benefits of using nondestructive testing to assess the deterioration of metal structures were identified (Young; 1979). Currently, nondestructive testing is used for in-service inspection, condition monitoring and measurement of components and their physical properties. NDT techniques are sometimes called nondestructive evaluation (NDE) or nondestructive inspection (NDI) techniques. The term nondestructive evaluation

will be used here. The main benefit of NDE is that the testing has no negative effects on the condition of the materials or structures that are tested. A wide range of NDE techniques are available today with different degrees of complexity and operational costs, as well as specific application areas and limitations. The techniques can vary from simple visual examination of a surface to more complex radiographic, ultrasonic or magnetic methods and finally to new advanced and highly specialised approaches. To select the optimal NDT method for a particular application, a comprehensive knowledge of both the method and the tested object is necessary.

A large number of contributions to the development and application of NDT techniques can be found in the literature. Reviews of different NDE techniques are presented in Eiswirth et al. (2001); Rajani and Kleiner (2004) and Sinha et al. (2003). In general, all NDE techniques can be divided into two main categories: (1) visual NDE methods and (2) non-visual NDE methods.

Visual NDE methods

Closed-circuit television (CCTV) inspection. CCTV inspection is the standard simple approach for pipe interior inspection. The CCTV camera is mounted on a wheeled platform capable of travelling along the pipe. The inner surface of the pipe is videotaped during the inspection and recorded images are reviewed by an engineer off-line. The engineer detects, classifies and rates the severity of defects against the documented criteria. The manual assessment procedure is labour intensive and time consuming and therefore increases the overall inspection costs. CCTV inspection may miss certain types of defects, especially those that are hidden from the camera by obstructions. This method is also dependent on the engineer's concentration, experience and the ability of the image to reveal important effects. Generally, results of CCTV inspection are recognized to have a lack of consistency and reliability, especially when the objective of the inspection is to track the process of deterioration for planning of the proactive management.

Pipe scanner and evaluation technology (PSET). Pipe scanner and evaluation technology (PSET) is an advanced new technology for obtaining images of the interior of the pipe. It overcomes some of the shortcomings of

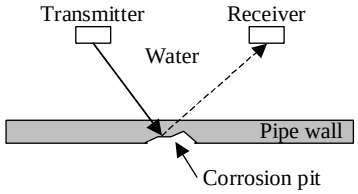

Figure 3.1: Schematic view of ultrasonic inspection

the CCTV inspection by using scanning and gyroscopic technology. The mechanics of the PSET inspection are similar to CCTV. PSET is designed to operate from a tractor platform, which is propelling the tool through the pipe. The main advantage of the PSET tool over the conventional CCTV is that the acquired images have a higher quality. Sinha et al. (2003) presented a system for application of computer vision techniques to the automatic assessment of PSET scanned images. The algorithm consists of image preprocessing, a sequence of morphological operations to accurately extract pipe joints and laterals, and statistical filters for detection of surface cracks in the interior wall of the pipe.

Laser-based scanning systems (LBSS). A laser-based profiler can be coupled to a CCTV camera to increase the accuracy of the inspection. This method, in theory, can make extremely accurate evaluations of the condition in a de-watered pipe. The equipment can be coupled with algorithms for automated detection and classification of pipe defects as shown by Duran et al. (2003). Laser-based scanning systems add real-time analysis capability to the visual inspection process and reduce the cost of the testing considerably. However, the technology is still in its development stage.

Non-visual NDE methods

Ultrasonic testing (UT). Ultrasonic inspection is performed using a beam of very high frequency coherent sound energy. The sound wave travels into the object that is being inspected and is reflected whenever there is a change in the density of the material (Figure 3.1). The transit times of a sound wave to travel through a pipe wall and back are measured. The technique is capable

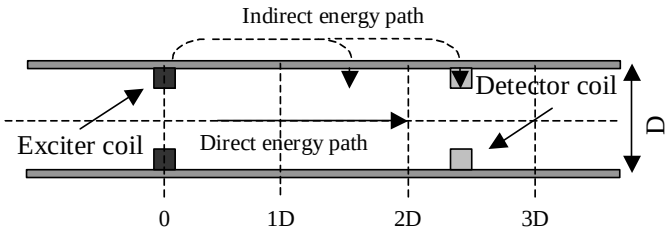

Figure 3.2: Schematic view of the RFEC principle

of detecting pits, voids and cracks. According to Rajani and Kleiner (2004), the UT methodology has some drawbacks. Crack orientation influences the precision of detection, the techniques is most suitable for metallic pipes and tuberculation on the pipe wall, which is quite common in water pipelines, degrades the performance of the method. The commercial products available are designed predominantly for oil and gas pipeline applications.

Guided waves (GW). A different type of ultrasonic approach is presented in Lowe et al. (1998) and Demma et al. (2004). It is based on the response analysis of ultrasonic guided waves excited at one location along the pipeline. These waves stress the whole pipe wall and propagate along the length of the pipe. While propagating, guided waves are partially reflected at the local changes of pipe geometry (including rust patches). The technique seeks to detect corrosion defects that remove 5-10% of the total cross-section area at a particular axial location. The scheme offers rapid inspection of sections of a pipe up to 50 m in length.

Magnetic flux leakage (MFL). The magnetic flux leakage is the most common technique used for in-service corrosion inspection of oil and gas steel pipelines (Atherton; 1989). The exact location, size and shape of the defects are determined. MFL testing relies on active magnetization in which the pipe wall is magnetized to near saturation by using a strong permanent magnet. The flux leaking out around a defect is measured at the surface of the pipeline. The magnitude of the leakage flux density depends on the strength of the magnet, the width and depth of the defect, the magnetic properties of the pipeline material and running conditions such as velocity and stress. According to Rajani and Kleiner (2004), the MFL technique is not applicable to water pipelines due to the tuberculation on the pipe interior that might pro-

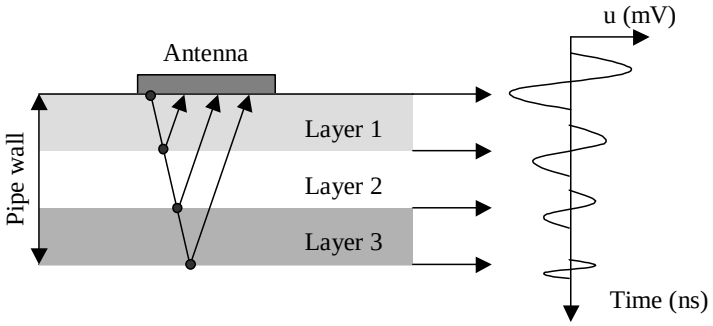

Figure 3.3: Sketch showing the principle of georadar

hibit good contact between the magnet and pipe wall. Babbar and Clapham (2003) presented a different MFL approach that is based on the measurement of the residual MFL signal after the pipe has been magnetized.

Remote field eddy current (RFEC). The remote field eddy current (RFEC) method (Atherton; 1995; Haugland; 1996) is based on measurements of the attenuation and phase delay of an electromagnetic signal as it passes throughout the wall thickness of a metallic pipe. The typical system consists of exciter and detector coils that are placed inside the pipe some distance (2-3 diameters) apart (Figure 3.2). The exciter generates an indirect (external) electromagnetic field that travels through the pipe wall. Changes in the field attenuation depend on the pipe wall thickness and therefore the measurement of the field attenuation can be used to estimate the thickness of the pipe wall. In Robinson (1998), laboratory and field trials of a prototype RFEC testing system are described. As stated in Rajani and Kleiner (2004), there are some disadvantages with the method. It can only be used for metallic pipes and requires prior cleaning of the pipe interior. Commercially available equipment is suited only for small diameter (up to 250 mm) pipes.

Georadar. Georadar testing is based on the measurement of the transit time and the signal strength attenuation of electromagnetic impulses as they travel through a pipe wall thickness (Figure 3.3). The technique is applicable for non-metallic pipes, such as asbestos cement (AC), where the deterioration forms soft layers on the internal or external (or both) pipe wall surfaces, forming several layers within the pipe wall. The properties of each layer

can be determined from the travel times and the strength of the electromagnetic impulses that can be identified in the signal measured by georadar. An application of the technique on asbestos cement (AC) pipes is described in Slaats et al. (2004). It can be applied without interrupting the operation of the pipeline, although the section of the pipe has to be uncovered.

Ground penetrating radar (GPR). Surface or ground penetrating radar (GPR) is considered as a proven nondestructive testing technique for inspection and location of buried objects. The radar operates by transmitting pulses of ultra-high frequency radio waves (microwave electromagnetic energy) down into the ground through a transducer or antenna. The transmitted energy is reflected from various buried objects or distinct contacts between different earth materials. The antenna then receives the reflected waves and stores them in the digital control unit. A GPR signal can be measured from the ground surface or from the inside of a pipe. The radar is moved along the pipe length and the image is acquired. One of the drawbacks of the technique is the difficulty of measurement interpretation. GPR inspection does not provide extensive information regarding the condition of the pipe. However, it can be used in combination with an electromagnetic system to evaluate the physical properties of the pipe and its surrounding soils.

Linear polarisation technique (LPT). The external corrosion of a metallic pipe can be correlated with the corrosivity of the surrounding soil. The linear polarisation technique is one of the most advanced methods that are using the measurement of polarisation resistance of the soil samples that are taken from the vicinity of the pipe. The measured polarisation resistance is then used to determine corrosion rates of the pipe material in various soil types. Some successful applications are mentioned in Eiswirth et al. (2001). The method can be applied for metallic pipes only and the density of sampling depends on the homogeneity of the soil surrounding the pipeline.

Field signature method (FSM). Strommen et al. (1993) described the field signature method, a technique for monitoring the condition of an in-service pipeline. The approach is based on a continuous monitoring of corrosion and remaining pipe wall thickness at a given point on the pipeline. An electric direct current is fed through the selected sections of the structure to be monitored and the pattern of the electrical field is derived by measuring small potential differences set up on the surface of the monitored object. The sen-

sor grid is permanently installed on a 1 m long section of the pipe. FSM enables the operator to create the baseline for the uninhibited corrosion rate so that FSM could be used to monitor subsequent performance of the corrosion inhibition program.

Acoustic emission (AE) monitoring. Acoustic emission monitoring involves listening to the sounds that are emitted by the tested structure. Usually, one or more ultrasonic microphones are attached to the pipe and the acquired signal is analysed with the help of computer-based instruments. The noise may be generated by the friction, crack growth turbulence and corrosion. The technique is especially suitable for prestressed concrete pipes where the sound is made by breaking reinforcement wires. An operational acoustic emission monitoring system is described in Travers (1997). The hydrophones are installed with an interval of 300 m to continuously monitor the acoustic emission of the pipeline for reinforcing wire failure.

In Samoilov (1998), the experiences of using an AE monitoring system in combination with the hydrostatic testing on an oil pipeline are described. Hydrostatic testing is a pipe integrity testing method. The pressure in the pipeline is changed in a sequence of four test-load levels: starting load, increasing load, intermediate hold and decreasing load. AE monitoring is performed continuously during the testing and the acquired data is analysed to distinguish signals generated by plastic deformation, crack initiation and crack growth from fatigue.

Impact echo (IE). The impact echo technique is based on the analysis of acoustic waves that are artificially generated by impacting the pipe wall with a solid object. A firm high frequency sound indicates an intact pipe, while a hollow low frequency sound is a sign of deterioration. The complexity of the analysis can vary significantly, from a manual striking of the pipe using a hammer and listening to a systematic controlled impact generation and measurements of reflection pulses using transducers (Robison; 1995). As indicated in Rajani and Kleiner (2004), the technique is not yet commercially available.

Mechanical (MAC) method. Diab (1995) presented a mechanical system which is used to apply cyclic load on a pipe from the inside of the structure and measure the produced displacement. The system is called MAC (French

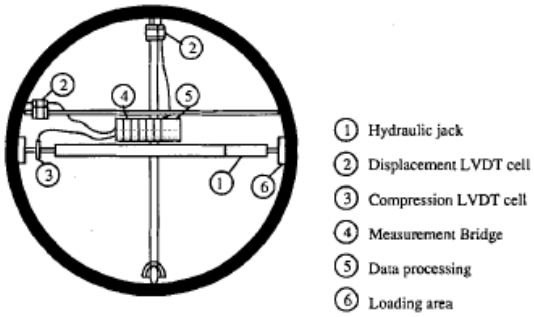

Figure 3.4: Components of MAC system. Source: Diab (1995)

abbreviation for buried pipes mechanical inspection) and is illustrated in Figure 3.4. The load is applied in horizontal direction and the displacement is measured by the LVDT (linear variable differential transducer) cells. Loading steps and limits are adapted in a real-time as a function of measured displacement. The system is primarily designed for sewer pipes and allows inspection of pipes with the horizontal span from 700 to 4 000 mm. It requires the pipeline to be empty and have access points large enough for the test equipment to be inserted. Tests are performed at the interval of 20 m and the nominal testing rate of 2 000 m/day is claimed.

Free-vibration (FV) method. The free-vibration method can be seen as an extension of the impact echo technique. In Murigendrappa et al. (2004a), an experimental investigation of the possibility of representing a crack with a straight front and normal to the axis in a straight pipe containing pressurised fluid by a spring for simulating its transverse free vibration is presented. A technique based on measurements of changes of natural frequencies has been employed to detect the location of an unknown crack in a pipeline at different pressures. Two pipe materials - aluminium and steel - were tested. The length of the pipe segments used in experiments was less than 1 m. The crack had a size-to-pipe-wall-thickness ratio in the range of 0.19 to 0.64. The maximum error in derived crack location was 2.6% of the pipe span. Data presented on the variation of the rotational spring (representing the crack) stiffness versus the ratio of crack size to thickness could be used for crack size prediction knowing the spring stiffness. The expected range of the technique is around 60 m. The same technique has been applied for a multiple

crack case as shown in Murigendrappa et al. (2004b). Locations of two simultaneous cracks (straight fronts) with a size-to-pipe-wall-thickness ratio in the range of 0.19 to 0.64 were found with an error less than 4.3% of the pipe span.

3.2 Comparison of NDE techniques for application in water pipelines

Different features of the presented NDE techniques are summarised in Table 3.1. Historically, NDE methods have been developed for large oil or gas pipelines, where inspection budget and failure risk are considerably larger than in water supply systems. As already noted earlier in Chapter 2, the main requirements for condition assessment techniques from the perspective of the water industry would be low cost and a fast inspection, whereas high precision of the inspection is less crucial. None of the existing NDE techniques can satisfy those objectives. Furthermore, the range and the speed of inspection are very small. As indicated in Table 3.1, a number of techniques require the inner surface of the pipe wall to be clean. Water pipelines often have an accumulation of tuberculation on the inside wall and therefore cleaning would be necessary before inspection. The cleaning would further increase the cost of inspection and, in many cases, water utilities are reluctant towards any disturbances due to health and safety concerns, i.e. intrusion of contaminants due to pressure drop or disinfection of the pipeline after inspection.

Currently CCTV inspection is the main tool for condition assessment of water pipes. Recent developments of the technology allow for good quality of the captured image, but a number of drawbacks still remain. The analysis of the data from CCTV inspection is usually done manually, which is extremely time and labour intensive. To be able to insert the camera and the transporter into the pipe, cutting the wall is often required. Since the range of CCTV inspection is only around 300 m on each side of the access point, a large number of access points will be necessary in a long pipeline. Finally, de-watering is usually required. The combination of all these factors and related health and safety issues prevent large-scale applications of CCTV inspection in water transmission pipelines. Other available NDE techniques reviewed earlier

Method	Type*	Pipe material	Inspection		Evaluation			Available	Comments
			range	speed	qualitative	quantitative	precision		
CCTV	*IL,I,Man.*	All	600 m	1500 m/day	Yes	Yes	Low	Yes	Most popular
PSET	*IL,I,Aut.*	All	600 m	1500 m/day	Yes	Yes	High	R&D	Automated
LBSS	*IL,I,Aut.*	All	600 m	1500 m/day	Yes	Yes	High	R&D	Real-time
UT	*IL,I,Man.*	Metallic	n/a	Slow	Yes	Yes	High	Yes	Cleaning required
GW	*Ex,I,Man.*	Metallic	50 m	300 m/day	Yes	Yes	Low	Yes	Pipe access required
MFL	*IL,I,Man.*	Metallic	<n/a	Medium	Yes	Yes	Low	Yes	Cleaning required
RFEC	*IL,I,Man.*	Metallic	1 m	Slow	Yes	Yes	Medium	R&D	Cleaning required
Georadar	*Ex,I,M*	AC	1 m	Slow	Yes	Yes	Medium	R&D	Pipe has to be uncovered
GPR	*Ex,I,Man.*	All	1 m	Slow	Yes	No	Low	Yes	Difficult data interpretation
LPT	*Ex,I,Man.*	Metallic	n/a	n/a	Yes	No	Low	Yes	Soil examination
FSM	*Ex,M,Aut.*	Metallic	1 m	-	Yes	No	Low	Yes	Corrosion monitoring
AE	*Ex,M,Aut.*	PCCP	100 m	-	Yes	Yes	Medium	Yes	Expensive installation/maintenance
IE	*Ex,I,Man.*	All	1 m	n/a	Yes	No	Low	Yes	Low precision
MAC	*IL,I,Aut.*	All	20 m	2000 m/day	Yes	No	Low	Yes	Sewer applications
FV	*Ex,I,Aut.*	Metallic	60 m	n/a	Yes	Yes	Medium	R&D	Early R&D stage

**IL* - applied in-line, *Ex* - applied from outside, *I* - inspection, *M* - monitoring, *Man.* - manual data analysis, *Aut.* - automatic data analysis

Table 3.1: Comparison of nondestructive evaluation (NDE) techniques for pipe condition assessment

in this chapter, have similar drawbacks to those of CCTV inspection. Thus, further development of NDE methods is required to make their use in water supply systems more frequent and systematic. New techniques, offering low cost and time-effective inspection, represent another alternative.

In Chapter 11 (Part IV) of this thesis, a new, hydraulic transient-based condition assessment technique is presented.

Chapter 4

Review of pipe failure detection and location techniques

In this chapter, reactive failure detection and location techniques will be reviewed. The review covers both techniques that have already been applied for failure detection and location in pipelines and pipe networks and techniques that are in the stage of research and development. Approaches that have been used or designed for water industry applications and methods applied in the oil and gas industries are considered. A summary of available numerical, experimental and field validation results is presented. At the end of the chapter, the application of failure detection and location techniques in water supply systems is discussed.

4.1 Classification

As discussed in Chapter 2, pipe failure has different types depending on the size and the character. Due to the fact that for most of the techniques that are described in the literature the type of failure is not specified, a leak will be used as a general term here. Depending on the application, leak detection can be associated with two different operations. In larger transmission pipelines, where larger failures are common, leak detection is usually associated with identifying discrete pipe failure events. Subsequent leak location

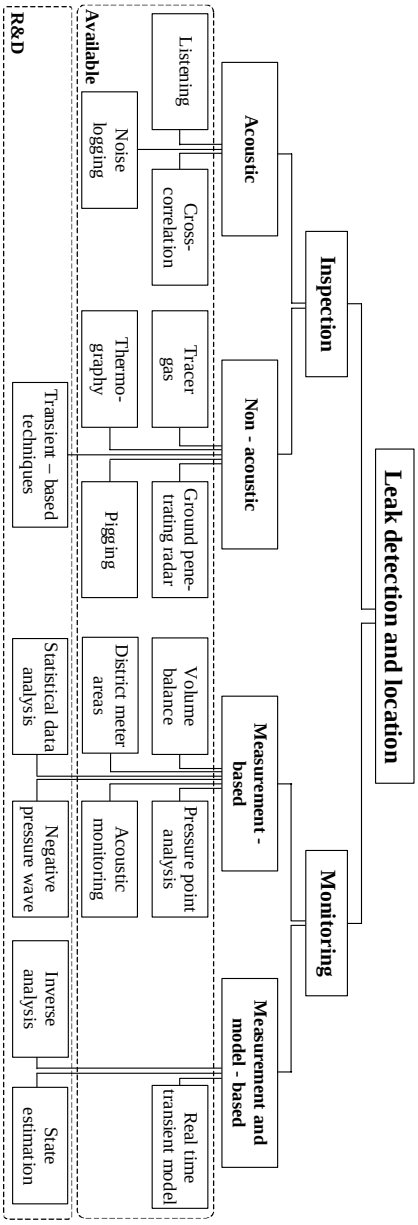

Figure 4.1: Active leak management techniques

involves the identification of the actual position of the leak. In distribution networks, leakage detection is often integrated with leakage assessment, where the amount of water that is lost due to leaks present in the system is estimated. Leakage is detected collectively and the identification of a particular leak is part of the location process. Generally, two leakage detection and location (sometimes also referred to as leakage control) strategies can be used for both pipelines and pipe networks.

- **Passive or manual.** The reaction to a leak incident is based on visual observations. For example, the appearance of water on the ground surface following pipe failure is visually detected by the staff or reported by custumers. Manual location techniques are then used to identify the actual location of the failure.
- **Active or automatic.** Active leakage control includes management policies and processes that are used to locate and repair unreported leaks from the water supply system (Tripartite Group; 2002). Active leakage control can involve systematic manual leak inspections or continuous monitoring for automatic detection of leaks. Manual leak location techniques are usually used, although some leak monitoring systems provide automatic location.

Passive leakage detection is straightforward, simple and does not involve any systematic action. Thus, it will not be discussed in this thesis. The main focus of the work presented here is on active leakage detection and location strategies. Active leakage control techniques can further be divided into two groups:

- **Inspection (survey).** Inspection or survey leak detection is a planned action that is performed at discrete time instances. The inspection involves checking the whole or a part of the system to assess the level of leakage and find leaks that are already present.
- **Monitoring.** Continuous failure monitoring is used for detection of leak events in real-time. A monitoring system is installed on a pipeline or in the network permanently and is continuously checking for new leaks. Some monitoring systems can perform periodical leak checks (repeated at a certain time interval).

A large number of leak detection and location techniques have been applied in real systems or have been described in the literature. The classification of different approaches is shown in Figure 4.1. Some of the existing techniques are designed for detecting leaks only and are not capable of locating them. Other methods are developed specifically to locate leaks. Finally, there are methods that allow for both detection and location. No specific division is made in this review to separate existing approaches into detection, location and detection and location groups. The inspection techniques are reviewed first followed by the review of monitoring approaches. At the end of the chapter, a summary of performance for different methods is presented along with a discussion on the application in water supply systems.

4.2 Leakage inspection techniques

Commercially available leakage inspection methods can generally be divided into two large groups - acoustic inspection techniques and non-acoustic inspection techniques. In addition to these two groups, transient-based leak inspection methods are reviewed here. Although not yet available commercially, transient-based approaches have been given a lot of attention from the research community.

Acoustic inspection techniques

Listening. Listening is the oldest leak detection technique that has been in use since 1850s (Pilcher; 2003). Pipe inspection is conducted manually, using mechanical or electronic devices that are sensitive to leak-induced noise or vibrations. The leak inspector walks along the pipe and listens to the leak noise at ground level or on a fitting connected to the pipe. Modern equipment incorporates amplifiers and noise filter to enhance the resolution of the signal. A listening stick is the most common device used for leak inspection. A ground microphone is another tool that can be applied at the ground surface above the pipe. There is a number of factors that influence the effectiveness of the listening survey (Chastain-Howley; 2005). The distance between the leak and the monitoring point will affect the precision of the detection and location. The noise attenuation rates in different soil types are discussed in Hunaidi and Chu (1999). In case when the listening device is attached to the

pipe fitting, the acoustic leak detection is generally more efficient. However, since fittings on large transmission pipelines are far from each other, leak detection becomes difficult. Pipe material has a considerable influence on the attenuation of the leak noise. Acoustic leak detection is not well suited for plastic pipes, which have higher noise attenuation rate than metallic lines. Since the sound waves generated by the leak travel through the pipe wall and water together, pipes with larger diameter have a higher attenuation of the leak noise. Finally, the noise from traffic, water flow as well as the degree of detail of the survey and the experience of the inspector can influence the performance of the leak detection and location. Lange (2005) suggested that an advanced acoustic signal processing might considerably improve the leak detection capabilities in plastic and larger diameter metallic pipes. The author reported the detection of a 0.17 L/s leak in a plastic pipe using a listening stick when the distance from the leak point to the monitoring point was 95 m.

Acoustic monitoring (AM). Acoustic emission monitoring is performed using vibration sensors or hydrophones, which are temporarily or permanently attached to the pipe fittings, typically 200 to 500 m apart. In case of temporal setup, data loggers are coupled to sensors to store the measured data. Usually, noise loggers are left overnight and are programmed to collect data during the period of low water use, usually between 2 and 4 am. Collected data is then downloaded to a computer and statistical analysis is performed to detect leak signals. Rajtar and Muthiah (1997) described the expected performance of a real-time acoustic emission leak detection system for low pressure pipelines in oil and gas gathering installations. The system was tested on a closed field-scale two phase flowloop. Both gas and liquid leaks were tested. Sensor spacing of 61 m was used. Liquid leaks with flow rates less than 0.003 L/s were detected and located. The location of the error was approximately 15% of the detetector spacing. The main disadvantage of acoustic monitoring is the high cost. van der Kleij and Stephenson (2002) studied the application of acoustic loggers in well established district metering areas (DMAs). It was shown that acoustic loggers, when used as a temporary survey tool (moved from area to area), are less cost effective than traditional manual leakage inspection (fitting sounding using a listening stick). When a permanent deployment of loggers was considered, a minimum payback period of 26 years was estimated (235 units covering 50 km

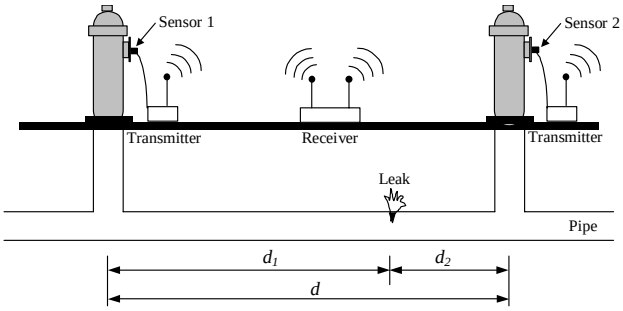

Figure 4.2: Measurement arrangement for leak detection using correlation

of mains). It was also noted that the detailed manual inspection survey identified 40% more leaks than an acoustic logger survey. Using acoustic loggers can be beneficial in situations when a manual survey is difficult, e.g. in parts of the network that have high surrounding noise.

Cross-correlation. In leak detection surveys using acoustic signals, the most common technique of leak location is the cross-correlation. The cross-correlation technique is fairly straight forward. Vibrations or acoustic signals are measured using either accelerometers or hydrophones at two access points (typically fire hydrants), on either side of the inspected pipe length (Figure 4.2). The signals from the sensors are transmitted to the leak noise correlator, which computes a cross-correlation function of the two signals. If a leak is present between the sensors as shown in Figure 4.2, the cross-correlation function will have a distinct peak. A corresponding time delay, τ_{peak}, indicates the difference in arrival times of the leak noise signals at each sensor and is related to the locations of the sensors:

$$\tau_{peak} = \frac{d_1 - d_2}{a} \tag{4.1}$$

where d_1 is the distance from the leak to sensor 1, d_2 is the distance from the leak to sensor 2 and a is the wave speed of the pipe. By substituting $d_1 = d - d_2$ into Equation (4.1), the location of the leak with respect to sensor 1 can be calculated:

$$d_2 = \frac{d - a\tau_{peak}}{2} \tag{4.2}$$

The distance between the sensors, d, influences the performance of the leak detection and location. Generally, shorter sensor-to-sensor spacing is better. A number of factors, such as pipe material and type of sensors, have an influence on the maximum spacing between monitoring points. As indicated by Hunaidi and Wang (2004), for plastic pipes, it may not be possible to locate leaks if the distance between sensors is greater than 100 m. For metal pipes, a sensor spacing limit of 200 m is recommended.

Cross-correlation testing results are presented in Hunaidi et al. (2000). The leaks were simulated in a 150 mm diameter PVC pipe and the sensors were placed on the fire hydrants that were 103 m apart. Two types of instruments were used - hydrophones and accelerometers. The smallest detectable leak flow rate was between 0.03 and 0.05 L/s for the hydrophone tests and between 0.08 and 0.1 L/s for the accelerometer tests. Results from the same experimental study were analysed in Gao et al. (2004) and the error in the derived leak location was shown to be less than 0.6 m. However, it was also noted that, in the noise-free case, the ratio between distances d_1 and d_2 has to be within the limits of 0.1 and 10 for a leak to be located. Due to background noise, sufficient levels of correlation might be further restricted in real applications. Effects of other factors, such as pressure level, type of leak (service connection, crack or joint), measurement connection type (fire hydrant, service connection) are discussed in Hunaidi and Chu (1999). A number of manufacturers of acoustic leak detection equipment are listed in Hunaidi et al. (2000). The main disadvantage of the cross-correlation method is the short range and slow speed of the survey.

Non-acoustic inspection techniques

Tracer gas technique. The integrity of an isolated section of the pipe can be tested by injecting a non-toxic, water insoluble and lighter-than-air gas and scanning the ground surface above the pipe with a highly sensitive gas detector (Heim; 1979). If a leak is present in the tested section of the pipe, the tracer gas will escape through the leak opening and, being lighter than air, will penetrate the ground surface. Tracer gas methodology is widely used for machinery testing (Heitbrink et al.; 1999), but its wide application for leak inspection in pipelines is prohibited by the high cost.

Thermography. Infrared thermographic pipeline inspection has been used to test pipelines in chemical plants, water supply systems, steam lines, natural gas pipelines and sewer systems (Weil et al.; 1994; Weil and Graf; 1996). An infrared camera is used to scan the soil around the pipe for thermal anomalies. The leak detection method is based on the assumption that the water leaking from the pipe will affect the thermal characteristics of the surrounding soil, i.e. make it a more effective heat sink than the dry soil. Several case studies are reported in Weil et al. (1994) that indicate the potential of the method to detect leaks in pipes as well as erosion voids. A number of factors affect the performance of the technique: surface conditions of the test area, solar radiation, cloud cover, ambient temperatures, wind speed and the moisture of the ground.

Ground penetrating radar (GPR). The application of ground penetrating radar for leak detection has been given a lot of attention during the last few years (Hyun et al.; 2003; Stampolidis et al.; 2003; Nakhkash and Mahmood-Zadeh; 2004). Ground penetrating radar inspection is a nondestructive geophysical method that produces a continuous cross-sectional profile or record of subsurface features. The radar operates by transmitting pulses of ultra high frequency radio waves (microwave electromagnetic energy) down into the ground through a transducer or antenna. The transmitted energy is reflected from various buried objects or distinct contacts between different earth materials. The antenna then receives the reflected waves and stores them in the digital control unit. The time lag between the transmitted and reflected waves corresponds to the depth of the reflecting object. To detect a leak, GPR is used to either (a) identify voids in the soil around the pipe that are created by the leak, or (b) detect sections of the pipe that appear to be deeper than they actually are due to changes in dielectric properties of the water saturated soil. The testing procedure is quite time-consuming. As an example, Stampolidis et al. (2003) described testing of the piping along a 330 m long street. 60 GPR profiles were measured with a total length of $1\,350$ m. Measurements along the profiles were taken with a spatial interval of 0.1 m.

Pig-based methods. A pipeline pig acts like a free moving piston inside the pipe. In oil and gas pipelines, pigs are used for various purposes such as cleaning, inspection, leakage detection, etc. (Anon; 1997; Lima and Neto;

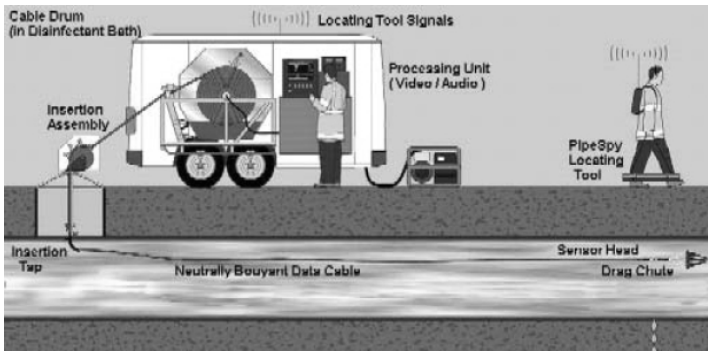

Figure 4.3: Sahara system. Source: Mergelas and Henrich (2005)

1995; Licciardi; 1998). According to Chastain-Howley (2005), the Sahara leak detection and location system developed by the Water Research Centre in the UK is the only technology currently available to assess the exact location of a leak in water transmission mains. The performance of the Sahara leak detection system is described in Mergelas et al. (2005). A sensor is introduced into the pipe through a tapping of 50mm or larger. The sensor travels along with the flow; as it passes any leak it detects the sound generated and gives an indication to the operator. Passing close to each leak means the system will work in pipes of any material. Every leak can be individually identified and its relative size assessed. Leaks as small as 1 L/h ($2.7 \cdot 10^{-4}$ L/s) can be detected. The sensor is mounted on an umbilical cable which allows its position along the pipe to be controlled precisely. This, coupled with a built in tracing device, allows the sensor position to be tracked accurately from above ground. Survey lengths of up to $2\,000$ meters can be achieved with a location precision of 20m.

Transient-based methods

A number of hydraulic transient-based techniques for detecting and locating existing leaks are described in the literature. The main objective of all transient leak detection methods is the same – extract information about the presence of a leak from the measured transient trace. For the generation of a transient event, system elements (i.e. inline valves and pumps) or special

devices (such as solenoid side discharge valves) are used. The fact that the transient wave speed can be over 1000 m/s means that a high sampling frequency of pressure measurements is required. The choice of measurement position and the characteristics of generated transients depend on the method that is used for further analysis.

Leak reflection method (LRM). The leak reflection method (Brunone; 1999; Brunone and Ferrante; 2001; Jönsson and Larson; 1992; Jönsson; 1995, 2001) is probably the most straightforward and simple application of transient analysis for leakage detection. A transient wave travelling along the pipeline is partially reflected at the leak. If the reflected wave (usually the first reflection is considered) can be identified in a measured pressure trace, the location of the leak can be found using simple calculations. The method is based on the principle of time domain reflectometry (TDR), which is a well-established technique in electric power systems (Cowan; 1975; Harding; 1976). For the best results, a sharp transient wave has to be used. The detection of change in the measured pressure caused by leak reflection can be difficult. A magnitude of the reflection from the leak depends on the ratio between the size of the generated transient wave and the size of the leak orifice. In Brunone (1999), a leak with $C_d A_o$ approximately equal to $3.5 \cdot 10^{-5}$ m^2 was detected and located in a 94 mm laboratory plastic pipeline. A pressure wave with the magnitude ΔH=10 m was generated. Jönsson (2001) was able to detect a 0.04 L/s leak corresponding to 5 % of the pipe flow, however, the transient with the magnitude of 45 m was used. Transients of that size can be dangerous for a real pipeline. Jönsson (2001) also showed that both positive and negative transients can be used. A negative transient with the magnitude of 30 m was generated in a 200 mm diameter polyethylene pipeline. The analysis of the results indicated two possible leaks. After examination, one 7 L/s leak was discovered. The location error was 100 m. The application of the leak reflection method is limited to the single pipe case.

Inverse transient analysis (ITA). The inverse transient analysis method (ITA) was introduced by Liggett and Chen (1994). The approach uses least squares regression between modelled and measured transient pressure traces. The leak is modelled at discrete positions (usually nodes) in the network and the minimisation of the deviation between the measured and calculated pressures produces a solution of leak location and size. Since its introduction, the

ITA method has been the topic of many research papers (Liggett and Chen; 1994; Kapelan et al.; 2003a,c; Covas et al.; 2001, 2003, 2004; Vítkovský et al.; 2000, 2001; Stephens et al.; 2004; Ivetic and Savic; 2003). However, the main effort has been focused on the development of the mathematical part of the technique and not on experimental validation or field testing. Limited experiences from laboratory and field tests (Vítkovský et al.; 2001; Stephens et al.; 2004; Covas et al.; 2005) include single pipe cases where a controlled transient is introduced to detect and locate a leak. The challenge for applying ITM is the accurate modelling of the transients and boundary conditions of the pipe system. In Stephens et al. (2004), a 10 mm leak was detected in a 94 mm dead-end branch of the network using a reasonably small transient (magnitude of 6 m). Covas et al. (2005) presented results from a 300 mm diameter field pipeline, where a 13 m transient was used to detect and locate a 3 L/s leak with the precision of 50 m.

Impulse response analysis (IR). When propagating along the pipeline, a transient is affected by the friction of the pipe wall and other loss elements such as leaks. This effect results in damping of the transient wave. By comparing the transient damping in the same pipeline with and without a leak, the leak can be detected. Liou (1998) has presented an impulse response analysis method for detecting and locating leaks. The impulse response can be extracted by using cross-correlations between a low amplitude pseudo random binary disturbance input and the system's output. The feasibility of using the impulse response to detect and locate a leak in real time was demonstrated using a simulation example. A 10 L/s leak was simulated in a 300 mm diameter pipeline. The amplitude of the pseudo random binary disturbance was 2 m. The precision of leak location was dependent on the discretization of the pipeline length. The implications that may arise when applying the technique on real pipelines are not discussed.

Transient damping method (TD). The analytical solution derived by Wang et al. (2002) showed that the friction related transient damping in a pipeline without a leak is exactly exponential and the corresponding damping in a pipeline containing a leak is approximately exponential. The rate of the leak-induced damping depends on leak characteristics, the pressure in the pipe, the location of the transient generation point and the shape of the generated transient. Based on the analytical solution, a leak detection and lo-

cation technique was developed. Tests on a laboratory pipeline showed that 1 mm diameter leak can be detected and located in a 22.1 mm diameter pipeline. However, in a real situation, friction in not the only cause of transient damping. Other physical elements, such as joints, connections, fire hydrants and pipe wall deterioration products can cause transient damping. The modelling of these elements can be complicated and, in some cases, impossible. Thus, it may be difficult to estimate the leak-free damping for a real pipeline.

Frequency domain response analysis (FDR). The frequency response method (Mpesha et al.; 2001, 2002; Ferrante and Brunone; 2003a,b; Lee et al.; 2005) uses the analysis of transient response in the frequency domain. Fourier transforms are used to transform time-domain data into the frequency domain. By comparing the dominant frequencies of no-leak and leaking pipelines, the leak location can be obtained. Performance of the method is strongly influenced by the shape of the transient and the measurement location. Only pipeline applications of frequency response analysis are presented in literature. In Lee et al. (2005), the detection and location of a leak with $C_d A_o = 1.4 \cdot 10^{-4}$ m^2 in a 300 mm diameter pipeline is demonstrated using a simulation example. The generated transient had the magnitude of 26 m and the location precision was around 500 m.

4.3 Measurement-based leak monitoring techniques

Leak monitoring approaches can be divided into measurement-based and model-based techniques. Measurement-based methods are using the analysis of measured parameters to detect leaks.

Acoustic monitoring (AM)

Acoustic monitoring, already presented as an inspection technique in the previous section, can be performed permanently to detect leaks. In Grimaud and Pascal (1991), a permanent leak/burst monitoring system is presented. The system is installed on a 420 m long section of a large diameter ($1\,250$ mm) pipeline that runs from a reservoir ($450\,000$ m^3) and across a highway. The failure of such a pipeline could have catastrophic consequences, and therefore a continuous monitoring scheme had been chosen. The alarm level for

the acoustic monitoring system was set to 1.94 L/s (7 m^3/h), resulting in a leak detection time of 10 min. The alarm was set up to be transmitted to the control room. The flow rate comparison was implemented as a parallel monitoring system setup to detect 97 L/s leak in 1 min. In Brodetsky and Savic (1993), a permanent acoustic leak monitoring system for high-pressure underground gas pipelines is described. A classifier is implemented to distinguish between leak and non-leak signals. A distance between sensor units of 600 m allows for a 6 mm leak to be detected. Location of the leak is not discussed.

For the combined detection and location of leaks, a permanent acoustic monitoring (AM) system can be installed in the network. Short-term deployment of acoustic monitoring sensors for leak detection has already been discussed in a previous section. In Sánchez et al. (2005), a pilot study of a permanent acoustic monitoring system is presented. A total of 75 km of distribution mains in three different areas in the autonomous region of Madrid, Spain were monitored using 460 items of equipment. The study was conducted during 6 months and a total of 49 leaks were detected (excluding leaks that were already present in the network at the time of installation of the monitoring system). Exact locations of detected leaks were determined using geophones and correlators. The cost-benefit analysis performed in the study has indicated that the high installation cost of permanent acoustic loggers can be justified if the number of bursts in the network is higher than 20 bursts/100 km/year. In other words, the continuous monitoring is beneficial in systems that have a higher deterioration level.

Volume balance method (VB)

The volume balance method is one of the earliest computer-based methods developed to detect the presence of a leak in a pipeline. Conservation of mass serves as a main principle of the method: the difference between the amount of fluid that goes into the pipe and the amount that goes out of the pipe over any time interval must be equal to the change of mass inventory inside the pipe (line pack) over the same time interval:

$$VB = V_{in} - V_{out} - \Delta V \tag{4.3}$$

where V_{in} is metered inlet volume of the pipe segment, V_{out} is metered outlet volume of the pipe segment and ΔV is a volume of fluid contained in the pipe segment (line pack). Ideally, in a leak-free situation the volume balance VB should be equal to zero. In a case of leak, VB would have a positive value equal to the volume of water that escaped the pipe. The accuracy of the volume balance method depends on the precision of flow measurements and the accuracy of calculated line pack ΔV. Water hammer equations can be used to calculate ΔV (Liou; 1994). The sensitivity of the volume balance leak detection increases with the increase of the time interval for which the volumes are calculated. When calculating volumes balance based on a longer time period, errors of calculated line pack are diluted and measurement noise is averaged out.

The optimal length of a leak detection period depends on the pipeline system, instrumentation and SCADA sampling rate. However, periods shorter than 30 minutes are not generally effective. If the threshold value is set to be low, operational transients in the pipeline might trigger false alarms of the leak detection system. When the detection period is extended, the influence of transients is reduced. Larger leaks can be detected when the shorter detection period is used, but for maximum sensitivity of the method, the volume balance should be calculated for an interval of up to 24 hours. The main drawback of the volume balance method is the assumption of the steady state. Due to this assumption, the detection period has to be increased in order to avoid false alarms. Consequently, the response time to the leak will be extended, which is undesirable. Another significant disadvantage of the approach is the lack of leak location. Other techniques have to be applied after the leak has been detected to find its location. In real applications, the volume balance method is implemented as a stand-alone leak detection system or in combination with other methods.

A volume-balance based leak detection system is described in Mactaggart and Myers (2000). The system was implemented on a 140 km long 350 mm diameter crude oil pipeline. The flow rate, pressure and temperature were monitored at all inlet and outlet points and additional pressure measurement points were installed on all platforms (18 in total). The largest spacing between two pressure monitoring points was 67 km. The sampling interval of measurements was 30 s. The line pack was recalculated each sampling inter-

val and analysed using different length time windows (from a few minutes to several days). Threshold values were selected for each window length separately. Thresholds were increased during transient operations in the pipeline to avoid false alarm situations. The estimated detection time of a 1 L/s leak was 4 hours, while a complete line failure should be detected in less than 3 minutes.

Pressure-point analysis (PPA)

Pressure-point analysis is another widely used technique that monitors the pressure measurement to detect the leak-induced pressure drop. The level of advancement can vary from detection of abnormally low pressures, to the monitoring of pressure change rate and further to the use of statistical techniques to identify the leak signature in the measured pressure trace. The latter approach is described in Whaley et al. (1992).

The main principle of the PPA is that the leak will be followed by a decrease in pressure. To identify the pressure decline, the buffer of the most recent values of pressure can be divided into two parts and statistical properties (mean and standard deviation) of the two parts are calculated. If the mean of the newer portion of data is significantly smaller than the mean of the older portion, a leak can be suspected. To increase the sensitivity of the leak detection, a longer buffer of data should be used. Consequently, the response time to a leak will be increased. Other events in the system (operational changes) can cause similar changes in pressure as the one of the leak. Thus, to reduce the rate of false alarms, the operation of the leak detection system can be inhibited until the pressure of the system resumes the steady-state level after the operational change.

The primary advantage of the PPA system is low complexity and cost. The amount of instrumentation that is installed in a pipeline can vary from a single measurement point to a number of pressure transducers distributed along the pipeline. The weaknesses of the approach are the high probability of false alarms and inability to locate or size the leak. In case when the density of measurement points is higher and the sampling interval is shorter, the locations of the transducer that produces the earliest leak alarm can be used to reduce the search space for the location of the leak.

In Schlattman (1991) experiences from the real operation of the PPA system on two crude oil pipelines (with diameters of 600 and 650 mm) are presented. The system is reported to be able to detect leaks with flow rates from 10 L/s in 10 minutes when three pressure monitoring points (sampling interval of 10 s) are installed on a 130 km long pipeline. The location capabilities are not discussed. Since only three pressure measurement points are available, the precision of the leak location is expected to be approximately equal to half the length of the pipeline. A leak detection system combining volume balance and pressure point analysis methods is described in Bose and Olson (1993).

Negative pressure wave (NPW) method

Silva et al. (1996) presented a pipeline burst monitoring system that is based on the monitoring of pressure for the leak-induced pressure wave. The location of the leak is derived based on the wave arrival times at different pressure monitoring stations and the wave speed of the pipe. Experimental results from two PVC pipelines with diameters of 75 mm and lengths of 433 and $1\,248$ m, respectively, are reported. Four pressure transducers were used to monitor the pressure and the burst was simulated by opening a side-discharge solenoid valve. The size of the burst was defined using the ratio between the flow rate of the leak and the flow rate in the pipeline prior to the leak. Tested bursts had flow rates between 5 and 50% of the initial pipeline flow rate and were located with an error of less than 5 m.

Statistical pipeline leak detection (SPLD)

Atmos pipe© (Zhang; 2001), a statistical leak detection system that uses flow rate, pressure and temperature measurements has been installed on a number of pipelines. The main principle of the statistical pipeline leak detection is the sequential probability ratio test (SPRT). Data received from a SCADA system is validated prior to calculating the corrected flow imbalance. SPRT is used to decide if there is an increase in flow imbalance and, finally, pattern recognition is applied to distinguish between a leak and operational changes. SPLD system apply three different computational pipeline monitoring (CPM) methods: (1) modified mass balance, (2) pressure and

flow monitoring and (3) statistical analysis. The main objective of the system is to minimise the rate of false alarms. The leak is identified based on probability calculations at regular sampling intervals. The probability calculation combines mass-balance with hypothesis testing – leak against no leak. Hypotheses are tested using SPRT. Different SPRT parameters are used for steady-state operation and during operational changes.

A statistical leak detection system presented in Beushausen et al. (2004) is installed on a 700 mm diameter and 353 km long oil pipeline. The flow and pressure are monitored at the inlet and outlet points and an additional 31 pressure, 19 temperature and 7 density monitoring stations are installed along the pipeline. The measurement data is transferred to the control room a over local area network (LAN) with a 3 s interval. Results from 47 leak tests are presented that were carried out under both steady-state and transient conditions. Leaks with flow rates between 14 and 100 L/s were detected during steady-state operation with detection times between 4 and 35 minutes. During transient operation, leaks with flow rates between 19 and 72 L/s were detected in 2 to 14 minutes. The location of the leak was estimated based on the leak-induced wave arrival times at the pressure monitoring stations. Since the sampling time was quite long, the precision of the leak location was around 10 km.

Statistical data analysis-based (SA) methods

Wang et al. (1993) presented an approach based on autoregressive modelling which requires four pressure measurements along a pipeline (two at each extreme). Two consecutive time sequences of pressure gradients at both ends of the pipeline are fitted to autoregressive (AR) models. The parameters and residual variances of the fitted models are dependent on the condition of the pipeline and are analysed to detect the leak. The approach has been tested on a 120 m long experimental pipeline with a diameter of 10 mm. The pressure was monitored at 0, 20, 100 and 120 m along the pipe with the sampling frequency of 50 Hz. Two leaks, 1% and 0.5%, were simulated and both were detected almost instantly. The nominal flow in the pipe is not given. The sensitivity of the proposed method to operational changes in pressure is not discussed.

District meter areas (DMAs)

In present practice of water companies, the most common technique for identifying leakage is to conduct a water audit. A detailed account of water flows into and out of the distribution system, or parts of it, is recorded. At the level of the whole system, this consists of a total water supply balance, i.e. the summation of water consumed (billed and unbilled authorised consumption) and not consumed (apparent and real losses) compared with the total system input volume (Lambert; 2003). District flow metering extends this to monitoring individual zones. The distribution system is subdivided into discrete zones, or district meter areas (DMA), by the permanent closure of valves. The concept of DMA management was first introduced to the UK water industry in the early 1980s, in Report26 (1980). A DMA will generally comprise 500-3000 properties. Flow (and sometimes pressure) sensors are placed on the DMA boundaries and collected data are subsequently analysed for leakage trends. The most popular operational use of the flow data is the analysis of measured minimum night flows. Night flows (usually measured between midnight and 5:00 am) are used because the water usage is at its minimum and it is easier to identify and subtract legitimate flows. Any remaining unusual changes in volumes will signify leakage in the absence of any other factors. SCADA systems are used for collecting the data. The analysis is often performed manually. If it is established that the leakage has increased sufficiently to warrant further investigation, then a manual leakage detection is carried out in the entire DMA using labour and time demanding methods like step testing, listening and leak noise correlation.

Several approaches have been described in the literature proposing a systematic analysis of the DMA flow rate data for a more efficient leak detection. In Buchberger and Nadimpalli (2004), a leak detection algorithm based on the statistical analysis of the flow rate reading is presented. Continuous high resolution (1 s sampling interval) flow rate data measured at the entry point of a DMA and the mean and standard deviation of the measured flow rate is repeatedly computed as the data set is truncated progressively from below. The truncation process is continued until the data set is reduced to zero. Derived statistics are plotted against the truncation level and compared to the standardised curve. Artificial flow rate data sets (1 hour long) were generated for a hypothetical neighbourhood containing 200 homes for cases of no

leak, constant leak and variable leak. The average water demand during this one-hour period was 0.17 L/s and the maximum flow rate value was 0.87 L/s. The constant leak had a flow rate of 0.063 L/s, which corresponds to 26% of the average flow (including the leakage itself). The variable leakage had a mean of 0.15 L/s and a standard deviation of 0.03 L/s (47% and 9% of the total flow, respectively). For all tests presented in the paper, the leak flow rate error in the case of constant leakage was less than 6 %. In the case of variable leakage, more than 85 % overlap of simulated and estimated leak flow rate intervals was observed. The proposed methodology is only suitable for leak detection and does not provide the location of the leak.

An approach described in Mounce et al. (2003) is designed for burst detection and location on a DMA level. The approach is based on analysis hydraulic parameters (flow and pressure) measured within the DMA. A neural network knowledge-based system was developed for automatic and continuous monitoring of the measured flow rate data from DMA level sensors for normal and abnormal behavior. The detection system adopts an empirical model based on pattern recognition techniques applied to time series data. Each DMA level flow sensor is modelled by one mixture density network neural network (MDN ANN), which learns to forecast the sensor output. A rule-based module performs a fusion on the ANNs' outputs to produce an overall state classification. Analysis of the pressure gradient across a DMA is also presented to measure the spatial distribution of the burst-induced pressure drop to identify the location of the failure. A set of successful tests on a real water distribution network is presented where bursts were simulated by hydrant flushing. Bursts at four different locations were simulated. The maximum burst flow rate between 5 and 7 L/s (approximately 10% of the total DMA inflow) was established over 0 to 7 minutes and maintained from 30 minutes to 5 hours for different tests. Flow rate data from two flow meters were continuously monitored with a 1 minute sampling interval. In all cases except one, burst events were detected from the flow rate measurements with a detection times varying between 23 minutes and 2.5 hours. The pressure gradient plots were generated for two burst locations and the correct identification of the burst location was indicated.

As a part of the same work, Khan et al. (2002) developed a low-cost failure sensor design. The design of sensors was based on correlation between ab-

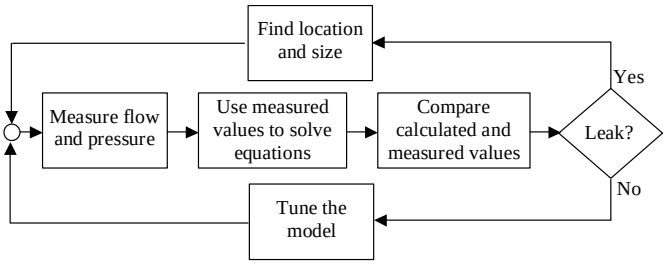

Figure 4.4: The procedure of model-based leak detection

normal flows and the opacity of the water. Sensors were placed within the DMA and measured the opacity of the water flow. Significant correlation between abnormal flows and the opacity was observed for several sensors during field trials.

4.4 Model-based leak monitoring techniques

Model-based leak monitoring techniques combine the modelling of the system with the measurement analysis.

Real-time transient model-based methods (RTTM)

Two main techniques are used for model-based leak detections: (1) deviations analysis and (2) model compensated volume balance methods.

To simulate the unsteady flow in a pipeline, the momentum and continuity equation have to be solved (Wylie; 1983). To accurately solve these equations, detailed information about pipeline and instrumentation is necessary. Parameters including length, diameter, wall thickness, roughness, wave speed, errors in measurements have to be included into the transient model. Not all of these parameters can be known precisely and therefore, a tuning process is conducted using the measurement data and assuming that there is no leak in the pipeline. The overall transient model based leak detection procedure is shown in Figure 4.4.

The transient simulation model of an intact pipeline is run in real-time. Simultaneously, real-time pressure and flow measurements are performed at

the pipeline boundaries. Using flow rate and pressure values measured at one boundary, flow rate and pressure at another boundary can be calculated and compared to the corresponding measured values. If no leak is present along the pipeline, calculated and measured values of flow rate and pressure should match. In the case of a leak, leak-induced transient waves will propagate towards the boundaries and will affect the measured values. Consequently, the discrepancy between the measured and calculated (leak-free) values will be observed, thus indicating a leak. This method is called the pressure-flow deviation method.

Normal fluctuations in the measurements can cause small deviations between modelled and measured values. Thus, threshold values are introduced to define the acceptable deviation. Usually, the deviation should exceed the threshold value at more than one point along the pipeline for a leak alarm to be issued. The size of the leak is determined based on the observed deviation in flow rate. The location of the leak can be derived by analysing the pressure deviations at different locations along the pipeline (Kiuchi; 1993), based on the timing of the sudden changes of discrepancy traces at the boundaries (Liou and Tian; 1995) or, alternatively, the leak can be simulated at multiple locations and obtained results compared to the measured data.

The main advantage of the transient model-based leak detection is the ability to detect leaks even when large transients are present in the pipeline. The detection time usually varies in the range of minutes. In addition to the leak detection, the modelling can provide other useful information about the operation of the pipeline. However, more instrumentation and information about the pipeline is required when using model-based approaches in comparison to other techniques. Another drawback of the method is the vulnerability to modelling errors.

The model compensated volume balance approach is another application of real-time transient modelling. The method is based on the real-time comparison of the measurement generated flow balances and model generated line packing rates. The packing rate is computed by the model from measured pressures and temperatures at the end points of the pipeline segment. As the model tracks the hydraulics of the pipeline, operational transients that can cause negative or positive measured flow balance will affect the modelled line packing in the same way. Only in the case of a leak, the measured flow

balance and the model generated line packing will diverge. A threshold is used to account for small deviations that are caused by measurement fluctuations. The main advantage of using a model generated packing rate is that it is not sensitive to the degree to which the model is in tune.

In Liou and Tian (1995), a transient simulation-based leak detection scheme is presented. Leaks were simulated in a 225 km long field pipeline with an outside diameter of 219 mm. The SCADA system was collecting flow rate, pressure and temperature measurements at the boundaries of the pipeline with a sampling time of 15 s. Three leaks were simulated during different operational regimes: pump shutdown, pump startup and steady-state flow. The smallest leak had a flow rate of 0.32 L/s (steady-state) and the largest leak had a flow rate of 6.41 L/s. All leaks were successfully detected. The time of detection is not given and the location of leaks is not discussed. In Fukushima et al. (2000), the implementation of a transient simulation-based leak detection system on a 250 km long natural gas pipeline is discussed. The flow and pressure are measured with 30 s sampling intervals and the simulation is performed every 5 seconds. Based on the tuning of the algorithm, 2.5 L/s leaks should be detected and located in 4 to 8 minutes. The location error is expected to be 4-20% of the total pipeline length. Not all applications of the RTTM-based monitoring systems were successful. An extremely high false alarm rate was reported in Threlfall (1999). Several reasons were identified that could prevent the system from normal operation - slow measurement update frequency (6 s), low precision of instrumentation, different fluid properties along the pipeline (30-40 different batches at the same time) and unstable operation (large number of pump-induced transients).

Liou (1996) has compared the performance of the mass-balance based and transient simulation-based leak detection systems. The test pipeline was a 869 km long, 300 mm diameter crude oil pipeline equipped with flow meters at all inflow and outflow points, as well as pressure and temperature sensors at multiple points along the pipe. The measurement sampling time of 20 s was used. Leaks with flow rates from 1 to 10 L/s were successfully detected and the detection time varied from 20 minutes (10 L/s leak) to 100 minutes (1 L/s leak). Detection times are very similar for both mass-balance and transient simulation methods. The location of leaks is not discussed.

Inverse analysis methods

Steady-state inverse analysis (IA). Leak detection and location can be accomplished by solving an inverse problem using measurements of pressure and/or flow rate. Equivalent orifice areas of possible leaks are used as unknowns. These areas are determined by minimising the difference between measured and simulated values of pressure.

In Pudar and Liggett (1992), the steady-state inverse problem was analysed. A small example network was used having 7 nodes and pipe diameters between 150 and 250 mm. Three cases were considered: (1) one leak with a diameter of 55 mm, (2) two leaks, each one with a diameter of 55 mm, and (3) two leaks with diameters of 55 mm and one leak with a diameter of 11 mm. Three possible leak locations were selected. For the overdetermined problem (the number of measurements exceeds the number of possible leaks), successful detection and location of leaks was observed. However, when the underdetermined problem was considered, the performance of the technique degraded significantly. The conclusion was made by the authors that, although the exact location of the leak is not provided in case of a smaller number of measurement points, the continuous monitoring is able to give valuable information. The main disadvantage of the inverse steady-state problem is the fact that precise estimates of the pipe roughness coefficients as well as the nodal demand are required.

Mukherjee and Narasimhan (1996) presented a model-based method to detect, locate and size leaks (single or multiple) that occur in a pipe network. The method is an adaptation of the generalised likelihood ratio (GLR) test, which utilizes flow rate and pressure measurements and a steady- state model of the network. The simulation study on a 22 node and 36 pipe (diameter 150 mm) network and the experimental study on a bench-size 6 node and 9 pipe (diameter 12.5 mm) network were used to verify the method. In the simulation study, leaks with sizes between 10 and 20 L/s were used and a success rate of 70% was observed for the single leak case. The corresponding rate for a case of 4 leaks was around 50%. The random noise with variance of 1% of the measured value was added to the nodal flow rate and pressure measurements (measured at all nodes). In the experimental study, leaks with sizes between 0.02 and 0.04 L/s were detected and located with the success

rate of 63% for a single leak case and 33% for a two-leak case. Pressure measurements were available at nodal positions. As noted by the authors, calibration of pipe friction factors in the model is absolutely necessary if real applications are considered.

In Caputo and Pelagagge (2002) an architecture of an ANN-based inverse analysis approach for monitoring network status in order to identify abnormal conditions is presented. The approach is based on flow rate and pressure measurements. The actual implementation and performance are not discussed.

Inverse transient analysis (ITA). Inverse transient analysis has been applied to the unsteady flow situation by Liggett and Chen (1994). It was proposed to solve the problem of model calibration and leak detection simultaneously. The main advantage of the inverse transient analysis (ITA) approach is that a higher sensitivity of the measured pressure to the parameters (roughness, leaks) can be achieved. Also, longer intervals of measurement data can be used for more accurate calibration of model parameters. The performance of the approach was evaluated using the same numerical example as in Pudar and Liggett (1992) and promising results were observed. Since the introduction of ITA, the method has been developed by many researchers. The main effort was put to the improvement of the mathematical part of the approach and not much has been done in terms of experimental and field validation. As a result, the ITA method has not been applied to the real network situations yet. Although some positive results for single pipelines can be found in the literature (see the review in Section 4.2), only leaks of substantial size (that could be referred to as bursts) could be detected and located.

The main problem of the ITA method is the transient modelling error. As was shown by McInnis and Karney (1995), reasonable agreement between the simulated and measured transient response traces can only be observed within the short time interval after the first transient wave arrival. The deviation between measured and simulated traces is increasing rapidly with time indicating a poor long-term transient decay representation. The same problem was further stressed by Stephens et al. (2005). Even when a short interval of data is used for ITA, the model precision may be a limiting factor when the minimum detectable leak size is considered.

In Liggett and Chen (1994), the possibility of using inverse transient analysis for on-line pipe break detection and location was briefly discussed. Sudden events that would initiate a transient wave were considered. Using the path information and travel times as calculated for the network, the origin of the transient wave can be located. Another example of on-line monitoring is discussed in Shinozuka (1999). Pipe failures caused by earthquakes or severely cold weather were considered. A neural network-based inverse analysis method was proposed for detecting the extent and location of damage based on the variation of the water pressure. The scheme is applied for idealised noise-free conditions.

State estimation (SE) approaches

A state estimator or a filter can be designed for the distributed parameter (DP) system that represents flow in pipelines. Some of the state estimation approaches do not include leak in the model (fault sensitive approaches). Since the leak is not modelled, systematic observer errors develop if a leak occurs in a real pipeline. The residual errors can be used to detect and locate the leak by assuming a linear cause/effect relationship. Another type of approaches is fault-model approaches that include the leak in the model. In Benkherouf and Allidina (1988), a method for detecting and locating leaks in gas pipelines is described that is based on modelling of multiple leaks at chosen positions along the pipeline. An extended Kalman filter (EKF), that is commonly used as a state estimator for non-linear systems, is used to estimate those leaks and relations and the size and location of the real leak can be derived from the sizes and locations of the estimated leaks. Simulated results were used to test the method. Three pressure measurements were assumed along a 90 km long, 785 mm diameter pipeline. A 4 L/s leak (2% of the nominal flow rate) was simulated. The leak was successfully detected, located and sized using the filter with the division of the pipeline into three sections. The detection time and location time was less than 140 minutes.

A multiple-model modified extended Kalman filter (MEKF) state estimation together with a dynamic feed-forward leak computation was proposed for detecting and locating leaks by Emara-Shabaik et al. (2002). Simulations were used for testing. Verde (2001, 2005) presented a multi-leak detection

system that is using a bank of unknown input observers that estimate leaks at discrete locations along the pipe. The flow rate and pressure measurements at the extremes of the duct are then used to calculate the residuals for each observer. Residuals are robust to one location of the leak and sensitive to the others. Experiments were performed on a 132 m long laboratory pipeline with a diameter of 0.1 m. The pressure and flow measurements were sampled at a frequency of 1 Hz. The pipe was divided into three sections and three Kalman filters were designed. Two cases were tested - a single leak and two simultaneous leaks. The flow rates of the leaks were approximately equal to 0.5 L/s. In both cases (single and two leaks) the sections where the leaks were present were successfully identified.

A number of state-estimation approaches for pipe networks have been presented in the literature (Andersen and Powell; 2000; Andersen et al.; 2001; Nagar and Powell; 2002). In Andersen and Powell (2000), an implicit weighted least squares (WLS) state-estimation method is outlined and its potential for leak detection and location is discussed. A numerical example with 36 nodes and 60 pipes (diameter of 150 mm) was used to illustrate the performance of the approach. Flow rate and pressure measurements were assumed at four external flow entry points. Proportional demand indicators were also assumed to be known. A leak of 10 L/s was introduced as an increase in the nodal demand. Six different leak locations were successfully identified, however, network uncertainty, measurement errors or insufficient meter coverage are not considered.

Using model-based approaches, leak detection and location is performed by correlating measured changes in hydraulic characteristics and changes in the hydraulic model of the system. The model is updated so that its predictions match the measured data. The model matching procedure is an inverse problem that often suffers from the lack of sensitivity of the hydraulic characteristics to the reasonably sized leaks. Non-unique solutions are likely to be found when the amount of available measurement data is insufficient to match the complexity of the system. Typical problems experienced while trying to solve the inverse problem are: (1) modelling errors, (2) measurement noise/errors, and (3) lack of measured data. Many model-based approaches for leak detection and location presented in the literature assume ideal noise-free conditions. In Poulakis et al. (2003), the reliability of the

results obtained from the modelling procedure is discussed. A Bayesian system identification methodology is proposed for leakage detection and location. The approach provides estimates of the most probable leak events and uncertainties of the estimates. The technique was tested on a numerical example network containing 31 nodes and 50 pipes. A single-leak and a two-leak case were investigated. Perturbations were introduced separately to pipe roughness coefficients, node demands and measurement data. Pressure and flow rate measurements were considered as two different alternatives. A total of 7 measurement points were distributed throughout the network. The analysis showed that both the uncertainty level of network parameters or measurements and the placement of measurement points have a significant influence on the leak detection and location results. These uncertainties can prohibit the successful application of model-based leak detection and location methods.

4.5 Summary of performance for different techniques

Validation results of different leak detection and location techniques that are found in the literature are summarised in Tables 4.1 and 4.2. Table 4.1 shows the results for leak inspection techniques and Table 4.2 shows the results for leak monitoring approaches for pipeline and network cases. For better evaluation of the performance, common performance indicators were chosen:

- the size of the leak;
- the leak detection time;
- the precision of the leak location (where applicable);
- the amount of measurements required (network applications).

The review above shows that the definition of the leak size varies considerably for different case studies. A number of parameters were used to define the size of the leak: (a) the diameter of the corresponding circular orifice (D_l), (b) the ratio between the cross sectional area of the leak and the cross-sectional area of the pipe (A_l/A), (c) the lumped discharge coefficient of the

leak ($C_d A_o$), (d) the discharge flow rate of the leak (Q_l), and (e) the ratio between the leak flow rate and the nominal flow rate in the pipe (Q_l/Q). To compare the performance of different leak detection techniques, a common leak size expression is necessary. The size of the leak orifice is a more general parameter than the leak flow rate, since it does not depend on the pressure in the pipeline. The orifice size can be defined by the cross-sectional area, however, using the diameter of an equivalent circular orifice (D_l) has more physical meaning. The leak size alone is not sufficient to evaluate the performance of the leak detection method. The effect of a 10 mm leak in a 50 mm diameter pipe is definitely more significant than the effect of the same size leak in a $1\,000$ mm pipe. To incorporate the size of the pipeline, the ratio D_l/D is used where D is the diameter of the pipe. The ratio D_l/D was not given in the literature for all reviewed techniques. Thus, post-processing of available data was used to derive common performance indicators. In cases when the corresponding information was not provided, a steady-state pressure of 50 m was considered and the orifice discharge coefficient $C_d = 0.75$ was used. It has to be noted that the information presented in Tables 4.1 and 4.2 are the results from case studies. In some cases, these results may not indicate the limits of the performance for the applied leak detection techniques.

Some general observations can be made before the application of the reviewed techniques can be discussed.

Leak inspection techniques

Validation results for nine different techniques are presented in Table 4.1. Twelve test cases were considered. 44% of the techniques (4 out of 9) are comercially available, while the rest are still under development. All approaches can be applied on single pipelines. However, only 3 out of the 9 techniques are suitable for application in networks. It has to be noted that the method was not considered to be applicable in the network in case when it can only be applied on a single branch of the network. Only 2 out of 5 methods that are under development were tested in the field and leaks that were detected using those methods were at least $2-3$ times larger (D_l/D) than the leaks that can be detected using available techniques. All available

Leak inspection												
Method	Reference	Application[1]						Tests[2]	D (mm)	D_l/D (%)	Q_l (L/s)	Location error (m)	Comments
		D	L	P	N	I	A						
Listening	Lange (2005)	+	-	+	+	-	+	*F*	180	1.7	0.17	n/a	Range=95m
AM	Rajtar and Muthiah (1997)	+	+	+	+	-	+	*F*	n/a	n/a	0.003	9.15	Range=61m
Correlation	Hunaidi et al. (2000)	+	+	+	+	-	+	*F*	150	0.93	0.03	<0.6	Range=103m
Pigging	Mergelas et al. (2005)	+	+	+	-	+	+	*F*	>300	<0.3	n/a	<20	Range=2000m
LRM	Jönsson (2001)	+	+	+	-	-	-	*L*	50	2.8	0.04	2.8	ΔH=45m
								F	200	10	7	100	ΔH=-30m
	Brunone (1999)	+	+	+	-	-	-	*L*	94	25	0.007	4	ΔH=10m
ITA	Covas et al. (2005)	+	+	+	-	-	-	*L*	50	5.4	0.1	5	ΔH=16m
								L	108	8	0.35	24	ΔH=8m
								F	300	4.8	3	50	ΔH=13m
	Vítkovský et al. (2001)	+	+	+	-	-	-	*L*	22.1	6.8	0.025	2.3	ΔH=20m
	Stephens et al. (2004)	+	+	+	-	-	-	*F*	94	10	1.5	n/a	ΔH=6m
TD	Wang et al. (2002)	+	+	+	-	-	-	*L*	22.1	4.52	0.01	0.38	ΔH=2m
IR	Liou (1998)	+	+	+	-	-	-	*S*	300	7.8	10	2000	ΔH=2m
FDR	Lee et al. (2005)	+	+	+	-	-	-	*S*	300	5.13	4.73	<500	ΔH=26m

[1] D - detection, L - location, P - pipeline, N - network, I - intrusive, A - available
[2] *S* - numerical simulation, *L* - lab, *F* - field

Table 4.1: Summary of available experimental and field test results for different leak inspection techniques

Pipeline monitoring

Method	Reference	D	L (1)	A	Pipeline length (km)	Sensors Q	Sensors H	Sensors Δt	Tests (2)	D (mm)	D_l/D (%)	Q_l (L/s)	Location error	Detection time
AM	Grimaud and Pascal (1991)	+	-	+	0.42	4*		n/a	*F*	1250	1.1	13.7	-	10 min
VB	Mactaggart and Myers (2000)	+	+	+	140	2	18	30 s	*F*	350	2.1	1	67 km	4 hours
PPA	Schlattman (1991)	+	+	+	130	0	3	10 s	*F*	600	2.18	3.15	65 km	10 min
SPLD	Beushausen et al. (2004)	+	+	+	353	2	33	3 s	*F*	700	3.9	14	10 km	34 min
RTTM	Fukushima et al. (2000)	+	+	+	250	2	5	30 s	*F*	n/a	n/a	2.5	10 km	4 min
SE	Benkherouf and Allidina (1988)	+	+	-	90	0	3	33 s	*S*	785	1.87	4	0	140 min
SA	Wang et al. (1993)	+	+	-	0.12	0	4	20 ms	*L*	10	n/a	n/a	n/a	15 s
NPW	Silva et al. (1996)	+	+	-	1.248	0	4	0.5 ms	*F*	100	8.6	0.63	5 m	0

Network monitoring

Method	Reference	D	L (1)	A	Network size	Sensors Q	Sensors H	Tests (2)	D (mm)	D_l/D (%)	Q_l (L/s)	Location error	Comments
AM	Sánchez et al. (2005)	+	+	+	75km of mains	460*		*F*	n/a	n/a	0.067	n/a	49 leaks found in 6 months
IA	Pudar and Liggett (1992)	+	+	-	7nodes	3	3	*S*	200	5.5	1.7	0	1-3 leaks
ITA	Liggett and Chen (1994)	+	+	-	7nodes	0	5	*S*	200	1.8	n/a	0	Noise-free case
GLR	Mukherjee and Narasimhan (1996)	+	+	-	6nodes	0	6	*L*	12.5	n/a	0.02	3%	1-2 leaks
SE	Andersen and Powell (2000)	+	+	-	36nodes	4	4	*S*	150	15.5	10	0	Noise-free case
BSI	Poulakis et al. (2003)	+	+	-	31nodes	7 or 7		*S*	300	11.6	22.8	0	Uncertainty analysis
SA	Buchberger and Nadimpalli (2004)	+	-	-	200 homes	1	0	*S*	n/a	n/a	0.063	-	Detection only
SF	Mounce et al. (2003)	+	+	-	DMA	2	17	*F*	150	7.3	5	n/a	$t_{detection}$ = 0.4-2.5 hours

(1) D - detection, L - location, A - available (2) *S* - numerical simulation, *L* - lab, *F* - field * listening units

Table 4.2: Summary of available experimental and field test results for different leak monitoring techniques

techniques, except pigging (the only intrusive method), have quite a short range, i.e. are labour-intensive. Available inspection techniques have mainly been applied in water pipelines and networks.

Leak monitoring techniques

A total of sixteen presented monitoring methods are equally divided between pipeline and network applications. However, only 1 out of 8 network approaches is commercially available, whereas 63% of pipeline leak monitoring techniques are applied in the field. This situation can be explained by the fact that most of the existing leak monitoring applications are implemented in oil or gas transmission pipelines. The instrumentation level of oil and gas pipelines is fairly high and the monitoring techniques used in these pipelines require more measurements. Due to the high risk assosiated with failure of oil or gas pipelines, monitoring approaches are chosen. Acoustic monitoring is the only available approach for the network case. It requires a large number of sensors and therefore is labour intensive.

4.6 Application in water supply systems

It is extremely difficult to find one leak detection and location technique that would have the best performance in all cases. There is a number of aspects that have to be considered before making conclusions regarding the performance of a particular method. It is clear that the main parameter that is used as a performance indicator is the cost-benefit ratio. However, evaluation of the cost and the benefit is not that straightforward. First of all, limitations may apply to the maximum allowable cost in the water industry. On the contrary to the oil and gas industries, large investments cannot be made by water utilities. At the same time, evaluation of the benefit of using one or another leak detection technique is not a simple process. Very limited practical experiences of using different techniques can be found. Some general conclusions can be made from the review of available techniques presented in this chapter:

1. Since leak inspection techniques are labour intensive, leak inspections are not frequently performed. This results in long leak detection and location times.
2. To achieve a quick response to a leak, continuous monitoring is necessary.
3. Most of available monitoring techniques can only be applied on single pipelines and, in some cases, single branches of the network.
4. Monitoring of every single branch in a network is financially infeasible.
5. Available pipeline monitoring approaches require the pipeline to be well instrumented.
6. Failure location capabilities have to be improved in both pipelines and networks.

Considerable differences exist between water transmission pipelines and distribution networks in terms of the topology and hydraulics, the regime of operation as well as types and consequences of failure. The differences are also reflected in the choice of failure detection and location techniques. The overall conclusion is that failure monitoring techniques have to be developed separately for pipeline and network applications. As discussed in Chapter 2, the cost-benefit ratio of failure detection depends on the cost of failure. Medium and large pipe breaks (bursts) present the highest risk and have the most expensive consequences out of all types of pipe failures observed in the water supply systems. With system getting older, the frequency of these failures is increasing. The techniques that are currently used in the water industry are not suitable for quick reaction to pipe bursts. Thus, the following directions have been formulated for the work on failure detection and location in pipelines and pipe networks presented in this thesis:

- medium and large bursts are the primary target;
- continuous monitoring or periodical diagnosis;
- low installation and maintenance costs;

- automatic analysis.

Automatic techniques that have been developed for the pipeline failure monitoring, detection and location are presented in the second part of this thesis. Automatic techniques that have been developed for the network failure monitoring, detection and location are presented in the third part of the thesis.

Part II

Automatic failure monitoring, detection and location in pipelines

---

Summary: *Losses associated with a pipeline failure can be reduced considerably if a failure detection and location time is minimal. Examples form the oil and gas industries show that a continuous monitoring is an effective tool for a quick reaction to the failure. However, the available pipeline monitoring systems that are reviewed in Chapter 4 have a high cost and cannot be installed on water transmission pipelines. Existing leak inspection methods (review in in Chapter 4) are either time and labour consuming or are only able to detect large leaks.*

Part II of this thesis describes two techniques for a pipeline failure management. The first method, presented in Chapter 5, is used for a periodical leak diagnosis and is based on the hydraulic transient response difference monitoring. The second approach, described in Chapter 6, is a pipeline burst monitoring system based on the continuous monitoring of the pressure for a burst-induced transient wave. A successful validation results on the laboratory and field pipelines are presented. Chapter 7 discusses the performance, application and implementation of the proposed techniques.

Related publications: *Part of the work has been presented in Misiunas et al. (2003), Misiunas et al. (2005e) and Misiunas et al. (2005b).*

Chapter 5

Periodical leak diagnosis

As was stated in Chapter 4, the performance of existing transient based leak detection and location techniques can be considerably enhanced by resolving model error-related problems. In this chapter, a periodical leak diagnosis system is presented that can be implemented on water transmission pipelines. The technique is based on the transient response difference monitoring. The approach does not use the transient model and therefore does not suffer from model-related problems observed while applying earlier methods. The technique is presented using test results from the real water transmission pipeline. The method is also shown to be effective for detecting and locating air pockets and blockages. More extensive discussion of the performance, implementation and application of the proposed technique can be found in Chapter 7.

5.1 Modelling limitations when applying transient-based leak detection and location techniques

In Figure 5.1, the transient response pressure traces from a real pipeline are shown. Parameters of the pipeline will be presented later in this chapter. The transient was artificially generated by a sudden closure of the side-discharge valve and the response was measured for no leak and leak situations. Approximately 15 L/s leak was created artificially by opening a fire hydrant.

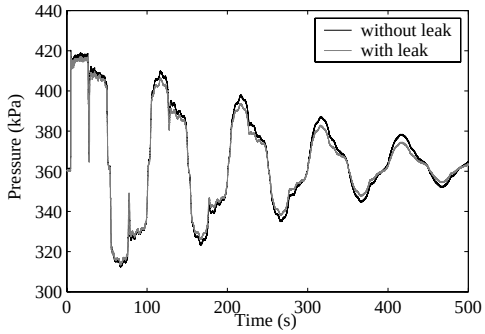

Figure 5.1: The comparison of pressure traces with and without leakage

Two well-researched transient-based leak detection and location methods, the leak reflection method (LRM) and the inverse transient analysis (ITA), have been applied to detect the leak. These methods were reviewed in Chapter 4. To detect the leak and to derive its location, both LRM and ITA methods rely on the information that is concentrated mainly within the data window that corresponds to the first period of the transient wave ($4L/a$) starting from the first rise of the pressure in the measured trace. In fact, LRM only uses the data window from the first transient wave arrival to the arrival of its reflections from the boundaries ($2L/a$). An example of such window is shown in Figure 5.2.

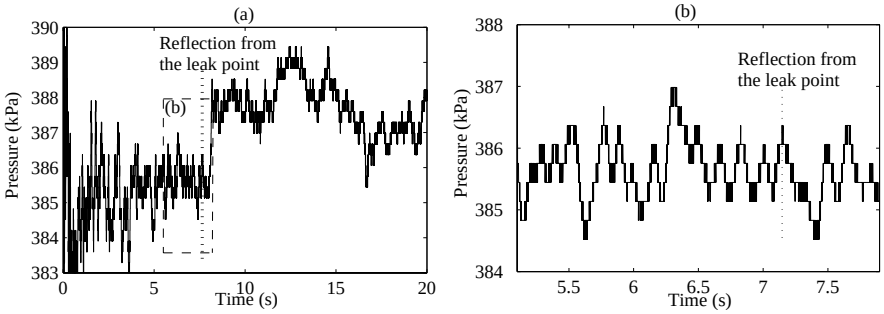

Figure 5.2: (a) Measured pressure response for a leak case with the vertical line indicating the reflection from the leak and (b) a closer view of the part of the trace showing the reflection from the leak

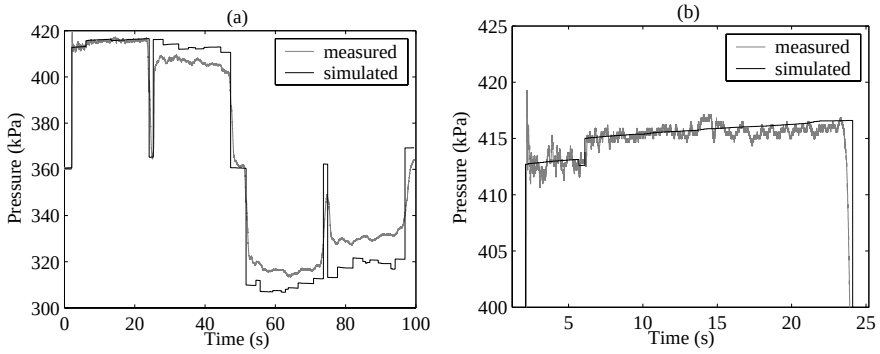

Figure 5.3: The comparison of simulated and measured traces with a leak

Traditionally, the LRM approach was based on timing of the transient wave reflection from the leak observed on the measured traces. From Figure 5.2 it is clear that the task becomes very difficult when a real pipeline is considered. The vertical dashed line indicates the time instance that corresponds to the actual location of the leak. It is unlikely that the reflection from the leak can be identified visually or by using data analysis techniques. The LRM method is designed assuming that the measured pressure trace in between the first rise and the reflection from the boundary will have a flat profile. In that case, the reflection of the generated wave from the leak point will cause a noticeable change on the measured trace. In the real pipeline, high frequency oscillations are present on the trace (Figure 5.2). Those oscillations is a composition of the measurement noise and reflections from different elements of the pipeline. Any change of the physical properties of the pipe will cause a reflection of the transient wave as it propagates along the length of the pipeline. Many of these reflections have similar character as the reflection from the leak, which makes the detection of the latter difficult and sometimes even impossible as demonstrated in Figure 5.2.

The ITA approach is based on minimizing the difference between measured and simulated traces. The leak is placed at different location in the model and the simulation results are compared to the actual measurement. An example is shown in Figure 5.3, where the leak is simulated at the actual location and the obtained trace is compared to the measured one.

Simulated leak location (m)	Objective function	
	Long data window	Short data window
9656	42885	370.2783
11886	44633	361.5068
12076	44749	331.5617
12266	44856	360.6017
13026	45313	361.6719
13406	44380	361.5416

Table 5.1: Results of the IT analysis

The length of the data window length that is used for inverse fitting is a subject of choice. In Figure 5.3, a data data window with a length of one pipeline period ($4L/a$) is shown. The agreement between measured and simulated data is really poor. Figure 5.3b shows a shorter data window that includes data prior to the arrival of the transient wave reflections from the boundaries. The fit between measured and simulated traces is slightly better. The leak was simulated at six different locations, including the actual leak point. The square root of the sum of squared differences between the measured and simulated traces for all samples was used as the objective function. Results of the IT analysis are summarised in Table 5.1.

The discrepancy between the simulated and measured responses is large for all tested leak locations as indicated by large values of the calculated objective function. To compare the results of the objective function for different leak locations, derived values were normalized applying the division by the optimal (minimum) objective function. The distribution of the normalized objective function at different points along the pipeline for both short and long data windows is shown in Figure 5.4.

The leak simulated closest to the the actual leak location did not have the best fit when using both short and longer data windows. Actually, the difference between the outputs of the objective function for all three leak locations that were tested was less than 5%. The location having the best fit was 155 m away from the actual leak location when the shorter data window was used and $4\,130$ m away from the actual leak location when the longer data window was used. As already mentioned, the error in the results is mainly due to lack of information about the physical state of the pipeline or, in other words,

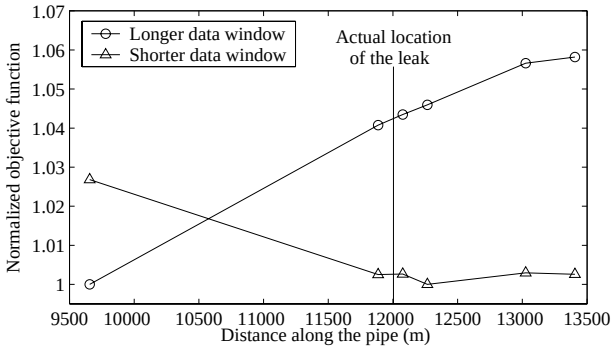

Figure 5.4: Distribution of the normalized objective function for different locations along the pipeline

the low quality of the model. Increasing the complexity of the model might provide a better agreement between modeled and measured traces. However, often detailed information about the physical structure of the pipeline is not available. In cases when a more precise model of the system can be built, longer computational times are required. Higher computing power demands might become an issue due to the fact that the ITA method requires a large number of simulations.

There are two possible solutions to the problem described above. The first solution, as already suggested, is to increase the complexity and, consequently the precision, of the model. This is a rather difficult task. Alternatively, the methods have to be modified so that modelling is not required. In the following section, a leak detection and location approach that eliminates the influence of the modelling error is described.

5.2 Methodology

The fundamental principle of the proposed methodology is the assumption that leak diagnosis will be performed periodically. Leakage detection is considered to be a repetitive procedure that is a part of the active failure monitoring system, which is permanently installed on the pipeline. The initial pressure trace, i.e. the trace measured directly after the installation of the

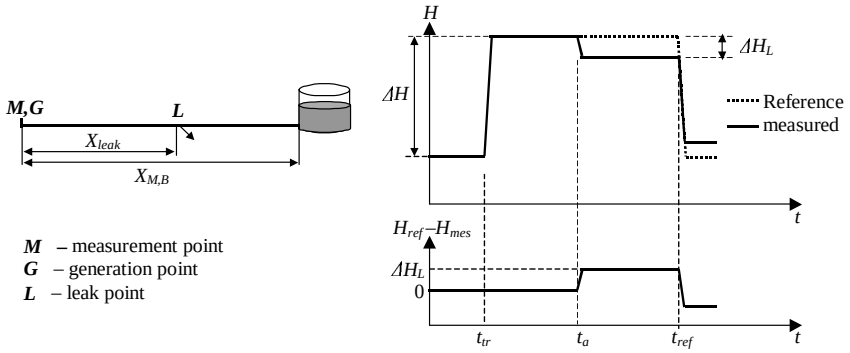

Figure 5.5: Difference between the reference and measured pressure traces caused by reflection from the leak point

monitoring system, is considered to be leak-free and represents the transient response of the intact pipeline. This trace is used as a reference for the consequitive tests, substituting the modelled trace. Relative changes in the transient pressure response are used to detect and locate pipeline abnormalities. Any discrepancies between the last measured transient response and the reference trace are attributed to a change of the pipeline's physical properties, i.e. leakage. Figure 5.5 illustrates the way the proposed technique works.

A pipeline running between a dead-end and a tank is considered as an example. The transient is generated at point G and the pressure is measured at point M (Figure 5.5). Both G and M are placed at the dead-end boundary of the pipeline. The leak, L, is located along the pipe at a distance X_{leak} away from the measurement and generation point. Figure 5.5 also shows generalised pressure traces for leak-free and leak situations (upper plot) and the difference between the two traces (lower plot). The traces are adjusted to compensate for the difference in steady-state pressure ($H_{noleak} - H_{leak} = 0$ for $t < t_{tr}$).

To locate the leak, the classical theory of LRM is used. The transient wave is artificially generated at time t_{tr} and propagates along the pipeline. When the wave reaches the leak, part of it is reflected. The size of the reflection, ΔH_L, depends on the size of the leak, the size of the generated transient and frictional effects in the pipeline. When the reflection from the leak

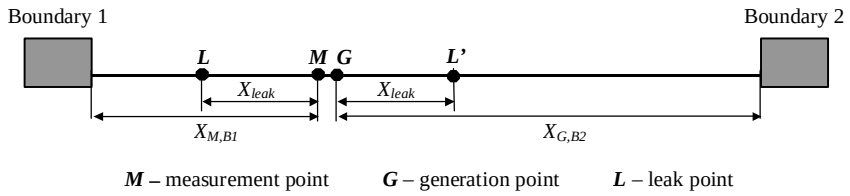

Figure 5.6: Two possible locations of the leak

reaches the measurement point it will affect the difference between the reference trace and the measured trace. The time instance t_a when the difference $|H_{noleak} - H_{leak}|$ becomes greater than zero is used to derive the location of the leak:

$$X_{leak} = \frac{a(t_a - t_{tr})}{2} \tag{5.1}$$

Modifications for transmission pipelines

The measurement and generation setup shown in Figure 5.5 represents the ideal case. In reality, it might not be possible to generate the transient and measure the pressure at the dead-end boundary. It is preferable that the operation of the pipeline is not interrupted by the leak detection procedure. Furthermore, in some cases the generation and measurement equipment might have to be installed separately, at two different locations along the pipeline. Figure 5.6 shows the case where the generator and the measurement station are installed at different points along the pipeline.

The measured pressure trace will look similar to the one in Figure 5.5. The time t_{tr} will correspond to the arrival of the generated transient wave at the measurement station. The time of change in the difference $H_{noleak} - H_{leak}$ will correspond to the arrival of the transient wave reflection from the leak at the measurement station. Using t_{tr} and t_a, the distance X_{leak} can be calculated using Equation 5.1. However, since the transient generation point is placed along the pipeline, two waves will be generated and will propagate in opposite directions from the generation point. Thus, as indicated in Figure 5.6, there will be two possible locations of the leak: (a) location L, distance X_{leak} away from the transient generation point in the direction of boundary 2

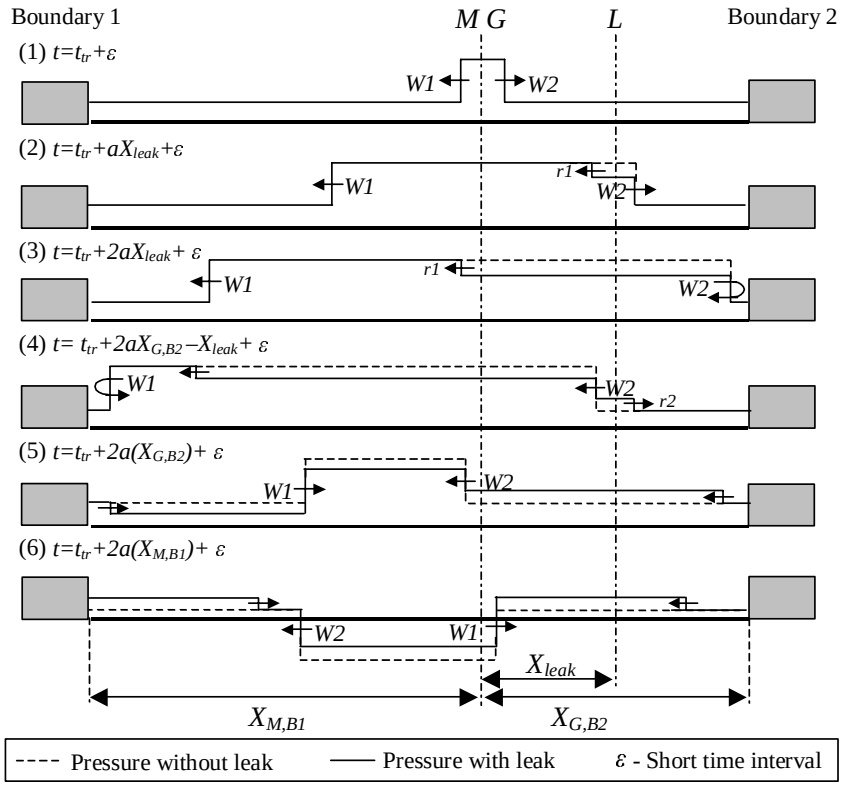

Figure 5.7: Transient wave propagation and refletions from leak and pipeline boundaries

or (b) location L', distance X_{leak} away from the measurement point in the direction of boundary 1. The timing of the transient reflection from the leak does not provide enough information to identify whether L or L' is the actual location of the leak.

The actual location of the leak can be identified from the analysis of transient wave reflections from the boundaries of the pipeline. In Figure 5.7, the transient wave propagation and its reflections from the leak and from pipeline boundaries are shown in sequential steps. The pipeline system from Figure 5.5 is considered and the leak is assumed to be located at L. Pressure profiles are shown for cases when there is no leak and when the leak is present at L.

The transient generation and pressure measurement are assumed to be placed at the same point. To better visualise the pressure changes at the measurement point, pressure distributions are shown a short time interval (ϵ) after different waves have passed the measurement point. The following sequence of events can be identified:

1. At time t_{tr} two transient waves ($W1$ and $W2$) are generated at point G and propagates in both directions along the pipe

2. At time $t_{tr} + aX_{leak}$ the wave $W2$ is partially reflected at the leak. The magnitude of the reflection $r1$ is equal to ΔH_L.

3. At time $t_{tr} + 2aX_{leak}$ reflection $r1$ reaches the measurement point. At this time instance, the difference between the pressure for no-leak and leak cases, i.e. $H_{noleak} - H_{leak}$, becomes equal to ΔH (neglecting frictional effects).

4. The wave $W2$ reaches the boundary at the time $t_{tr} + aX_{G,B2}$ and is reflected from it. The reflection depends on the reflection coefficient of the pipeline boundary P_{B2}. At time $t_{tr} + 2aX_{G,B2} - X_{leak}$ the reflected wave reaches the leak point and a part of it is reflected ($r2$). The reflected $r2$ will have a magnitude slightly smaller than ΔH_L.

5. At time $t_{tr} + 2aX_{G,B2}$, the remaining part of $W2$ reaches the measurement point. Due to reflections $r1$ and $r2$ the change in the difference $H_{noleak} - H_{leak}$ is observed at the time $t_{tr} + 2aX_{G,B2}$. The size of the change is approximately equal to $P_{B2}(r1 + r2)$.

6. Since there is no leak between the measurement point and boundary 1, the wave $W1$ reaches the measurement point at time $t_{tr} + 2aX_{M,B1}$ (after it was reflected from the boundary) with the same magnitude as for the no-leak case. Thus, the arrival of $W2$ has no effect on the difference $H_{noleak} - H_{leak}$.

The following conclusions can be made after the sequence presented above is analysed: assuming that the leak is located between the measurement/generation point and one of the boundaries, the actual location of the leak can be identified by observing the effect of the transient wave reflections from the

boundaries on the difference $H_{noleak} - H_{leak}$. If the reflection of the boundary causes the change in $H_{noleak} - H_{leak}$, the leak is located between the measurement/generation point and that boundary. The window of the data that is necessary to find the location of the leak starts from t_{tr} and has a length equal to

$$2\max(X_{M,B1}, X_{G,B2})/a$$

Alternatively, a transient model of the system can be used to simulate the leak at both L and L'. The simulated traces can then be subtracted from the simulated no-leak trace and the resulting differences compared to the difference between measured traces.

Size of a leak

The size of the leak can be defined using the lumped orifice discharge parameter C_dA_o. The coefficient C_d is an orifice discharge coefficient and A_o is the cross-sectional area of the orifice. An approximate value of C_dA_o can be estimated using the magnitude of the transient wave reflection from the leak point as derived in Appendix E:

$$C_dA_o = \frac{2gA\ |\Delta H_L|}{a\sqrt{2gH_0}\left(\sqrt{1+\frac{\Delta H}{H_0}-\frac{|\Delta H_L|}{H_0}}-1\right)} \tag{5.2}$$

where
C_dA_o	=	lumped orifice discharge parameters
g	=	gravitational constant
A	=	pipe cross-sectional area
a	=	wave speed of the pipe
H_0	=	steady-state head
ΔH	=	magnitude of the generated transient wave
ΔH_L	=	magnitude of the reflection from the leak

5.3 Placement of measurement and generation points

The analysis presented in the previous sections can be used to derive basic guidelines for the placement of transient generation and measurement points:

1) The generation and measurement points should be placed as close to each other as possible. If the leak occurs in between the measurement and generation points, the location of it becomes more complicated. The generated transient wave is reflected from the leak before it reaches the measurement point. This means that the reflection of a generated wave from the leak is no longer detected in the measured trace. Only the change in difference $H_{noleak} - H_{leak}$ that occurs upon arrival of the reflections from the pipeline boundaries can be used to detect and locate the leak.

2) It is beneficial to have both generation and measurement points at the dead-end boundary of the pipeline. There are two main benefits of such a setup: (i) both the generated wave and its reflection from the leak will be magnified two times due to the immediate reflection from the dead-end boundary and (b) there will be only one possible leak location corresponding to the distance $a(t_a - t_{tr})/2$ at all times. It is likely that most pipelines will not have a permanent dead-end as one of the boundaries. Since the leak diagnosis is performed periodically at selected time instances, the dead-end boundary can be artificially created for the time of the procedure. It could be a check valve of a pump that is not running or a valve that is closed during the time of the leak diagnosis procedure. At all other times the pipeline can be kept in its normal operational state.

3) In case generation and measurement points cannot be located at the dead-end boundary, the leak will have two possible locations only in case when

$$t_a - t_{tr} < 2\min(X_{M,B1}, X_{G,B2})/a$$

This suggests that placing measurement and generation points close to the boundary will increase the probability of only one possible location of a leak. On the other hand, to reduce the effect of friction, it is desired that the measurement point is as close to the leak as possible. To minimise the distance from the measurement station to the leak for all possible leak locations, the measurement point has to be placed not far from the middle point of the

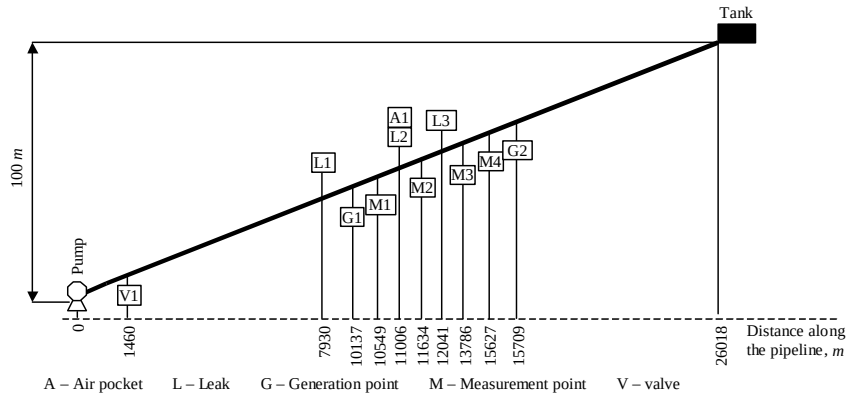

Figure 5.8: Layout of the test pipeline

pipeline. However, to avoid the simultaneous arrival of reflections from the boundaries to the measurement point, placement at the middle point is not recommended. The setup of transient generation and measurement points has to be designed specifically for a particular pipeline. The guidelines listed above should be considered along with the physical parameters of the pipeline to find the optimal solution.

5.4 Validation on a field pipeline

The proposed leakage detection and location technique was tested on a large water transmission pipeline. The layout of the pipeline is shown in Figure 5.8. A $26\,018$ m long mild-steel concrete-lined (MSCL) pipeline has a diameter of 750 mm and an experimentally estimated wave speed of 950 m/s. At the downstream end there are two storage tanks and on the upstream end there is a treatment plant and a pumping station. For all tests presented in this chapter, inline valve (V1 Figure 5.8) was used as an upstream boundary. The transient was artificially generated by fast closure (around 10 ms) of the side-discharge valve mounted on a scour valve. Two sizes of the side-discharge valve nozzle were used - 40 mm and 50 mm. The pressure was measured at the sampling rate of $2\,000$ Hz and the resolution of the pressure measurement was 0.049 kPa. More information about the test equipment and procedure can be found in Appendix A.

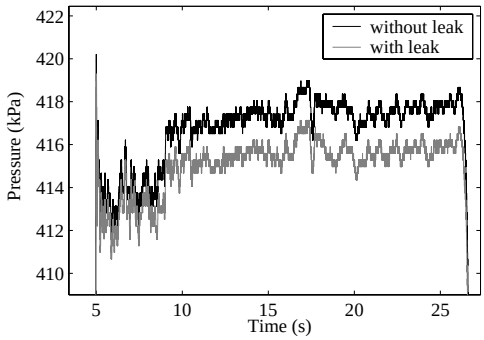

Figure 5.9: Comparison of pressure traces measured at M3 with and without leakage

The performance of the proposed method was tested for single and a multiple leak cases. Additionally, the capability of detecting and locating an air pocket and blockage was explored.

Single leak

The proposed methodology was first tested for a single leak case. Two pressure traces were measured. In the first trace, which was to be used as a reference trace, the transient response of the intact pipeline was recorded. The transient was generated at position G2 (Figure 5.8) using a closure of the side-discharge valve with a diameter of 50 mm. In the second trace, the same transient was generated with a leak (approximately 15 L/s) opened at position L3 (Figure 5.8). The diameter of the leak orifice was around 30 mm (4% of the pipe diameter). The pressure was measured at position M3. Figure 5.9 shows the comparison of data windows for no leak and leak cases. The data window corresponds to the time interval between the first transient wave arrival to the measurement station and the arrival of its reflections from the boundaries. The change in difference between the two traces in Figure 5.9 indicates the presence of a leak. The actual difference between measured pressures can be analysed to get a better resolution as shown in Figure 5.10.

Measured data was pre-processed for better visual presentation. A steady-state pressure baseline was subtracted from the measured traces and data

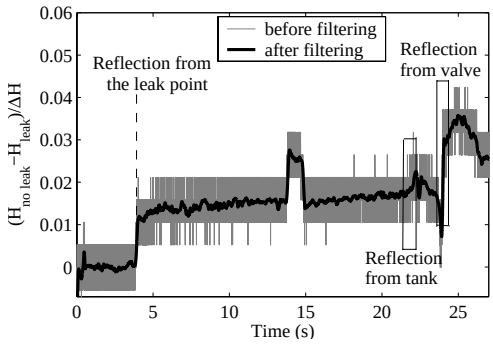

Figure 5.10: Difference between pressure without leak and with leak. Measurements at M3.

was normalised by the magnitude of the generated transient. However, these procedures are not essential, since leaks are detected from changes of the difference between pressures rather than the absolute value of the difference. A Butterworth low-pass filter with a cutoff frequency of 5 Hz was applied to reduce the measurement noise as shown in Figure 5.10.

The first positive change in difference between measured pressures at around 3 s indicates the reflection from the leak point. An important feature of the change in the difference between measured traces, which is caused by the reflection from the leak, is that is remains unchanged until the reflection from the boundaries arrive to the measurement point. In other words, if, after the change, the value of $H_{noleak} - H_{leak}$ goes back to what is was before the change, the change was not caused by the leak. As an example, the first positive change (around 3 s) in the trace in Figure 5.10 changes the value of $(H_{noleak} - H_{leak})/\Delta H$ from 0 to approximately 0.012 and the difference between measured traces does not change back to zero. This indicates that the change at around 3 s was caused by the reflection from the leak. Meanwhile, the positive change at around 13 s is followed by a negative change of the same size (at around 15 s) which shows that this change is not induced by the reflection of the leak. This change was caused accidentally when the side discharge valve that was used to generate the transient was slightly opened and closed within two seconds. Although the discharge through the valve was very small, its effect is obvious.

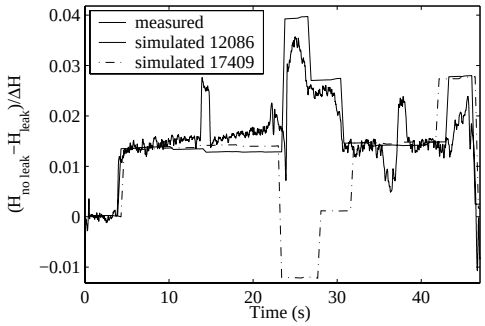

Figure 5.11: Differences between leak and no leak cases derived for two candidate leak locations using simulation results and compared to the measured (filtered) one

As explained in Section 5.2, there are two possible locations of the leak (see Figure 5.6). The reflection in Figure 5.10 can be coming from $12\,086$ m or from $17\,409$ m along the pipeline. To identify the actual location of the leak, the effect of reflections from boundaries on the difference $H_{noleak} - H_{leak}$ is analysed. As indicated in Figure 5.10, no substantial change in $H_{noleak} - H_{leak}$ is observed at the time corresponding to the arrival of the reflection from the tank. Thus, the conclusion can be made that the leak is located between the measurement station and the valve, i.e. at $12\,086$ m along the pipeline. To provide additional confirmation, the time that corresponds to the arrival of the reflection from the valve is indicated on the trace in Figure 5.10.

There is an obvious change in difference $H_{noleak} - H_{leak}$ at that point, which confirms that the leak is at $12\,086$ m along the pipeline. An alternative approach of identifying which out of the two possible leak locations is the actual one was also tested. The leak was simulated at both possible locations ($12\,086$ m and $17\,409$ m) using a hydraulic transient simulation model based on the method of characteristics (MOC) (Wylie and Streeter; 1993). The implementation of the model is described in Chapter B. Differences between the two cases and the simulated leak-free case were compared to the difference between measured and reference traces. The comparison is shown in Figure 5.11.

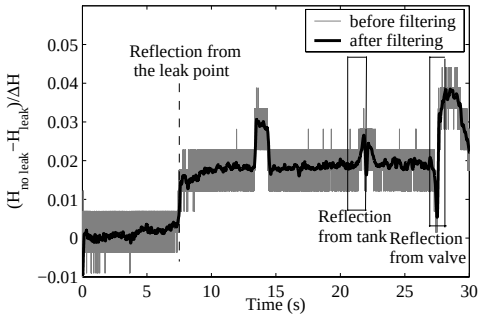

Figure 5.12: Difference between pressure without leak and with leak. Measurements at M4.

Results of a leak simulated at $12\,086$ m along the pipeline match the difference between measured traces better indicating that the reflection coming from $12\,086$ m represents the leak. The actual location of the leak was at $12\,041$ m and the error of the location estimated by the technique is 45 m.

For the second test, the same transient generation point and the same leak location were used. The pressure was measured at M4. The difference between the measured trace and the reference (leak-free) trace is shown in Figure 5.12.

The change in difference between measured pressures indicates that the reflection from the leak point is coming from $12\,082$ m or from $19\,254$ m. The true location of the leak can be identified in the same way as for the previous case. The actual location of the leak is at $12\,041$ m and the error of the estimated location is 41 m.

Using two measurement locations can give a direct estimate of the true leak location. Two possible locations of the leak are estimated for each measurement point. If two measurement points are used, two out of four calculated locations should coincide (or be close) indicating the actual location of the leak. If measurements at M3 and M4 are considered, locations at $12\,086$ and $17\,409$ m were estimated from measurements taken at M3, and locations at $12\,082$ and $19\,254$ m were found from measurements at M4. It is clear that $12\,086$ m (M3) and $12\,082$ m (M4) are indicating the same point. The average of 12084 m can be used to define the real location of the leak.

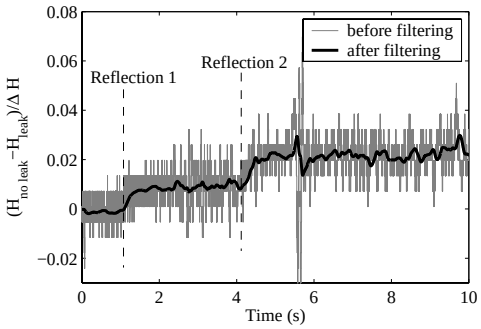

Figure 5.13: The difference between measured pressure traces for no leak and two-leaks cases

Multiple leaks

The technique was also tested for the case of multiple leaks. The transient was generated at G1, the pressure was measured at M1 and two leaks were present at L1 (approximately 8 L/s) and L2 (approximately 15 L/s). The changes in difference between measured pressures shown in Figure 5.13 indicate the reflection from leak points. Reflection 1 is coming from $9\,631$ m or from $11\,077$ m. Reflection 2 is coming from $8\,124$ m or from $12\,483$ m. The same principles as for the single leak case were used to identify the actual leak locations. The data window was extended to include the reflections from pipeline boundaries as shown in Figure 5.14.

Changes in the difference $H_{noleak} - H_{leak}$ that can be observed on the trace in Figure 5.14 indicate that the leaks are located on both sides of the generation/measurement point. Based on the size of the change in the difference between reference and measured traces, the exact locations of the two leaks can be found. Since the change in $H_{noleak} - H_{leak}$ caused by the reflection from the tank is smaller than the change caused by the reflection from the valve, the conclusion was made that the smaller leak was located between the measurement point and the tank, i.e. at $11\,077$ m along the pipeline and the larger leak was located at $8\,124$ m along the pipeline. The actual locations of the leaks were at $11\,006$ m and $7\,930$ m, respectively. The errors were 71 m and 194 m.

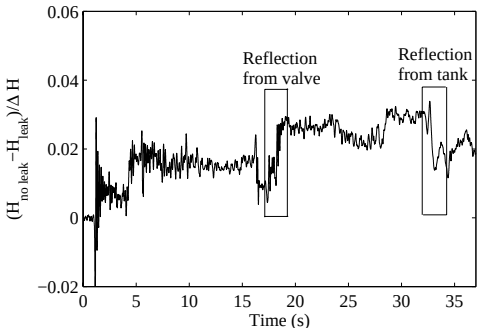

Figure 5.14: Longer data window including reflections from pipeline boundaries that are used to identify leak locations

Test No.	1	2	3	4
Leak location (m)	12041(L3)	12041(L3)	12041(L3)	7930(L1) and 11006(L2)
Measurement at	M3	M4	M3 and M4	M1
Generator	G2	G2	G2	G1
Estimated leak location (m)	12086	12082	12084	8124(L1) 11077(L2)
Leak location error (m)	45	41	43	194(L1) 71(L2)
ΔH(m)	5.62	5.52	5.57	4.55
ΔH_L(m)	0.0924	0.0919	0.0922	0.0615(L1) 0.03(L2)
$\Delta H_L/\Delta H$	0.0164	0.0167	0.0166	0.0135(L1) 0.0066(L2)
$C_d A_o$(m^2)	$4.52{\cdot}10^{-4}$	$4.58{\cdot}10^{-4}$	$4.56{\cdot}10^{-4}$	$4.52{\cdot}10^{-4}$(L1) $2.02{\cdot}10^{-4}$(L2)
D_l/D(%)	3.69	3.72	3.71	3.69(L1) 2.47(L2)
Q_L(L/s)	13.4	13.6	13.5	16.6(L1) 6.8(L2)

Table 5.2: Summary of leak detection and location tests and results

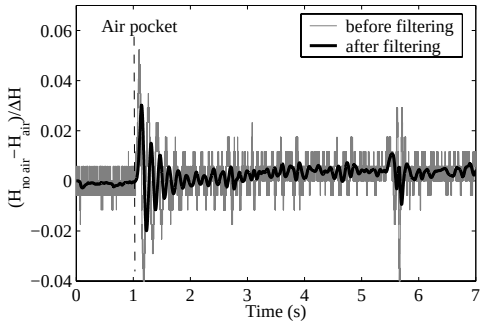

Figure 5.15: Difference between measured pressure traces for no air and air pocket cases

5.5 Extension of the methodology for other hydraulic faults

The leakage detection technique described in this chapter can be applied for detecting other hydraulic faults, such as blockage or entrapped air pocket. As an example, results of the detection and location of (1) air pocket and (2) blockage are presented in this section.

Air pockets

In the addition to leaks, the approach was also tested for entrapped air. An air chamber was attached to the fireplug at location A1, the transient wave was generated at G1 and the pressure was measured at M1 (Figure 5.8). The measured trace was compared to the reference air-free trace and the difference between the two traces is shown in Figure 5.15.

The difference between an air pocket and air-free traces in Figure 5.15 contains an oscillation that indicates an air pocket in the pipeline. The reflection is coming from $9\,655$ m or $11\,053$ m along the pipeline. By using the model or having two measurement locations, the actual location of the air pocket can be identified. The true location of the air pocket is $11\,006$ m and the error of the estimate is 47 m.

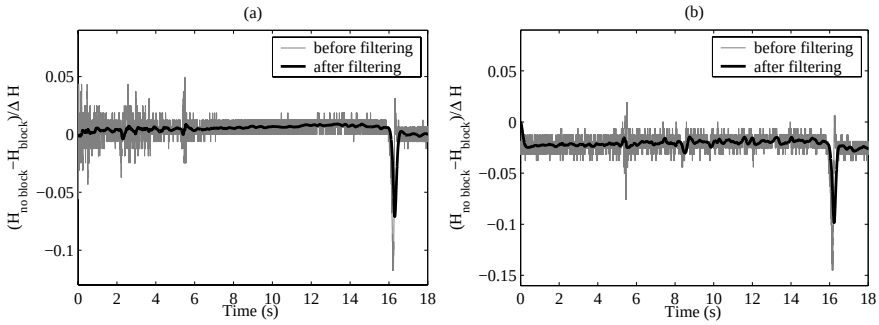

Figure 5.16: Difference between measured pressure traces without blockage and with blockage. The measurement was taken at (a) M1 and (b) M2.

Blockage

The last set of tests was performed to test the ability of the proposed technique to detect partial blockage in a pipeline. To simulate blockage, the inline valve V1 (Figure 5.8) was closed and the bypass of the valve with a diameter of 250 mm was open. The difference between measured pressure traces without blockage (valve open and bypass closed) and with blockage (valve closed and bypass open) are shown in Figure 5.16.

The pressure was measured at two stations - M1 and M2 (see Figure 5.8 for positions). As shown in Figure 5.16, the spike (around 16 s) is present in the pressure difference trace for both measurement stations. According to the traces measured at M1, the spike indicates a reflection that is coming from $1\,457$ m or $19\,229$ m along the pipeline. From the traces measured at M2, the reflection is coming from $1\,518$ or $20\,253$ m along the pipeline. One of the two alternative locations is common for both stations ($1\,458$ and $1\,518$) and the blockage location was selected to be at the middle point between the two estimates, i.e. 1487.5 m along the pipeline. The actual blockage was at $1\,460$ m along the pipeline. The technique was able to determine the location of the blockage with an error of 27.5 m.

Further discussion on the performance, implementation and application of the proposed transient response difference monitoring approach is presented

in Chapter 7 in conjunction with the discussion of the automatic failure monitoring, detection and location technique described in Chapter 6.

Chapter 6

Burst monitoring, detection and location

In this chapter, an automatic pipe failure monitoring, detection and location technique is presented. The approach is based on the continuous monitoring of pressure for sudden failure-induced transients. A sudden failure can also be referred to as a burst and the latter term will be used throughout this chapter. The proposed algorithm uses a single pressure measurement point to detect and locate pipeline bursts of medium and large sizes. Results of a successful validation in a laboratory pipeline, a single branch of a distribution network and a large transmission pipeline are presented. Further discussion on the performance, implementation and application of the technique can be found in Chapter 7.

6.1 Burst location based on wave timing

Location of a burst in a pipeline can be determined based on timing of the burst-induced pressure transient wave reflections from the pipeline boundaries. When a sudden rupture of a pipe wall or other element in the pipeline occurs, the resulting burst flow generates a negative pressure drop. This negative pressure drop initiates two pressure transient waves that propagate in both directions away from the burst location. Eventually, both waves reach

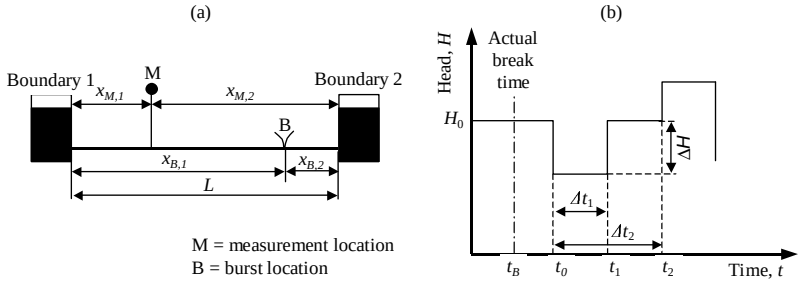

Figure 6.1: The example pipeline system and the generalised pipe burst transient for the example pipeline system

the boundaries of the pipeline and are reflected. Timing of the reflections depends on the location of the burst relative to the positions of the boundaries. The travel times of the transient waves can be found using a pressure measurement sampled at high frequency at one point along the pipeline. Consider the simplified example pipeline in Figure 6.1a where a burst occurs at point B and the pressure is measured at point M. Distances $x_{B,1}$ and $x_{B,2}$ are the distances from the burst point to the boundaries 1 and 2, respectively, and $x_{M,1}$ and $x_{M,2}$ are the distances from the measurement point to boundaries 1 and 2, respectively. Figure 6.1b shows the generalized burst-induced transient pressure trace measured at point M. The propagation of a burst induced transient wave can be explained using the following time sequence:

$t < t_B$: Before the burst event the pressure along the pipeline is equal to the steady-state pressure.

$t = t_B$: The burst even occurs at point B and a sudden decrease in pressure is generated at the burst point B.

$t_B < t < t_0$: Two negative pressure waves are travelling in both directions along the pipeline away from burst point B. The pressure at the measurement point M is still equal to the steady-state pressure.

$t = t_0$: The first wave reaches (travelling to the left from B) the measurement point M causing a negative change in the measured pressure trace. Meanwhile the second wave (travelling to the right from B) is reflected from Boundary 2, changes direction and propagates towards

M. Since Boundary 2 is a reservoir, the sign of the second wave is inverted.

$t_0 < t < t_1$: Both waves continue travelling along the pipeline. Eventually, the first wave reaches Boundary 1 and is reflected. Since Boundary 1 is a reservoir, the sign of the first wave is inverted.

$t = t_1$: The second wave reaches the measurement point M causing a positive change in the measured pressure trace.

$t_1 < t < t_2$: The first wave, reflected from Boundary 1 is approaching M.

$t = t_2$: The first wave reaches measurement point M causing a positive change in the measured pressure trace.

The sequence of wave reflections continues until the transient wave magnitude is equal to zero. The wave is dampened. For the burst detection and location, the time interval $[t_B : t_2]$ is of the main interest.

The magnitude of the burst-induced transient wave, ΔH, will depend on the size of a burst and the sign and magnitude of transient pressure changes at t_1 and t_2 will depend on the reflection characteristics of the pipeline boundaries. As already noted, the timing of the changes in the transient trace (t_0, t_1 and t_2 in Figure 6.1b) depends on the position of the burst. If the example trace is considered, the position of the burst can be estimated from time differences $\Delta t_1 = (t_1 - t_0)$ and $\Delta t_2 = (t_2 - t_0)$. If the distance from the burst to the closest boundary $\min(x_{B,1}, x_{B,2})$ is shorter than the distance from the measurement point to the closest boundary $\min(x_{M,1}, x_{M,2})$, the time difference Δt_1 will correspond to $\min(x_{B,1}, x_{B,2})$. The time difference Δt_2 in this case will be proportional to the distance from the measurement point to the other boundary (not necessary the closest one). Alternatively, if $\min(x_{B,1}, x_{B,2}) > \min(x_{M,1}, x_{M,2})$ the time difference Δt_1 will correspond to $\min(x_{M,1}, x_{M,2})$. Since $x_{M,1}$ and $x_{M,2}$ are known, Δt_1 and Δt_2 can be determined from the measured pressure trace. The times associated with the measurement point location with respect to both boundaries are derived from:

$$\begin{aligned} t_{M,1} &= \frac{2x_{M,1}}{a} \\ t_{M,2} &= \frac{2x_{M,2}}{a} \end{aligned} \tag{6.1}$$

where a is the wave speed of the pipe, $t_{M,1}$ is the time required for a transient wave to travel from the measurement point to boundary 1 and back, and $t_{M,2}$ is the time required for the transient wave to travel from the measurement point to boundary 2 and back. The following rules can then be used to determine the burst position:

$$\begin{aligned}
&\text{if} \quad \Delta t_1 = t_{M,1} \qquad \text{then} \qquad x_{B,2} = \frac{a\Delta t_2}{2} \\
&\text{if} \quad \Delta t_1 = t_{M,2} \qquad \text{then} \qquad x_{B,1} = \frac{a\Delta t_2}{2} \\
&\text{if} \quad \Delta t_2 = t_{M,1} \qquad \text{then} \qquad x_{B,2} = \frac{a\Delta t_1}{2} \\
&\text{if} \quad \Delta t_2 = t_{M,2} \qquad \text{then} \qquad x_{B,1} = \frac{a\Delta t_1}{2}
\end{aligned} \tag{6.2}$$

where $x_{B,1}$ and $x_{B,2}$ are the distances from the burst point to boundary 1 and boundary 2, respectively. Since, in many cases, the precise value of the wave speed of the pipeline is not known, an error will be introduced when the burst position is calculated. To reduce this error, the wave speed can be eliminated. The rules in Equation 6.2 then become:

$$\begin{aligned}
&\text{if} \quad \Delta t_1 = t_{M,1} \qquad \text{then} \qquad x_{B,2} = \frac{x_{M,1}\Delta t_2}{\Delta t_1} \\
&\text{if} \quad \Delta t_1 = t_{M,2} \qquad \text{then} \qquad x_{B,1} = \frac{x_{M,2}\Delta t_2}{\Delta t_1} \\
&\text{if} \quad \Delta t_2 = t_{M,1} \qquad \text{then} \qquad x_{B,2} = \frac{x_{M,1}\Delta t_1}{\Delta t_2} \\
&\text{if} \quad \Delta t_2 = t_{M,2} \qquad \text{then} \qquad x_{B,1} = \frac{x_{M,2}\Delta t_1}{\Delta t_2}
\end{aligned} \tag{6.3}$$

Due to the uncertainty of the wave speed estimate and detected pressure change times t_0, t_1 and t_2, conditions in Equation 6.3 may not hold exactly. Thus, the case having the best fit should be used to determine the burst location.

6.2 Size of burst

The lumped orifice discharge parameter $C_d A_o$ can be used to define the size of a burst. Coefficient C_d is an orifice discharge coefficient and A_o is the

cross-sectional area of the orifice. An approximate value of $C_d A_o$ can be determined from the magnitude of the burst-induced pressure wave (ΔH in Figure 6.1b) using the Joukowsky pressure rise formula (adjusted for a side discharge situation) combined with the orifice equation (see Appendix D for derivation). From the method of characteristics analysis (Wylie and Streeter; 1993) the flow rate downstream from the burst point after the burst has occurred is equal to $Q_0 - 0.5Q_B$, where Q_0 is the initial flow in the pipeline and Q_B is the flow rate through the burst orifice. The flow rate upstream from the burst point is $Q_0 + 0.5Q_B$. After applying Joukowsky's pressure rise formula ($\Delta H = -(aQ_B)/(2gA)$) and substituting into general orifice equation $Q_B = C_d A_o(2g(H_0 - |\Delta H| - z))^{1/2}$ the burst size estimate is:

$$C_d A_0 = \frac{A|\Delta H|\sqrt{2g}}{a\sqrt{H_0 - |\Delta H| - z}} \tag{6.4}$$

where ΔH = head change due to the burst
H_0 = initial system head
A = pipe cross-sectional area
$C_d A_0$ = lumped orifice discharge parameter
g = gravitational constant
z = elevation

After the burst position is determined using the rules in Equation 6.3 and the size of the burst is estimated from Equation 6.4, the obtained parameters can be confirmed by simulating a burst of the estimated size at the derived position using a transient model (Appendix B) and comparing the model results with the measured data.

6.3 Burst detection and location system

The proposed continuous burst monitoring algorithm is illustrated in Figure 6.2. Since the method is based on analysis of transients induced by a burst, the pressure in the pipeline has to be continuously monitored at a high sampling frequency. To reduce the burst detection time, the measured pressure is analysed on-line. In the case when the negative change in pressure induced by a burst is detected, data necessary for burst location is stored and

analysed off-line. The continuous burst monitoring algorithm can be divided into three parts: (1) continuous monitoring of measured pressure for a burst event, (2) gathering of the data window necessary to estimate burst parameters, and (3) analysis of the gathered data and burst parameter estimation.

Monitoring for a burst event

In the first part of the burst monitoring algorithm, the measured pressure trace is continuously monitored for the burst event. In case of a burst, a negative change in the measured pressure trace is expected (ΔH in Figure 6.1). Figure 6.1 shows the ideal burst pressure trace when the instantaneous burst opening (the time from the start of the burst event to the moment when the maximum flow through the burst orifice is established) is assumed. In reality, the opening time can vary considerably for different bursts. The assumption is made that the burst flow develops linearly. The opening time of the burst will affect the slope of the burst-induced transient wave front. The magnitude of the wave front depends on the size of the burst. The on-line cumulative sum (CUSUM) test (Basseville and Nikiforov; 1993; Page; 1954) can be used to analyse the measured pressure trace and detect changes. Since the pressure measurement from the real system can contain a considerable amount of noise, the data is pre-filtered using an adaptive Recursive Least Squares (RLS) filter. The filter estimates the signal θ_t from the measurement y_t (containing noise) as:

$$\theta_t = \lambda\theta_{t-1} + (1-\lambda)\, y_t \tag{6.5}$$

where $\lambda[0,1)$ is the forgetting factor. The value of the forgetting factor limits the smoothing effect of the filter. The noise suppression of the filtering increases with increasing values of λ. Residuals $\epsilon_t = \theta_t - \theta_{t-1}$ are fed into the CUSUM test algorithm to determine whether a change has occurred. Mathematically, the CUSUM test is formulated as the following time recursion:

$$\begin{aligned} &S_0 = 0 \\ &S_t = \max\left(S_{t-1} - \epsilon_t - \nu, 0\right) \\ &\text{if } S_t > h \text{ then issue the alarm and set } t_a = t,\ S_t = 0 \end{aligned} \tag{6.6}$$

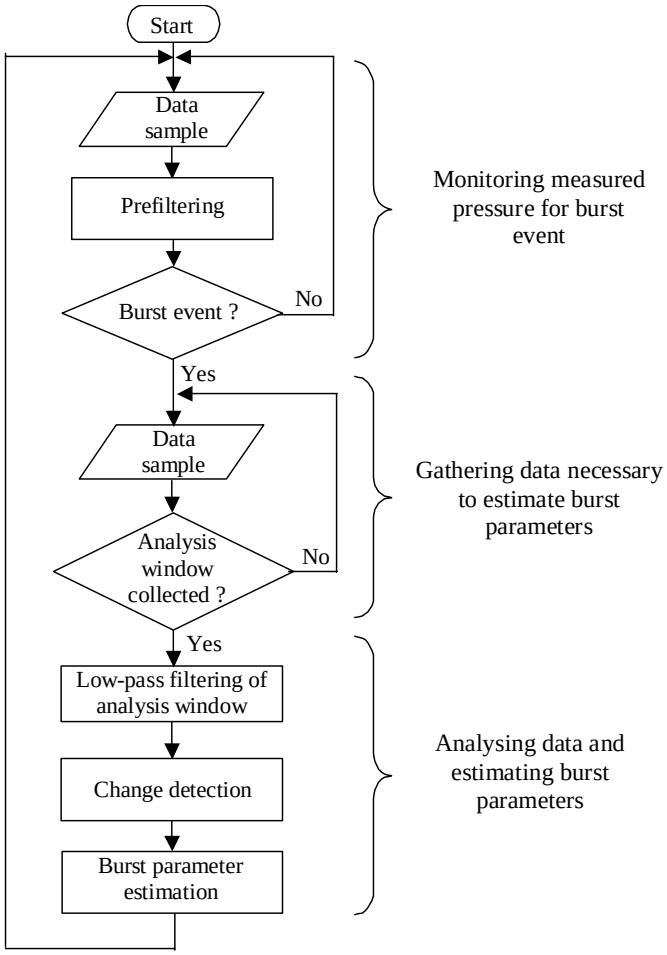

Figure 6.2: Continuous burst monitoring algorithm structure

where S_0 is the cumulative sum value at the start of the test, S_t and S_{t-1} are the cumulative sum values at the current and previous time steps, h and ν are threshold and drift parameters, respectively. For every sample of data, the part of the change in signal ϵ_t that exceeds the drift value (the expected variation) is added to the cumulative sum S_t. When S_t reaches the threshold value h, the alarm is issued and the time of change t_a is recorded. The algorithm then resets S_t to zero. The formulation of the CUSUM test used for burst monitoring (Equation 6.6) detects only negative changes in the measured pressure trace.

The performance of the CUSUM change test is controlled by two parameters - threshold h and drift ν. Since the size and the opening time of the burst are not known prior to the burst event the shape and the magnitude of the burst-induced change in the measured pressure cannot be predicted. Therefore CUSUM test parameters have to be tuned for as wide range of bursts as possible. For a given set of CUSUM parameters, the minimum size of the change in pressure that will be detected, ΔH_{min}, and the longest opening time of the burst that will be detected, $t_{opening,max}$, can be calculated:

$$\Delta H_{min} = h + \frac{\nu t_{opening}}{\Delta t} \tag{6.7}$$

$$t_{opening,max} = \frac{\Delta H - h}{\nu} \Delta t \tag{6.8}$$

where Δt is the sampling interval of the pressure measurement. The minimum size of the burst that will be detected can be calculated by putting ΔH_{min} into Equation 6.4. Equations 6.7 and 6.8 indicate that successful detection depends on the combination of both size and opening time of the burst. Smaller values of drift and threshold will extend the range of detectable burst sizes and opening times. However, the success rate of the technique is not the only performance indicator. Another important factor is the false alarm rate. False alarms can be caused by oscillations in the pressure measurements that are the result of measurement noise of legitimate hydraulic activity in the system. Both the level of measurement noise and typical operational changes in pressure can be evaluated from historical data. The combination of h and ν has to be chosen so that the rate of false alarms is minimised.

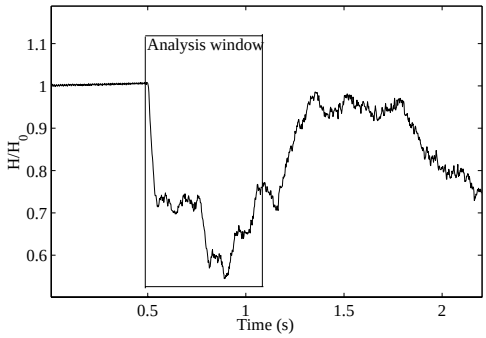

Figure 6.3: Example of measured burst transient pressure trace

Analysis window

After the burst-induced negative change in the measured pressure is detected and the time of the change, t_a, is set, a window of the data (not filtered with the RLS filter) is collected for further analysis. The analysis window has to contain an amount of data, which is sufficient for deriving the location of the burst. In other words, the changes in pressure caused by the initial transient wave induced by the burst and its reflections from both boundaries of the pipeline have to be within the window. The length of the analysis window is set to be proportional to the maximum distance from the measurement point to the boundary, defined as

$$t_W = \frac{2\max\left(x_{M,1}, x_{M,2}\right)}{a} \tag{6.9}$$

where t_W is the analysis window length in time units. To identify the timing of all changes in the data, including the one induced by the first arrival of the burst wave, the wider data window $[t_a - \varepsilon : t_a + t_W]$ is used, where ε is the short interval of data preceding t_a. An example of analysis window selection is shown in Figure 6.3. A more conservative approach would be to use $t_W = 2L/a$.

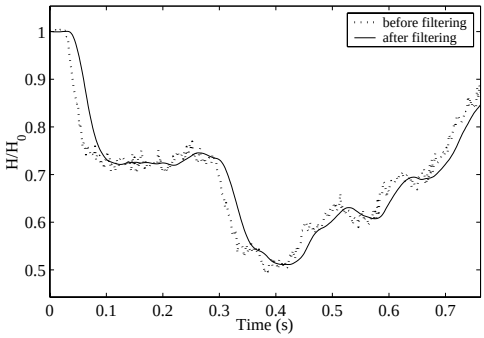

Figure 6.4: Example of analysis window and the effect of filtering

Filtering and change detection

Further analysis of the data window is performed offline. To remove the high frequency noise, the data is filtered using a Butterworth low-pass filter. An example of analysis window selection is shown in Figure 6.3 and the effect of filtering is illustrated in Figure 6.4. It may be observed that the filtering introduces a certain time lag. This time lag has no influence on the results of burst detection and location, since the burst position is proportional to the difference between time instances t_0, t_1 and t_2 (Figure 6.1) and not the absolute time (the time lag introduced by the filter is the same for t_0, t_1 and t_2). After filtering, the change detection is performed. Three time instances (t_0, t_1 and t_2 in Figure 6.1) have to be identified. The pressure trace in Figure 6.1 is valid for instantaneous bursts; however, in reality the burst occurs over some finite time.

An example of the experimental pressure trace is shown in Figure 6.5. The burst flow develops from zero to its maximum value over a time period from t_1 to t_2. As a result, the front of the burst-induced transient wave in the pressure measurement will have a slope, $\Delta H/(t_2 - t_1)$, corresponding to the burst flow development profile. The measured pressure trace can be divided into two states: (1) steady state, and (2) transient state. In Figure 6.5, the steady state corresponds to the time intervals $[t < t_1]$, $[t_2 < t < t_3]$, $[t_4 < t < 5]$ and $[t > t_6]$, whereas the transient state corresponds to the time intervals $[t_1 < t < t_2]$, $[t_3 < t < t_4]$ and $[t_5 < t < t_6]$. The transitions

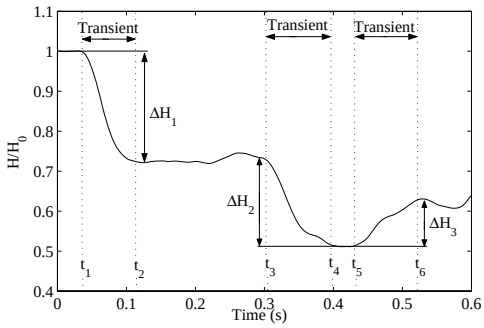

Figure 6.5: Division of analysis window. Vertical lines indicate changes between states.

from steady state to transient state are detected by means of the two-sided CUSUM test (Equation 6.10). Using a two-sided test, both positive and negative changes in the measured signal are detected.

$$
\begin{aligned}
&S_0^1 = 0 \text{ and } S_0^2 = 0 \\
&S_t^1 = \max\left(S_{t-1}^1 + \epsilon_t - \nu, 0\right) \text{ and } S_t^2 = \max\left(S_{t-1}^2 - \epsilon_t - \nu, 0\right) \\
&\text{if } \left(S_t^1 > h \text{ or } S_t^2 > h\right) \text{ then issue the alarm and set} \\
&t_a = t,\ S_t^1 = S_t^2 = 0
\end{aligned}
\tag{6.10}
$$

To illustrate how these times are found, Figure 6.6 shows the generalized burst-induced pressure transient trace measured at the measurement point together with the variations of the positive cumulative sum S^1 and negative cumulative sum S^2 from Equation 6.10. Alarm times t_{a1}, t_{a2} and t_{a3} do not correctly indicate arrivals of the burst-induced transient wave and its reflections. As stated in Skalak (1956) and evident from experimental data, the transient wave front gradually disperses over a finite length as the wave propagates along the pipeline. The delay between the actual wave front arrival and the time when it is detected as reflections from boundaries ($t_{a2} - t_3$ and $t_{a3} - t_5$) is therefore likely to be longer than the corresponding delay for the first wave ($t_{a1} - t_1$). For better precision in the burst location estimate, times t_1, t_3 and t_5 should be used. The gradient of the cumulative sum S can be used to identify the time of the wave front arrival. As shown in Figure 6.6, dS/dt becomes greater than zero when the change in pressure

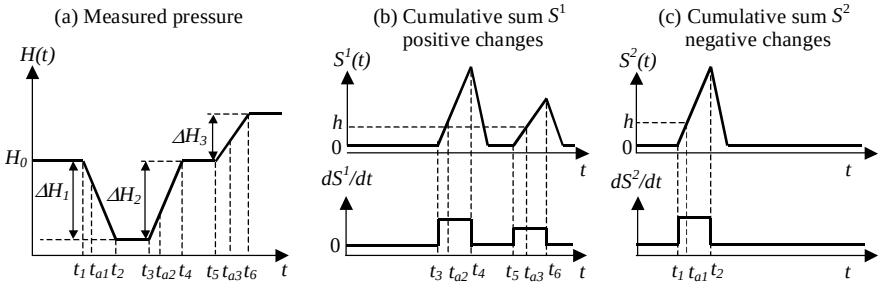

Figure 6.6: Generalised trace of pressure, cumulative sums and gradients of cumulative sums for a two-sided CUSUM test

(transient state) starts and becomes equal or less than zero when the transient stage is finished. This rule is introduced into the CUSUM test to find times t_1, t_3 and t_5 and the burst opening time $t_2 - t_1$.

Adaptive parameter tuning

For better performance of the change detection algorithm, an adaptive tuning of the threshold and drift parameters is implemented. The initial values of threshold (h) and drift (ν) that were chosen in the monitoring part of the algorithm are used to detect the first change in the pressure trace (ΔH_1 in Figure 6.5). As the noise is filtered out from the pressure measurement, the initial drift value (ν) is no longer equal to the noise bandwidth of the filtered signal. The initial value of ν was set to 20% of h. After the first change has occurred and the magnitude of the change is identified (ΔH_1), the threshold and drift values are tuned to detect reflections of the burst-induced wave from the boundaries ΔH_2 and ΔH_3. The main purpose of parameter tuning is to prevent the technique from detecting smaller changes in pressure trace, such as reflections of the transient wave from physical elements in the pipeline, pressure oscillations caused by demand changes, etc. The drift is adjusted to account for the dispersion of the transient wave front that was discussed earlier in this section:

$$\nu_{tuned} = C_1 \nu \tag{6.11}$$

where C_1 is a coefficient describing the dispersion of the wave front with a value between 0 and 1. C_1 is selected arbitrary or based on historical data.

For most pipelines it should be close to 1. The threshold, h, is adjusted based on the magnitude of the already detected change ΔH_1. Since the boundaries of the pipeline are known, the smallest magnitude of the reflection that has to be detected can be derived:

$$\Delta H_{ref} = \min\left(\Delta H_1 P_1, \Delta H_1 P_2\right) \tag{6.12}$$

where ΔH_{ref} is the magnitude of the smaller reflection from pipeline boundaries. Coefficients P_1 and P_2 are wave reflection coefficients for boundaries 1 and 2, respectively, and can be derived using the method of characteristics (Wylie and Streeter; 1993) as shown in Appendix C. An uncertainty of ΔH_{ref} is introduced by neglecting the frictional effects while calculating coefficients P_1 and P_2. The adjusted threshold value can be derived using the following expression:

$$h_{tuned} = C_2 \left(\Delta H_{ref} - \frac{\nu(t_{f0} - t_0)}{\Delta t}\right) \tag{6.13}$$

The time $t_{f0} - t_0$ defines the burst opening time as shown in Figure 6.5 and C_2 is a coefficient that compensates neglecting frictional effects while deriving P_1 and P_2. C_2 should have a value close to 1. Tuned CUSUM test parameters ν_{tuned} and h_{tuned} are used to detect reflections from the pipeline boundaries ΔH_2 and ΔH_3.

After all three changes in the measured pressure trace are detected and the time differences $\Delta t_1 = (t_1 - t_0)$ and $\Delta t_2 = (t_2 - t_0)$ are calculated, the burst position may be derived according to the rules in Equation 6.3. The size of the burst is then estimated from Equation 6.4. To increase the confidence, the burst with estimated parameters can be simulated and simulation results compared with the measured trace. The transient simulation model based on the MOC is described in Appendix B. Once the burst is located, the section of the pipeline that contains the burst can be isolated and then repaired.

6.4 Limitations and considerations

There are a number of issues that influence the performance of the continuous monitoring technique for pipeline burst detection and location. The

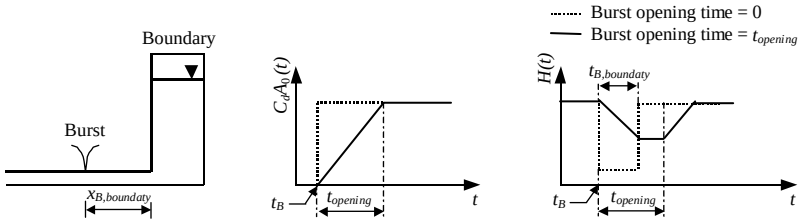

(a) Burst near boundary (b) Burst opening profile (c) Head response at burst point

Figure 6.7: Occurrence of a burst near a pipeline boundary

situations addressed in this section are (1) occurrence of bursts near boundaries, (2) speed of burst opening, (3) measurement position, (4) false alarms caused by normal pipeline operation and (5) pipeline bursts resulting from transients induced by normal operation of the system.

Burst near boundary. When a burst occurs near the boundary of the pipeline, the burst size estimate may contain an error. The situation is illustrated using Figure 6.7. The burst is located at a distance $x_{B,boundary}$ from the reservoir, which is one of the most common boundaries for transmission mains. When the burst occurs, a negative transient wave is generated. Since the burst orifice size is increasing continuously for a time $t_{opening}$ starting from time t_B as shown in Figure 6.7b, the transient wave is also generated continuously. That is evident in the measured pressure trace - the slope of the wave front is inversely proportional to the opening time of the burst. The time required for the burst-induced wave to travel from the burst point to the boundary and back $t_{B,boundary}$ is equal to

$$t_{B,boundary} = \frac{2x_{B,boundary}}{a} \tag{6.14}$$

The transient wave generated immediately after t_B will propagate to the boundary and be reflected. The reflection coefficient P of a reservoir is equal to -1 which means that the wave will be reflected with the same magnitude and the opposite sign. The reflection of the wave will reach the burst point at time $t_B + t_{B,boundary}$. If the burst opening time $t_{opening}$ is greater than $t_{B,boundary}$, an interaction will occur between the wave that is generated by the burst and reflected wave. This interaction will affect the measured pressure trace as shown in Figure 6.7c. The pressure traces for an instantaneous

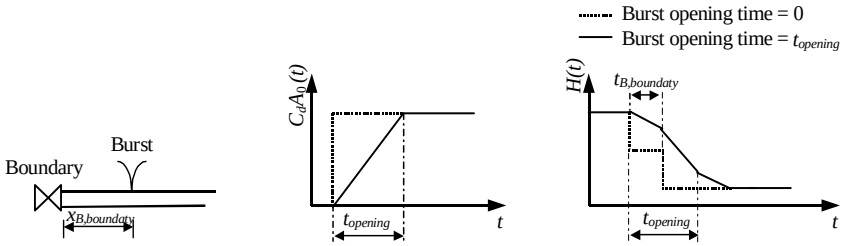

(a) Burst near dead-end (b) Burst opening profile (c) Head response at burst point

Figure 6.8: Occurrence of a burst near a pipeline boundary

burst ($t_{opening} = 0$) and a burst with $t_{opening} > t_{B,boundary}$ are compared. In the case when $t_{opening} > t_{B,boundary}$ the magnitude of the transient wave and the timing of the reflection from the boundary that are found from the measured trace are incorrect. Thus, the derived location and the size of the burst will contain an error.

If the burst occurs near the dead-end of a fully closed valve, the measured pressure trace will look slightly different. Figure 6.8 is an equivalent of Figure 6.7 for a dead-end boundary. Since the dead-end boundary has a reflection coefficient P equal to 1, the wave will be reflected with the same sign and magnitude. Thus, the measured change in pressure will have two times larger magnitude than the burst-induced wave. It is also likely that the arrival time of the reflection from the boundary could not be detected from the measured trace.

Speed of burst opening. As stated earlier in this section, correct burst parameters will not be found if the burst opening time is greater than the time required for a burst wave to travel to the closest boundary and back. It is likely that slow bursts with $t_{opening} >> 2x_{B,boundary}/a$ might be detected but not located. Depending on the burst opening time, the length of pipeline sections adjacent to the boundaries where the burst will not be located correctly, can be calculated. The length of these sections depends on the burst opening time and can be derived using the following expression:

$$x_{B,boundary} = \frac{t_{opening} a}{2} \tag{6.15}$$

It has to be noted that $x_{B.boundary}$ does not depend on the length of the pipe-

line. If the technique is implemented on a long pipeline, the probability of the burst occurring in the region within $x_{B.boundary}$ away from the boundary is quite low.

Measurement position. The choice of the measurement position is an important issue that can be the source of error in the burst position. An example of such an error is Test 8 in Section 6.6. The problem arises when the burst and measurement positions are symmetrical with respect to the boundaries ($x_{M,1} = x_{B,2}$). In this case, after being reflected from the boundaries, waves induced by a burst reach the measurement point at the same (or almost the same) time. In such a situation, the waves interact and it is not possible to identify their exact arrival times to the measurement site. This causes an error in the burst position estimate. In the case when another measurement position was used, the correct location of the burst can be found. Thus, a separate analysis has to be performed in order to find the position of the measurement that would minimise the probability of such an error. Another potential problem results from taking the pressure measurement at the centre of the pipeline ($x_{M,1} = x_{M,2}$) when both boundaries have the same reflection characteristics. In this case, the arrival times of the pressure reflections coincide making determination of the true burst location difficult. If one of the pipeline boundaries is a dead-end or a fully closed valve, it might be beneficial to place the measurement station at that boundary. Since the dead-end boundary has a reflection coefficient $P = 1$, the burst-induced transient wave measured at the dead-end will be magnified twice. However, all pressure oscillations caused by demand changes and other activities in the pipeline will also be magnified at the dead-end.

False alarms caused by normal operation. Pressure transients caused by normal operation of the system have a potential to cause false alarms from the pipeline burst detection technique. Pressure transients initiated by a pump shutdown, a valve operation or a sudden increase in demand can initiate pressure transients similar to the ones induced by the burst. The location of where the transient originated will still be derived by the technique. The false alarms can be quickly assessed as to whether the derived location and the timing correspond to a particular operation - pump shutdown, valve opening, etc. The pressure transients caused by a sudden variation in demand are most likely to be associated with industrial consumers with known location

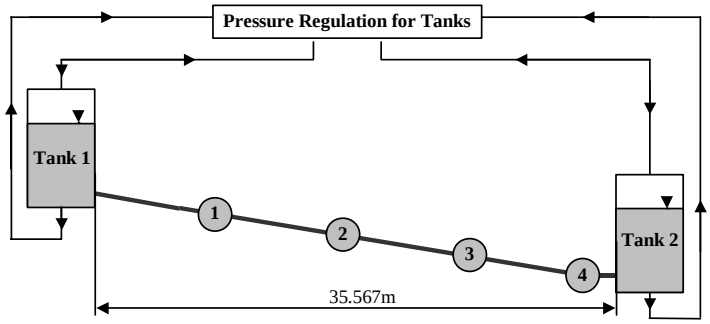

Figure 6.9: Layout of the laboratory experimental apparatus

and, in some cases, operation times. Thus, false alarms could be dismissed based on the transient source location derived by the burst detection technique.

Bursts resulting from transients induced by normal operation of the system. In certain situations, a pipeline burst can occur during a pressure transient that is a part of the normal operation of the system. A common example is pump switching. When the pump is turned on or off, a pressure transient is generated. Detection and location of a burst that is caused by pump switching requires special analysis. A transient model of the pipeline can be used to predict the expected pressure variation during a transient initiated by pump operation. The simulated trace can then be compared with the measured trace. The discrepancy between predicted and actual pressure traces would indicate a burst event.

6.5 Laboratory validation

To validate the proposed technique under controlled conditions, the continuous monitoring technique for burst detection was tested in a laboratory pipeline shown in Figure 6.9. The laboratory pipeline and testing procedure are described in more detail in Appendix A. The laboratory apparatus comprises a 37.53 m long copper pipeline with diameter of 22.1 mm and wave speed of $1\,327$ m/s. An initial flow in the pipeline was generated by a head dif-

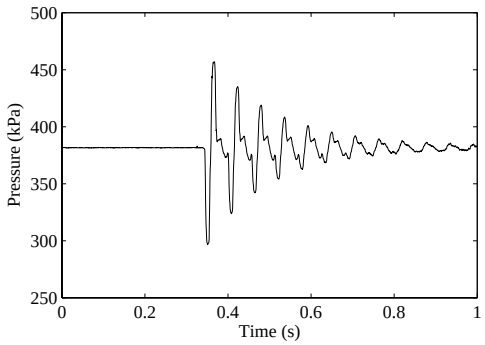

Figure 6.10: An example of the measured trace (test 3)

ference between two computer-controlled pressurised tanks. The burst was simulated using a fast-opening (opening time of 4 ms). Additionally, a manually actuated side-discharge valve was used for simulating bursts with longer opening times. A pressure was measured with a sampling rate of $2\,000$ Hz.

Tests 1 to 4 consider a fast-opening burst located at various positions along the pipeline. The burst positions were at 0.1784, 0.4985, 0.7476, and 0.9936 (expressed as a fraction of the total pipeline length) along the pipeline for Tests 1 to 4, respectively. These positions correspond to points 1 to 4 in Figure 6.9. The pressure was measured at 0.1784 along the pipeline (point 1 in Figure 6.9). The calibrated size of the burst in each case was $C_d A_o = 1.7665 \cdot 10^{-6}$ m^2. Test 5 was designed to assess the effectiveness of the continuous monitoring burst detection technique when the burst opening occurs over a greater time period. In this case, a manually actuated side discharge valve was used to generate the burst at a position of 0.1784 along the pipeline (point 1 in Figure 6.9). The estimated opening time of the burst was 12 ms and the calibrated size of the burst orifice was $C_d A_o = 6.019 \cdot 10^{-7}$ m^2. A pressure measurement was taken at a position of 0.7476 along the pipeline (point 3 in Figure 6.9). For all tests, the burst event was generated a few seconds after the measurement was started. An example of the measured pressure trace is shown in Figure 6.10.

The burst detection and location algorithm shown in Figure 6.2 was applied for all measured traces. Parameters of the algorithm used for Test 1-5 are presented in Table 6.1. The measured data was first monitored for a burst

Part of the algorithm	Parameter	Value
Monitoring for a burst event	λ	0.7
	h	1.5 kPa
	ν	0.04 kPa
Filter for analysis window	type	Butterworth, low-pass
	order	2
	f_{cutoff}	500 Hz
Burst parameter estimation	C_1	0.8
	C_2	0.85

Table 6.1: Parameters used for tests 1-5. Measured data were converted to pressure units (kPa).

event. Since measurements had little noise, the smoothening effect of an RLS filter used for pre-filtering was low ($\lambda = 0.7$). The drift and threshold parameters were selected considering that no operational oscillations in the pressure were expected in the laboratory pipeline. After the first change in pressure was detected, the data window was selected for further analysis. Low-pass filtering using a second order Butterworth filter was applied on the data window. After the filtering the change detection was performed for the whole length of the data window. The values of CUSUM test parameters were tuned after the first change in pressure was detected as explained in Section 6.3. The experimental pressure traces and the change detection algorithm results for all tests are shown in Figure 6.11.

The burst detection and location results can be found in Table 6.5. In each test case the burst was quickly detected and located. The range of bursts that will be detected when monitoring the measured pressure can be identified using Equations 6.7 and 6.8 from Section 6.3. Since both the size and the opening time of the burst influence the success if its detection, the detectable bursts are described by the combination of the two parameters. The burst with the opening time of 4 ms and size $C_d A_o = 3.33 \cdot 10^{-8}$ m^2 will still be detected as well as the burst with size $C_d A_o = 1.7665 \cdot 10^{-6}$ m^2 (Tests 1-4) and opening time of 0.98 s.

For Tests 1, 2 and 3, the error of the derived location was less than 0.33 m (0.9% of the total length of the pipeline) and the estimate of the burst orifice size was within 2% of the correct value. Results from Test 4, where the burst

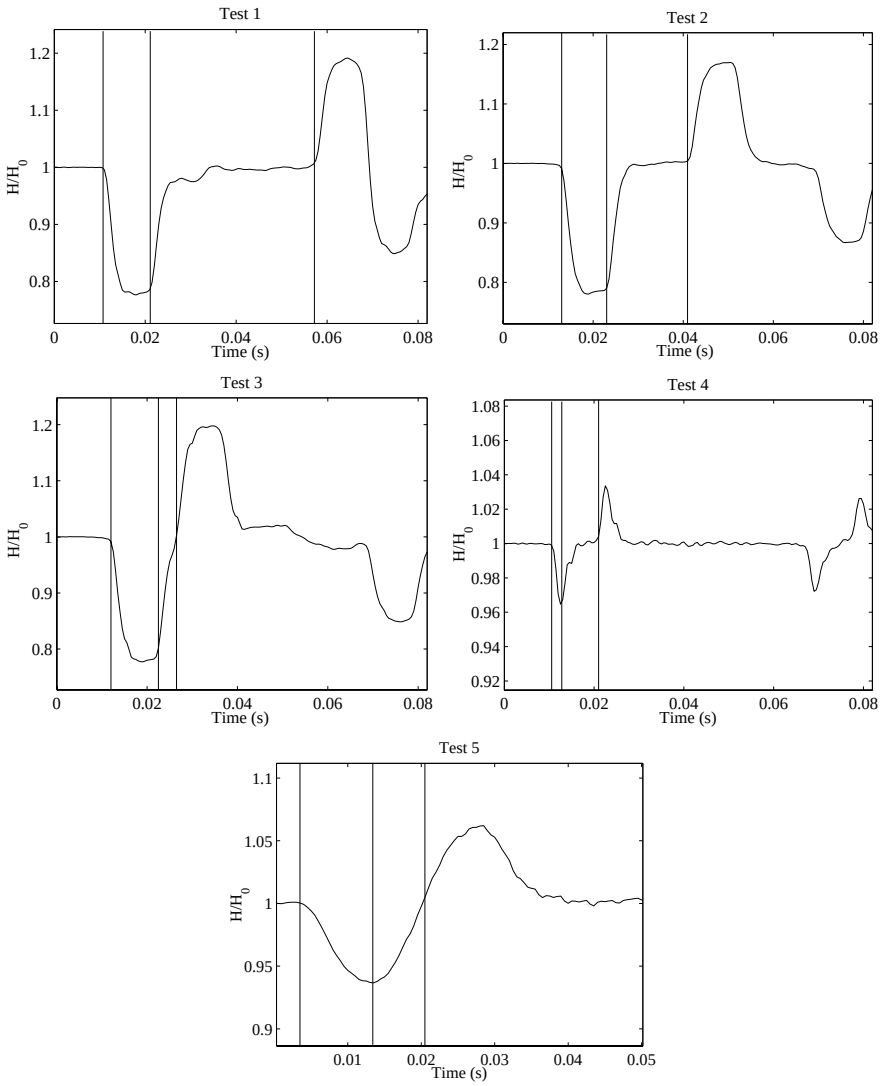

Figure 6.11: Burst at 0.1784 (Test 1), 0.4985 (Test 2), 0.7476 (Test 3), 0.9936 (Test 4), and 0.1784 (Test 5) along the pipeline. Measurement at 0.1784 (Tests 1-4) and 0.7476 (Test 5) along the pipeline. Vertical lines indicate change points detected by the change detection algorithm.

Test	Actual position[a] Actual C_dA_0 (m^2)	Estimated position[a] Estimated C_dA_0 (m^2)	Absolute error in position (m) Relative error in C_dA_0 (%)
1	0.1784 1.7665×10^{-6}	0.1767 1.7635×10^{-6}	0.0642 -0.1691
2	0.4985 1.7665×10^{-6}	0.5073 1.7356×10^{-6}	0.3294 -1.7496
3	0.7476 1.7665×10^{-6}	0.7536 1.7530×10^{-6}	0.2266 -0.7622
4	0.9936 1.7665×10^{-6}	0.9624 2.7098×10^{-7}	1.1693 -84.66
5	0.1784 6.0192×10^{-7}	0.1683 5.1955×10^{-7}	0.3802 -13.685

[a] burst positions given as a fraction of the total pipeline length

Table 6.2: Summary of laboratory burst detection tests.

has occurred in the vicinity of the right-hand tank, and from Test 5, where the the opening time of the burst was 12 ms, were less accurate. As explained in Section 6.4, if the burst opening time is 4 ms, the estimated location and size of the burst might contain an error if the burst occurs closer than 2.65 m from the boundary (Equation 6.15). The burst from Test 4 was located 0.24 m away from the boundary. In the case of Test 5, where the the opening time of the burst was 12 ms, the corresponding distance from the boundary is 7.96 m. Since the burst was located 6.7 m away from the boundary, results from Test 5 contain some error. However, the largest burst location error was less than 1.2 m.

6.6 Field validation on a dead-end branch of a network

In this section, the validation of the proposed burst detection and location technique under controlled field conditions is described and the results are presented. The technique was tested on a 356.53 m long 100 mm diameter pipe in a real water distribution network. The layout of the test pipeline is illustrated in Figure 6.12. The pipe is a dead-end branch connected to the rest of the system by a tee-junction. A total of 15 residential household connections with diameters between 15 mm and 25 mm are attached to the

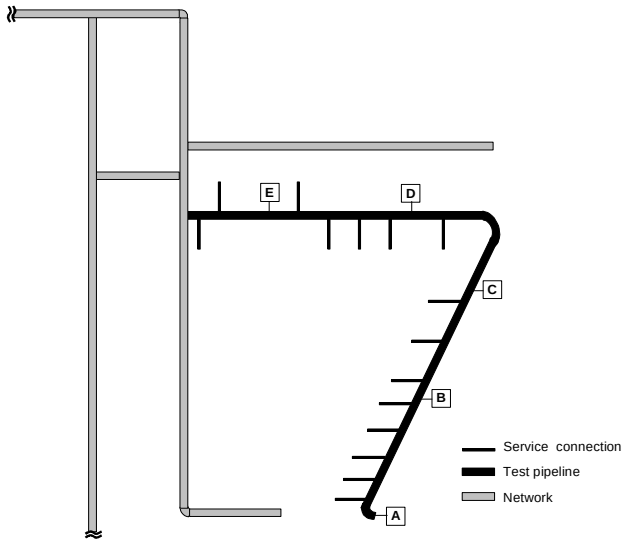

Figure 6.12: Layout of field experimental pipeline

pipe section. The calibrated wave speed of the pipe was $1\,150$ m/s. The fire hydrant plugs were used as connection points for both the measurement and burst simulation equipment. The burst was simulated using a 10 mm diameter solenoid side discharge valve with opening time of 50 ms. The size of the simulated burst was $C_d A_0 = 5.4978 \cdot 10^{-5}$ m^2. The pressure measurements were collected at a sampling frequency of 500 Hz. Appendix A contains more detailed description of the site and measurement equipment.

Tested burst locations are defined as the ratio of the distance from the dead-end of the pipe to the burst point and total length of the pipeline. Four locations were used – 0.1421, 0.3999, 0.4981 and 0.7991 along the pipeline (points B, C, D and E in Figure 6.12, respectively). Two different measurement sites were used. The first one (Tests 6-9) was located at the dead-end of the pipe (point A in Figure 6.12) and the second one (Tests 10-13) was 0.3999 along the pipeline (point C in Figure 6.12). The burst event was generated a few seconds after the measurement was started. An example of a measured trace is shown in Figure 6.13.

The burst detection and location algorithm shown in Figure 6.2 was applied

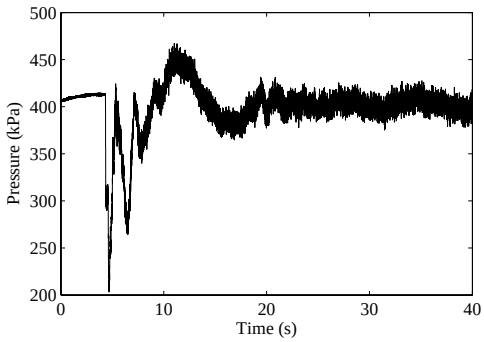

Figure 6.13: An example of measured pressure trace (Test 6)

Part of the algorithm	Parameter	Value Tests 6-9	Value Tests 10-13
Monitoring for a burst event	λ	0.95	0.95
	h	5.0 kPa	10.0 kPa
	ν	0.15 kPa	0.2 kPa
Filter for analysis window	type	Butterworth, low-pass	
	order	2	2
	f_{cutoff}	12.5 Hz	12.5 Hz
Burst parameter estimation	C_1	0.8	0.8
	C_2	0.75	0.75

Table 6.3: Parameters of burst detection and location algorithm used for Tests 6-13. Measured data were converted to pressure units (kPa).

for all measured traces. Parameters of the algorithm used for Tests 6-13 are presented in Table 6.3. The first step of the analysis was monitoring of measured pressure traces for a burst event. Pre-filtering was applied with a higher degree of smoothening than for the laboratory tests, since the field measurements contained more noise. Higher values of drift and threshold parameters for the CUSUM test had to be selected to account for pressure oscillations caused by demand changes. After the first change in pressure was detected, an analysis data window was selected and filtered. To illustrate the effect of the filtering, the pressure traces before and after filtering for Test 6 are presented in Figure 6.14. After the filtering the change detection was performed for the whole length of the data window. The values of CUSUM test were tuned after the first change in pressure was detected as explained

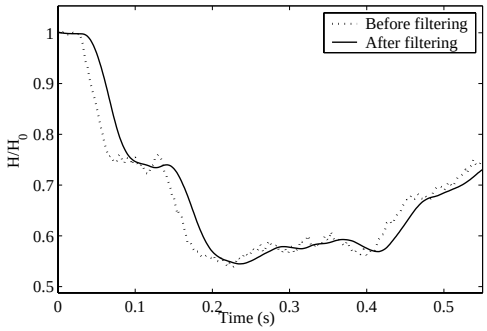

Figure 6.14: Effect of filtering (Test 6). Butterworth low-pass filter with cut-off frequency of 12.5 Hz was used.

in Section 6.3. Detected changes for all tests are shown in Figures 6.15 and 6.16. The burst detection and location results are summarised in Table 6.4.

Only two changes in pressure had to be detected for Tests 10-13 since the pressure was measured at the dead-end of the pipeline. Thus, the reflection from the dead-end boundary coincided with the arrival of the burst-induced wave. Since the dead-end boundary has a reflection coefficient $P = 1$, the measured change in pressure is two times greater than the actual burst wave. The reflection from the other boundary will also have double magnitude in the measured trace. As noted in Section 6.4, measuring at the dead-end boundary might extend the limit for the minimal size of the burst that will be detected. All bursts were successfully detected. The range of detectable bursts can be determined using Equations 6.7 and 6.8. If an opening time of 40 ms is considered, the smallest detectable burst would have $C_dA_o = 4.23 \cdot 10^{-6}$ m^2 if the pressure is measured at 0.3999 along the pipe and $C_dA_o = 7.3 \cdot 10^{-6}$ m^2 if the pressure is measured at the dead-end. If the burst with $C_dA_0 = 5.4978 \cdot 10^{-5}$ m^2 is considered, the slowest detectable burst will have an opening time of 1 s if the pressure is measured at 0.3999 along the pipe and 0.7 s if the pressure is measured at the dead-end.

The errors in location of the burst were within 15 m (4% of the total length of the branch) and the errors in size were within 15% except for the large error in the burst position for Test 8. After further investigation of the pressure trace it became apparent that the transient waves reflected from the bound-

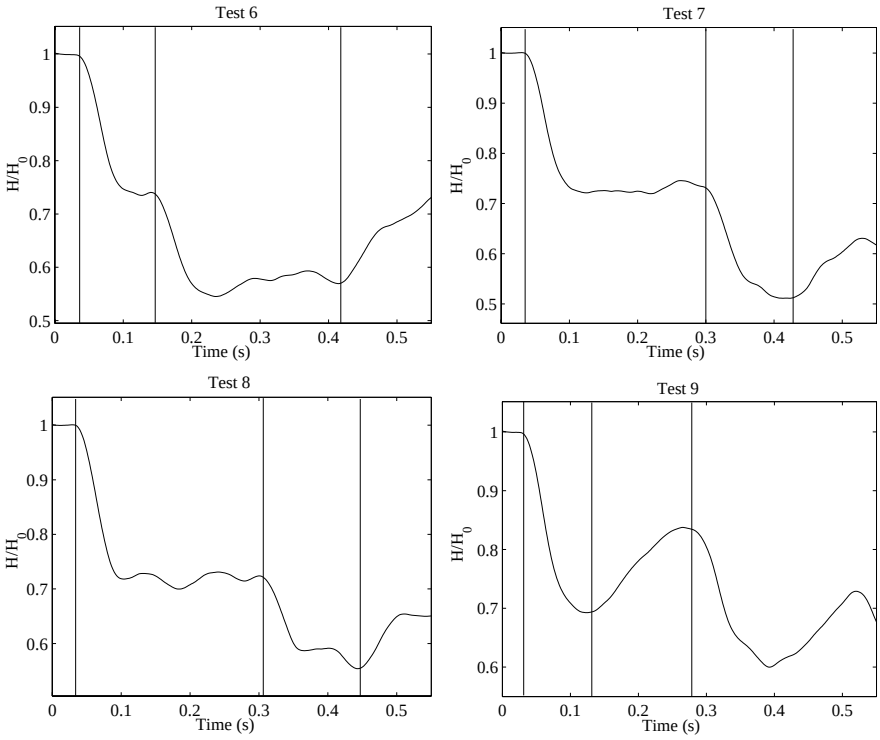

Figure 6.15: Burst at 0.1421 (Test 6), 0.3999 (Test 7), 0.6013 (Test 8) and 0.7991 (Test 9) along the pipe. Measured at 0.3999 along the pipe. Vertical lines indicate change points detected by the change detection algorithm.

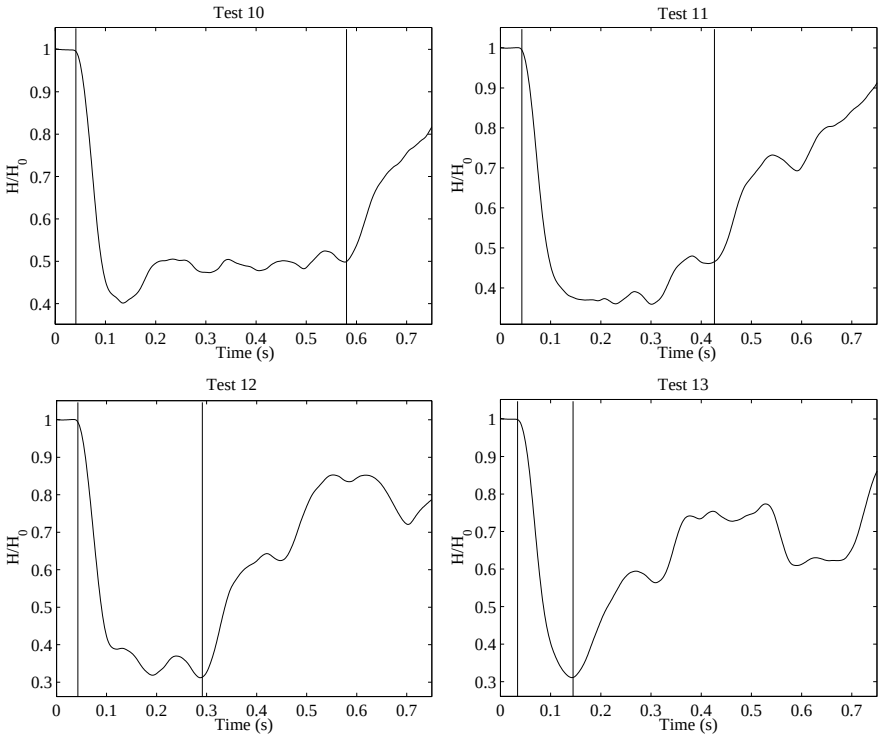

Figure 6.16: Burst at 0.1421 (Test 10), 0.3999 (Test 11), 0.6013 (Test 12) and 0.7991 (Test 13) along the pipe. Measured at the dead-end. Vertical lines indicate change points detected by the change detection algorithm.

Test	Actual position[a] Actual C_dA_0 (m^2)	Estimated position[a] Estimated C_dA_0 (m^2)	Absolute error in position (m) Relative error in C_dA_0 $(\%)$
Measured at 0.3999 along the pipe			
6	0.1421 5.4978×10^{-5}	0.1670 5.1182×10^{-5}	8.8902 -6.9043
7	0.3999 5.4978×10^{-5}	0.3850 5.3733×10^{-5}	5.3171 -2.264
8	0.6013 5.4978×10^{-5}	0.3885 5.5841×10^{-5}	75.85 1.5694
9	0.7991 5.4978×10^{-5}	0.7985 5.8136×10^{-5}	0.2158 5.7447
Measured at the dead-end			
10	0.1421 5.4978×10^{-5}	0.1000 4.7160×10^{-5}	14.9830 14.22
11	0.3999 5.4978×10^{-5}	0.3678 5.4744×10^{-5}	11.4460 -0.4256
12	0.6013 5.4978×10^{-5}	0.5807 5.9784×10^{-5}	7.3515 8.7417
13	0.7991 5.4978×10^{-5}	0.7871 6.0740×10^{-5}	4.2731 10.48

[a] burst positions given as a fraction of the total pipeline length

Table 6.4: Setup and results of Tests 6-13

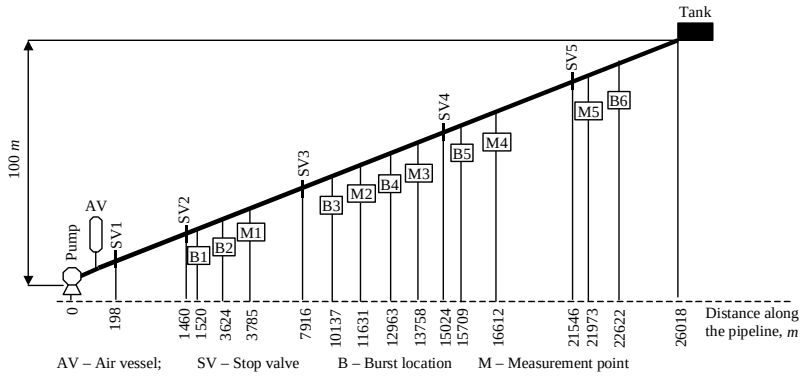

Figure 6.17: Layout of the pipeline

aries arrived at the measurement point almost at the same time. The interaction of the waves occurred at the measurement point and the arrival times were not accurately captured in the pressure data. Results could be improved with an additional measurement point or a measurement point located elsewhere in the pipeline. As an example, Test 12 can be considered where the burst was located at the same position as in Test 8. In this case the pressure was measured at the dead-end of the pipe and the correct position of the burst was found (see Table 6.4).

6.7 Field validation on a large water transmission pipeline

An operational water transmission pipeline was used for testing the burst detection and location technique. The 26 km long pipeline is a part of a larger system and conveys water to remote areas in South Australia. A schematic view of the pipeline is shown in Figure 6.17.

The MSCL (mild steel concrete-lined) pipeline has a diameter of 750 mm and consists of three segments with different wall thicknesses (starting from the upstream end) – 5614 m of 7.94 mm, 6126 m of 6.35 mm, and 14278 m of 4.76 mm. Wave speeds of 1100 m/s, 1030 m/s and 950 m/s were estimated for the three segments, respectively (starting from the upstream boundary). The bursts were simulated using the opening of a side-discharge valve (with

Part of the algorithm	Parameter	Value
Monitoring for a burst event	λ	0.95
	h	2.0 kPa
	ν	0.001 kPa
Filter for analysis window	type	Butterworth, low-pass
	order	2
	f_{cutoff}	10 Hz
Burst parameter estimation	C_1	0.8
	C_2	0.75

Table 6.5: Parameters used for Tests 14-24. Measured data were converted to pressure units (kPa).

diameters of 40 mm and 50 mm) or a fire plug air valve (FPAV) (with diameter of 30 mm). The pressure was measured at a sampling frequency of 2000 Hz. A more detailed description of the pipeline, measurement equipment and tests procedure can be found in Appendix A.

Parameters of the burst monitoring, detection and location algorithm used for Test 6-13 are presented in Table 6.5. A total of 11 tests numbered as Tests 14 to 24 were performed. Burst detection and location under three different operational regimes was considered: (1) pump off, (2) pump on (3) pump switching.

Case 1 - pump off

For the first 9 tests (Tests 14-22) there was no flow in the pipeline to represent the situation when no pumping is performed. A closed inline valve was acting as an upstream boundary. Burst locations and measurement point that were used in Tests 14 to 22 are shown in Figure 6.17 and listed in Table 6.6. Different burst locations, sizes and opening times as well as measurement positions were used to evaluate the performance of the burst detection and location algorithm. Different inline valves were closed for different tests to alternate the length of the pipeline and extend the range of tested burst locations.

The first step of the analysis was monitoring of measured pressure traces for

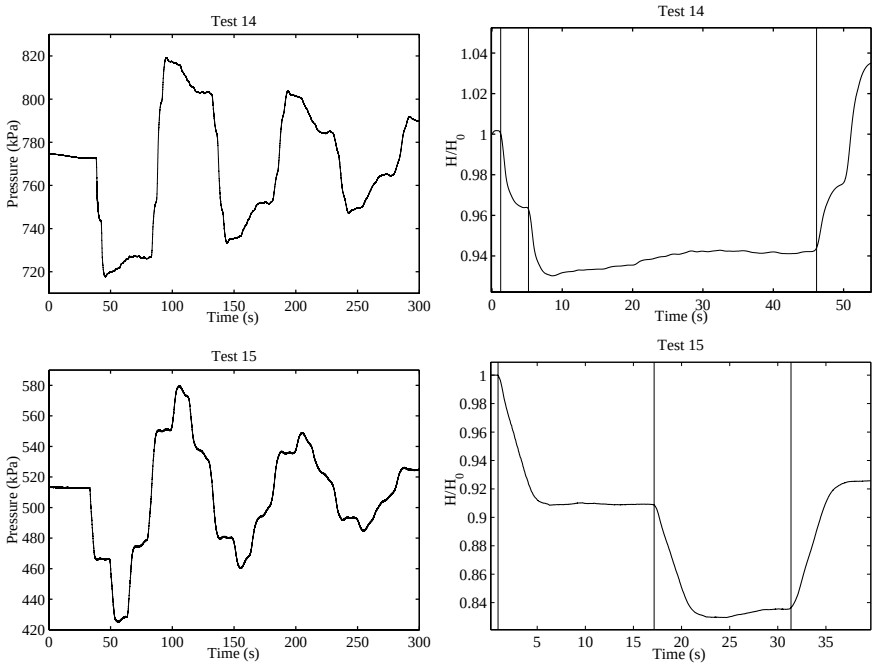

Figure 6.18: Test 14 (burst at B2) and Test 15 (burst at B3). Measurement point at M1. Measured burst traces (left) and filtered data windows (right). Vertical lines indicate the changes detected by CUSUM.

a burst event. Pre-filtering was applied with a higher degree of smoothening than for the laboratory tests, since field measurements contained more noise. Quite low values of drift and threshold parameters for the CUSUM test were selected since no pressure oscillations caused by demand changes were present on a steady-state pressure trace. After the first change in pressure was detected, an analysis data window was selected and filtered. After the filtering the change detection was performed for the whole length of the data window. The parameters of the CUSUM test were tuned after the first change in pressure was detected as explained in Section 6.3. As an example, measured pressure traces, analysis windows and CUSUM test results are shown in Figure 6.18 and Figure 6.19 for Tests 14, 15 and 20, 21 respectively. The detailed results for all tests are given in Table 6.6.

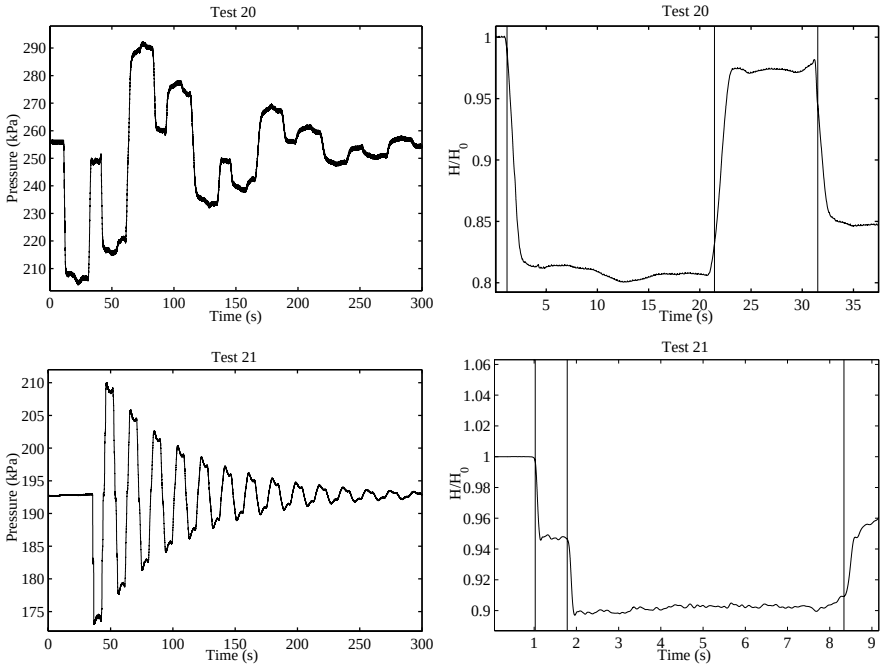

Figure 6.19: Test 20 (measurement at M4 and burst at B5) and Test 21 (measurement at M5 and burst at B6). Measured pressure traces (left) and filtered analysis windows (right). Vertical lines indicate changes in pressure detected by CUSUM.

Test No.	Upstream boundary	Measured at, m	Burst size*, L/s	Burst opening, s	Burst location, m		
					Actual	Found	Error
14	SV2**	M1	19.3	1.25	3624(B2)	3638	14
15	SV2	M2	35.5	3.22	10137(B3)	10143	6
16	SV1	M2	40.8	1.56	10137(B3)	10217	80
17	SV2	M3	43.0	4.20	15709(B5)	15614	95
18	SV3	M3	43.0	6.74	15709(B5)	15619	90
19	SV2	M4	44.5	2.84	12936(B4)	13026	90
20	SV1	M4	37.5	1.23	15709(B5)	15674	35
21	SV5	M5	8.8	0.13	22622(B6)	22618	4
22	SV2	M2	19.9	0.86	1520(B1)	1460	60

All locations are given as a distance from the upstream pump station

* Burst size was calculated from the measured change in pressure. ** SV = stop valve.

Table 6.6: Summary of burst detection and location tests. Tests 14-22

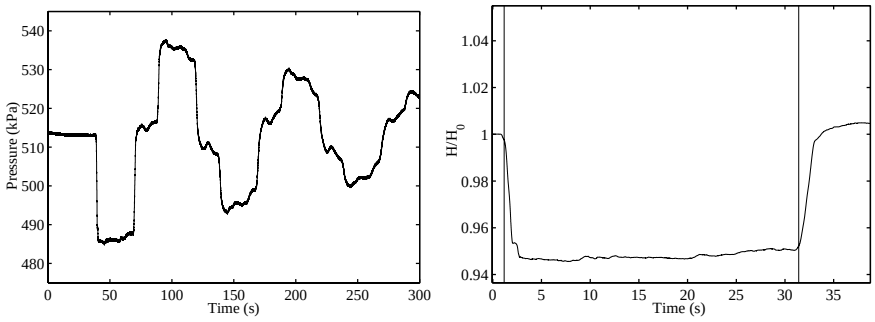

Figure 6.20: Test 22, measurement at M2 and burst at B1. (a) Burst trace and (b) filtered analysis window. Vertical lines indicate changes detected by CUSUM.

The transient wave reflection from the closed valve has the same sign as the wave itself, whereas the reflection from the tank has the opposite sign (see Appendix C). In Figure 6.18 and Figure 6.19, the influence of the burst location on the timing and the arrival order of the transient wave reflections from the tank and the valve can be observed. Only two changes in pressure were detected in the measured trace from Test 22 (Figure 6.20). Since the burst has occurred close to the boundary, the first change that is detected in the measured trace is a composition of the burst-induced transient wave and its reflection from the boundary. A more detailed explanation of the situation is given in Section 6.4 (Figure 6.8). If the analysis window for Test 22 is extended (Figure 6.21) it appears that the third change in pressure corresponds to the distance $2L/a$ where L is the length of the pipeline. This together with the fact that the second detected change indicates the reflection from tanks (sign opposite to the initial wave) suggests that the reflection from the valve has not been detected. Thus, the burst is assumed to be located within the distance of $0.5(t_{opening}a)$ from the valve (Equation 6.15). To verify this assumption, the burst was simulated 50 m away from the valve using a pipeline model. The transient pressure is solved by the method of characteristics (see Appendix B). A good match between simulated and measured pressure traces is shown in Figure 6.21 and proves that the burst was located close to the valve.

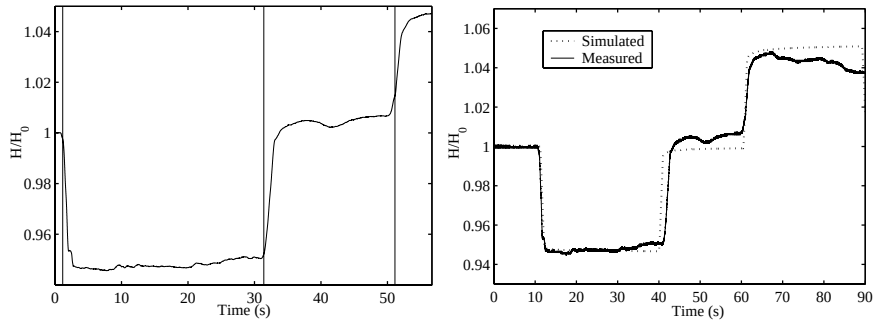

Figure 6.21: (Left) Extended analysis window for Test 9. Vertical lines indicate pressure changes detected by CUSUM. (Right) Comparison between simulated and measured pressure traces for Test 9.

Case 2 - pump on

Two tests were conducted with the pump running. Two locations of the bursts were tested for the same measurement point (Tests 23 and 24). The nominal flow in the pipeline was 496 L/s. As an example, the measured burst pressure trace, analysis window and results of the CUSUM for Test 10 are shown in Figure 6.22. More details for both tests are given in Table 6.7. Since the pump was running, air vessels adjacent to the pump station were acting as an upstream boundary condition for a burst-induced wave. Therefore reflections from both boundaries have the same sign as shown in Figure 6.22.

Test No.	Uptream boundary	Measured at, m	Burst size*, L/s	Burst opening, s	Burst location, m		
					Actual	Found	Error
23	Pump	M3	34.6	3.07	10137(B3)	10193	56
24	Pump	M3	45.1	6.63	15709(B5)	15566	143

All locations are given as a distance from the upstream pump station

* Burst size was calculated from the measured change in pressure

Table 6.7: Summary of burst detection and location tests. Tests 23-24.

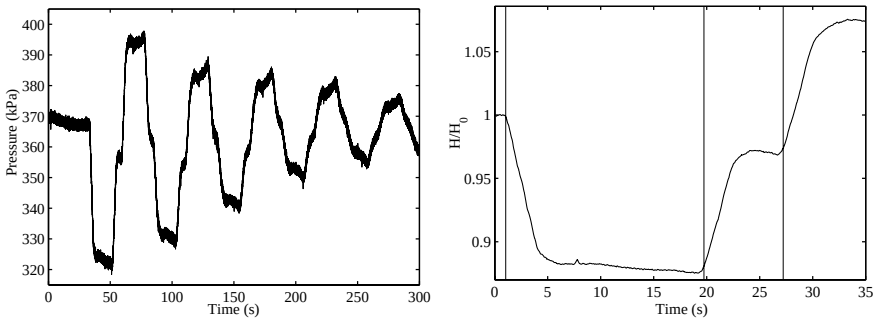

Figure 6.22: Test 23, measurement at M3 and burst at B3. (a) Measured burst trace and (b) filtered data window. Vertical lines indicate changes detected by CUSUM.

Case 3 - pump switching

Two operational regimes of the pipeline have been considered so far - the pump being off and the pump being on. The third regime is transition between two abovementioned ones, i.e. pump start-up and shutdown. Figure 6.23 shows typical pump start-up and shutdown traces (no burst) measured at M4. In certain situations, a pipeline burst can occur during a pressure transient that is caused by a pump start-up/shutdown. Dealing with bursts that are initiated by pump operation requires special attention. One option is to model the pressure response of a transient initiated by the pump and compare the simulated trace to the measured one. The discrepancy between modelled and actual pressure traces would indicate a burst event. Since there is a standard procedure for pump operation and the hydraulic environment of the pipeline does not vary considerably, is it likely that the traces of pump start-up/shutdown will be similar each time. Thus, historical measurements of pump start-up/shutdown can be used as a reference instead of the model. Due to the complexity of the experimental setup, testing for bursts that are initiated by pump start-up/shutdown was not conducted.

The overall performance of the burst detection and location technique is very promising. Different burst sizes between 8 and 50 L/s and burst opening times from 0.1 s up to 6.8 s were tested. Six different burst locations and five measurement points were used. Most bursts were successfully detected

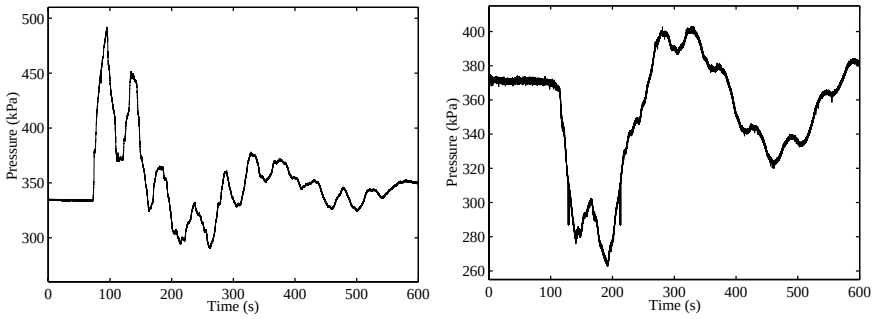

Figure 6.23: The pressure traces of (a) pump start-up and (b) pump shutdown

and located. As shown in Table 6.6 and Table 6.7, the error of the burst location varies between 4 and 143 m (0.015–0.55% of the total pipeline length), which is sufficiently small to be able to identify the section of the pipeline that has to be isolated.

Further discussion of the performance, implementation and application of the proposed automatic pipeline failure monitoring, detection and location approach is presented in Chapter 7 in conjunction with a discussion of the transient response difference monitoring approach that was described in Chap ter 5.

Chapter 7

Pipeline failure monitoring - discussion

In this chapter, a discussion of automated failure monitoring, detection and location in pipelines is presented. Two different techniques, described in Chapters 5 and 6, are considered. The discussion focuses on the performance, implementation and application of the two failure monitoring techniques.

7.1 Performance limits

Validation results from the laboratory and field pipelines have demonstrated that the techniques presented in Chapters 5 and 6 are capable of detecting and locating leaks and bursts of a certain size. However, the limited flexibility of the tests does not always allow for validation of the method for the whole range of failures that may occur. Thus, the performance limits of the techniques have to be estimated. The performance of the failure management techniques can be evaluated using three main parameters: (1) the minimum size of the failure that can be detected and located, (2) the precision of the derived location and (3) the detection and location time, i.e. the time from the actual failure to the time when it is detected and located.

Periodical leak diagnosis

The minimum size of a detectable leak. The minimum size of a leak that can be detected by the technique depends on the following parameters: the resolution of pressure measurements; the level of measurement noise; the size of the transient that is generated; and the intensity of the hydraulic activity in the pipeline. High resolution pressure measurements can be achieved using modern measurement equipment. In the tests that were conducted to validate the approach, a 12 bit A/D card was used together with a variable-gain amplifier. As a result, pressure measurements had a calculated resolution of 0.049 kPa. The observed reflection from the 15 L/s leak was 0.92 kPa, i.e. almost 20 times larger than the resolution. Theoretically, if there was no measurement noise present, a 2.1 L/s ($D_l/D = 1.4\%$) leak should be detected. Furthermore, if a 16 bit A/D card was used, the resolution would increase to 0.0023 kPa and the corresponding minimum leak size would be 0.1 L/s ($D_l/D = 0.31\%$). The actual limit of the detectable leak size for a real installation is expected to be higher and would depend on the measurement noise level.

The size of the transient that is generated has considerable influence on the size of the reflection from the leak and, consequently, affects the minimum size of the leak that will be detected. The larger the magnitude of the generated wave, the smaller the leak that will be detected. However, a too large transients can be hazardous to the pipeline. In the presented tests, transients with magnitudes around 50 kPa were generated. On a large pipeline, such transients are not likely to have any damaging effect. If a higher resolution-to-noise ratio can be achieved in pressure measurements, the size of the generated transient can be further reduced.

Hydraulic events in the pipeline have the potential to corrupt the measured pressure trace and lead to false alarm situations. As already mentioned in Chapter 5, to avoid this problem, tests have to be conducted during the time when the pipeline system is in its most stagnant state. It is preferable that the variation in demand is minimal and no pumping is performed during the leak diagnosis tests. These conditions are likely to be feasible on most water transmission pipelines as a part of the normal operation. If the pipeline leak diagnosis cannot be made when the pipe is online, a temporary suspension of the operation can be used.

Tests	D (mm)	h (kPa)	ν (kPa)	Opening time 10 ms		Opening time 1 s	
				$D_{l,\min}/D$	Q_l	$D_{l,\min}/D$	Q_l
Branch in the network	100	5	0.15	2.6 %	0.1 L/s	22.6 %	8.4 L/s
Transmission pipeline	750	2	0.001	1.27 %	1.7 L/s	1.79 %	3.3 L/s

Table 7.1: Performance limits of the burst monitoring system

The precision of the location. The average error of the derived leak location for the validation tests was less than 80 m (0.3% of the total length of the pipeline). This error can be further reduced by increasing the precision of the estimated wave speed value for the pipeline. If necessary, the exact location of the leak can be confirmed using noise correlators or other sounding equipment. A pipeline section of 80 m can be inspected using a single correlator setup and, therefore, the inspection procedure should take relatively little time.

The detection and location time. The time required for detecting and locating a leak primarily depends on the frequency of leak tests. A period of leak diagnosis has to be selected by the operator. More frequent checks will allow for faster reaction to the leak. However, in some cases, the operational regime of the pipeline may limit the frequency of leak diagnosis. Some additional time may be required when listening equipment is used to find the precise location of the leak after it has been detected. Generally, the location time is likely to be reduced considerably using the proposed techniques in comparison to the current practice.

Burst monitoring

The minimum size of a detectable burst. To evaluate the performance limits for the burst monitoring system, the minimum size of a detectable burst can be used. This size is defined as a combination of two interdependent parameters: the size of the burst and the opening time of the burst. As an example, the validation results from Chapter 6 can be used. The minimum size of detectable bursts for different tests and different burst opening times is presented in Table 7.1. In this table, $D_{l,\min}/D$ is the ratio of the minimum diameter of the burst that will be detected and the diameter of the pipeline

and Q_l is the flow rate through the burst orifice. Two discrete values of the burst opening time were chosen to illustrate the performance of the technique. In the first case, a sudden burst was considered with an opening time of 10 ms. The second case was a slower break with 1 minute opening time. For the transmission pipeline, the algorithm was tuned to be sensitive to both sudden and slower bursts. This was achieved by setting a low value of the CUSUM drift parameter (ν). For tests conducted on the dead-end branch in the network, the system was tuned to be sensitive to sudden events and a higher value of drift was used to prevent false alarms caused by normal operational oscillations, such as sudden changes in demand. A set of parameters has to be specifically tuned for a particular system to minimise the rate of false alarms and maximise the number of bursts that are detected.

The precision of the location. The average error of the derived burst location for the eight tests conducted on the dead-end branch in the network was less than 8 m (2.25 % of the total length of the branch). The corresponding error for the nine tests on the transmission pipeline was less than 53 m (0.2 % of the total length of the pipeline). The precision of the derived location can be further improved by calibration of the wave speed value.

The detection and location time. The burst detection and location time is approximately equal to the time it takes for the pressure wave to travel from the burst point to the furthest boundary, be reflected and reach the measurement point. This time will always be less than $2L/a$, where L is the length of the pipe and a is the wave speed of the pipe. If the transmission pipeline that was used for the validation testing is considered (L=26 km), the detection time of a burst would be approximately 50 seconds. The corresponding time for the 356 m long dead-end branch in the network would be less than 1 second.

7.2 Application

The developed techniques were designed for applications on single pipelines. In a water supply system the primary example of single pipelines are transmission pipelines. However, if considered individually, distribution mains can also qualify as single pipelines.

Transmission pipelines

The primary application of the proposed techniques is failure monitoring in water transmission pipelines. Large, long mains often present a challenge to the conventional failure detection and location methods. Leak detection and location times can be increased due to the extensive length and remote location of the pipeline. The periodical leak diagnosis system can provide an alternative to the frequent visual inspection, which is time and resource consuming. The consequences of failure in transmission pipelines can be hazardous and expensive, especially when pipelines are located close to other urban infrastructure assets, such as gas mains, communication networks, etc. In such situations, it is essential to react to the pipe failure as quickly as possible; therefore, a continuous monitoring is preferable.

Distribution mains

It is practically infeasible to extensively apply the proposed failure monitoring methods in water distribution networks. In order to apply these techniques to a network, installation of a separate monitoring system on every single branch in the network would be required, which is cost prohibitive. However, pipes that are the most critical in the network can be chosen for burst monitoring or leak diagnosis systems. The burst monitoring technique presented in Chapter 5 has been tested on a single dead-end branch in a distribution network. Despite the presence of service connections and the uncertainty in demands, burst detection and location was successful. In fact, the method can be applied to any single pipeline under two conditions: (1) side pipe connections are considerably smaller in diameter compared to the pipeline and (2) approximate reflection characteristics of end boundaries can be derived. Periodical leak diagnosis can also be applied on a single branch in a network.

7.3 Implementation

Generally, a pipeline failure monitoring system would have three main components: sensors and actuators, data analysis unit and communication sys-

tem. Due to differences in operation, the implementation of these components has to be considered separately for the periodical leak diagnosis and burst monitoring systems.

Periodical leak diagnosis system

Since only one pressure measurement point and a single transient generation point is required for the operation of the proposed leak diagnosis system, its implementation on an actual pipeline should be fairly straightforward. A transient generator and pressure measurement unit are the two main components of the periodical leak diagnosis system. As already noted in Chapter 5, it is beneficial to install the generator and the pressure monitoring point as close to each other as possible. The actual location along the pipe has to be chosen for a particular pipeline. A micro controller can be used to operate the transient generator and collect the required data. The length of the data window that has to be collected depends on the length of the pipeline. Once measured, the transient response trace can be analysed locally (compared to the reference leak-free trace) or sent to a control room.

Burst monitoring system

For the implementation of the burst monitoring system, a single pressure monitoring point is required. The data acquisition system is slightly different from the one used for leak diagnosis. The pressure has to be sampled continuously and stored in a memory buffer for on-line analysis and checks must be made for the burst-induced pressure change. If such a change is not detected, the data can be erased from the buffer and a new batch loaded. Such a pre-emptive scheme does not require large memory capacity. When a burst-induced change in pressure is detected, the longer window of data can be collected and sent to the control room or, alternatively, the burst parameters can be derived on-site and sent to the operator.

Integrated system

Considering that the two systems discussed above operate on different time scales and principles, it may be beneficial to combine these two approaches into an integrated pipeline failure management system. The integrated system would have a transient generator combined with the continuous pressure monitoring unit. With a moderate increase in installation and maintenance costs, a combined system would have several advantages including:

- immediate detection and location of sudden bursts by the continuous burst monitoring system;
- detection and location of single or multiple leaks using a periodical leak diagnosis system;
- detection and location of slower bursts that cannot be detected by the burst monitoring system with the help of the periodic leak diagnosis system;
- detection and location of slowly developing leaks once their sizes are greater than the detectability limit; and
- confirmation of the presence and location of the burst detected by the burst monitoring system using the leak diagnosis system (immediately after an alarm).

For the integrated system, a transient generation unit has to be installed on the pipeline in addition to the architecture of the burst monitoring system. The same pressure measurement point can still be used. Thus, the increase of installation and maintenance costs should be limited. Benefits associated with such an upgrade are likely to make the investment return period short.

7.4 Calibration

The same level of calibration is required for the leak diagnosis and burst monitoring systems. The only parameter that has to be calibrated to derive

the precise location of a leak is the wave speed of the pipeline. A theoretically calculated wave speed value usually contains some error, and better precision of the wave speed can be achieved by estimating the value from experimental data. The calibration procedure is simple. By measuring the time it takes for the generated transient wave to travel from the measurement point to the boundary of the pipeline and back to the measurement point, the wave speed can be calculated. Alternatively, two measurement points can be used and the wave speed can be calculated based on the wave travel time between the two points. Other parameters of the pipeline do not have to be known precisely for failure detection and location.

7.5 Tuning

Tuning of the failure monitoring system involves the adjustment of system's parameters for the optimal operation. The optimal operation is associated with a high reliability, where reliability is generally understood as a measure measure of the certainty that the system will perform as intended. The failure monitoring system can be unreliable in two ways: (1) it may not generate an alarm in the case of a failure, or (2) it may generate an alarm when no failure has occurred (false alarm). Thus, the reliability of the failure monitoring system can be defined using the following expression:

$$reliability = \frac{alarms - false\ alarms}{failures}$$

To increase the reliability, the number of successfully detected failures has to be increased. However, at the same time, the rate of false alarms has to be minimised. The main purpose of the tuning process is to enhance the reliability of the failure monitoring system.

As every pipeline has individual physical and hydraulic characteristics, it is clear that tuning has to be performed once the failure monitoring system is installed on a particular pipeline.

7.6 Conclusions

Whether only one of the presented systems is installed on a pipeline or both approaches are applied in a combined way, the efficiency of the pipeline failure detection and location process can be increased considerably in comparison to the current situation. At the cost of installing a single pressure monitoring point, sudden bursts can be detected and located at any point along the pipeline. The burst monitoring technique offers an immediate reaction to potentially hazardous pipe ruptures. Losses associated with pipe failure can be reduced significantly if the monitoring system is installed. By adding the hydraulic transient generator, the range of detectable failures can be extended further, including events that occur over a longer time period and also leaks that are too small to be detected by the burst monitoring system. As mentioned previously, most leaks are likely to increase in size over time and eventually become large enough to be detected by the proposed methods. Additionally, as was shown during field testing, the periodic leak diagnosis approach allows for the detection and location of air pockets and partial blockages in the pipeline.

The application of the described methods can be extended to monitoring of illegal consumption and detection of hydraulically dangerous events in pipeline systems. In some cases, normal operation of the pipeline may involve some hydraulic events (i.e. transients) that can be potentially hazardous to the system and often pipeline operators are not aware of these disturbances. It is beneficial to maintain as steady pressure in the pipeline as possible and the continuous pressure monitoring can serve as a tool to identify sources of disturbances and eliminate them.

Part III

Automatic failure monitoring, detection and location in pipe networks

---

Summary: *To reduce losses associated with a pipe failure in a network, the failure detection and location time has to be minimised. Currently, pipe failures are often detected visually, when the water appears on the ground surface. Available active leakage control techniques reviewed in Chapter 4 are either expensive and time consuming or have a long leak detection and location time.*

Part III of this thesis describes two techniques for failure monitoring, detection and location in pipe networks. The first method, presented in Chapter 8, is based on a steady-state analysis of a network and is designed to detect and locate slower pipe breaks. The second approach, described in Chapter 9, is based on a unsteady-state analysis of a network and is capable of detecting and locating sudden bursts. Chapter 10 discusses the performance, application and implementation of the proposed techniques.

Related publications: *Part of the work has been presented in Misiunas et al. (2004), Misiunas et al. (2005a) and Misiunas et al. (2005f).*

Chapter 8

Failure monitoring, detection and location based on steady-state analysis

In this chapter, the methodology for failure detection and location in pipe networks (on the level of DMA) is presented. The approach is based on monitoring of the steady-state flow rate at the entry point of a network for a burst-induced change. The location of the failure is derived from the distribution of the steady-state pressure throughout the network. The approach was validated for simulated data and an uncertainty analysis was performed. Further discussion on the performance, implementation and application of the proposed technique is presented in Chapter 10.

8.1 Modelling of steady-state flow in pipe networks

A water distribution network basically consists of a set of nodes (junctions) joined to each other by links (pipes). The principles of conservation of mass at nodes and conservation of energy between nodes and in loops are used to model pressure, flow and hydraulic elements in the network. *Conservation of mass* dictates that the fluid mass entering any node will be equal to the

mass leaving the node:

$$\sum_{j=1}^{pipes} Q_j - D_M = 0 \tag{8.1}$$

where Q_j is the inflow to the node from the j^{th} pipe and D_M is the demand at the node. The conservation-of-mass equation is applied to all nodes in a network, resulting in one equation for each node.

Conservation of energy dictates that the difference in energy between two points must be the same regardless of the path taken (Bernoulli; 1738):

$$Z_1 + \frac{P_1}{\gamma} + \frac{{V_1}^2}{2g} + \sum h_a = Z_2 + \frac{P_2}{\gamma} + \frac{{V_2}^2}{2g} + \sum h_f + \sum h_m \tag{8.2}$$

where:

Z	=	elevation
P	=	pressure
γ	=	fluid specific weight
V	=	velocity
g	=	gravitational constant
h_a	=	head added by pumps
h_f	=	head loss due to pipe friction
h_m	=	head loss due to minor losses

When a series of links and nodes constitute a closed path, they form a loop. In a distribution network, the sum of all energy losses in an independent closed path or loop must equal zero. Additionally, energy must be conserved between two nodes of known energy. As a result, one energy equation must be developed for each pipe (or loop) depending on the method used. In this study, the EPANET hydraulic solver (Rossman; 2000) was used to simulate the flows and pressures in a pipe network.

From Equations 8.1 and 8.2 it can be seen that change of demand at one node (i.e. due to a burst) will influence the flow rates and pressure at that node and the distribution of pressures and flow rates at other nodes. As it will be shown in the following sections, a burst can be detected and located by observing the flow rate and pressure throughout the network. There are two basic conditions that have to be satisfied while applying the proposed methodology:

(1) all flow rates into the network are measured and (2) knowledge exists about the distribution of demand within the network. Since a network with measured inflow rate (DMA) is considered in this study, the burst flow rate will be fully realised in the flow rate measurement at the entry point of the system.

8.2 Monitoring of flow rate for a burst event

A burst event may be detected from the continuous flow rate measurement at the entry point of the network. The burst discharge will increase the measured total flow rate, Q_m, entering the network. The increase of Q_m may be detected using a cumulative sum (CUSUM) change detection test (Page; 1954). The CUSUM test has been extensively applied for change detection in different time series analysis problems (Basseville and Nikiforov; 1993). If the flow rate measurement contains a high level of noise pre-filtering is applied using a Recursive Least Squares (RLS) filter. The filter estimates the signal θ_t from the measurement Q_t^m (containing noise) as $\theta_t = \lambda\theta_{t-1} + (1-\lambda)Q_t^m$. The parameter $\lambda \in [0, 1)$ is the forgetting factor limiting the smoothing effect of the filter. Residuals $\epsilon_t = \theta_t - \theta_{t-1}$ are fed into the CUSUM test to determine whether a significant change has occurred in the measured signal:

$$\begin{aligned} &S_0 = 0; \\ &S_t = \max(S_{t-1} + \epsilon_t - \nu, 0) \\ &\text{if } S_t > h \text{ then issue alarm and set } t_a = t \end{aligned} \tag{8.3}$$

where S_t is the cumulative sum value at time t, while h and ν are threshold and drift parameters, respectively. For every sample of data, the part of the change in signal ϵ_t that exceeds the drift value (the expected variation) is added to the cumulative sum S_t. When S_t reaches the threshold value h, an alarm is issued and the time of change, t_a, is recorded. It has to be noted that the formulation of the CUSUM change detection test that is used here (Equation 8.4) is only sensitive to positive changes in flow rate. Negative changes do not influence the cumulative sum and are therefore ignored by the change detection test. To illustrate the change detection procedure, Figure 8.1 shows an idealized burst flow rate, total flow rate and cumulative sum

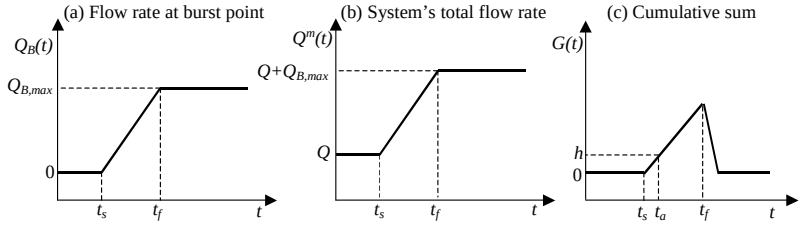

Figure 8.1: Generalised traces of (a) flow rate at burst point, (b) total flow rate at the entry point and (c) cumulative sum.

traces. The maximum burst flow rate $Q_{B,max}$ and the time ($t_f - t_s$) for Q_B to reach $Q_{B,max}$ are unknown and can vary considerably for different bursts. As it will be shown later in this chapter, for determination of a burst location it is beneficial to register the maximum change in pressure induced by the burst. To achieve that, pressure measurements before the burst event ($t = t_s$) and after the burst flow rate has reached its maximum value ($t = t_f$) have to be determined. As shown in Figure 8.1c, t_s corresponds to the time when dS/dt becomes positive and t_f corresponds to the time when dS/dt becomes zero or negative. This is a modified form of the CUSUM test. In the classical form only time t_a is used and G_t is reset to zero directly after t_a (i.e. when $S_t > h$).

The drift ν is chosen so that it is larger than typical operational flow rate oscillations in the system, which can be determined from historical flow rate data. Usually water demand changes quite rapidly during certain periods of the day and can be rather stagnant at other times, especially during night time. Thus, variable drift selection can be introduced to improve the performance of the burst detection and location technique. The specific drift set points can be derived for every hour or peak/off-peak periods based on the observed fluctuations of flow rate in a particular network. Theoretically, the threshold h can have a small positive value (resulting in $t_a \approx t_s$). However, in reality, the fluctuations in flow rate due to demand changes can exceed the drift value which would result in $G > 0$. To prevent false alarms triggered by such situations, h is set to be larger than the drift, i.e. $h = 2\nu$.

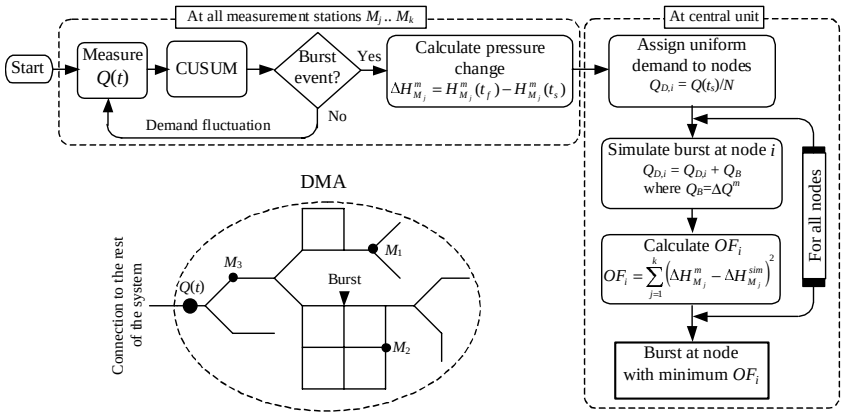

Figure 8.2: Structure of the continuous burst monitoring algorithm

8.3 Burst location algorithm

A schematic view of the complete burst detection and location algorithm is shown in Figure 8.2. Once the presence of a burst is detected in the flow rate measurements at the entry point of the network, the location of the burst is found by searching for the burst node based on the observed changes of pressure at a number of measurement points throughout the network. Using the burst start time t_s and the time when the burst flow reached its maximum t_f, as identified by the CUSUM change detection test, the total change in flow rate due to the burst and the changes in pressure at the monitoring points can be calculated:

$$\Delta Q^m = Q^m(t_f) - Q^m(t_s) \tag{8.4}$$

$$\Delta H^m_{M_j} = H^m_{M_j}(t_f) - H^m_{M_j}(t_s) \tag{8.5}$$

The demand value for an individual node is assigned as a proportion of $Q^m(t_s)$ based on historical demand information at that node. If no demand information is available, an average demand of $Q_{D,i} = Q^m(t_s)/N$ is assigned uniformly to all nodes. A burst of size $Q_B = \Delta Q^m$ is simulated by assigning $Q_{D,i} = Q_{D,i} + Q_B$ to one burst candidate position and calculating the pressure and flows in the network. In this study, all the nodes in the network were nominated as burst candidate locations. Simulated pressure

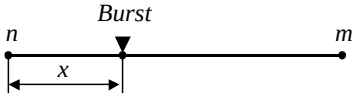

Figure 8.3: Burst location along a pipe

values at the measurement points are used to calculate the objective function:

$$OF_i = \sum_{j=1}^{k} \left(\Delta H_{M_j}^{m} - \Delta H_{M_j}^{sim} \right)^2 \qquad \forall i \in [1, N] \tag{8.6}$$

where ΔH^m is the measured change in pressure, ΔH^{sim} is the simulated change in pressure, k is a number of pressure measurement points in the system and $M_1, \ldots, M_k$ are the nodes where the measurement points are located. The objective function is calculated for all burst candidate locations and the node having the smallest OF_i value is declared to be the burst position. The burst size is equal to the detected change in the flow rate observed at the inlet point of the network ($Q_B = \Delta Q^m$).

Based on the knowledge available about different types of pipe failures, which was summarized in Chapter 2, it is reasonable to assume that bursts may occur both at junctions (nodes) and along pipes (in between nodes). During the search for the burst location using the procedure described earlier in this section all candidate burst locations are tested and the one having the best fit is selected as the burst location. Every node in the model of the network is used as candidate location of a burst. Thus, when a burst occurs in between two network nodes, the node that is closest to the burst will be selected as the burst location. Depending on the level of detail in the network model, the identification of the node closest to the burst location may be satisfactory. A further increase in the precision of the burst location is possible. An example of a burst that occurs along a pipe is shown in Figure 8.3, where n and m are nodes adjacent to the burst pipe and x is the distance from node n to the burst. After the search for a burst location is performed, nodes n and m are likely to have the best fit (OF not equal to zero). The distances x can be derived using the values of the objective functions of the two nodes with the best fit:

$$x = \frac{OF_n}{OF_n + OF_m} L \tag{8.7}$$

where L is the distance between nodes n and m.

Issues related to the uncertainty in the derived burst location caused by measurement and model errors and other aspects limiting the performance of the burst detection and location technique are discussed in Section 8.6.

8.4 Optimal measurement placement

As declared in the beginning of the chapter, the proposed burst detection and location technique requires two types of continuous measurements. The flow rate has to be monitored at all points of supply into the network and the pressure has to be monitored at one or more points within the network.

Flow rate measurements

The proposed technique requires the flow rates to be measured at all entry points to the network. Thus, the selection of flow rate measurement points is straightforward and limited to the point(s) where the monitored network is connected to the rest of the system. In some cases, the network can be fed by an elevated storage tank, which is filled using the pumping station connected to the rest of the system. In that case, both the pump flow (during pumping operation) and the outflow from the tank have to be monitored.

Pressure measurements

The optimal placement of the pressure monitoring points is an important factor that influences the performance of the proposed technique. A large number of measurement positioning (also called sampling design) approaches are described in the literature (Bush and Uber; 1998; Kapelan et al.; 2003b; Vítkovský et al.; 2003). There are two parameters that have to be chosen: (1) the number of measurement stations and (2) the distribution of measurement stations throughout the network. Therefore, the optimal measurement placement is a multi-objective problem.

Number of measurement stations. The choice of the number of pressure monitoring stations depends on two main factors: the maximum allowable installation cost and the minimum required level of performance of the burst location technique. It can be intuitively assumed that a larger number of measurement points will enhance the precision of the estimated burst location. However, at the same time, the installation and subsequent maintenance costs will increase. Therefore, a compromise has to be found for a particular system. The selection of the number of measurement points can be seen as an iterative procedure initiated with one pressure monitoring station. After the optimal position of the station is found, the expected performance of the burst monitoring technique is re-evaluated. The number of measurement points is increased by one, the optimal placement is found and the performance is evaluated. The same procedure is repeated until a satisfactory level of the performance is reached or until the limit of the investment for the measurement system is approached.

Distribution of measurement stations. Most of the sampling design techniques found in the literature are based on sensitivity analysis. The sensitivity matrix can be derived using a perturbation method (Bush and Uber; 1998) where every element represents the change in a state variable due to the change of a single parameter:

$$S_{i,j} \equiv \left| \frac{\delta H_j}{\delta Q_{D,i}} \right| = \left| \frac{H_j(Q_{D,i}) - H_j(Q^*_{D,i})}{Q_{D,i} - Q^*_{D,i}} \right| \tag{8.8}$$

$$\forall i \in [1, N], \forall j \in [1, N]$$

where $H_j(Q_{D,i})$ is the computed head at node j for the assumed demand $Q_{D,i}$ at node i and $H_j(Q^*_{D,i})$ is the computed head at node j after alternating the assumed demand $Q_{D,i}$ at node i to $Q^*_{D,i}$. The value of Q_D depends on the average demand in the system and can be determined from historical flow rate data. Ideally, the perturbation Q^*_D should be equal to the burst size. Since the size of the burst is not known in advance, a range of expected burst sizes can be selected and Q^*_D can be set to the average value of that range.

Sampling design is a set of monitoring points $Z = (M_1, \ldots, M_k)$ where M_j is the position of the j^{th} monitoring point ($j \in [1, k]$) and k is the number of monitoring points. Before a search for the optimal sampling design can

be performed, the points in the network where a measurement station can be installed have to be identified. Usually, all the nodes in the model of the network are considered as possible measurement point locations. Thus, the optimal sampling design task is to find the best possible distribution of k monitoring points among N nodes. The number of possible configurations is equal to:

$$n = \frac{N!}{k!(N-k)!}$$

When the number of possible configurations becomes too high to be handled by a fully enumerated analysis, combinatorial techniques can be used. In the analysis presented here, it was assumed that full enumeration is possible. Two performance indicators may be used to measure the merit of a particular sampling design:

(1) Cumulative sensitivity. Since the size of the burst is not known in advance, it is beneficial to maximize the range of the burst sizes that will be detected and located by the technique. The pressure change observed at the measurement point depends on the sensitivity of the pressure at that point to the burst. Larger sensitivity would allow for a pressure change induced by a smaller burst to be detected at the measurement point. Thus, to maximise the range of detectable bursts, the nodes with the maximum sensitivity have to be selected as measurement sites. The sum of sensitivities at all monitoring points in sampling design Z for every possible burst location can be used as a performance indicator for a particular sampling design:

$$\eta_{1,Z} = \sum_{i=1}^{N} \sum_{j=1}^{k} \left(S_{i,M_j}\right)^2 \tag{8.9}$$

The upper limit $\eta_{1,\max}$ can be derived from the sensitivity matrix by setting $k = N$. The lower limit $\eta_{1,\min}$ is zero.

(2) Uniqueness of the solution. The objective of the burst location algorithm is to identify a unique location in the network where the burst has occurred. Since all network nodes are used as candidate burst locations, there is a possibility of two candidate locations having the same value of the objective function. In that case, a non-unique location of the burst will be found. The objective function for a particular node depends on the difference between

the measured and simulated change in pressure ($\Delta H_M^m - \Delta H_M^{sim}$). Thus, if the simulated change in pressure at measurement point M has the same value for two burst candidate locations i and j, a unique location of the burst will not be found. The difference between simulated changes in pressure at the measurement point M for burst candidate locations i and j will depend on the size of the pressure change at the burst point and the sensitivities $S_{i,M}$ and $S_{j,M}$. Since the same size of the burst is assigned to all candidate locations while searching for the burst node, the difference between the objective function values for any two candidate nodes in the network will be proportional to the difference in the sensitivities $S_{i,M}$ and $S_{j,M}$. The uniqueness of the burst location can be maximised by maximising the probability that the difference between measurement point sensitivities for a pressure change at two different candidate burst locations will exceed a certain threshold value β:

$$\eta_{2,Z} = \Pr\left[\sum_{j=1}^{k}\left(S_{i,M_j} - S_{p,M_j}\right)^2 > \beta\right] \tag{8.10}$$

$$\forall i \in [1,N], \forall p \in [1,N], i \neq p$$

The choice of β can be based on the resolution of pressure measurements and the average expected size of the burst. The limits $\eta_{2,\max}$ and $\eta_{2,\min}$ are assumed to be 1 and 0, respectively.

To combine the two performance indicators (Equations 8.9 and 8.10) into one objective function a compromise programming approach is used. Compromise programming is a multi-criterion distance-based technique designed to identify compromise solutions. The following objective function is used:

$$OF_Z = \sqrt{\sum_{n=1}^{2} w_n \left(\frac{\eta_{n,Z} - \eta_{n,\max}}{\eta_{n,\min} - \eta_{n,\max}}\right)^2} \tag{8.11}$$

where w_1 and w_2 are the weights for η_1 and η_2, respectively. The distribution of the measurement points Z that gives the minimum value of OF_Z is selected as the optimal measurement placement.

As stated earlier in the section, the optimal distribution of measurement stations has to be evaluated to decide whether the additional measurement point

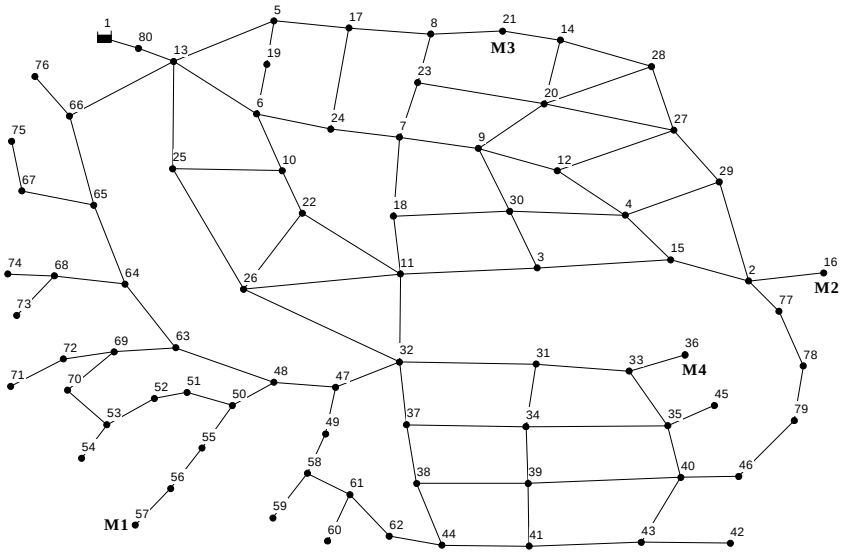

Figure 8.4: Layout of the pipe network used for the case study.

is required. The probability of finding the unique burst location (Equation 8.10) as well as the sum of sensitivities (Equation 8.9) can be used to evaluate a particular sampling design.

8.5 Case study

The example network model shown in Figure 8.4 was used to verify the proposed method for burst detection and location. The network has 108 pipes and 79 nodes. Pipes have diameters between 100 and 200 mm, lengths between 40 and 210 m and a roughness height of 0.2 mm. The node elevations are in the range of 140 to 160 m. The network is fed from a fixed head (56 m) reservoir. The topology of the network was chosen to represent both looped and branched structures. The case study network can be treated as a single DMA, since it has only one supply point (the tank) and all demand is distributed within the network.

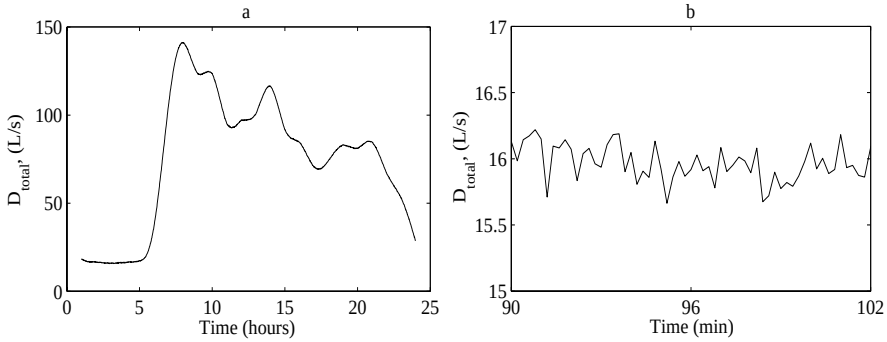

Figure 8.5: (a) 24-hour demand curve and (b) zoom in on the demand curve to show noise characteristics. 1 minute sampling time.

Generation of demand pattern

The burst is detected from the measurement of the flow rate at the input of the DMA. Since the simulation case study is used to validate the proposed technique, the flow rate measurement was generated artificially. The test network is assumed to supply 300 households with a typical residential demand characteristics. A 1 minute sampling interval was used to generate a 24-hour demand pattern. The experimental residential consumption data presented in (Guercio et al.; 2001) was used as a guideline for selecting hourly demand factors. Interpolation was then used to generate the demand pattern having 1 minute sampling interval. Additionally, white noise was added to the demand pattern as shown in Figure 8.5b to represent discrete demand changes corresponding to household appliance use as described by (Buchberger and Nadimpalli; 2004). The generated demand pattern was used to substitute the flow rate measurement.

Measurement placement

The placement of pressure monitoring stations was selected following the procedure described in Section 8.4. To investigate the influence that different numbers of measurement stations have on the performance of the failure detection and location technique, four cases were tested - one, two, three and

No. of sites	No. of configurations	β	w_1	w_2	Selected nodes
1	79	0.00008	0.5	0.5	57
2	3,081	0.00016	0.5	0.5	16 57
3	79,079	0.00024	0.5	0.5	16 21 57
4	1,502,501	0.00032	0.5	0.5	16 21 36 57

Table 8.1: Parameters and results of the search for optimal measurement placement

four pressure measurement stations. Parameters used in the search for an optimal measurement distribution as well as results of the search are summarised in Table 8.1 Selected nodes are labelled as measurement stations M1 (node 57), M2 (node 16), M3 (node 21) and M4 (node 36) as shown in Figure 8.4.

Generation of measured data

To simulate a burst, a change in a flow rate was added on the derived diurnal flow rate pattern (Figure 8.1a,b). The change had a size corresponding to the actual size of the burst and a slope being proportional to the burst opening time. The measured pressure changes at the monitoring points were obtained by simulating a burst of the actual size at the actual location and subtracting pressure values before and after the burst event: $\Delta H^m_{M_j} = H^m_{M_j}(\text{after burst}) - H^m_{M_j}(\text{before burst})$ for all measurement sites $j \in [1, k]$. The precision of the numerically generated measurement data was the same as the precision of the simulated data. Although using modern data acquisition hardware can allow for a reasonably high precision, it is not likely that real pressure measurements would have the same precision as the simulated values. As a compromise, a resolution of 0.1 kPa was selected to represent the real measurements. All the numerically generated measurement data was rounded to the precision of 0.1 kPa.

Detection of bursts that occur at different times of the day, with different sizes and opening times

The variable drift value for the CUSUM test is obtained by dividing a 24-hour period into two parts - night (22:00-06:00 hours) and day (6:00-22:00

Burst No.	Actal burst parameters			Detected burst parameters		
	Time of burst	Opening, min	Size, L/s	Time of burst	Opening, min	Size, L/s
1	4:20	3	10	4:20	3	10.2
2	6:00	2	15	6:00	2	14.76
3	9:00	8	20	9:00	8	19.07
4	20:00	5	12	20:00	5	12.21
5	22:30	1	5	22:30	1	4.78

Table 8.2: Burst detection tests and results

hours). The drift was chosen to be larger than the maximum changes in flow rate during the night and day time intervals and set to 0.939 and 1.763 L/s. The threshold was set to twice the drift value, i.e. 1.878 and 3.526 L/s for night and day parts respectively.

The CUSUM change detection test with parameters selected as above was applied to the generated flow rate measurement that contained a burst signature. Results are summarised in Table 8.2. Five different bursts with sizes between 5 and 20 L/s (6 to 25 % of the average total demand of the DMA) and opening times in the range of 1 to 8 minutes were successfully detected. Errors in the estimated size of the burst were less than 2.5%.

Location of bursts that occur at nodal locations

To test the ability of the proposed technique to locate bursts, a series of tests were performed. The assumption was made that only one burst at a time occurs within the network. The search for the burst location was performed as shown in Figure 8.2. The objective function was calculated for all burst candidate locations (all nodes in the network) and the node having the smallest value of the objective function was selected as the burst location. All possible burst locations were tested for the five different bursts described in the previous section. Each of the five bursts was tested by placing it at all 79 nodes in the network (one node at a time). The same procedure was repeated using one, two, three and four measurement stations. Results are summarised in Table 8.3.

Measurement location	Burst No.	Actual burst node	Burst location [% (No. of tests)]		
			found	non-unique	not found
57	1	1-79*	75 (59)	30 (24)	25 (20)
	2	1-79*	82 (65)	30 (24)	18 (14)
	3	1-79*	87 (69)	30 (24)	13 (10)
	4	1-79*	84 (66)	23 (18)	16 (13)
	5	1-79*	66 (52)	18 (14)	34 (27)
16,57	1	1-79*	95 (75)	28 (22)	5 (4)
	2	1-79*	98 (77)	28 (22)	2 (2)
	3	1-79*	92 (73)	24 (15)	8 (6)
	4	1-79*	91 (72)	17 (13)	9 (7)
	5	1-79*	87 (69)	18 (14)	13 (10)
16,21,57	1	1-79*	96 (76)	28 (22)	4 (3)
	2	1-79*	95 (75)	25 (20)	5 (4)
	3	1-79*	90 (71)	14 (11)	10 (8)
	4	1-79*	91 (72)	17 (13)	9 (7)
	5	1-79*	90 (71)	18 (14)	10 (8)
16,21,36,57	1	1-79*	100 (79)	28 (22)	0(0)
	2	1-79*	100 (79)	28 (22)	0 (0)
	3	1-79*	89 (70)	9 (7)	11 (9)
	4	1-79*	87 (69)	6 (5)	13 (10)
	5	1-79*	91 (72)	13 (10)	9 (7)

* all 79 nodes were tested as burst location, one node at a time

Table 8.3: Burst location tests and results for bursts that occur at network nodes

Burst	Burst pipe	Burst location along the pipe
B1	Between nodes 32 and 11	100 m from node 32
B2	Between nodes 63 and 64	60 m from node 63
B3	Between nodes 17 and 24	130 m from node 17
B4	Between nodes 39 and 40	100 m from node 39

Table 8.4: Bursts along pipes

As mentioned earlier, the numerically generated pressure measurement data was rounded to the precision of 0.1 kPa to represent real pressure measurements. As a result of the testing, for each setup with different number of measurement points and different type of the burst, the number of tests for which the correct burst location was found is listed in Table 8.3. For some bursts, a non-unique solution was found. The number of such cases is indicated in Table 8.3. Finally, the number of tests for which the correct location of the burst was not found is given. As can be observed, the rate of successfully located bursts varies for different burst types and is on average equal to 78.8% for one measurement station, 92.6% for two measurement stations, 92.4% for three measurement stations and 93.4% for four measurement stations. The unique location was found for 70 to 94% of the cases. When a non-unique location was found, 2 to 4 nodes had the same objective function. Further analysis showed that nodes with the same values of the objective function were located at the same dead-end branch of the network.

Location of bursts that occur at non-nodal locations

To assess the performance of the burst location technique for bursts that occur along pipes in the network (not at the candidate burst locations), four burst locations along different pipes in the network as described in Table 8.4 were tested. Five different burst types (Table 8.2) were simulated at each location and the sequence was repeated for the setup with one, two, three and four measurement stations. The results of the burst location are shown in Table 8.5.

Results show that using only one pressure monitoring point gives quite a high error in the location of bursts along pipes. The average error is decreasing

Measurement location	Burst No.	Error in burst location (m)				
		Burst B1	Burst B2	Burst B3	Burst B4	Average
57	1	943.6*	1.3	12	98*	277
	2	903.6*	2.6	20	117*	
	3	776*	6.5	14	355*	
	4	774*	9.1	10	355*	
	5	738*	10.4	30	355*	
16 57	1	2	1.3	54	118*	47
	2	8	2.6	50	125*	
	3	12	7.8	42	131*	
	4	10	9.1	40	131*	
	5	8	11.7	42	132*	
16 21 57	1	2	1.3	8	118*	46
	2	8	2.6	58	127*	
	3	12	7.8	50	131*	
	4	10	7.8	44	131*	
	5	8	11.7	50	132*	
16 21 36 57	1	14	1.3	8	20.7*	30
	2	8	2.6	56	8.3*	
	3	6	7.8	50	37*	
	4	4	9.1	44	34*	
	5	0	11.7	48	214*	

* derived burst location was not on the same pipe as the actual burst. The shortest path was used to calculate the error

Table 8.5: Burst location tests and results for bursts that occur at non-nodal locations

with increasing number of measurement points and is as low as 30 m for the setup with four pressure measurement stations.

8.6 Uncertainty analysis

To evaluate performance limits of the proposed burst detection and location technique, an uncertainty analysis was performed using the example network from the case study described in the previous section with four pressure measurement points. In the case of a real application, there are two potential sources of errors - measurement errors and model errors. Tradi-

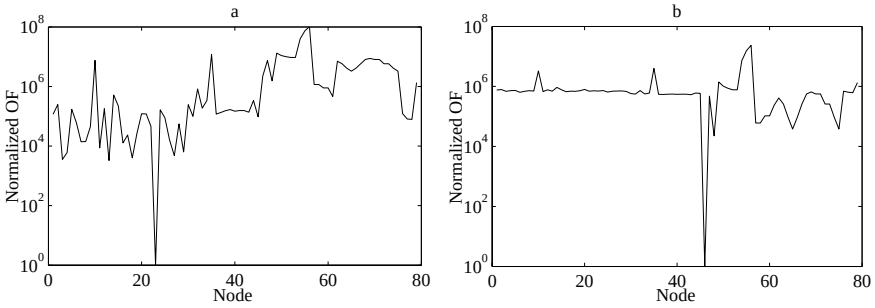

Figure 8.6: Normalized mean values of the OF for all candidate burst locations for a burst at (a) node 24 and (b) node 47

tionally, measurement errors are considered to be caused by measurement equipment and are typically defined as a percentage of the measured value. Model errors can be attributed to the uncertainty of pipe friction coefficients and demand distribution. A third type of error is introduced for a proposed application - error in the detected changes of measured values. Both changes in flow and changes in pressure have to be determined from the measured traces, which include oscillations caused by normal demand dynamics. Consequently, some errors in estimated changes ΔQ^m and ΔH^m are expected. This error will not be proportional to the actual value that is derived and can be expressed in the units of the parameter that is measured. Since the precision of the burst size derived by the burst detection and location technique is not crucial, only the derived burst location will be considered in the uncertainty analysis. Instead of analysing the effect of different types of errors separately, a lumped error e is introduced that accounts for measurement, model and change detection errors collectively. It is assumed that e will be normally distributed with zero mean and standard deviation $\sigma_e = b$ and will have pressure units (kPa).

The value of the lumped error is randomly selected from the distribution and added to the objective function (Equation 8.6):

$$OF_i = \sum_{j=1}^{k} \left(\Delta H^m_{M_j} - \Delta H^{sim}_{M_j} + e \right)^2 \qquad \forall i \in [1, N] \tag{8.12}$$

As noted earlier in this chapter, the measured changes in pressure are rounded

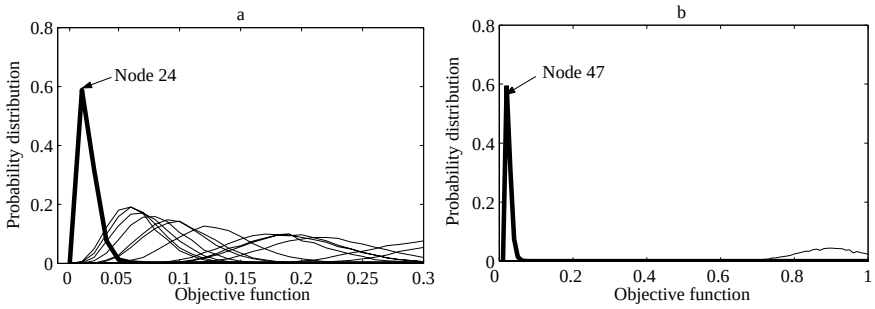

Figure 8.7: Distribution of objective function values for different candidate burst locations for a burst at (a) node 24 and (b) node 47. Perturbation $b = 0.5$ kPa was applied. A step of 0.01 was used in the distribution.

to the precision of 0.1 kPa to represent real measurements. Rounded values are used to calculate the objective function while searching for the burst location. To illustrate results of the search, Figure 8.6 shows values of the calculated objective function for all candidate locations in the case when the burst occurs at node 24 (a) and at node 47 (b). Objective function values are normalized applying division by the optimal (minimum) value. As shown in Figure 8.6, the correct location of the burst can be easily identified. Actually, values of the objective function for all other candidate locations are at least three orders of magnitude larger.

To investigate the effect of uncertainty, the lumped error e was introduced with the standard deviation $b = 0.5$ kPa. The same nodes (24 and 47) were used as an example. A Monte Carlo type simulation was performed by randomly selecting values of e from a normal distribution with zero mean and standard deviation equal to b. 10000 runs were executed and the probability distributions of the objective function values for all candidate burst locations were derived. In Figure 8.7, distributions of the objective function values are shown for burst at node 24 (a) and 47 (b). Only low values of the objective function are shown in figures. In both cases, the actual node of the burst has the objective function distributed close to zero. For the burst at node 24, the distribution of the objective function of the burst node slightly overlays with distributions of some other nodes. However, the probability of node 24 having the best fit is still considerably larger. In case of a burst at node 47, the

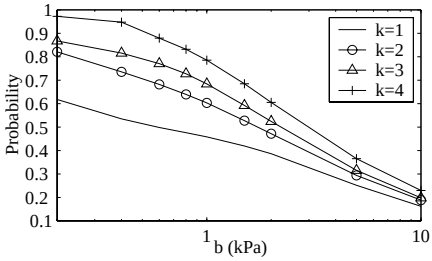

Figure 8.8: Effect of perturbation b on the probability of successful burst location for different number of measurement points k

distribution of the objective function does not overlap with the distribution of any other candidate node.

To evaluate the influence of the error on the overall performance of the burst location technique, all possible burst locations were tested and the probability of finding the correct burst location was calculated. The error term was added to the objective function for each burst location as shown in Equation 8.12 and the search was performed. The probability of finding the correct burst location was calculated as the ratio between the cases where the burst was successfully located and the total number of possible burst locations (the number of nodes in the network). The procedure was repeated 10000 times and an average value was derived. The described analysis was performed for a number of different error sizes ($d \in [0\ \ 10]$ kPa). The obtained results are shown in Figure 8.8 ($k = 4$). As can be expected, increasing the size of the error decreases the probability of successful location of the burst.

Effect of the number of measurement points

To evaluate the influence of the number of measurement sites on the sensitivity of the proposed technique to the error, the relationship between the probability of finding the correct burst location and the size of the lumped error was derived for one, two, three and four pressure monitoring stations. The results are presented in Figure 8.8.

Increasing the number of measurement stations reduces the sensitivity of the burst location technique to the error. The exponential character of the curves in Figure 8.8 becomes more evident when a larger number of measurement points are used. This means that, when more pressure monitoring stations are installed, the probability of finding the correct burst location will remain the same for a wider range of error sizes. Figure 8.8 also shows that, in case when no error is added (only the rounding of the measured values) the probability of successfully locating the burst is higher for a larger number of measurement stations. That was already identified earlier in the chapter (Table 8.3).

The performance, application and implementation of the steady-state analysis based pipe failure monitoring technique described here are discussed in Chapter 10. The discussion in Chapter 10 also considers the unsteady-state analysis based burst monitoring approach, which is presented in Chapter 9.

Chapter 9

Failure monitoring, detection and location based on unsteady-state analysis

In this chapter, the concept of a burst monitoring system for water distribution networks is presented. The proposed approach offers a low-cost alternative to expensive acoustic monitoring systems and fast reaction-to-failure, which is missing in currently practiced DMA analyses. The approach is based on continuous monitoring of pressure at a number of locations throughout the network and analysis of burst-induced transient waves. Results from field validation as well as uncertainty analysis are included in the chapter. The discussion of the performance, application and implementation of the technique can be found in Chapter 10.

9.1 Methodology

The technique presented in this chapter originates from the burst detection and location method described in Chapter 6. In the case of a sudden pipe rupture a transient wave is generated and propagates throughout the network away from the burst point. If the pressure is continuously measured at two or more points within the network and measurements are synchronised in time, the arrival times and magnitudes of the burst-induced wave at the measure-

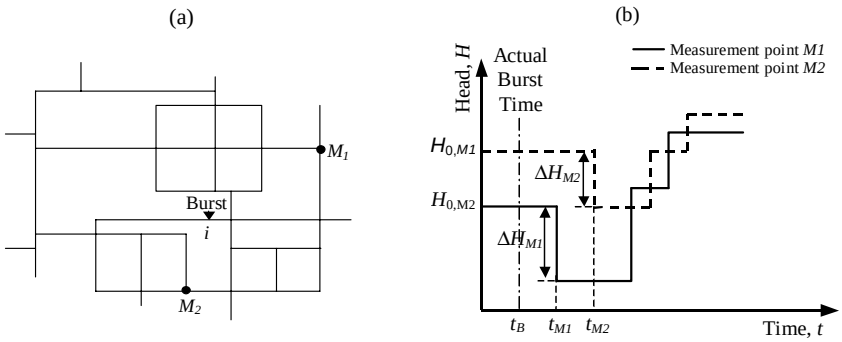

Figure 9.1: (a) Schematic view of the burst monitoring system in a water distribution network and (b) generalized burst-affected pressure traces at measurement points

ment points can be used to derive the location of the burst. The schematic view of the burst monitoring system and the generalised pressure traces at two measurement points are shown in Figure 9.1. The burst occurs at time t_B, which is assumed to be unknown. Two parameters can be obtained from the pressure trace at each monitoring point - transient wave arrival time, t_M, and the magnitude of the wave, ΔH_M.

Timing of transient waves

If the pressure is measured at points M_1 and M_2, the travel times from the burst origin to the measurement sites $t_{M_1} - t_B$ and $t_{M_2} - t_B$ cannot be determined. However, since the measurements are synchronised in time, the difference between the arrival times $t_{M_1} - t_{M_2}$ is known. Using a model of the network and the method of characteristics (MOC) (Wylie and Streeter; 1993) the shortest transient wave travel time between any two points within the network $\tau_{i,j}$ can be derived. The wave travel time for a single pipe is equal to

$$\tau_p = \frac{L_p}{a_p} \tag{9.1}$$

where L_p is the length of the pipe and a_p is the wave speed of the pipe. One or more pipes connect any two points i and j in the network. The transient wave travel time between those points $\tau_{i,j}$ is equal to the sum of the wave

travel times τ_p of all pipes connecting i and j. In case when alternative routes between two points exist, the route with the shortest travel time is selected. As τ_p depends on both length of the pipe and wave speed (Equation 9.1), the route having the shortest travel time does not necessarily correspond to the shortest distance between the nodes. Although, theoretically it is possible that the transient travel time along two alternative routes between nodes i and j will be exactly the same, it is highly unlikely that such situations will occur in a real network. Wave speed values can vary considerably for different pipe materials and roughness and the topology of a network is usually asymmetrical, which suggests that the probability of having a unique route between two nodes with the shortest wave travel time is high.

If a burst occurs at node i, the wave arrival times at two measurement points t_{M_1} and t_{M_2} are measured and the wave travel times $\tau_{i,j}$ and $\tau_{i,k}$ are calculated, the following equation holds:

$$(t_{M_1} - t_{M_2}) - (\tau_{i,M_1} - \tau_{i,M_2}) = 0 \tag{9.2}$$

where t_{M_1}, t_{M_2} are the measured wave arrival times at points M_1 and M_2, τ_{i,M_1} and τ_{i,M_2} are the calculated wave travel times from point i to points M_1 and M_2, respectively.

Magnitude of transient waves

While propagating in the network, the negative pressure wave initiated by a burst may interact with a number of pipe junctions before it reaches the measurement points. A certain portion of the wave is reflected at each junction, while the rest is transmitted. Since the route between any two points i and j, corresponding to the shortest travel time $\tau_{i,j}$, can be derived for a particular network, the wave transmission coefficient $T_{i,j} = \Delta H_j / \Delta H_i$ can be calculated. ΔH_i and ΔH_j represent the transient wave magnitudes at points i and j respectively. $T_{i,j}$ is the multiplication of transmission coefficients at every junction that the wave has to pass while propagating from point i to point j. Using the analysis of Wylie and Streeter (1993), the wave transmission coefficient T_n can be derived (see Appendix C). For a general junction n, connecting P pipes, in the case when the wave is approaching from pipe 1,

T_n is equal to

$$T_n = \frac{(H_J - H_0)}{(H_W - H_0)} = \frac{\dfrac{2A_1}{a_1}}{\displaystyle\sum_{k=1}^{P} \frac{A_k}{a_k}} \tag{9.3}$$

where H_0 is the initial head at the junction, H_J is the head at the junction after the wave has interacted with it and H_W is the magnitude of the initial wave. A_i is the cross-sectional area of the i^{th} pipe. Additionally, the friction in the pipes will also affect the transmission coefficients. However, the effect of friction is neglected in Equation 9.3. In the case when the burst occurs at node i, the following relation should be true

$$\frac{\Delta H_{M_1}}{\Delta H_{M_2}} - \frac{T_{i,M_1}}{T_{i,M_2}} \approx 0 \tag{9.4}$$

where ΔH_{M_1} and ΔH_{M_2} are pressure wave magnitudes registered at measurement points M_1 and M_2, T_{i,M_1} and T_{i,M_2} are transmission coefficients for a wave travelling from point i to points M_1 and M_2 respectively. The effects of friction along the pipe length and at the junctions have been neglected and therefore the left-hand-side of Equation 9.4 will be close, but not necessarily equal to zero.

To estimate the size of a burst, the magnitude of the burst-induced pressure change at the burst location has to be known. It is back-calculated from Equation 9.4:

$$\Delta H_i = \Delta H_{M_1} \frac{1}{T_{i,M_1}} = \Delta H_{M_2} \frac{1}{T_{i,M_2}} \tag{9.5}$$

Once the head change ΔH_i is known, the approximate burst size can be calculated using the Joukowsky pressure rise formula combined with the orifice equation (see Appendix D).

$$C_d A_0 = \frac{A|\Delta H_i|\sqrt{2g}}{a\sqrt{H_0 - |\Delta H_i| - z}} \tag{9.6}$$

where H_0 is the head at the burst point before the burst event and $C_d A_0$ is a lumped discharge parameter describing the size of the burst. Since friction at the junction and along the pipes is not considered, Equation 9.6 will not

provide the exact size of the burst. However, the main objective of burst monitoring is to locate the burst and evaluate the severity of it, not to determine the exact size.

9.2 Burst detection and location system

Based on the principles described in the previous section, the complete structure of the burst detection and location system was derived and is shown in Figure 9.2. The algorithm can be divided into two parts: (a) pressure is continuously monitored at a monitoring station and, in case of a detected burst-induced wave, arrival time and magnitude of the wave are sent to the central unit (b) data sent from all measurement stations are processed at the central unit and burst location and size are derived.

Monitoring pressure for burst events

To locate the burst, a transient wave has to be detected at two or more measurement points. The cumulative sum (CUSUM) change detection test (Page; 1954) may be used to monitor the measured pressure for a negative burst-induced pressure wave. The CUSUM test has been extensively applied for change detection in different time series analysis problems (Basseville and Nikiforov; 1993). The measured pressure trace contains a certain level of measurement noise and other oscillations that are caused by changes in demand or other operational actions in the network. The term hydraulic noise can be used to collectively describe variations of the pressure trace during normal operation of the network. To reduce the level of hydraulic noise, pre-filtering is applied using an adaptive Recursive Least Squares (RLS) filter. The filter estimates the signal θ_t from the measurement H_t (containing noise) as

$$\theta_t = \lambda\theta_{t-1} + (1-\lambda)H_t \tag{9.7}$$

where the parameter $\lambda \in [0, 1)$ is the forgetting factor that limits the smoothing effect of the filter. Depending on changes in the measured data, the forgetting factor is exponentially adjusted in real-time between selected minimum and maximum values. In other words, the smoothening effect of the

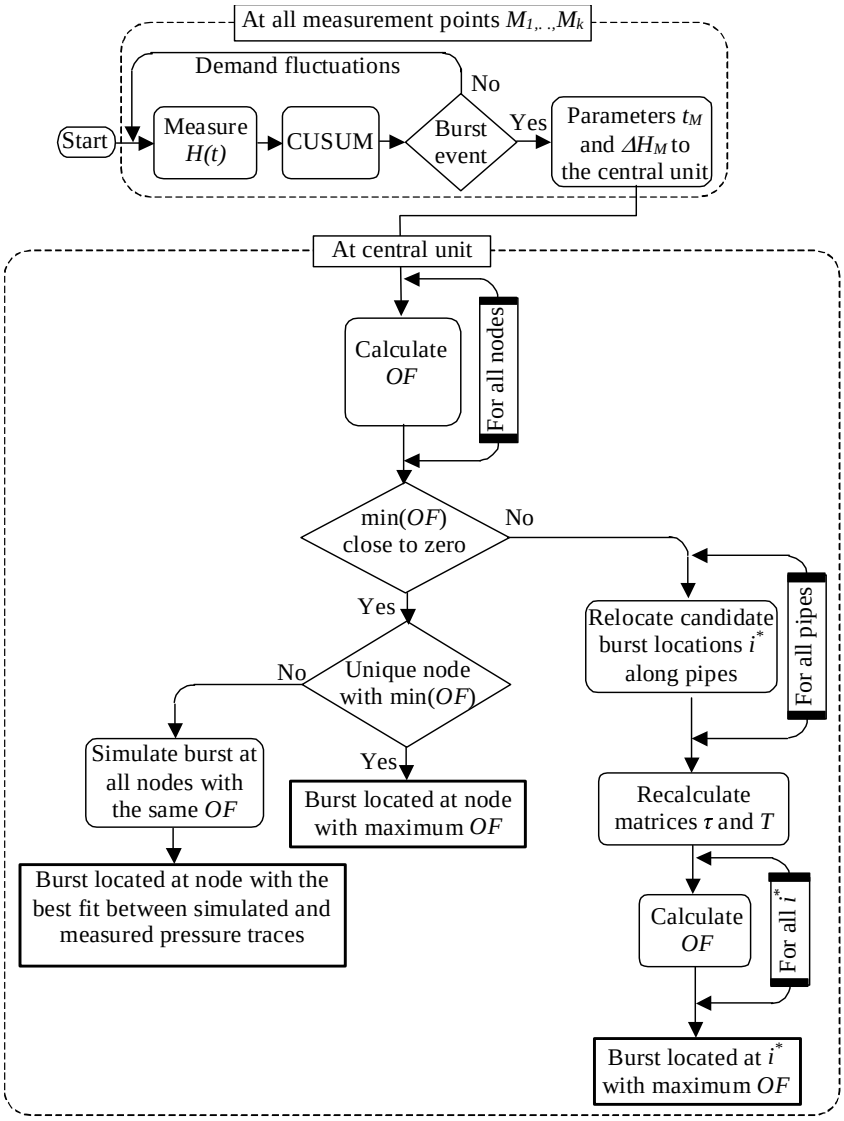

Figure 9.2: Structure of continuous burst monitoring algorithm

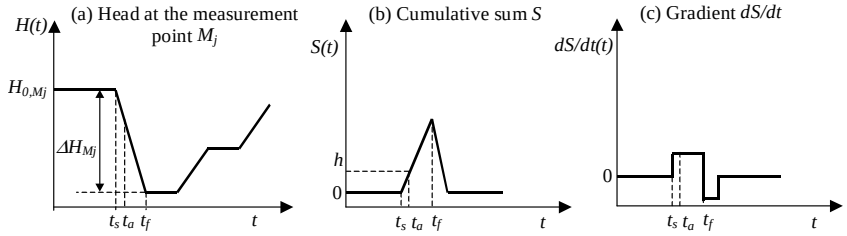

Figure 9.3: Generalised traces of (a) head at burst point and (b) cumulative sum and (c) gradient of cumulative sum

filter is controlled based on the size of changes in the measurements. The residuals $\epsilon_t = \theta_t - \theta_{t-1}$ are fed into a CUSUM test, which is used to determine whether a change has occurred in the measured signal. Mathematically, the CUSUM test is formulated as the following time recursion:

$$\begin{aligned} &S_0 = 0 \\ &S_t = \max(S_{t-1} + \epsilon_t - \nu, 0) \\ &\text{if } S_t > h \text{ then issue alarm and set } t_a = t \end{aligned} \tag{9.8}$$

where S_t is the cumulative sum value at time t, h and ν are threshold and drift parameters, respectively. For every sample of data, the part of the change in signal ϵ_t that exceeds the drift value ν (the expected variation) is added to the cumulative sum S_t. When S_t reaches the threshold value h, the alarm is issued and the time of change t_a is recorded (Figure 9.3). To obtain the actual transient wave arrival time t_{M_j} and the transient wave magnitude at the measurement point ΔH_{M_j} times t_s and t_f have to be identified. As shown in Figure 9.3, time t_s corresponds to the time when the slope dS/dt becomes positive and time t_f corresponds to the time when dS/dt becomes zero or negative. Then $t_{M_j} = t_s$ and $\Delta H_{M_j} = H_{M_j}(t_s) - H_{M_j}(t_f)$.

The performance of the CUSUM change test is controlled by two parameters - threshold h and drift ν. Since the size and the opening time of a burst are not known prior to the burst event the shape and the magnitude of the burst-induced change in the measured pressure cannot be predicted. Therefore the CUSUM test parameters have to be tuned for as wide a range of bursts as possible. For a given set of CUSUM parameters, the minimum size of the change in pressure that will be detected ΔH_{min} and the longest opening time

of a burst that will be detected $t_{opening,max}$ can be calculated:

$$\Delta H_{min} = h + \frac{\nu t_{opening}}{\Delta t} \tag{9.9}$$

$$t_{opening,max} = \frac{\Delta H - h}{\nu} \Delta t \tag{9.10}$$

where Δt is a sampling interval of the pressure measurements. The minimum size of the burst that will be detected can be calculated by putting ΔH_{min} into Equation 6.4. Equations 9.9 and 9.10 indicate that successful detection depends on the combination of both size and opening time of the burst. Smaller values of drift and threshold will extend the range of detectable burst sizes and opening times. However, the success rate of the technique is not the only performance indicator. Another important factor is the false alarm rate. False alarms can be caused by oscillations in the pressure measurements. which are the result of measurement noise of legitimate hydraulic activity in the system. Both the level of measurement noise and typical operational changes in pressure can be evaluated from historical data. The combination of h and ν has to be chosen so that the rate of false alarms is minimised.

Search for burst locations

Once a burst event is detected in the pressure measurements at two or more monitoring stations, identified wave arrival times and magnitudes are sent to the central unit where the search for the burst location is performed. The search space is defined by selecting candidate burst locations. The number of candidate burst locations is chosen arbitrary. However, it is logical to use the nodes in the network model as candidate burst locations. A network model is then used to calculate transient wave travel times τ_{i,M_j} and transmission coefficients T_{i,M_j} for $\forall i \in [i, N]$ and $\forall k \in [1, k]$ where N is the number of nodes in the network model and k is the number of measurement stations. Resulting matrices τ and T with sizes $(N \times N)$ together with results from the CUSUM test are used to calculate two objective functions, which are based on Equations 9.2 and 9.4:

$$OF1_i = \sum_{j=1}^{k-1} \sum_{p=2}^{k} \left[\left(t_{M_j} - t_{M_p} \right) - \left(\tau_{i,M_j} - \tau_{i,M_p} \right) \right]^2 \ \forall i \in [1, N] \tag{9.11}$$

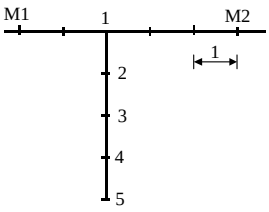

Figure 9.4: Dead-end branch with all nodes having the same OF value

$$OF2_i = \sum_{j=1}^{k-1} \sum_{p=2}^{k} \left(\frac{\Delta H_{M_j}}{\Delta H_{M_p}} - \frac{T_{i,M_j}}{T_{i,M_p}} \right)^2 \qquad \forall i \in [1, N] \tag{9.12}$$

Both $OF1$ and $OF2$ have to be minimised in order to find the burst node. To combine the two objective functions (Equations 9.11 and 9.12) a compromise programming approach is used. Compromise programming is a multi-criterion distance-based technique designed to identify compromise solutions. The following objective function is computed:

$$OF_i = \sqrt{\sum_{n=1}^{2} w_n \left(\frac{OFn_i - OFn_{\min}}{OFn_{\max} - OFn_{\min}} \right)^2} \tag{9.13}$$

where w_1 and w_2 are the weights of $OF1$ and $OF2$ respectively. The objective function is calculated for all burst candidate locations and the node having the smallest value of the OF is declared to be the burst position.

Non-unique solution. In some cases more than one candidate burst location will have the minimum value of the objective function. In such situation, a unique burst location cannot be identified from the search results. A particular example of such a problem is a dead-end branch of a network. If burst occurs somewhere along the branch, all candidate burst locations at that branch will have the same (optimal) objective function. To illustrate this situation, a simple example network, consisting of one tee-junction, is shown in Figure 9.4. The distance between any two adjacent nodes is equal to one and the wave speed is 1000 m/s for all pipes. If a burst has occurred at node 1, the transient wave travel times will be $\tau_{1,M_1} = 0.2s$ and $\tau_{1,M_2} = 0.3s$. The pressure is monitored at points M_1 and M_2. If the burst has occurred at node 5, the transient wave travel times will be $\tau_{5,M_1} = 0.6s$

and $\tau_{5,M_2} = 0.7s$. However, since the time of the burst event is not known, the difference between the travel times is used to find the burst location (Equation 9.11). This difference is the same for both nodes 1 and 5, i.e. $\tau_{5,M_1} - \tau_{5,M_2} = \tau_{1,M_1} - \tau_{1,M_2} = 0.1s$. The same is true regarding the ratio of wave transmission coefficients that is used to calculate $OF2$ (Equation 9.12): $T_{1,M_1}/T_{1,M_2} = T_{5,M_1}/T_{5,M_1}$. In fact, the same situation will apply for any node on the dead-end branch. As a result, the actual burst location cannot be identified. The same situation might arise when the burst occurs along a single pipe that is a part of a loop in the network. If the shortest path from the burst point to all measurement stations is going along the same pipe and in the same direction, all points on that pipe will have the same value of the objective function.

The branch or the pipe where the burst has occurred is still identified and the model can be used to find the exact location of the burst. The inverse fitting approach is an effective tool in this situation, since the search space is well defined. The burst is simulated at every node of the branch and simulation results are compared to measured traces. The node having the best fit between simulated and measured responses is the actual burst location. Alternatively, once the bursting branch is identified, closer-range leak detection techniques may be applied.

Extension for bursts that occur along pipes. Based on the knowledge available about different types of pipe failure, which was summarized in Chapter 2, it is reasonable to assume that bursts may occur both at the junctions (nodes) and along the pipes (in between nodes). When using the burst location algorithm described earlier in this section, it was assumed that the true burst location was one of the candidate burst locations. However, in cases when a burst occurs along a pipe and not close to a node, the precision of the derived burst location might be low or, in some cases, the burst might not be located correctly. The difference between the actual and derived burst parameters affects the value of the objective function. Ideally, when burst occurs at the node, the objective function will be equal to zero. In reality, this value will be slightly larger, since frictional effects are not accounted for and some imprecisions in parameters that are derived from pressure measurements are expected. However, a value of the objective function considerably larger that zero indicates that the burst has not occurred at the node. In that

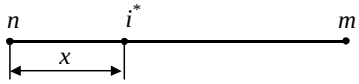

Figure 9.5: Relocation of candidate burst locations

case, the algorithm is extended as shown in Figure 9.2. The candidate burst locations are relocated from network nodes to new positions along pipes as shown in Figure 9.5. In Figure 9.5, n and m are any two network nodes adjacent to the same pipe, i^* is the new burst candidate location and x is the distance from node n to i^*. Distances x are derived for each pipe separately using the objective function $OF1$ (Equation 9.11):

$$x_p = \frac{OF1_n}{OF1_n + OF1_m} L_p \tag{9.14}$$

where p is any pipe in the network model, x_p is the distance from node n to the new candidate burst location i^* and L_p is the length of the pipe. Once new burst candidate locations are found for all pipes, matrices τ and T are recalculated and the search for the burst location is repeated using Equations 9.11, 9.12 and 9.13.

9.3 Sources of uncertainty

There are two main sources of errors that can limit the performance of the proposed failure detection and location technique: (1) measurement error and (2) model error. Since parameters of the burst-induced wave are derived from measured traces and not measured directly, the measurement error will include both instrument error and the change detection error. Actually, the error associated with the change detection test is likely to be considerably higher than the instrument error and therefore latter can be neglected. The model error is dependent on the reliability of the information about network topology and pipe characteristics. There is a number of parameters that can contain errors, such as lengths of pipes, wave speed values, materials, topology, etc. Model errors are affecting the values of wave travel times, τ, and wave transmission coefficients, T, between all candidate burst locations and

measurement points. Measurement errors are affecting values of wave arrival times, t, and wave magnitudes, ΔH, for all measurement points. However, due to the character of the objective functions, which are used in the search for the burst location (Equations 9.11, 9.12 and 9.13), measurement and model errors are affecting results of the burst detection and location collectively. Thus, an uncertainty analysis can be performed using only one common error that represents both the measurement and the model errors. The uncertainty analysis for the proposed technique was conducted using the example network and is described later in this chapter (Section 9.6)

9.4 Optimal placement of measurement stations

The optimal placement of the pressure monitoring points is an important factor, which influences the performance of the proposed technique. There are two decision variables - the number of measurement stations and the set of measurement positions. A number of measurement positioning (also called sampling design) approaches are described in the literature (Bush and Uber; 1998; Kapelan et al.; 2003b; Vítkovský et al.; 2003). Although these methods are designed for a specific problem, such as network model calibration, leakage detection, etc., they all involve a search procedure. A search is performed where an objective function is calculated for every possible set of measurement positions (sampling design) based on problem-specific criteria.

Selection criteria

Sampling design is a set of measurement stations $Z = (M_1, \ldots, M_k)$ where M_j is the position of the j^{th} measurement station ($j \in [1, k]$). Thus, the optimal sampling design task is to find the best possible distribution of k measurement stations among N nodes. Two performance indicators may be used to measure the merit of a particular sampling design:

(1) Observability of the network. While propagating throughout the network, the burst-induced transient pressure wave is reflected at pipe junctions and other network elements as well as dampened by friction. As a result,

after traveling a certain distance, the transient wave magnitude will decay to zero. In other words, there is a certain region around the burst point outside of which the transient wave is completely dampened and the wave can only be detected if the pressure is measured within the region. The size of that region is a function of the initial magnitude of the burst-induced wave, which depends on the size of the burst. Since the size of the burst is not known in advance, the region where the burst-induced wave can be detected cannot be determined. As an example, if the wave transmission coefficient between the burst point and the measurement station is 0.1, the 50 kPa wave generated at the burst point will have a magnitude of 5 kPa at the measurement station. Such a small change in pressure might be hard to distinguish from the pressure oscillations that are part of the normal operation of the network. However, if a 200 kPa wave is generated at the burst point, it will be measured as a 20 kPa change in pressure at the measurement station. Thus, two limit values have to be selected in order to define the propagation region of the burst-induced wave - the minimum change in pressure that can be measured at the measurement station M_j ($\Delta H_{M_j,min}$) and the minimum size of the burst that should be detected ($\Delta H_{B,min}$). Knowing these two parameters, the wave propagation region for a specific burst location can be derived. The corresponding regions can be derived for all measurement stations by selecting nodes with

$$T_{i,M_j} > \frac{\Delta H_{M_j,min}}{\Delta H_{B,min}} \qquad \forall i \in [1, N] \tag{9.15}$$

For successful location of a burst, a burst-induced wave should be detected at two (or more) measurement stations. This condition together with the one from Equation 9.15 can be used to check the observability of the network for a particular placement of measurement stations. The observability here is the probability that a burst that occurs at any location within the network will be detected at two or more measurement stations. It has a value between 0 and 1, where 1 represents the optimal case.

In some cases, limits $\Delta H_{M_j,min}$ and $\Delta H_{B,min}$ may not be available. From Equation 9.15 it can be seen that a higher value of the wave transmission coefficient T allows for higher $\Delta H_{M_j,min}$ and lower $\Delta H_{B,min}$, which improves the performance of the technique. Therefore, the observability of the network can be maximized by maximizing the sum of wave transmission co-

efficients at all monitoring points in sampling design Z for every possible burst location:

$$\eta_{1,Z} = \sum_{i=1}^{N} \sum_{j=1}^{k} T_{i,M_j} \tag{9.16}$$

The upper limit $\eta_{1,max}$ can be derived from the sensitivity matrix by setting $k = N$. The lower limit $\eta_{1,min}$ is zero.

(2) Uniqueness of the solution. As shown in a previous section, in some cases a unique burst location cannot be found by the technique. Although it can be derived using a model of the network, it is desirable to maximize the probability of a unique solution. The probability that a unique burst location will be derived is found using the following expression:

$$\eta_{2,Z} = \Pr\left[\sum_{j=1}^{k-1} \sum_{p=2}^{k} \left(\left(\tau_{m,M_j} - \tau_{m,M_p}\right) - \left(\tau_{n,M_j} - \tau_{n,M_p}\right)\right)^2 > \beta\right] \tag{9.17}$$

$$\forall m \in [1, N], \forall n \in [1, N], m \neq n$$

Parameter β can be selected based on the precision of pressure measurements. In the ideal case, β is equal to the sampling time of the measurements. The limits $\eta_{2,max}$ and $\eta_{2,min}$ are assumed to be 1 and 0, respectively.

To combine the two performance indicators (Equations 9.16 and 9.18) into one objective function a compromise programming approach is used. Compromise programming is a multi-criterion distance-based technique designed to identify compromise solutions. The following objective function is used:

$$OF_Z = \sqrt{\sum_{n=1}^{2} w_n \left(\frac{\eta_{n,Z} - \eta_{n,\max}}{\eta_{n,\min} - \eta_{n,\max}}\right)^2} \tag{9.18}$$

where w_1 and w_2 are the weights for η_1 and η_2, respectively. The sampling design Z that has the smallest value of OF_Z is selected as the optimal sampling design.

Number of measurement points

The choice of the number of measurement stations is influenced not only by the performance of the technique. The actual installation cost my become an important factor. Thus, the measurement station placement procedure can be started assuming that only two stations will be used (the least number of measurement stations possible). Once the search for the optimal placement is done, the decision has to be made, based on the resulting observability and uniqueness values, whether an extra station needs to be added. After adding another station, the search for optimal placement is repeated and new values of observability and uniqueness are obtained. Ideally, new stations should be added until the whole network is observable and the probability of the unique solution is equal to 1. However, this might require a large number of measurement stations and may be infeasible. A compromise can be reached by allowing lower value of uniqueness - the simulation and inverse fitting can be used when a non-unique solution is found. In some cases, the situation where a network is not fully observable might be acceptable. It is also possible to introduce weighting factors for different nodes proportional to the level of damage that would be caused if a burst occurs at the node.

Influence of network topology

As mentioned in a previous section, in the situation when the burst occurs in a dead-end branch of the network, a non-unique burst location is derived by the technique. This indicates that the topology of the network is an important factor, which is affecting the performance of the method. Two main observations can be made:

- Uniqueness of the burst location derived by the technique for the looped network is higher than for the branched network. The same size of the network as well as identical distribution of measurement stations is considered.
- Observability of the branched network is higher than the observability of the looped network. The same size of the network as well as identical distribution of measurement stations is considered.

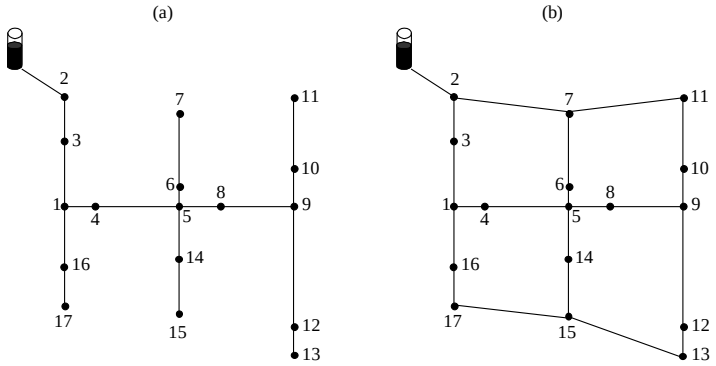

Figure 9.6: The example branched (a) and looped (b) networks

The above statements are illustrated using two networks presented in Figure 9.6. The branched (Figure 9.6a) and looped (Figure 9.6b) networks have identical size. The pipe lengths were selected so the networks are not symmetrical. Assuming that there are two measurement stations, the optimal measurement placements were found for both networks. Nodes 11 and 17 were identified as the optimal sampling design in both cases. However, in case of the branched network, the probability of a unique solution for burst location was only 0.35, whereas the corresponding probability for the looped network was 1 or 280% higher than for the branched network. At the same time, the average wave transmission coefficient value between any point in the network and the selected measurement points for the branched network was 57% larger than the corresponding value for the looped network indicating higher observability of the branched network.

9.5 Validation on a real network

A real water distribution network was used to verify the proposed method for burst detection and location. Around 250 households are connected to the network, which is fed from a fixed-head reservoir. To calculate theoretical transient wave travel times and transmission coefficients between different points in the system a network model was built containing 110 pipes and 107 nodes. The pipes are mainly asbestos cement and have diameters between

100 and 250 mm, lengths between 2 and 212 m and a roughness height of 2 mm. A wave speed of 1 120 m/s was used for all the pipes in the model. The node elevations are in the range of 116 to 180 m and the steady-state pressure at the nodes varies between 20 and 80 m.

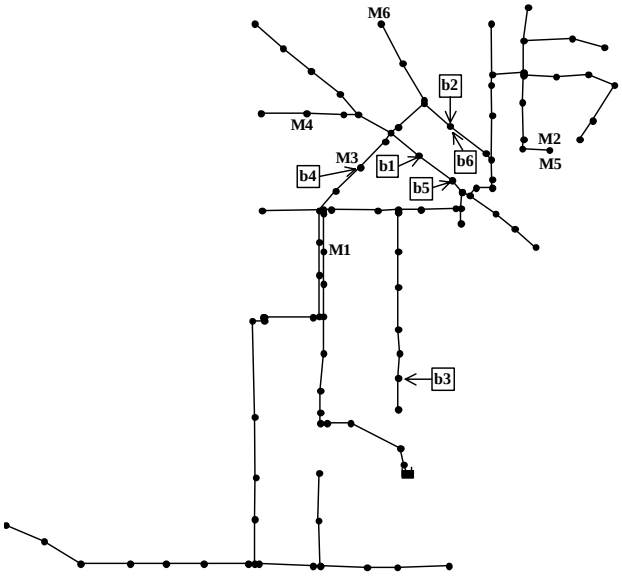

Figure 9.7: Layout of the network with locations of measurement points (M) and bursts (b)

The pressure was measured at a sampling rate of 2 000 Hz. Pressure measurements at all measurement stations were synchronised in time. The data acquisition system integrating variable-gain amplifiers and 16 bit A/D conversion cards enabled high-resolution (0.023 kPa) pressure measurements. The burst was simulated by opening a solenoid valve attached to a standpipe, which was connected to a fire hydrant. The solenoid valve had a diameter of 10 mm, an opening time of approximately 40 ms and an estimated discharge coefficient $C_d A_o = 5.5 \cdot 10^{-5}$ m^2. All tests were conducted between 3:30 and 5:00 pm on a summer day; thus relatively high demand variations were likely to be present in the system.

The burst monitoring, detection and location procedure was conducted fol-

Tests	Measurement position	λ_{min}	λ_{max}	ν (kPa)	h (kPa)
1-3,7-8	M1	0.7	0.995	0.014	4
	M2	0.7	0.8	0.01	10
	M3	0.7	0.95	0.02	7
4-6,9-10	M4	0.7	0.8	0.02	12
	M5	0.7	0.8	0.01	10
	M6	0.7	0.8	0.015	15

Table 9.1: CUSUM change test parameters used for data from Tests 1-10

lowing the structure shown in Figure 9.2. To mimic a real burst event situation, where the actual time instance of the burst event is not known in advance, the burst was simulated by opening the solenoid valve after the pressure measurement was started at all stations. Having this setup allows to assume that the pressure was monitored continuously. The pressure was recorded for 3 minutes during every test.

The whole validation procedure consisted of 10 tests and can be divided into three parts: (a) bursts that occur at network nodes and pressure measurement stations are positioned arbitrary (Tests 1-3), (b) bursts that occur at network nodes and pressure measurement station positioning is optimised (Tests 4-6), and (c) bursts that occur along network pipes and pressure measurement station positioning is optimised (Tests 7-10). The burst was simulated at a total of six different locations and the pressure was simultaneously monitored at three nodes within the network during each test. Two setups of three pressure measurement stations were used. The layout of the test network and locations of simulated bursts and measurement points is shown in Figure 9.7.

Burst detection

[t] As the first part of the burst detection and location procedure, the CUSUM change detection test described in Section 9.2 was applied on the recorded traces to detect the negative burst-induced pressure wave and derive parameters necessary to locate the burst. The time of burst-induced transient wave arrival ($t_{s,Mj}$), the wave magnitude ($\Delta H_{M_j} = H_{M_j}(t_f) - H_{M_j}(t_s)$) and the burst opening time ($t_{f,Mj} - t_{s,Mj}$) were derived from each measured trace. A separate set of CUSUM test parameters was selected for every measurement

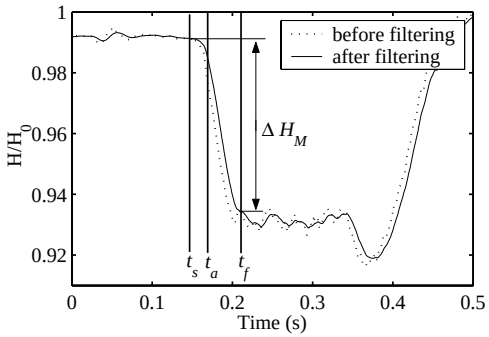

Figure 9.8: Example of CUSUM test

station, since these parameters depend on the hydraulic environment of the measurement station, i.e. noise level and pressure sensitivity. The CUSUM parameter selection is presented in Table 9.1. It has to be noted that the data was in pressure units (kPa) when the CUSUM test was applied. An example of the CUSUM test is shown in Figure 9.8.

The limits of detectable burst sizes and opening times can be identified from Equations 9.9 and 9.10. If an opening time of 40 ms is considered, the minimum detectable change in pressure will vary between 5 and 16 kPa for different measurement stations. The corresponding size of the burst will depend on the location of the burst. As a reference, the average measured pressure change for all tests described in this section was 29.9 kPa (burst with $C_d A_o = 5.5 \cdot 10^{-5}$ m^2). This suggests that up to three times smaller bursts will still be detected by the technique.

Burst location

The second part of the burst monitoring, detection and location algorithm is focused on finding the location of the burst. After the burst-induced pressure waves were detected in all measured traces by the change detection test, the acquired data were used in the burst location search procedure that was described in Section 9.2. All nodes in the network model were used as candidate burst locations.

Modelled parameters. To calculate objective functions from Equations 9.11, 9.12 and 9.13, the theoretical transient wave travel times (τ) and transmission coefficients (T) had to be calculated using the model of the network. Since τ and T between any two nodes in the network had to be derived, two matrices ($N \times N$) were built. A wave speed value of 1120 m/s was experimentally derived for a single branch in the network and used as the common wave speed for all pipes in the model. Such a choice is favoured by the fact that all pipes in the network had the same material (asbestos cement) and were installed around the same time. The theoretical value of the wave speed for asbestos cement pipes is 1109 m/s. The small difference between theoretical and measured values suggests that, in case when no experimental data are available, theoretical values of the wave speed could be used to construct matrices τ and T. Theoretically calculated wave transmission coefficients T are likely to contain some error, since frictional effects are ignored. Also, in some cases, the wave magnitude might be subjected to secondary reflections, which are not accounted for when deriving transmission coefficients from the model. An example of such a situation could be the reflection of the slower burst-induced wave from the end of a short dead-end branch that changes the magnitude of the wave front.

If a higher precision of matrices τ and T is desired or the available network data is suspected to be imprecise, an initial calibration can be performed. The calibration process would involve the generation of artificial bursts of known size at known locations in the network and measuring wave arrival times and magnitudes at measurement stations. Calibration would only be required once, since the burst monitoring system would be operated continuously with the same distribution of measurement stations. Thus, the cost of such an exercise could be justified.

Bursting nodes. The first part of the validation process was used to test the performance of the proposed algorithm for bursts that occur at network nodes. Two sets of tests were performed with different measurement station locations. For the first set of tests, measurements were positioned arbitrary, based on the quality of fire hydrants that were used to connect transducers. The burst was simulated by opening a solenoid valve. Three burst locations were tested. The measurement positions and burst nodes are shown in Figure 9.9. Measured pressure traces for the three tests are shown in Figure 9.10.

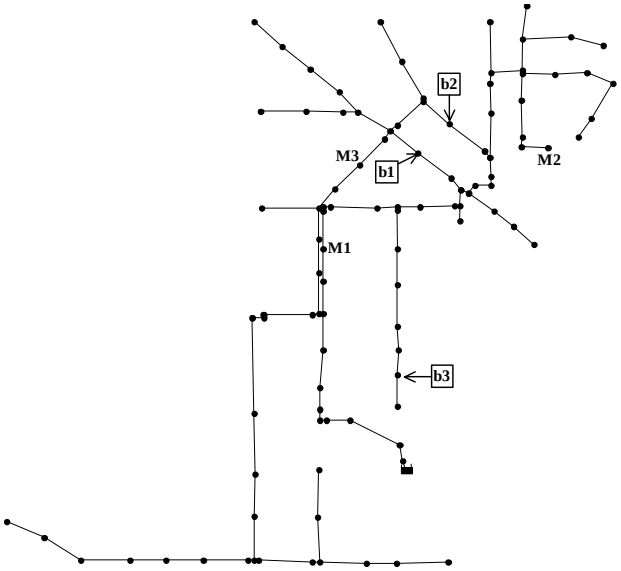

Figure 9.9: Layout of the network with locations of measurement points (M) and bursts (b) for Tests 1-3

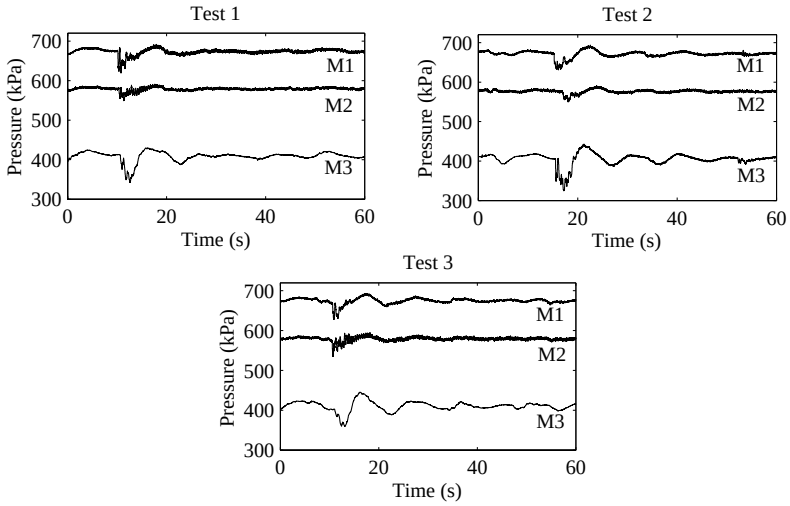

Figure 9.10: Measured pressure traces at all measurement points for Tests 1-3. The pressure measured at M2 was reduced by 100 kPa to avoid overlaying of traces.

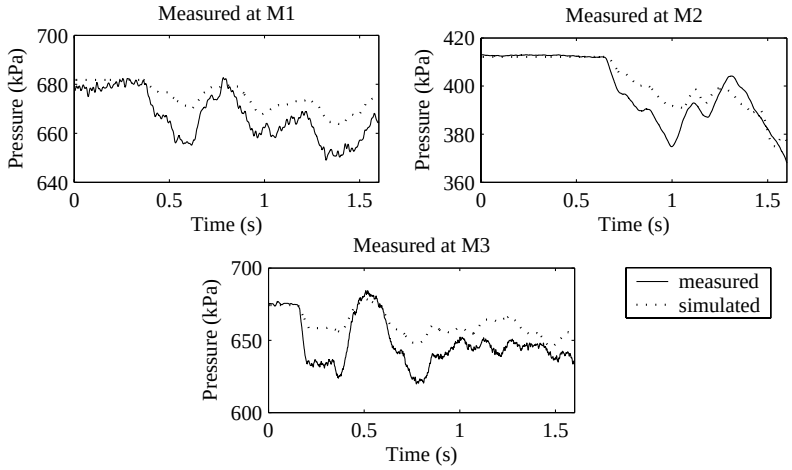

Figure 9.11: Test 1, validation

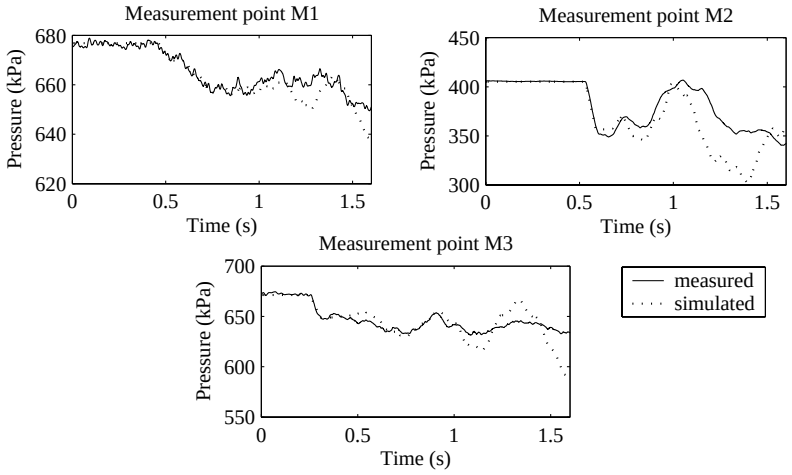

Figure 9.12: Test 2, validation

Test	Actal burst parameters			Detected burst parameters		
No.	Location	Opening (s)	$C_d A_o$ (m^2)	Location	Opening (s)	$C_d A_o$ (m^2)
1	b1	0.04	$5.5 \cdot 10^{-5}$	b1	0.049	$2.3 \cdot 10^{-5}$
2	b2	0.04	$5.5 \cdot 10^{-5}$	b2	0.047	$6.6 \cdot 10^{-5}$
3	b3	0.04	$5.5 \cdot 10^{-5}$	b3*	0.083	$6.0 \cdot 10^{-5}$

* Several nodes on the same branch as b3 had equal OF.

Table 9.2: Burst location results for Tests 1-3. Pressure was measured at points M1,M2 and M3.

The objective function for all candidate locations was calculated using Equation 9.13 and the node having the best objective function was selected as an actual burst location. Weights $w_1 = 0.7$ and $w_2 = 0.3$ were used in Equation 9.13, giving more weight to the match in wave arrival times than to the match in wave magnitudes. The main reason for such a choice of weights is the above mentioned uncertainty in theoretically calculated wave transmission coefficients. Results of the burst location are summarized in Table 9.2. The burst locations for Tests 1 and 2 were found successfully. Results were validated by simulating the burst with derived parameters at the found locations and comparing simulation results with measured traces (model is described in Appendix B). The validation of results for Test 1 is shown in Figure 9.11 and the validation of Test 2 is shown in Figure 9.12

Results of Test 3 indicated that several nodes were selected as the burst location with the same value of the objective function. In fact, all nodes of the dead-end branch shown in Figure 9.13, including the actual burst location, showed identical results. To find the real burst location, the network model was used to simulate the burst at locations 1, 2 and 3 as indicated in Figure 9.13. The comparison between simulated and measured data is presented in Figure 9.14. It is rather difficult to identify the node that has the best fit. The simulated pressure traces have to be treated with caution. It has been shown by a number of researchers that achieving good fit between simulated and measured pressure traces when modelling hydraulic transients in networks is a challenging task. Generally, the precision of the modelled trace is decreasing along the time axis starting from the arrival of the first wave. Thus, giving more weight to the part of the trace directly after the arrival of the burst-induced wave, node 3 can be selected as the actual burst location.

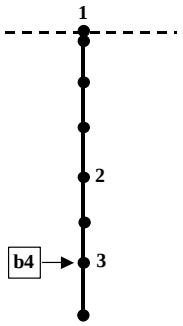

Figure 9.13: Test 3, dead-end branch with all nodes having the same OF

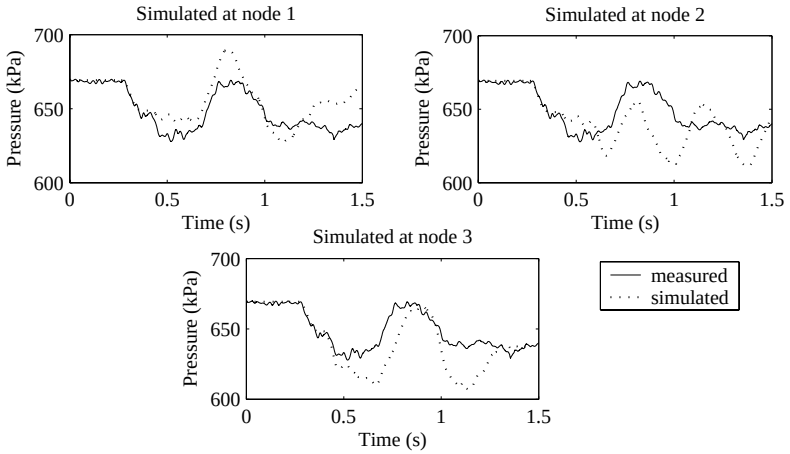

Figure 9.14: Test 3, deriving the actual location of burst by comparing measured and simulated traces

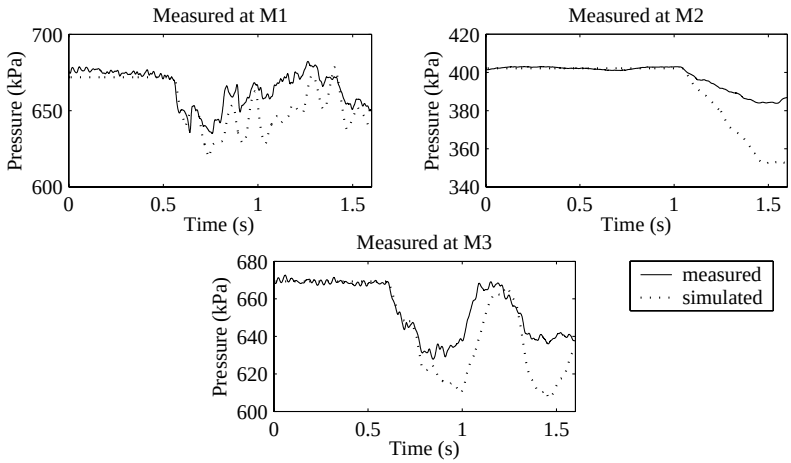

Figure 9.15: test 3, validation

Figure 9.15 shows the comparison between simulated and measured traces at all measurement stations.

Repositioning of measurement stations. Since the proposed burst detection and location technique is primarily designed for looped networks, the main focus of the second set of tests was concentrated on the looped part of the test network. To increase the efficiency of the burst detection and location technique, the optimal measurement placement was found using the algorithm described in Section 9.4. A reduced network model (Figure 9.16) was used in a search for the best distribution of three measurement stations. All fire hydrants in the network were used as candidate locations for measurement stations. Objective functions for all possible combinations were calculated using Equation 9.18 with weights $w_1 = 0.5$ and $w_2 = 0.5$. Measurement stations at M6, M7 and M8 (set No.1) were selected as the optimal placement. The connection of the measurement equipment to M7 and M8 was not feasible, therefore a new search was performed excluding nodes that were not suitable for connection and positions M6, M5 and M4 (set No.2) were selected as the optimal measurement placement. The performance indicators of both measurement station sets as well as the measurement placement used in Tests 1-3 (set No.3) are shown in Table 9.3. The positioning of measurement stations and locations of bursts for the second set of tests are shown in

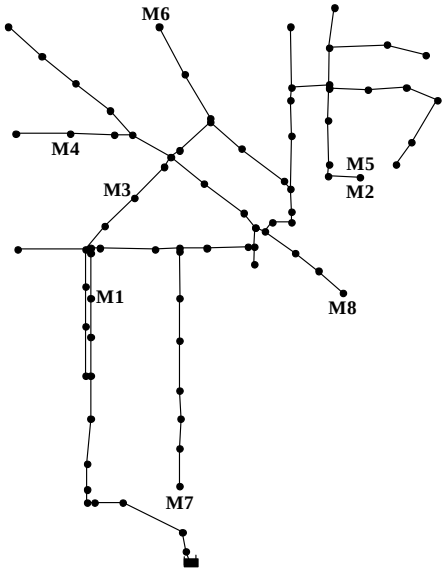

Figure 9.16: Network reduction used for optimal measurement placement selection to focussing on the looped part of the network

Figure 9.17. The burst was simulated at three different locations within the looped part of the test network and the measured traces for the three tests are shown in Figure 9.18. The average magnitude of burst-induced transient wave detected by the CUSUM test for all measured traces from Tests 4-6 was 74% larger than the corresponding value for Tests 1-3 where measurement stations were positioned arbitrary. This indicates the benefit of a systematic approach for measurement station placement. It has to be noted that the

Set No.	Measurement stations	Objective function	Uniqueness	Average T	Observability*
1	M6,M7,M8	0.5	0.4	0.59	0.99
2	M6,M5,M4	0.4	0.31	0.47	0.83
3	M1,M2,M3	0.36	0.34	0.38	0.46

*$\Delta H_{M,min}/\Delta H_{B,min} = 0.2$

Table 9.3: Performance indicators of different measurement position combinations for the reduced network (Figure 9.16)

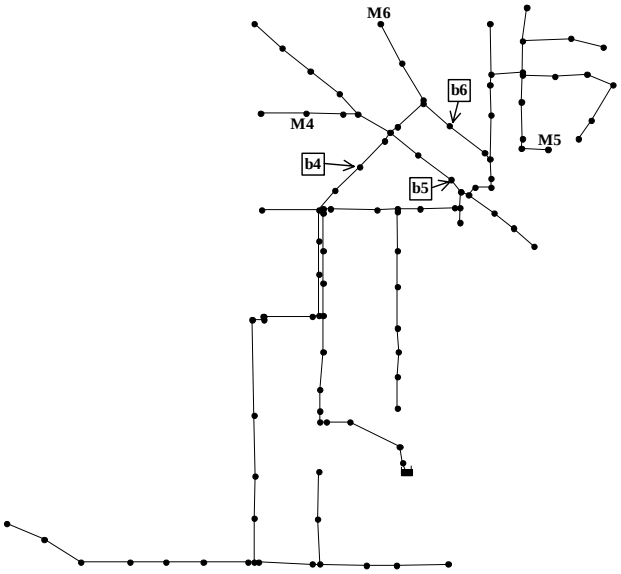

Figure 9.17: Layout of the network with locations of measurement points and bursts for setup No.2

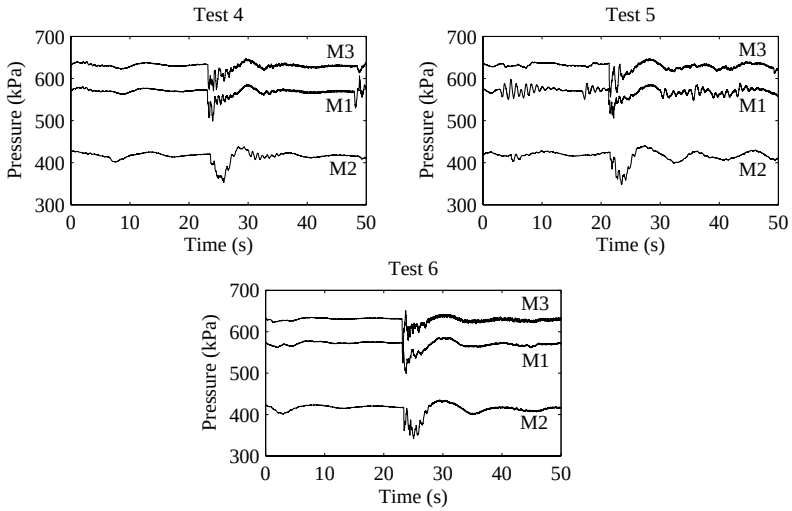

Figure 9.18: Measured pressure traces at all measurement points for Tests 4-6

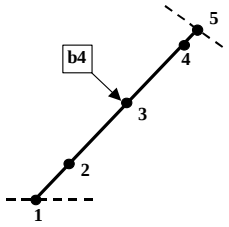

Figure 9.19: Test 4, closer view of the pipe with all nodes (1-5) having the same OF

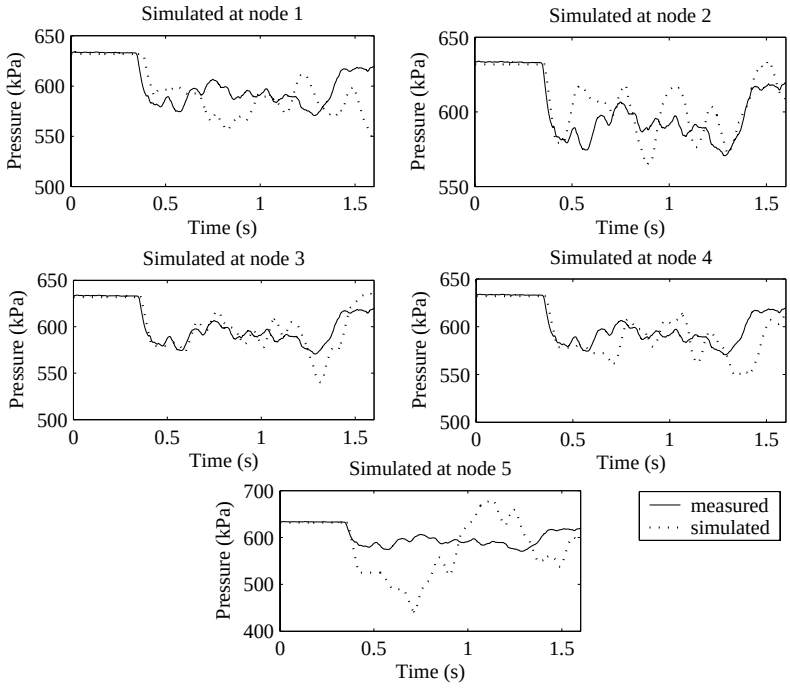

Figure 9.20: Test 4, finding the actual burst location. The burst was simulated at five different nodes and simulation results compared to the measured (at M3) trace.

Test	Actal burst parameters			Detected burst parameters		
No.	Location	Opening (s)	$C_d A_o$ (m^2)	Location	Opening (s)	$C_d A_o$ (m^2)
4	b4	0.04	$5.5 \cdot 10^{-5}$	b4*	0.042	$4.5 \cdot 10^{-5}$
5	b5	0.04	$5.5 \cdot 10^{-5}$	b5	0.042	$3.6 \cdot 10^{-5}$
6	b6	0.04	$5.5 \cdot 10^{-5}$	b6	0.045	$6.1 \cdot 10^{-5}$

* Several nodes on the same branch as b4 had equal OF

Table 9.4: Burst location results for Tests 4-6. Measurements at M4,M5,M6.

measurement placement could be further optimized, since some hydrants in the network were not suitable for connection of the equipment. The details and results of Tests 4-6 are presented in Table 9.4. For Test 4, a non-unique location of a burst was found. Five nodes on the same pipe that is a part of the loop had the same value of the objective function (Figure 9.19). To identify the actual location of the burst, the burst was simulated at all five nodes and results are compared with traces measured at M3 in Figure 9.20. The burst at node 3 has the best fit between the simulated and measured traces. To validate, the comparison of results for all three measurement stations is shown in Figure 9.21 confirming the burst location was identified correctly. In Tests 5 and 6, the correct location of the burst was found. Results are validated in Figure 9.22 and Figure 9.23 for Tests 5 and 6, respectively.

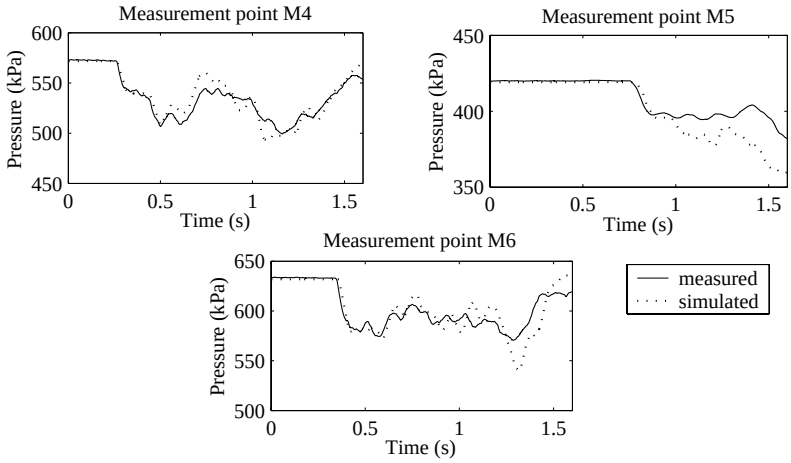

Figure 9.21: Test 4. The validation

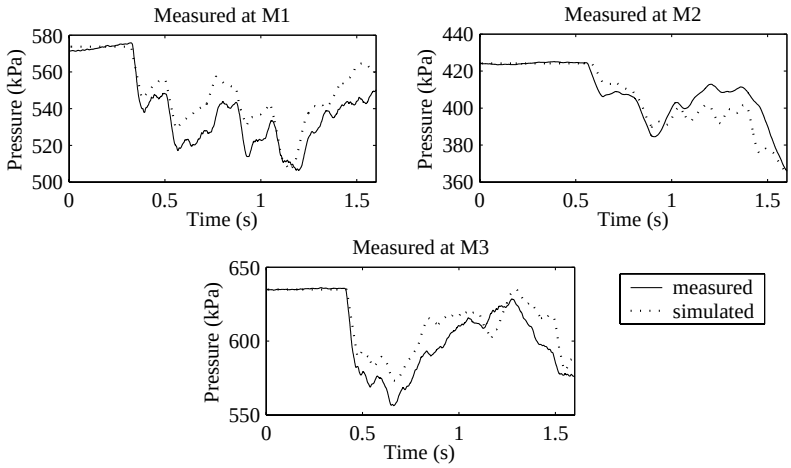

Figure 9.22: Test 5, validation

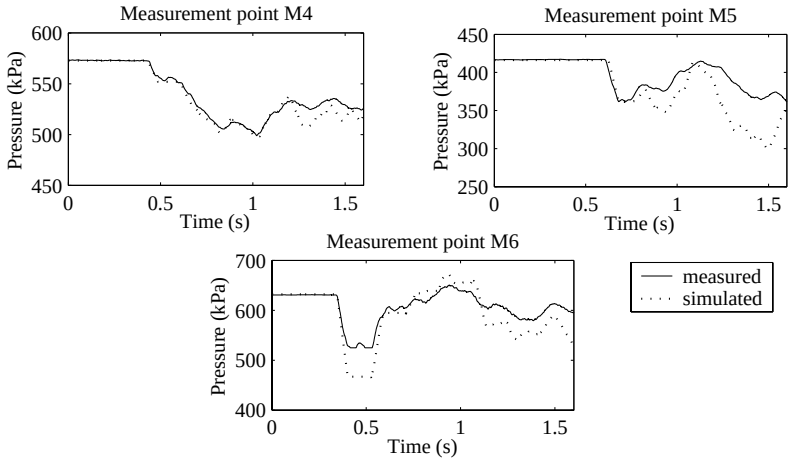

Figure 9.23: Test 6, validation

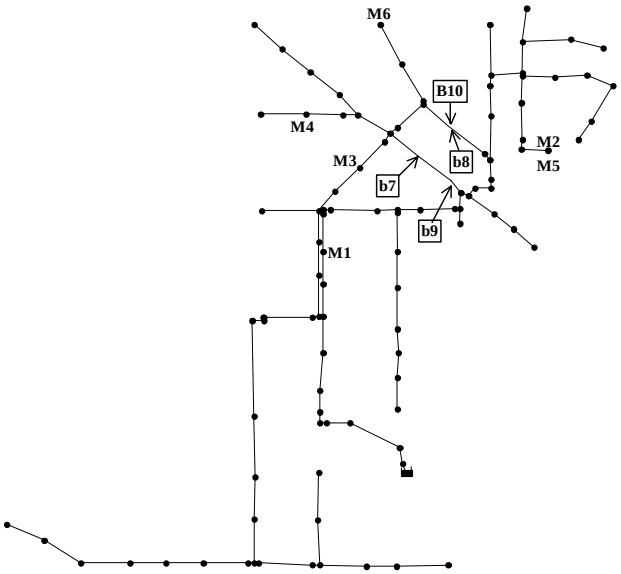

Figure 9.24: Setup for Tests 7-10

Bursting pipes. For Tests 1 to 6, it was assumed that the burst had occurred at a node of the network. To simulate the situation where the burst occurs along the pipe, the node where burst had occurred was not used as a candidate burst location. Four tests were conducted with burst and measurement locations shown in Figure 9.24.

Test No.	Actal burst parameters			Detected burst parameters		
	Location	Opening (s)	C_dA_o (m^2)	Location error (m)	Opening (s)	C_dA_o (m^2)
$7^{(1)}$	b7	0.04	$5.5 \cdot 10^{-5}$	8.0	0.047	$3.2 \cdot 10^{-5}$
$8^{(1)}$	b8	0.04	$5.5 \cdot 10^{-5}$	4.8	0.050	$3.8 \cdot 10^{-5}$
$9^{(2)}$	b9	0.04	$5.5 \cdot 10^{-5}$	9.0	0.042	$4.4 \cdot 10^{-5}$
$10^{(2)}$	b10	0.04	$5.5 \cdot 10^{-5}$	4.0	0.045	$2.8 \cdot 10^{-5}$

$^{(1)}$ Measured at M1,M2,M3 $^{(2)}$ Measured at M4,M5,M6

Table 9.5: Burst location results for Tests 7-10

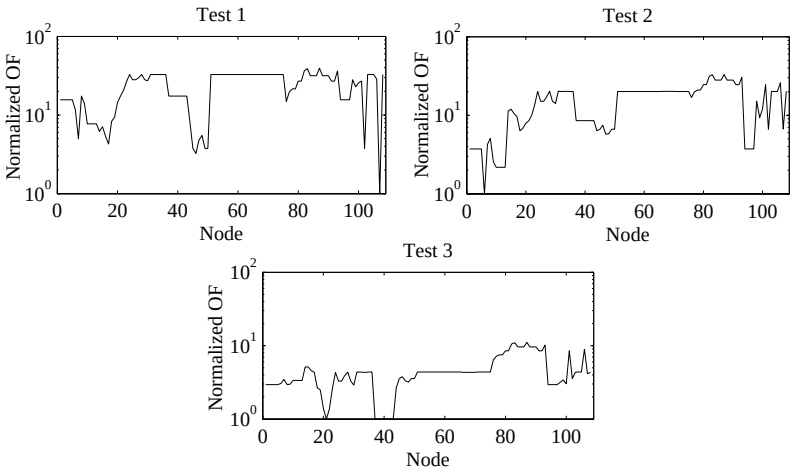

Figure 9.25: Tests 1-3, distribution of the normalized objective function values for all burst candidate locations

For Tests 7 and 8 the pressure was measured at M1, M2 and M3, and for Tests 9 and 10 the pressure was measured at M4, M5 and M6. Results of the burst location are presented in Table 9.5. All four bursts were successfully located with the location error being less than 9 m.

9.6 Uncertainty analysis

The uncertainty analysis was divided into two main parts: (1) evaluating the reliability of the derived burst locations and (2) testing the sensitivity of the proposed technique to the error.

In Figures 9.25 and 9.26, the distribution of the normalized objective function (OF) values for all candidate burst locations (all nodes in the network) are shown for Tests 1-3 and 4-6 respectively. Objective function values were normalized applying the division by the optimal (minimum) value. The actual burst location can be identified from the OF distributions for Tests 1-2 and 5-6. For Tests 3 and 4, the unique location of the burst was not derived and therefore more than one node has a minimum value of the OF. In all cases, the remaining nodes have larger objective functions (3-50 times).

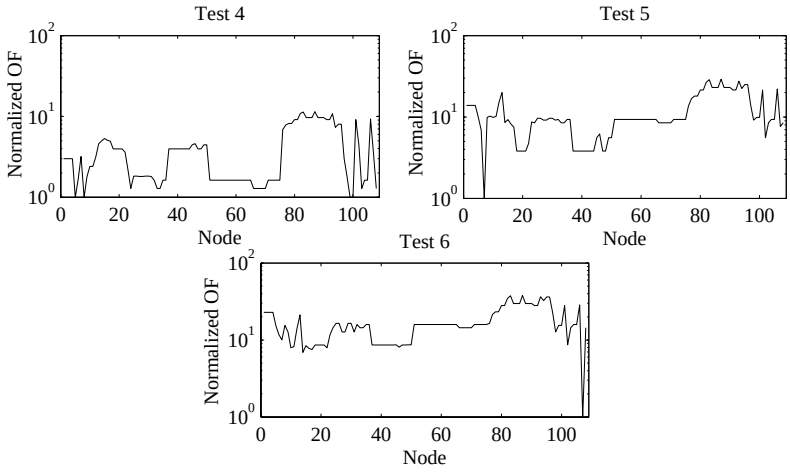

Figure 9.26: Tests 4-6, distribution of the normalized objective function values for all burst candidate locations

Results of tests were analysed to evaluate the level of error. As already mentioned earlier in this chapter, the influence of the measurement error and the model error can be evaluated collectively by using the common error term e. The first objective function used in the search for a burst location (Equation 9.11) depends on the timing of the burst-induced wave and the second objective function (Equation 9.12) depends on the magnitude of the wave. Two objective functions can have different weights when they are combined as shown in Equation 9.13. Therefore the error term e can be divided into e_t, which is the error related to the timing of the burst-induced wave, and e_m, which is related to the magnitude of the burst-induced wave so that

$$e = w_1 e_t + w_2 e_m \tag{9.19}$$

Weights w_1 and w_2 are the same as in Equation 9.13. Average values of e_t and e_m for all measurement points were calculated from the results of Tests 1-6 described in the previous section and are summarised in Table 9.6. Results in Table 9.6 show that the error related to the magnitude of the burst-induced wave is considerably larger than the error related to the timing of the wave. There are two main reasons for such a difference in error levels. First, the magnitude information at the measurement points can be

Test No.	1	2	3	4	5	6	Average
e_t (%)	3.08	3.62	6.31	9.78	2.50	1.97	4.54
e_m (%)	28.45	6.22	38.94	52.55	23.71	24.81	29.11

Table 9.6: Error values from Tests 1-6

affected by secondary reflections of the burst-induced wave within the network that arrive to the measurement point shortly after the transient wave itself. The second reason is that the frictional effects are not accounted for when calculating wave transmission coefficients for the model of the network. The fact that magnitude-related errors usually have larger values than the timing-related errors reflects on the selection of weights of the objective function from Equation 9.13. Error terms e_t and e_m can be combined as shown in Equation 9.19 to find the value of $e = 5.95\%$.

The second part of the uncertainty analysis included testing of the sensitivity of the proposed burst location technique to the error. A Monte Carlo type simulation was performed to evaluate the probability of finding the correct burst location for different levels of error e. The error e was defined as a percentage of the perturbation that was applied on measured variables - the wave arrival time t_M and the wave magnitude ΔH_M. In the uncertainty analysis the measured arrival time of the burst-induced wave was generated by adding the error term to the corresponding modelled value, i.e. $t_M = \tau_{i,M} + e_t$ where i is the burst node. The perturbation level was expressed as the percentage of the measured value and was randomly selected from the normal distribution with zero mean and standard deviation b. In the same manner, the ratio between measured wave magnitudes at two measurement stations was set to be equal to the sum of the modelled one and the error: $\Delta H_{M_1}/\Delta H_{M_2} = T_{i,M_1}/T_{i,M_2} + e_m$. The derived values were used to calculate objective functions from Equations 9.11, 9.12 and 9.13 and find the location of the burst. The same procedure was repeated for all possible burst locations (all nodes in the model of the network) and the probability of the successful burst location was expressed as a ratio between the number of bursts that were located correctly and the number of possible burst locations. Different levels of the error (b between 0 and 20%) were tested. 10000 runs were performed for each value of the error and resulting probabilities (average values) are shown in Figure 9.27. The error value in Figure

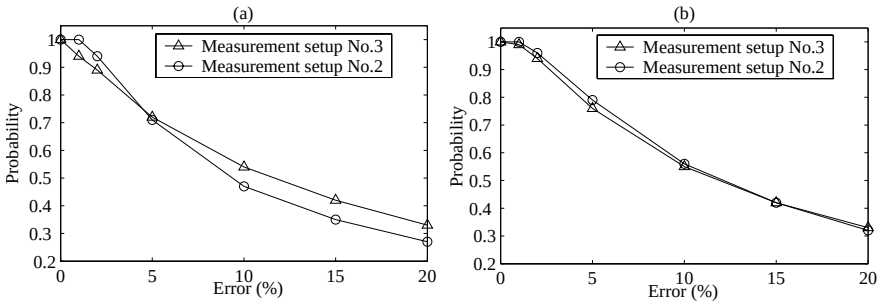

Figure 9.27: Relationship between the error and probability of successful burst location for (a) complete network and (b) reduced network with two measurement setups

9.27 corresponds to the standard deviation of the perturbation b. As can be expected, the probability of successful location of the burst decreases when the error is increasing. If the error level is assumed to be similar to the one that was observed in Tests 1-6, it can be expected that the burst occurring at around 70% of the possible locations will be located.

The difference in probability decay rates between the whole (Figure 9.27a) and reduced (Figure 9.27b) networks indicates that the performance of the technique depends on the ratio between the number of measurement points and the size of the network. When the same number of measurement sites (3) is used for a smaller network, the burst detection probability is higher for the same level of error. The small difference between two measurement setups can be explained by the small difference in the uniqueness parameter from Table 9.3. The benefit of systematic measurement station placement would become apparent for smaller bursts, since the measurement setup No.2 has a considerably higher observability.

The performance, application and implementation of the pipe failure monitoring technique described here are discussed in Chapter 10. The discussion in Chapter 10 also considers the steady-state analysis based pipe failure monitoring approach, which was presented in Chapter 8.

Chapter 10

Pipe network failure monitoring - discussion

In this chapter, the performance limits, implementation and application of the automatic failure monitoring, detection and location techniques presented in Chapters 8 and 9 are discussed. The first technique is based on a steady-state-analysis and the second approach is based on an unsteady-state analysis of the network.

10.1 Performance limits

The steady-state analysis-based pipe break monitoring, detection and location technique presented in Chapter 8 was tested using simulated data while the unsteady-state analysis-based approach (Chapter 9) was validated in the field. However, the results obtained from the validation tests do not completely represent the performance limits for the failure monitoring techniques. The performance of the two methods can be evaluated and compared by deriving common performance limits. The following parameters have been selected as the most significant performance indicators: (1) minimum size of detectable burst, (2) detection and location time, (3) precision of derived location of the burst (4) sensitivity to model error and (5) required number of measurements.

Steady-state analysis-based system						
Time of day	h (L/s)	ν (L/s)	Opening time 1 min		Opening time 10 min	
			$D_{l,\min}/D$	Q_l	$D_{l,\min}/D$	Q_l
22:00 - 06:00 hours	1.878	0.939	10.9 %	2.18 L/s	24.7 %	11.27 L/s
06:00 - 22:00 hours	3.526	1.878	16.9 %	5.29 L/s	33.9 %	21.16 L/s
Unsteady-state analysis-based system						
Measurement station	h (kPa)	ν (kPa)	Opening time 10 ms		Opening time 1 s	
			$D_{l,\min}/D$	Q_l	$D_{l,\min}/D$	Q_l
M6	15	0.015	3.4 %	0.23 L/s	5.9 %	0.65 L/s
M1	4	0.014	1.8 %	0.06 L/s	5.0 %	0.46 L/s

Table 10.1: Minimum burst size limits for network burst monitoring systems

Minimum size of a detectable burst. In Table 10.1, the minimum burst sizes that will be detected by the two techniques are summarised. These sizes are defined as a combination of two interdependent parameters: the size of the burst and the opening time of the burst. Two different burst opening times were selected for each technique. For the steady-state approach, opening times of 1 min and 10 min were selected, while a measurement sampling time of 1 min was used. Burst opening time values of 10 ms and 1 s were used to evaluate the performance of the unsteady-state method, where a measurement sampling frequency of 2000 Hz was used. Table 10.1 indicates that the unsteady-state-based method is capable of detecting smaller bursts than the steady-state approach. The estimated minimum detectable burst size for the unsteady-state method is at least six times smaller than the corresponding size for the steady-state technique. At the same time, the transient-analysis-based approach relies on the assumption that the failure will induce a transient wave into the network. If a pipe break occurs over a longer period of time (i.e. without creating a transient wave), the unsteady-state method will not be able to detect such a break.

Detection and location time. Both techniques have a short failure detection and location time. For the steady-state method, this amount of time depends on the opening time of the burst. The longer it takes for a burst to develop its maximum flow, the longer the time will be for its detection and location. The unsteady-state analysis-based burst monitoring system has shorter failure detection and location times. The time taken to detect and locate the burst in this case depends on the travel time of the burst-induced wave from the burst

point to the furthest measurement station. The communication time between the measurement stations and the control room also has to be accounted for when estimating the burst detection and location time.

Precision of the derived burst location. For the nodal burst tests, the candidate node with the best objective function value was selected as a burst location. Thus, the error of the derived burst location is assumed to be zero. For the non-nodal burst tests (i.e. bursts located along pipes), the error of the derived location was less than 9 m for the unsteady-state method and less than 30 m for the steady-state technique. Errors of this size are sufficiently small to enable operators to isolate the damaged section of the network.

Sensitivity to model error. An uncertainty analysis was performed for both the steady-state and unsteady-state approaches, where a perturbation was used to collectively represent both model and measurement errors. Different levels of perturbations were tested and the corresponding probabilities of successful detection and location of the failure were derived. For the steady-state technique, an error of 10% resulted in a decrease of the successfull location probability from 0.9 to 0.2. The corresponding decrease for the unsteady-state method was from 1.0 to 0.55. In both cases, three pressure measurement points were used. The result show that the transient monitoring approach is less sensitive to model or measurement errors than the steady-state technique. In fact, during the field validation, errors of approximately 5% and 30% were observed between measured and modelled values of travel time and magnitude of the burst-induced transient wave, respectively. Still, all bursts were successfully located.

Required number of measurement points. Similar size networks were used to test the steady-state and unsteady-state approaches, with 79 and 107 nodes, respectively. Three pressure measurement points were used for the unsteady-state technique (2.8% of the total number of nodes). The steady-state method was tested for a range of setups with the number of pressure monitoring points varying between 1 and 4 (1.3 to 4.1% of the total number of nodes). One flow rate measurement was also used for steady-state analysis-based failure monitoring. The required number of measurement stations depends not only on the size but also on the topology of the network. Having a branched structure would reduce the probability of deriving the unique location of the failure.

10.2 Application

Although both the steady-state and the unsteady-state failure monitoring techniques are designed for network applications, depending on the structure of a particular network, one of the methods may be more suitable. The main factor that has to be considered is the difference between the type and sampling frequency of the measurements that are required for the steady-state and the unsteady-state approaches.

Steady-state analysis-based failure monitoring system

As noted in Chapter 8, the steady-state break monitoring system is designed for application on the level of a DMA. Since the method requires continuous measurements of all inflow rates, its application is restricted to networks (subnetworks) that have flow rate meters at all points where the monitored network is connected to the rest of the system. An example of a system where the steady-state method would be suitable is a small, gravity-fed network. Most of the time, a reservoir would be the only source in the network, thus the flow rate can be easily monitored. Additionally, when applying the steady-state analysis-based failure monitoring system, the demand distribution in the network must be known. In a network where the demand information is poor, break detection and location may be difficult.

Unsteady-state analysis-based failure monitoring system

Application of the unsteady-state technique is flexible, since only pressure monitoring is required. A flow rate measurement is not necessary nor is knowledge of the demand distribution within the monitored network essential when the unsteady-state system is implemented. Therefore, the system can be installed to monitor a whole network, or part of a network that is not isolated from the rest of the system. For instance, if there is a section of the network where burst consequences are hazardous and expensive, or the risk of a pipe failure is high, the burst monitoring system can be installed in that part of the network only.

10.3 Implementation

A continuous burst monitoring system has three main parts - measurement, data analysis and communication. The three parts can be implemented in different ways for the steady-state and unsteady-state analysis-based systems.

Steady-state-analysis-based failure monitoring system

Installation of measuring devices for flow rate and pressure measurements is straightforward. Due to the quite low sampling frequency of the measurements, both local and centralised analyses of data are feasible. The flow rate data has to be continuously monitored for the burst-induced change, whereas analysis of pressure records is only necessary if the flow rate alarm is issued. Depending on the available data transfer capacity, an existing SCADA system may be utilised for the transfer of flow rate and pressure data to the control room.

Unsteady-state analysis-based failure monitoring system

As a high pressure sampling frequency is necessary to detect and locate sudden bursts, pressure data have to be monitored locally at the measurement point. A preemptive memory buffer, discussed in Chapter 7 as part of the pipeline burst detection system, can be used to minimise memory storage requirements. Once the burst-induced pressure wave is detected at one of the monitoring stations, wave parameters (arrival time and magnitude) have to be sent to a control room. In the control room, parameters from all stations are cross-checked and analysed to derive the location and the size of the burst.

Integrated system

The unsteady-state approach, being able to detect smaller bursts, less sensitive to model errors and having more flexible application possibilities, may

appear to be a more attractive option for burst detection and location in pipe networks. However, the steady-state-based technique allows detection and location of slower breaks. Ideally, both methods should be combined into one network failure monitoring system. In fact, even in the case when only pressure (and not flow rate) monitoring is feasible, the steady-state burst detection algorithm can be incorporated into the unsteady-state burst detection and location system. The same pressure data can be used, only with a different sampling rate. If the flow rate measurements are also available, confidence in the burst alarms can be further increased. The steady-state algorithm can even be used to confirm burst alarms generated by the unsteady-state technique.

10.4 Calibration

A network model is used to solve the forward problem in both the steady-state and unsteady-state burst monitoring methods. It is likely that the model will contain some errors, which may degrade the performance of the burst detection and location. To reduce the model error, calibration has to be performed.

Steady-state analysis-based failure monitoring system

Calibration may be necessary after the steady-state analysis-based burst detection and location system is installed in the network. For good performance of the technique, both the pipe friction and demand distribution have to be calibrated. The calibration of steady-state model parameters has been a popular topic ever since the use of models became an engineering practice and an extensive amount of research has been presented in the literature (Walski; 1983, 1986; Kapelan et al.; 2003b; Vítkovský et al.; 2000). The calibration process will not be discussed in detail here. The importance of having data of sufficient quality and quantity to use for calibration has been stressed by many authors. Since permanent installation of the steady-state failure monitoring system is considered, calibration of the model can be considered as an ongoing process. The quality of the model can be continuously improved,

even when the burst monitoring system is operational. The cost of the initial calibration of the network model can be justified, since it only has to be performed once.

Unsteady-state-analysis-based failure monitoring system

Generally, the unsteady-state burst detection and location technique is less vulnerable to model errors compared to the steady-state approach. The field validation discussed in Chapter 9 demonstrated that bursts can be detected and located without calibration of the model. The main advantage of the proposed unsteady-state burst location algorithm is that only the arrival times and magnitudes of the initial burst-induced wave are used to derive the location of the failure. If necessary, a relatively straightforward calibration process can be performed. Since the pressure monitoring points are permanently installed at certain points within the network, the calibration exercise would involve simulating bursts at different locations throughout the network and registering travel times and magnitudes of the burst-induced transient waves at the measurement points. Travel times of the burst-induced wave depend on the distance that the wave has to travel and on the wave speed of the pipe the wave is travelling along. The magnitude of the wave depends on the number and reflection characteristics of the junctions and other elements in the network, which the burst-induced wave has to pass on its way to the measurement point, as well as the friction of pipes. Thus, the number of burst locations that have to be used for calibration depends on how uniform the material, diameter and age of pipes in the particular network are.

10.5 Tuning

As discussed in Chapter 7, the main objective of the tuning process is to increase the probability of successful failure detection and to decrease the rate of false alarms. In a network situation, tuning of the monitoring system is very important, since the demand is likely to be highly dynamic. Changes in demand can cause pressure oscillations and increase the probability of a false alarm. Thus, in some networks, a higher value of the minimum detectable burst size may have to be chosen to reduce the false alarm ratio.

10.6 Conclusions

The overall performances of the burst monitoring, detection and location approaches presented in this chapter are promising. As demonstrated using the case studies, the proposed techniques are capable of detecting and locating bursts, which occur at different locations within the network, both at nodes and along pipes between nodes. Real-time continuous pressure monitoring allows for quick reaction to a failure in the network. As the required density of pressure monitoring stations is relatively low, the implementation of the failure monitoring system in water distribution networks may be feasible. If implemented, the continuous burst monitoring, detection and location system can considerably reduce the time of reaction to pipe failures and, consequently, increase the efficiency of the operation of the water supply system and minimise losses associated with failures.

In addition to the burst detection and location, continuous pressure monitoring offers other capabilities, such as detection of illegal consumption, demand monitoring and identification of abnormal pressure fluctuations. These applications are discussed as part of the future work directions in Chapter 13.

Part IV

Systematic asset condition assessment

Summary: *Proactive failure management can help to prevent pipe failures. An important part of the proactive failure management involves pipe condition assessment. The condition of a pipe can be evaluated using one of the nondestructive evaluation (NDE) techniques that are reviewed in Chapter 3. However, available NDE techniques cannot be systematically applied for condition assessment of water transmission pipelines, due to high cost and time requirements of the inspection.*

In Part IV of this thesis, a hydraulic-transient-analysis-based approach for a long range and low cost non-intrusive pipeline condition assessment is presented. The comparative evaluation of different segments of the pipeline is performed as well as critical points are identified along the length of the pipeline.

In the case of pipeline failure, inline valves are used to isolate the damaged section of the pipe. If the valve does not seal properly, the isolation will fail. In Chapter 12, a method is presented for fast, non-intrusive testing of inline valves.

Related publications: *Part of the work has been presented in Misiunas et al. (2005c) and Misiunas et al. (2005d).*

Chapter 11

Pipe condition assessment

In this chapter a possibility of using hydraulic transients as a non-intrusive tool for quantifying a deterioration level of transmission pipelines is investigated. The proposed approach is using the response characteristics of the artificially induced transient wave to evaluate the physical state of the pipeline. The proposed methodology can be used as a tool for initial testing to identify the areas of the pipe that are exposed to deterioration. Conventional NDE techniques (described in Chapter 3) can then be applied to the identified segments of the pipe.

11.1 Methodology

Nondestructive evaluation (NDE) techniques reviewed in Chapter 3 have one common disadvantage - they are labor demanding and have a high operation cost. As a result, only a small part of the whole water supply system is tested for condition assessment. The choice of the pipes that are tested is often arbitrary and not always optimal. Thus, it would be beneficial to perform an initial testing that would have a low cost and be time efficient. In that way, a rough judgment about the pipe condition could be made and the areas where further investigation is needed could be identified. This procedure would dramatically reduce the length of the pipe that has to be inspected using the conventional NDE techniques and make a periodical systematic testing of the whole system feasible.

In this chapter a possibility of using hydraulic transients as a non-intrusive tool for quantifying a level of deterioration is investigated. When propagating along the length of a pipeline, an artificially generated hydraulic transient wave is reflected at any point where a change in physical properties of the pipe is present. The change in physical properties can be part of the structure of the pipeline, i.e. change of the diameter or wall thickness, pipe junctions, fire hydrants, etc., or the result of deterioration process, i.e. leakage, blockage, crack or other change of wall properties due to corrosion. Since the pipe deterioration process depends on a number of parameters including those of the pipeline environment (soil properties, etc.), it is likely that the deterioration will not affect uniformly along the length of the pipeline. Some parts of the pipe will be exposed to the damage to a higher degree than other. The extent and the density of the damage can vary considerably. In some cases the damage can be localised, i.e. concentrated around one point along the pipeline, whereas in other cases the damage can be distributed, i.e. affecting a longer segment of the pipeline. Finding localised damage can help to prevent the failure of the pipeline, whereas identifying the segments of the pipeline that are affected by distributed damage can be part of the rehabilitation planning. The proposed nondestructive evaluation approach serves two main purposes: (1) assessment of the condition of different pipe segments and (2) identification of the points along the pipeline where the localised damage is present.

Condition assessment of pipeline segments

The presence of damage on the internal pipe wall will cause reflection of the transient wave from the point of damage. The size of the transient reflection is expected to be proportional to the level of the damage. Individually, small cracks or rust patches on the pipe wall might not always cause a substantial reflection of the transient wave that can be distinguished on the measured pressure trace. However, when a larger area of the pipe wall is exposed to the damage, the collective effect of that area on the transient wave will be significant. In other words, the cumulative reflection of the transient wave from the damaged section of the pipe can be distinguished in the measured transient response trace. Thus, evaluating cumulative transient reflections coming from the segment of the pipeline allows to assess the condition of that

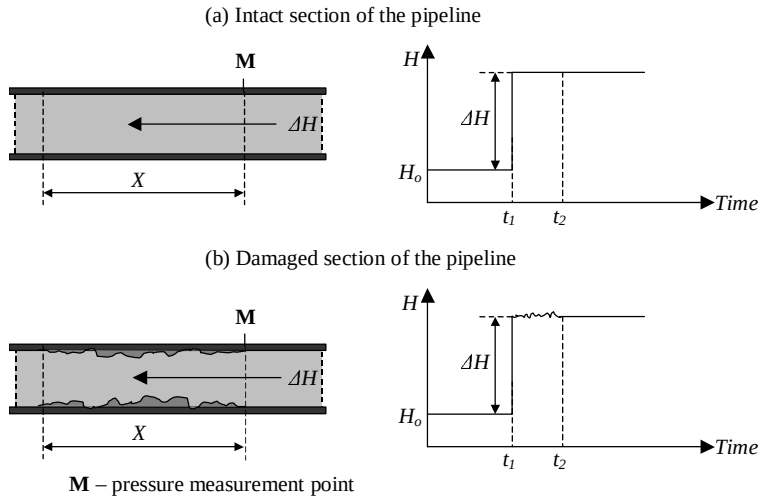

Figure 11.1: Pipe wall profiles (left) and transient response traces (right) for (a) intact and (b) damaged pipeline sections

segment. Figure 11.1 illustrates the main principle of the proposed methodology.

In Figure 11.1 time t_1 indicates the wave front arrival and ΔH is the magnitude of the generated transient wave. The time intervals $[t_1..t_2]$ on measured traces in Figure 11.1 correspond to the section of the pipeline with a length X. Given that a is the wave speed of the pipeline, X can be derived using the following expression:

$$X = \frac{a(t_2 - t_1)}{2} \tag{11.1}$$

As shown in Figure 11.1a, when the pipe is intact, the transient response trace between t_1 and t_2 contains no reflections. However, when the section of the pipeline is exposed to the damage as shown in Figure 11.1b, there are reflections present on the response trace (interval $[t_1..t_2]$). Thus, the condition of the pipeline segment can be evaluated based on the characteristics of the part of the transient response trace that corresponds to the segment.

The assumption can be made that in cases where the pipeline section is in

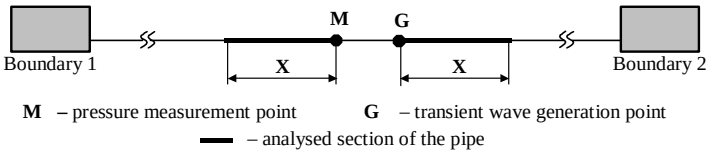

Figure 11.2: The section of the pipeline analyzed using transient response method

worse condition, the reflections coming from that section will have larger magnitude. The standard deviation of the pressure fluctuations can be used to quantify the size of reflections in each trace and can serve as a quantitative measure representing the level of deterioration of a pipeline segment.

Figure 11.1 represents the situation where the transient wave is generated at the dead-end of the pipeline. If testing on real transmission pipelines is considered, the transient generation and measurement points will have to be located at some position along the pipe (Figure 11.2). In that case the time intervals $[t_1..t_2]$ will include the reflections coming from a pipeline section of a proportional length (X) adjacent to the measurement site and transient generator as shown in Figure 11.2. Thus, the length of the analysed pipeline section will be equal to $2X$.

There are two points that have to be considered when using the transient response analysis for condition assessment of the pipeline:

- the reflections from different physical elements of the pipeline are subject to frictional damping that increases with the distance between the source of reflection and the measurement site;
- for clear reflections, the front of the transient wave has to be steep. The steepness of the wave front decreases as the transient wave travels along the pipe.

The two points above indicate that the length of the analysed pipe section X has to be chosen so that the frictional distortion of the pressure measurement is avoided. The transient generation and pressure measurement points should be located as close to each other as possible to keep the wave

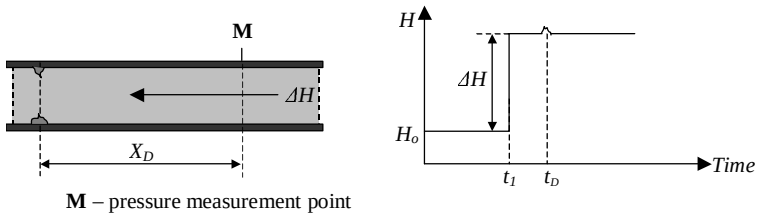

Figure 11.3: The mechanism of locating a discrete location of localized damage

front steep. The density of the transient generation points as well as pressure measurement sites will be proportional to X. The number of required generation/measurement sites for a particular pipeline can be estimated:

$$N_{sites} = \frac{L}{2X} \tag{11.2}$$

where L is the length of the pipeline. The choice of the segment length X is arbitrary and depends on the expected resolution of the pipeline condition information as well as limitations of the testing budget.

Detection of localised damage

In some cases a discrete point along the pipeline might be exposed to a high degree of damage. These critical points will then cause reflections of transient wave that can be identified in the measured trace (Figure 11.3). The following equation can be used to derive the location of the localized damage that corresponds to the observed transient wave reflection on the measured trace:

$$X_D = \frac{a(t_D - t_1)}{2} \tag{11.3}$$

In case when the generation/measurement point is located along the pipeline as illustrated in Figure 11.2, x_D will correspond to two locations. However, since usually more than one generation/measurement location would be used for testing of the pipeline, the actual location of the localised damage can be identified using data from two different measurement points.

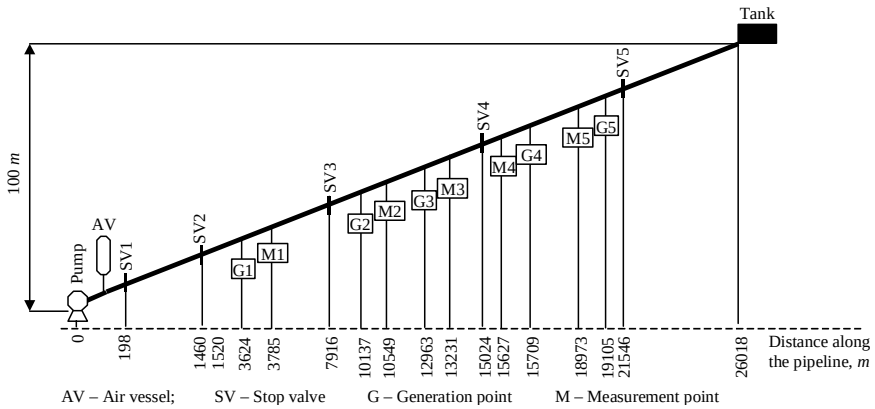

Figure 11.4: The layout of the test pipeline with locations of measurement and transient generation points

11.2 Testing on a large transmission pipeline

The testing was performed on a $26\,018$ m long mild steel concrete lined (MSCL) pipeline with a diameter of 750 mm. The layout of the pipeline with indicated transient generation and pressure measurement points is shown in Figure 11.4. At the downstream end of the pipeline there are two storage tanks and on the upstream end there is a treatment plant and a pumping station. The pipeline has three segments with different pipe wall thickness and estimated wave speed values: 7.94 mm (a=1100 m/s), 6.35 mm (a=1030 m/s) and 4.76 mm (a=950 m/s).

The transient was generated by the fast closure of the side-discharge valve mounted on a scour valve. Two sizes of the side-discharge valve nozzle were used - 40 mm and 50 mm. The custom-built fast release spring device was used to close the side discharge valve with the closing time around 10 ms. The pressure was measured at the sampling rate of $2\,000$ Hz using Druck 810 fast response pressure transducers with the measurement range of $0 - 1500$ kPa. Two setups of the measurement system were used. The first setup included a 16 bit A/D converted and the resolution of the pressure measurement was equal to 0.00305 kPa. In the second setup, a 12 bit A/D converter was used and a resulting resolution was equal to 0.049 kPa. More informa-

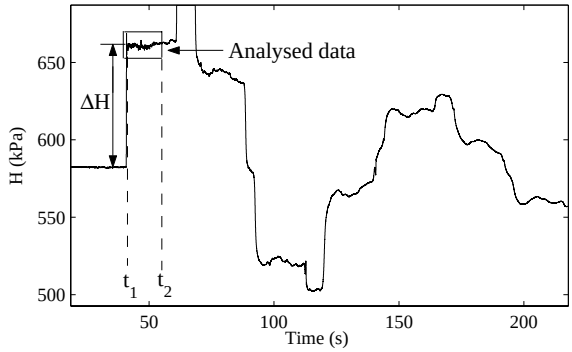

Figure 11.5: The part of the measured pressure trace that is analyzed for condition assessment of the pipeline section

tion on the test site, equipment and measurement system can be found in Appendix A.

In this study $X = 1\,000$ m was chosen. Consequentially, from each test data the assessment of the condition of $2\,000$ m long section of the pipeline was made. Five transient generation and pressure measurement sites were used and the total of 10 km of the pipeline was examined. The summary of tests and results are presented in Table 11.1.

The magnitude of the generated transient wave ΔH was between 30 and 80 kPa for different tests. An example of a measured trace with indicated analysed data window that corresponds to X is shown in Figure 11.5. The normalized pressure data windows from transient responses of all five tests are presented in Figure 11.6.

Trace Figure	Generated at, m	Measured at, m	Analised pipe section, m	Standard deviation	Rank
11.6a	3624	3785	$[2575 : 3575][3835 : 4835]$	0.0056	1
11.6b	10137	10549	$[8887 : 9887][10799 : 11799]$	0.0078	2
11.6c	12963	13231	$[11713 : 12713][13481 : 14481]$	0.0190	4
11.6d	15709	15627	$[14459 : 15459][15877 : 16877]$	0.0256	5
11.6e	19105	18937	$[17687 : 18687][19355 : 20355]$	0.0175	3

Table 11.1: Summary of tests and results

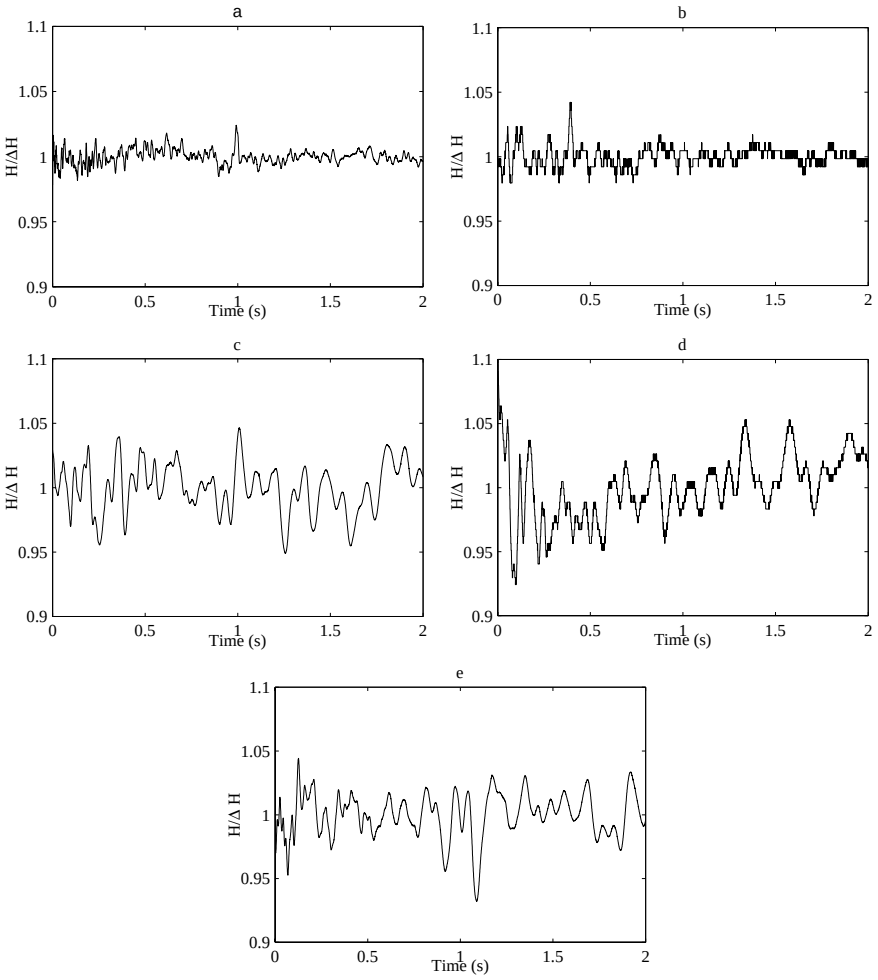

Figure 11.6: The analyzed pressure traces from pipeline No.1

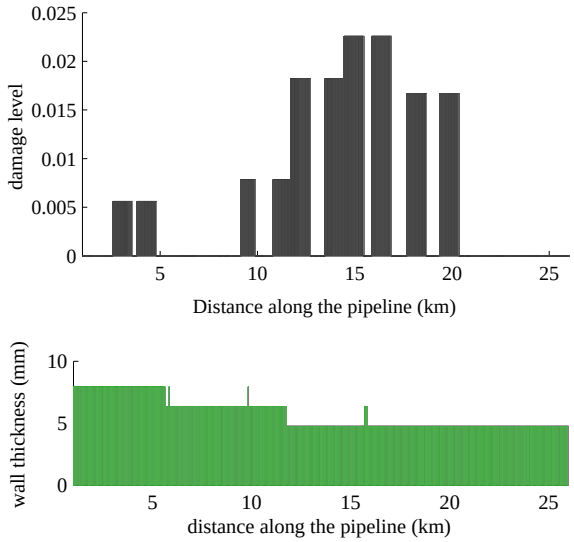

Figure 11.7: The distribution of damage level (upper plot) and pipe wall thickness (lower plot) along the pipeline. No tests were performed for intervals where damage level is zero.

Traces shown in Figure 11.6 were analysed to evaluate the condition of pipeline sections $a - e$ that are defined in Table 11.1. To evaluate the condition of different pipe section, standard deviation values were calculated for corresponding data windows. Larger value of standard deviation corresponds to a larger level of deterioration. thus, pipeline segments can be ranked accordingly. A graphical presentation of the results can be found in Figure 11.7.

The upper plot in Figure 11.7 represents the level of damage (defined by a standard deviation of the data window) for the tested pipe sections. Note that sections of the pipeline where damage level is equal to zero were not tested. There is a considerable difference in damage level between different sections of the pipeline. One of the reasons for this could be the fact that the wall thickness of the pipe is not constant throughout the length. The lower plot in Figure 11.7 shows the distribution of the pipe wall thickness. The comparison of two plots suggests that there might be a correlation between

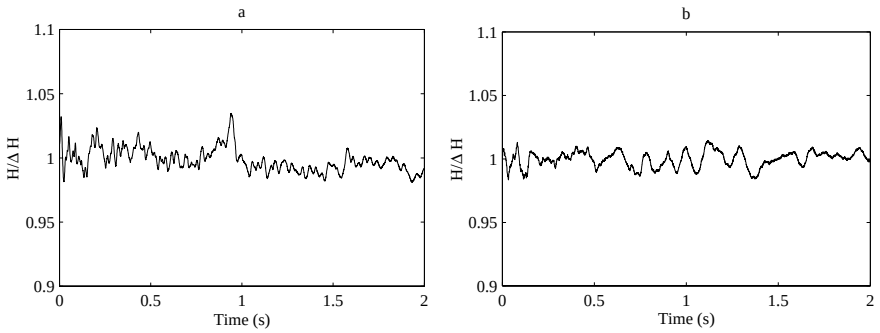

Figure 11.8: The analysed pressure traces from newer pipeline (parallel to the pipeline in Figure 11.4

the wall thickness and the level of the damage. As can be seen in Figure 11.7, the thicker-walled pipeline sections appear to be in better condition (smaller reflections). To provide a better perspective, two sections of a newer pipeline (built 15 years later parallel to the first pipeline) were tested using the same methodology. The measured transient responses are shown in Figure 11.8. The newer pipeline has the uniform pipe wall thickness of 7.94 mm. As expected, the transient response of the newer pipeline contains less reflections suggesting that the pipeline is in better condition. The standard deviation for tested segments was 0.0091 (Figure 11.8a) and 0.0062 (Figure 11.8b).

As indicated in Table 11.1, the length of the pipeline that was tested during the five tests that were conducted covers around 40 % of the total pipeline length. Additional tests would be required to assess the condition of the rest of the pipeline. The choice of the segment length X influences the speed of inspection. Having larger X will require less tests to inspect the same length of the pipeline. However, the resolution of the condition assessment results will be lower. The choice of X should be made for each system individually. Changing the experimental setup and using more sophisticated data analysis techniques could allow the evaluation of pipe segments on both sides of generation and measurement points separately. This is a subject of further development of the technique.

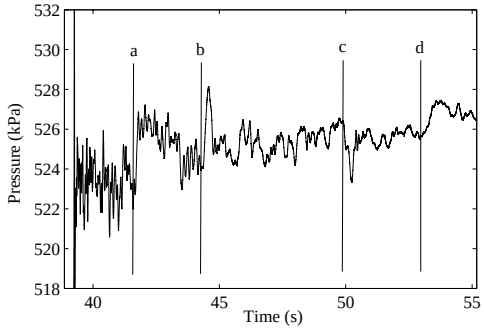

Figure 11.9: The transient pressure trace showing reflections from different physical elements

Identification of abnormalities

As suggested earlier in the chapter, discrete points (regions) of the pipeline can be identified where the observed transient reflections suggest some abnormal physical phenomena. In some cases transient wave reflections can be caused by a change in the physical properties of the pipeline due to the pipeline design. As an example, a fragment of the measured pressure trace is shown in Figure 11.9. Four reflections indicated by vertical lines (letters $a - d$):

a - the positive reflection at point a corresponds to the change in the pipe wall thickness from 4.76 mm to 6.35 mm at $11\,740$ m along the pipeline.

b - point b indicates the reflection coming from the 108 m long pipe section with a wall thickness of 6.35 mm pipe that is inserted in the section of the pipeline that has a wall thickness of 4.76 mm.

c - the negative reflection at point c comes from the closed cross-connecti with a parallel pipeline at $7\,250$ m along the pipeline.

d - the reflection at point d is due to the pipe wall thickness change from 6.35 mm to 7.94 at $5\,614$ m along the pipeline.

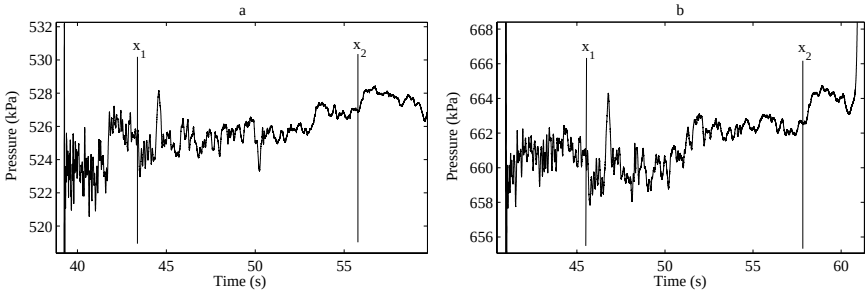

Figure 11.10: The transient pressure traces measured during two different tests (different test configurations) showing the reflections that indicate possible abnormalities

The available information about the pipeline allowed the identification of the sources of reflections described above. However, two other reflections (x_1 and x_2 in Figure 11.10) were evident on most of the measured traces that did not correspond to any physical element declared in the pipeline plan. Reflection x_1 matches the physical location at around $15\,300$ m along the pipe and is adjacent to the stop valve SV4 from the storage tank side. This area corresponds to a region where a CCTV camera inspection was previously performed by the water utility. The camera footage showed that a 30-meter long pipeline segment had lost most of its concrete lining and was highly affected by rust. Also, a large buildup of cement pieces was observed on the bottom of the pipe. It is likely that such a state of the pipe interior would result in the transient wave reflection that is observed at x_1.

The second reflection x_2 indicating the region where some abnormal condition of the pipe was suspected matches the physical location of around $21\,500$ meters along the pipe. A positive reflection of the pressure wave was detected. From the available information about the pipeline (extracted from the map) no known physical element could be identified that would cause the observed reflection of the transient wave. Furthermore, no CCTV footage was available from that region of the pipeline. It is possible that there are changes in the pipeline wall thickness at the points where reflections are coming from. These changes may not be indicated on the plan of the system. Therefore, CCTV inspection is suggested as a tool for validation.

11.3 Conclusions

This chapter uses field testing results to introduce and investigate the use of hydraulic transient analysis as the tool for the non-intrusive assessment of the pipeline condition. A level of deterioration has been quantified for 2 km long sections of a pipeline in the field based on the size of transient wave reflections coming from the segment of the pipeline. The size of the transient wave reflections was derived by calculating the standard deviation of the data window from the measured pressure trace that corresponds to the length of the analysed section of the pipeline. Results from the large transmission main tested showed that the pipe condition varies considerably along the length of the pipeline. Since the pipeline had wall thickness changes along the length, it was also suspected that the level of deterioration might be correlated with the wall thickness of the pipe.

Additionally, discrete points where the abnormal condition of the pipe interior was suspected were identified. Since the proposed technique is in the early stage of development, CCTV inspection is still required to validate the obtained results. Continued application on real pipelines will allow further investigation into the ability of hydraulic transient analysis to offer a low-cost and time-effective alternative for a non-intrusive pipeline condition assessment. The obtained information about the pipeline interior could be used for rehabilitation planning.

The proposed methodology can be used as a tool for initial rough testing to identify the areas of the pipe that are exposed to deterioration. Conventional NDE techniques (described in Chapter 3) can then be applied to the identified segments of the pipe.

Chapter 12

Diagnosis of inline valves

In this chapter, the method for systematic testing of inline valves on water transmission pipelines is described. Valves are the important asset that plays an important role in the reactive pipeline failure management, i.e. failure isolation. There has been little attention given to the problem of valve condition evaluation. Here, the results from two operational transmission pipelines are used to (a) identify the problem of poor valve seal quality and (b) validate the proposed technique for testing of the valve seal quality.

12.1 Introduction

Inline stop valves are important elements of a water supply system. Although during normal operation, valves have little or no function, they play a vital role when it comes to emergency situations or maintenance. A successful isolation of parts of the pipeline is essential for a quick reaction to the failure. Furthermore, a good closure of the valve is necessary when performing an inspection or maintenance of the pipeline. Often inline stop valves are not frequently operated, and as a result some of them might not seal properly when closed, particularly older valves. The current practice of water utilities includes the periodic exercise of inline valves. However, such a procedure does not provide the information about the quality of the valve's seal when fully closed. Thus, in most of the cases, valves with bad seal are identified

during the emergency situation or maintenance work when they fail to isolate the section of the pipeline. Some intrusive methods, primarily visual inspection, can be used to evaluate the condition of the valve. The costs of these procedures are high and they are both time and labour intensive. In addition, the operation of the pipeline has to be interrupted. Here, a non-intrusive pipeline valve testing technique based on the hydraulic transient analysis is presented.

12.2 Methodology

The description of the proposed methodology can be divided into two parts. The first part discusses how the reflection of the hydraulic transient wave at the valve can be used to quantify the quality of the valve seal. The second part describes the development of the method for the application on large water transmission mains.

Transient wave reflection at the valve

Hydraulic transients have proven to be able to collect the information about the physical configuration of the pipe interior as the pressure wave propagates along the pipeline length. The application of controlled hydraulic transients for inline stop valve testing is presented in this chapter. The quality of the valve closure can be evaluated based on the transient wave reflection from the valve. To quantify the degree of closure, the valve resistance coefficient K is used. Higher values of the valve resistance coefficient correspond to better valve sealing. The coefficient K depends on the ratio between the diameter of the pipe D and the diameter of the valve orifice D_o and the orifice discharge coefficient C_d:

$$K = \frac{(D/D_o)^4}{{C_d}^2} \tag{12.1}$$

The method of characteristics (MOC) (Wylie and Streeter; 1993) formulation for the orifice boundary condition is used to derive the expressions for

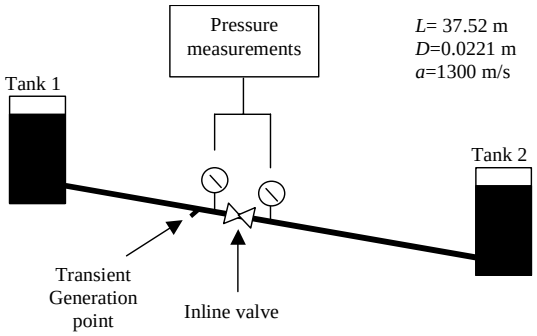

Figure 12.1: The laboratory pipeline system

calculating the magnitude of the transient wave transmitted through the orifice ΔH_T and the wave reflected from the orifice ΔH_R:

$$\frac{\Delta H_T}{\Delta H_W} = \frac{-(1 + H_o/BQ_o) + \sqrt{(1 + H_o/BQ_o)^2 + 2(Kg/2a^2)\Delta H_W}}{(Kg/2a^2)\Delta H_W} \tag{12.2}$$

$$\frac{\Delta H_R}{\Delta H_W} = 2 - \frac{\Delta H_T}{\Delta H_W} \tag{12.3}$$

where ΔH_W is the magnitude of the generated transient wave, $B = a/gA$ is the characteristic impedance of the pipe and a is the wave speed of the pipe. H_o is the steady state head loss across the orifice that corresponds to the steady state flow through the orifice, Q_o. Assuming that there will be no flow in the pipeline when the valve is closed for testing, the valve resistance coefficient K and corresponding valve orifice diameter D_o can be calculated as follows:

$$K = \frac{4a^2}{g}\left(\frac{\Delta H_W - \Delta H_T}{{\Delta H_T}^2}\right) \tag{12.4}$$

$$D_o = \frac{D}{({C_d}^2 K)^{0.25}} \tag{12.5}$$

where C_d is the discharge coefficient of the valve. To illustrate the relationship between valve closure and transient response the technique was tested on a laboratory pipeline (description of the system and testing procedure can be found in Appendix A). The experimental setup is shown in Figure 12.1.

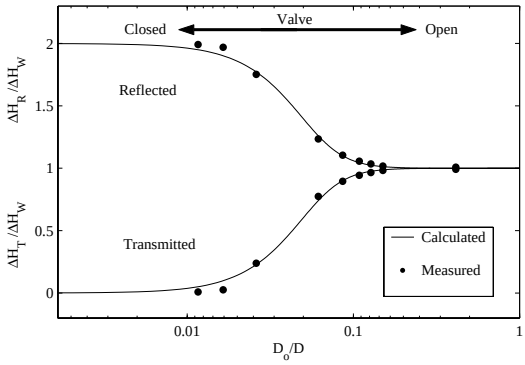

Figure 12.2: The transient wave transmission and reflection as a function of the valve opening

A gate valve was installed on a 37.52 m long cooper pipeline of the same diameter ($D = 0.0221$ m) connecting two pressurized tanks. For the tests, the entrance of tank 2 was closed and there was no flow in the pipeline. The transient ($\Delta H_W = 23$ kPa) was generated using a fast closure of the side-discharge solenoid valve and the pressure was measured at the sampling rate of $2\,000$ Hz on both sides of the gate valve.

Different values of the valve orifice D_o were tested between $D_o = 0$ (fully closed) and $D_o = D$ (fully open). The measured values are shown in Figure 12.2 (dots) along with the theoretical curves that represent the relationship between the transient wave reflection/transmission and valve opening (Equations 12.4 and 12.5). A good match between calculated and measured curves was found, indicating that the MOC formulation for the inline orifice boundary can be applied for a typical gate valve. Another feature that has to be noted in Figure 12.2 is that the transient wave reflection has the largest sensitivity when the valve is the position close to a complete closure ($D_o/D = (0.01 : 0.15)$). This feature is important for the seal quality testing of the valves, since it enables an identification and quantification of an incomplete sealing.

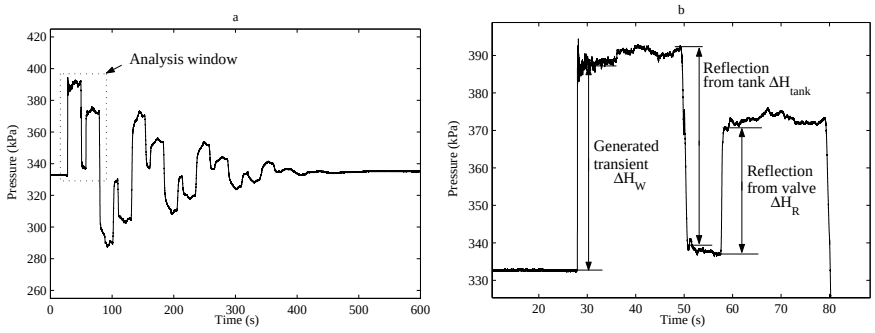

Figure 12.3: The example of (a) measured pressure response trace indicating the analysis window and (b) closer view of the analysis window showing the parameters used for evaluation of the valve seal

Modifications for large transmission mains

Since water transmission pipelines often have several valves distributed along the length at even intervals, it would be beneficial to be able to test all valves using one measurement and transient generation point. An example pressure response trace measured at the generation point is shown in Figure 12.3a. The transient is propagating in the pipeline that is terminated by a closed inline valve at one end and a tank at the other. A closer view of the data window used for further analysis (analysis window) is shown in Figure 12.3b, indicating the parameters that are used for valve condition assessment.

Equations 12.4 and 12.5 do not include frictional effects and are valid when the transient generation/measurement point is close to the tested valve. In the case when the valve is further away from the generation/measurement point, frictional losses have to be accounted for. Due to frictional losses, the magnitude of the transient wave that actually interacts with the valve is smaller than the magnitude of the transient wave measured at the generation/measurement point. In the same manner, the actual magnitude of the wave that is reflected from the valve is larger than the measured one. If a frictional loss is assumed to be uniform throughout the length of the pipeline, it can be estimated using the reflection from the tank ΔH_{tank} measured at the generation/measurement point. In a frictionless case, 100% of the

transient wave should be reflected from the tank. Since the transient wave has to travel the distance from the generation/measurement point to the tank and back, the measured friction loss $\Delta H_W - \Delta H_{tank}$ will correspond to the distance $2L_{M,tank}$, where $L_{M,tank}$ is the distance from the generation/measurement point to the tank. The friction loss for a unit length $h_{f,unit}$ can then be derived as:

$$h_{f,unit} = \frac{\Delta H_W - \Delta H_{tank}}{2L_{M,tank}} \tag{12.6}$$

At the moment of interaction with the valve, the magnitude of the transient wave ΔH_W is reduced by the friction loss corresponding to the distance from the generation/measurement point to the valve $L_{M,valve}$. The magnitude of the actual transient wave reflection from the valve ΔH_R^* is reduced by the friction loss corresponding to the same distance $L_{M,valve}$ when it is measured. Thus, the actual magnitude of the transient wave that interacts with the valve ΔH_W^* and the actual magnitude of the wave that is reflected from the valve ΔH_R^* are:

$$\Delta H_W^* = \Delta H_W - h_{f,unit} L_{M,valve} \tag{12.7}$$

$$\Delta H_R^* = \Delta H_R - h_{f,unit} L_{M,valve} \tag{12.8}$$

Since the pressure is measured only on the generation side of the valve, the magnitude of the wave that is transmitted through the valve is calculated from the magnitude of the reflected wave using Equation 12.3:

$$\Delta H_T = 2\Delta H_W^* - \Delta H_R^* \tag{12.9}$$

The actual magnitude of the transient wave interacting with the valve ΔH_W^* and the calculated wave transmission magnitude ΔH_T are then used in Equation 12.4 to calculate the valve resistance coefficient K. Equation 12.4 becomes:

$$K = \frac{4a^2}{g}\left(\frac{\Delta H_W^* - \Delta H_T}{{\Delta H_T}^2}\right) \tag{12.10}$$

and the corresponding valve orifice diameter D_o is then derived using Equation 12.5. The formulation derived above can be used for testing the seal quality of several valves on the same long pipeline when one generation/measu point is used.

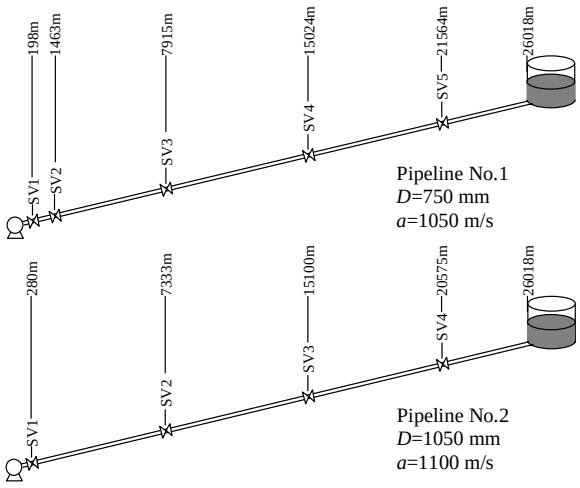

Figure 12.4: The layout of stop valves in Pipelines No.1 and No.2

12.3 Valve testing on large transmission pipelines

A total of nine inline stop valves from two parallel pipelines (No.1 and No.2, Figure 12.4) were tested using the method outlined in the previous section. The description of the pipeline system and measurement equipment can be found in Appendix A.

As noted in the previous section, to optimize the testing procedure, all the valves of each pipeline can be tested using the same transient generator location and pressure measurement location. Although, for the testing described below a total of four locations were used on each pipeline, only two generation/measurement locations were necessary. For each test, the test valve was closed by water utility's staff following the normal closure routine. One transient was generated to test each valve. The measured transient pressure responses for pipelines No.1 and No.2 are shown in Figure 12.5 and Figure 12.6 respectively.

For each trace, the data window was analysed to obtain magnitudes of the generated transient wave and its reflections from the valve and the tank as shown in Figure 12.3. Then, using Equations 12.7 to 12.10 and Equation

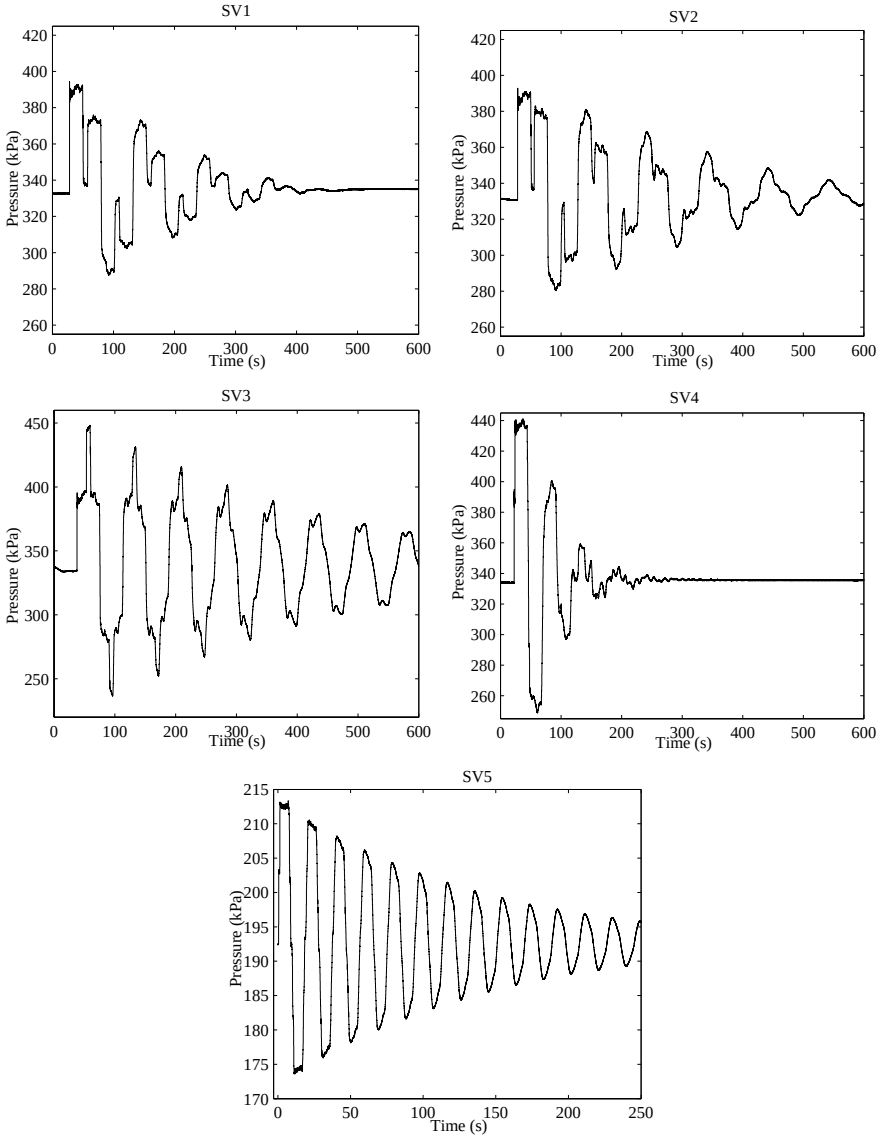

Figure 12.5: Pipeline No.1. Recorded transient propagation traces for tests of valves SV1-SV5.

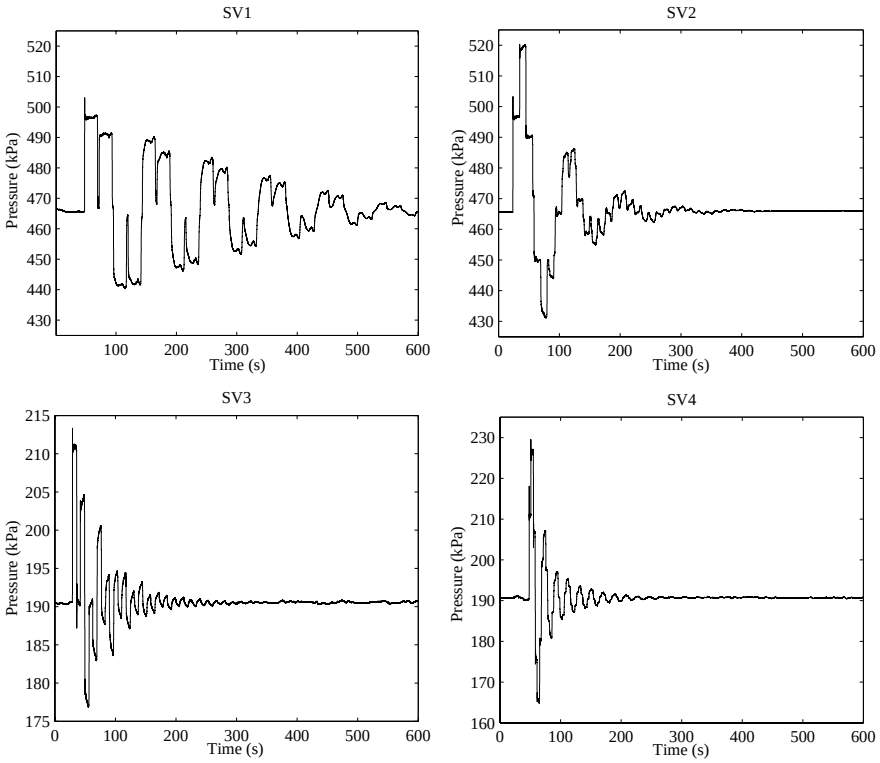

Figure 12.6: Pipeline No.2. Recorded transient propagation traces for testing valves SV1-SV4.

Valve	Reflection from valve,%	Reflection from tank,%	K	Closure %	D_o mm	Leak flow* L/s
Pipeline No.1						
SV1	58.50	95.65	$5.64 \cdot 10^5$	95.64	32.71	24.4
SV2	75.03	95.66	$2.65 \cdot 10^6$	97.04	22.21	10.8
SV3	81.25	95.46	$3.62 \cdot 10^6$	7.26	20.56	9.4
SV4	86.18	96.15	$3.39 \cdot 10^6$	97.25	20.59	6.5
SV5	93.72	99.24	$9.25 \cdot 10^7$	98.78	9.14	0.9
Pipeline No.2						
SV1	74.30	93.07	$5.64 \cdot 10^6$	97.55	25.76	15.32
SV2	66.28	93.99	$1.23 \cdot 10^6$	96.41	37.67	28.69
SV3	62.60	99.03	$1.25 \cdot 10^6$	96.42	37.57	21.72
SV4	72.09	96.12	$2.62 \cdot 10^6$	97.03	31.20	11.36

*an atmospheric discharge through D_o at the average steady state pressure and $C_d = 0.7$

Table 12.1: Results of valve tests

12.5, valve parameters were calculated. The test results for nine valves are shown in Table 12.1. Reflections from the valve and from the tank are shown for every valve as the percentage of the generated transient wave. The calculated diameter of the valve orifice D_o is used to derive the closure ratio (D_o/D). In the last column, the expected leak flow is estimated. It is found from the orifice equation, as an atmospheric discharge through the orifice with diameter D_o at the pressure equal to the average steady state pressure at each valve. This leak flow predicts the level of leakage in case the valve was closed for isolation and the downstream section of the pipeline was drained. However, the values are based on a theoretical calculation and need to be checked experimentally.

Based on the results presented in Table 12.1, the tested valves can be ranked in two different ways. The first approach is to rank valves by the resistance coefficient K. The larger the value of K, the better is the seal of the valve. The resistance coefficients of all tested valves are compared in Figure 12.7a. The second parameter that can be used to rank valves is the estimated leak flow. The smaller the estimated leak flow, the better the seal. The ranking based on the expected leak flow is shown in Figure 12.7b. In both cases, there is a considerable difference between the valves.

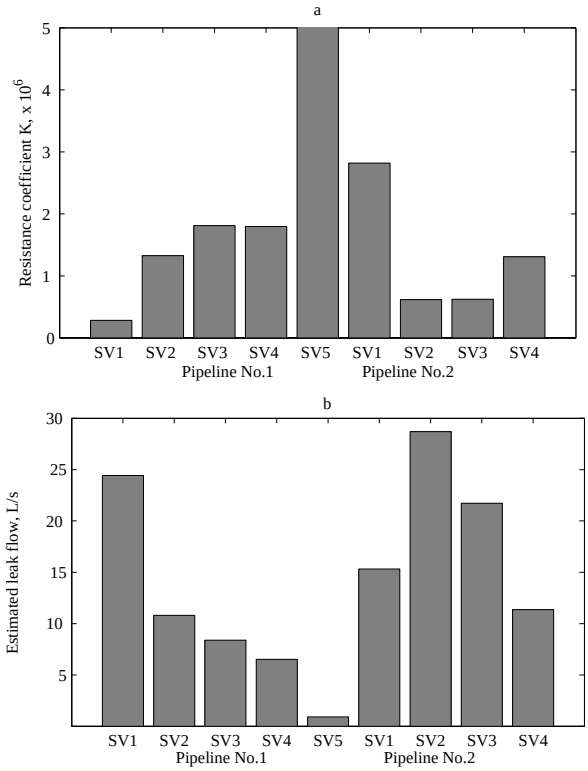

Figure 12.7: The ranking of all tested valves based on (a) the resistance coefficient K and (b) based on the estimated leak rate

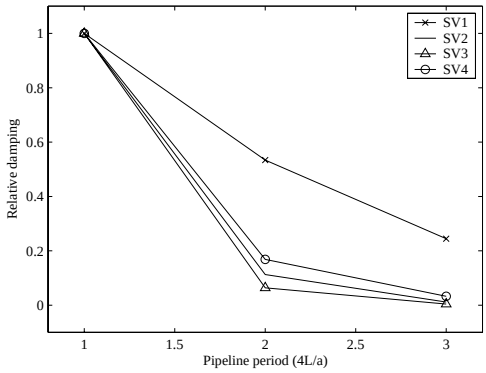

Figure 12.8: Hydraulic transient damping rates for different stop valve tests on pipeline No.2

Additionally to the transient wave transmission/reflection approach, transient wave damping analysis can be used to evaluate valve seal. A faster transient damping indicates worse seal of the valve, since more energy is dissipated through the valve. Damping rates for all valves on pipeline No.2 are shown in Figure 12.8. There is a good agreement with the resistance coefficient-based ranking presented in Figure 12.7a.

Figure 12.9 shows the measured relationship between the amplitude of the resonant frequency of the pressure response and the valve opening for a laboratory pipeline (Figure 12.1). The resonant frequency corresponds to the period of the transient wave oscillation and its amplitude is inversely proportional to the rate of the transient damping. Figure 12.9 confirms that the damping effect is increasing when D_o/D increases from 0 to 0.05. For larger openings ($D_o/D > 0.05$) the resonant frequency changes to the one corresponding to the total length of the pipeline. However, the change in the resonant frequency will not be usually relevant for valve seal testing.

12.4 Conclusions

Laboratory and field results have been presented in this chapter that show the potential of hydraulic transients for the evaluation of the valve closure. By inducing a controlled transient wave and recording the pressure response

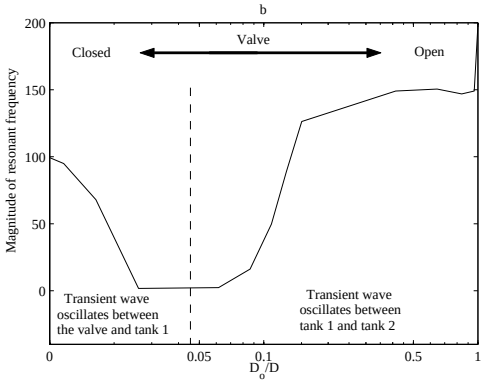

Figure 12.9: the magnitude of the resonant frequency as a function of the valve opening for a laboratory pipeline

at one point along the pipeline, it is possible to quantify the quality of the valve's seal. The valve resistance coefficient can be derived and the leak flow through the valve estimated. The approach has been verified for a laboratory pipeline, using a small gate valve. Nine large inline gate valves were tested on two field pipelines and results showed considerable variation in the seal quality. The proposed technique is a non-intrusive approach that can be used while planning the maintenance and replacement of inline stop valves. The testing can be performed under the normal operational regime of the pipeline. Only one generation/measurement station is required for all the valves that are present along the length of the pipeline. All this confirms the proposed methodology to be an inexpensive and efficient tool for evaluating the condition of inline stop valves. Although only the testing on the transmission pipeline was presented in this chapter, the proposed valve testing technique should be able to be used in distribution networks without any modifications.

Part V

Conclusions

Chapter 13

Concluding remarks

The overall objective of the work presented in this thesis was formulated in Chapter 1 as follows:

> to develop techniques that would utilise available measurement, data analysis, modelling and optimisation methods to reduce the risk of failure, minimise losses associated with failure and improve the reliability, availability, safety and efficiency of the urban water supply service.

Here, in the last chapter, the main conclusion that summarises the presented work is:

> it is possible to improve the current practices of failure management in urban water supply systems by applying systematic approaches that utilise the available measurement, data analysis, modelling and optimisation methods.

This chapter presents the main results of the work. A summary of the results is followed by a discussion of future work. Finally, some personal recommendations are given at the end of the chapter.

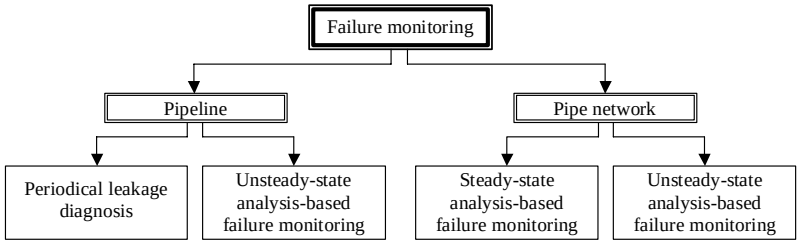

Figure 13.1: Techniques for failure monitoring

13.1 Main results

The work presented in this thesis was focused on the development of systematic approaches for effective failure management in urban water supply systems. Both proactive and reactive failure management techniques have been developed. The results can be divided into two parts: (1) failure monitoring, detection and location methods and (2) asset condition assessment techniques.

Failure monitoring, detection and location

Reactive failure management techniques that were presented in this thesis are summarised in Figure 13.1. Due to different topological and hydraulic characteristics, separate failure monitoring approaches were developed for single pipeline and pipe network applications. As knowledge about the burst development (burst opening) process is limited, two burst opening scenarios were considered. The first scenario assumes a sudden rupture of the pipe wall and the second scenario considers a burst, which develops over a longer period of time. Each scenario was applied to a pipe case and a network case and, as a result, a total of four approaches for failure monitoring, detection and location were developed. The first two techniques are applicable for automatic failure monitoring in pipelines and the other two methods were derived for automatic failure management in pipe networks.

Pipelines. For the pipeline case, two approaches were developed and tested. The first approach involves periodical diagnosis of leaks based on transient

response difference monitoring. An artificial hydraulic transient is periodically generated and the measured response trace is compared to the reference transient response that corresponds to a leak-free situation. It is sufficient to have a single pressure measurement point and a single transient generation point along the pipeline in order to detect and locate a leak. When the approach was validated on a full scale transmission pipeline, a relatively small leak was detected and located with a precision of 0.3% of the total length of the pipeline. In addition, the technique was shown to be capable of detecting an air pocket and a partial blockage in the pipeline.

The second technique is a burst monitoring, detection and location system designed for a quick reaction to sudden pipeline ruptures. A transient-analysis based approach is capable of issuing an alarm of a burst event and deriving the burst location automatically after the failure has occurred. Only one pressure monitoring station is necessary for the whole length of the pipeline, making the implementation and maintenance costs reasonably low. The proposed system has been successfully validated both in laboratory and field conditions. The results indicate that such a system can be applied in water transmission pipelines or in single branches of a distribution network, where immediate reactions to failures are critical.

The two pipeline failure monitoring approaches can be integrated into a multi-type failure monitoring, detection and location system. The integrated system would enhance the reliability and precision of failure detection and location.

Pipe networks. Two failure detection and location techniques were developed for application in water distribution networks. The first approach is based on steady-state analysis and can be applied on the level of a district metering area (DMA). The inflow rate is continuously monitored and the burst-induced change of flow rate is automatically detected. The location of the burst is derived using the distribution of the pressure, which is measured at a number of monitoring stations within the network. The method was successfully validated using simulated data. The optimal measurement point placement, uncertainty of the results, performance limits and implementation aspects of the technique were investigated. It was shown that a small DMA (300 properties) can be successfully monitored using one flow rate and between 2 and 4 pressure measurement points. The derived failure

locations had an error of less than 30 m.

The second approach for failure detection and location in a network is based on an unsteady-state analysis. Continuous monitoring of the pressure is performed at a number of locations within the network. In case of a sudden pipe failure, the burst-induced pressure wave is automatically detected at two or more monitoring stations. Arrival times and magnitudes of the transient wave measured at different monitoring stations are used to derive the location of the failure. The method enables quick and precise location of the failure regardless if it occurs at nodal or non-nodal (along pipes) locations. The technique has been successfully tested on a real water distribution network. Different aspects, such as the optimal placement of pressure monitoring stations, limits of burst sizes that can be detected, uncertainty of results and implementation aspects of the system, were investigated. Test results demonstrated that three pressure measurement stations were sufficient to monitor a network supplying around 250 households and bursts were located with a precision of 9 m without pre-calibration of the network model.

Combining the two systems into one would allow for a wider range of detectable failures as well as higher reliability of the failure detection and location.

Asset condition assessment

The asset-condition assessment-related part of the thesis is summarised in Figure 13.2. Two different assets of the water supply system were consid-

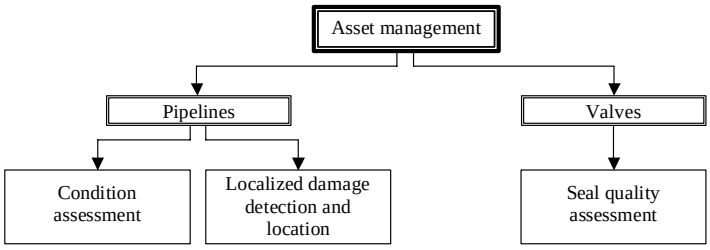

Figure 13.2: Asset management

ered – pipes and valves. Pipe condition assessment is part of the proactive failure management strategy, whereas valve condition testing is essential for isolation of the failure, i.e. is part of the reactive failure management exercise.

A nondestructive pipe evaluation (NDE) technique designed for condition assessment of transmission pipelines was presented. This technique can be used for two purposes: (1) as a proactive failure management tool and (2) for rehabilitation planning. The proposed inspection technique has a longer range and higher inspection speed than currently available NDE methods. A hydraulic transient wave is generated artificially and the measured response is analysed for pipe condition assessment. A comparative evaluation can be made where different sections of a pipeline are ranked depending on their condition. The proposed technique can also be used to identify sections of a pipeline where further inspection using more precise NDE techniques is necessary. The approach has been tested on a real transmission pipeline.

The last technique presented in this thesis was a transient-based inline valve seal testing methodology. For effective isolation of a failure, it is necessary that inline valves seal properly. Currently, there is no established methodology for testing the seal quality of valves. The developed approach is based on analysis of the transient wave reflection from a closed valve. The size of the valve opening is estimated and the corresponding leak flow rate through the valve is derived. The approach has been tested on inline valves in transmission pipelines.

13.2 Significance of results

The techniques presented in this thesis contribute to different points in the pipe asset management cycle and can improve *reliability, availability, safety* and *efficiency* of the urban water supply.

The developed transient-analysis-based nondestructive evaluation technique enables systematic condition assessment, which is faster and cheaper than currently practiced pipe inspection methods. A larger-scale condition assessment can make the proactive failure management more effective and increase

the *reliability* of the water supply system. More *efficient* planning of the rehabilitation process can be achieved by having more information about the current state of the assets. Proactive failure management prevents the failure itself, increasing the *availability* and *safety* of the water supply system.

Considering the average age and condition of pipe assets, it is reasonable to assume that, even if the proactive failure management practices are improved, the rate of pipe failures will increase in the future. Therefore, the reactive failure management practices have to be improved to reduce costs associated with failures. The techniques for leak and burst monitoring in pipelines and networks presented in this thesis can be used to reduce failure detection and location times. The presented valve testing methodology is designed to evaluate the quality of a valve's seal, which is essential to guarantee successful isolation of pipe failures. Quick and effective isolation of failures minimise associated losses, thus, increasing the *efficiency* of the supply system. At the same time, rapid and effective isolation reduces the probability that a failure will have consequences, which could be hazardous to society. The continuous failure monitoring system combined with the valve testing enhances the *safety* of the supply. By reduction of the reaction time to failure, the *availability* of the supply system is increased, since service interruption times are reduced.

13.3 Future work

The main goal for future work should involve further testing of the proposed techniques. Larger scale systems and a wider range of operational conditions have to be explored. In addition, some components of the work presented in this thesis should be completed or improved upon. These include:

The steady-state analysis-based network failure monitoring technique presented in Chapter 8 is the only method that has not been validated experimentally. Field validation of the approach is an important part of the future work.

The proposed condition assessment technique (Chapter 11) was developed during the late stage of the project and, due to time restrictions,

only an initial investigation was possible. Further testing and theoretical development are necessary to assess the applicability of the presented method. The data analysis should be automated.

Results from field testing have shown that conventional modelling of transients in pipelines and, especially, in networks does not offer reliable representation of reality. The improvement of existing models is a subject for future work. If improved, modelling can enable more extensive applications of inverse techniques which, in turn, would reduce measurement requirements.

13.4 Personal recommendations

Experiences and results of the work presented in this thesis have raised a number of considerations and ideas. This section is used to describe some personal impressions and recommendations regarding the future research and development (R&D) perspectives for the water industry.

For efficient failure management, the failure itself has to be identified. Historically, the term “leakage” described the whole range of failure sizes and types. However, the size and type of the failure is very important when selecting the methods that can be used for failure detection and location. As an example, hydraulic transient-based methods are not applied to leak inspection, since conventional leak inspection techniques (e.g. listening) are capable of detecting smaller leaks. However, as it was shown in this thesis, other types of failure exist, where transient analysis is superior to alternative methods for detection and location.

Continuous pressure monitoring is an essential step that has to be performed in order to take the operation and management of water supply systems to a more advanced level. Measured data are necessary for successful application of advanced techniques and methods, which have been developed during the last 10–20 years. Model-based techniques have shown potential which, unfortunately, has been limited by the reliability of models. Having high-quality data in real-time can change the situation. Continuous pressure monitoring has potential not only for failure detection and location, but

also for real-time pressure control, demand monitoring, detection of illegal consumption, identification of hydraulically dangerous activations in the system, model calibration and a number of other applications. Considering the potential benefit of pressure monitoring systems, the installation investment return time of the continuous monitoring system is likely to be short.

Asset management has been a topic of concern for the water industry for the last few years. In fact, the recent increase in the interest from the water industry side indicates that, in the near future, asset management can become the field where, in terms of R&D, the demand will exceed the supply. Increasing interest puts pressure on the research community for developing new asset condition assessment methods, which can offer extended capabilities at a lower cost. That is not an easy task. Focus has to be directed toward systematic approaches that offer full-scale application possibilities. The extent and age of existing pipe assets raise a concern that consequences of the deterioration process may become more apparent in the near future. The water industry is in need of techniques, which can offer fast and cost-effective evaluation of the current state of the assets that would allow for optimal planning of rehabilitation of these assets.

Part VI

Appendices

Appendix A

Laboratory and field testing

A total of 120 experimental tests were conducted in the laboratory and in the field as part of the work presented in this thesis. Experimental validation plays an important role in the overall contribution of the work. This appendix describes the measurement equipment, testing sites and procedures used in the experimental work.

A.1 Introduction

The literature review presented in Part I of the thesis has revealed the fact that few approaches described in the literature were validated experimentally, in a laboratory of in the field. Therefore, experimental validation was one of the objectives of this work. Table A.1 summarises the experimental work conducted during this research and, as it can be seen, a large part of the testing was conducted in afield conditions. In the following sections, the different test sites, the equipment used and test procedures followed are described.

A.2 Laboratory experiments

Two sets of tests were conducted on a laboratory pipeline - burst detection and location and inline valve testing. The results obtained were used in Chapters 6 and 12, respectively.

Testing	Type of system	Purpose of testing	Measurement system*	Results used in
Laboratory	Pipeline	Burst detection and location	1	Chapter 6
Field	Transmission pipeline	Leak detection and location	3	Chapter 5
Field	Branch in the network	Burst detection and location	2	Chapter 6
Field	Transmission pipeline	Burst detection and location	2,3,4	Chapter 6
Field	Network	Burst detection and location	3,4	Chapter 9
Field	Transmission pipeline	Condition assessment	2,3,4	Chapter 11
Laboratory	Pipeline	Inline valve testing	1	Chapter 12
Field	Transmission pipeline	Inline valve testing	2,3,4	Chapter 12

* Different setups of the measurement system are described in Table A.2

Table A.1: Summary of the conducted testing

The single pipeline system in the Robin Hydraulics Laboratory in the School of Civil and Environmental Engineering at The University of Adelaide, Australia was used for laboratory experiments. Figure A.1 shows the principal scheme of the pipeline. It is composed of a 37.527 m long copper pipe with an inside diameter of 22.1 mm and a wall thickness of 1.6 mm. There are 5 brass blocks along the pipeline (points A, B, C, D and E in Figure A.1). These blocks are used as connection points for pressure transducers and side-discharge valves. There is a ball valve at each end of the pipeline. Two pressurised tanks at each end of the pipeline control the steady state pressure and flow. The difference between the tank elevations is 2 m and the pressure is regulated by a computer control system. The maximum pressure of each tank is 70 m of head. A photograph of one Tank 1 is shown in Figure A.2.

The pressure was measured using Druck 810 flush fit pressure transducers, which were mounted in brass blocks, as shown in Figure A.3 (left). The flush fit prevents undesirable effects of the transducers interference with the fluid flow. The rise time of the transducers is 5×10^{-6} s, the absolute pressure range is 0 to 600 kPa and the uncertainty is $\pm 0.1\%$ of full span. The

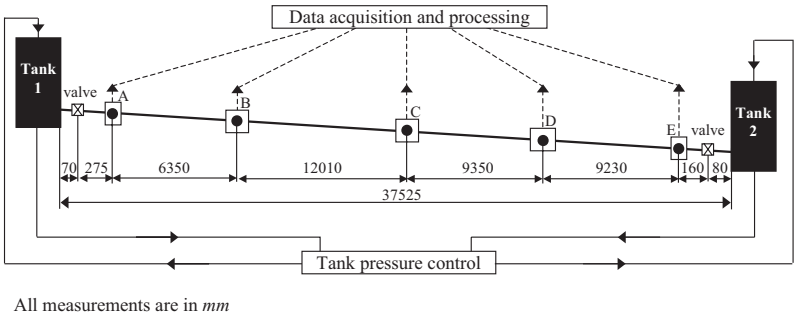

Figure A.1: Laboratory pipeline

transducers produce an output between 0 and 100 mV and an amplifier is required to amplify the measured pressure signal. The amplifiers used in the laboratory setup had a gain of 100, resulting in the amplifier output from 0 to 10 V. The data acquisition was performed on a 150 MHz Pentium computer using a Intelligent Instrumentation data acquisition card and visual designer software (see Figure A.2). A 12 bit A/D (analog to digital) converter was built into the card.

Burst detection and location - laboratory pipeline. The burst was simulated by opening a solenoid side-discharge valve (shown in Figure A.3 (right)). The calibrated lumped discharge parameter of the solenoid valve was $C_d A_0 = 1.7665 \times 10^{-6}$ m^2 and the opening time was estimated to be 4 ms. The manual opening of a side discharge valve was also used to simulate a slower burst. In that case, $C_d A_0$ was equal to 6.0192×10^{-7} m^2 and the estimated opening time was 30 ms. Since the burst had to be first detected and then located, the pressure measurements were started prior to the opening of the solenoid valve.

Inline valve testing - laboratory pipeline. To test the algorithm for an inline valve seal quality evaluation, a standard 1-inch inline gate valve (Figure A.4) was installed at the middle point of the laboratory pipeline (point C in Figure A.1). A fast closure (4 ms closing time) of the solenoid valve was used to generate a positive transient wave. Different degrees of opening of

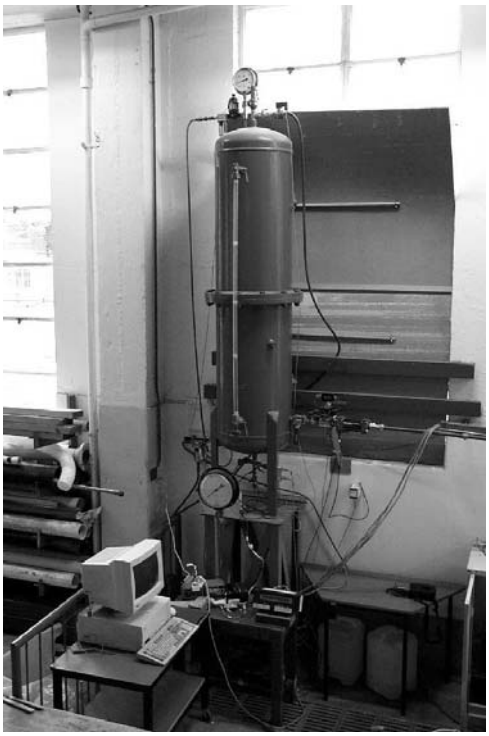

Figure A.2: Boundary tank (Tank 1) and data acquisition system.

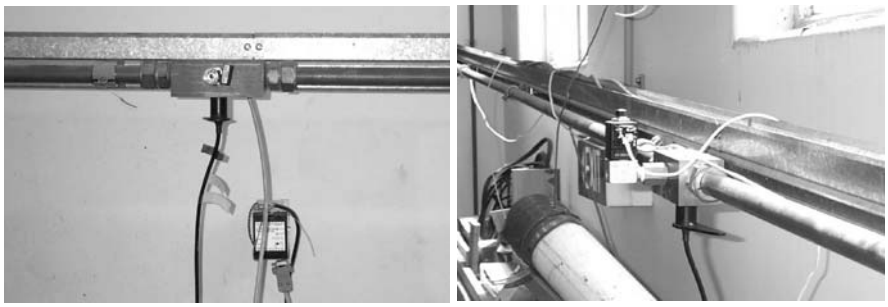

Figure A.3: Pressure transducer in a brass block (left) and solenoid valve (right)

Figure A.4: Inline gate valve used in the laboratory experiments

the inline valve were tested defined by the number of turns that the valve was open. After the testing, the inline valve was taken off the pipeline and the area of the valve orifice was measured for the number of turns corresponding to different tests.

A.3 Field experiments

The main part of the experimental work presented in this thesis was conducted in the field. Field tests can be divided into two parts: (1) tests in a distribution network, and (2) tests on transmission pipelines. All test systems were operational.

Network test

All network tests were performed in part of the Willunga network, corresponding to one of two pressure zones. Willunga is a township located on the southern edge of metropolitan Adelaide, South Australia. The local water utility divided the whole network into two pressure zones by permanently closing a number of isolation valves. Thus, the test network (single pressure zone) is completely isolated from the rest of the system. It has a size corresponding to a typical DMA and supplied around 250 households. A fixed-head reservoir is the main source of water and a pumping station is used to fill the reservoir, where pumping is controlled by the level of the reservoir. The pumping station is the only connection point to the rest of the system. The network has approximately $7\,550$ m of pipes with three discrete diame-

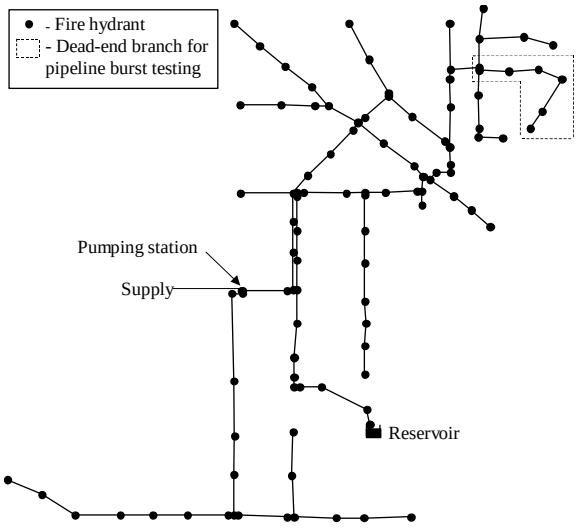

Figure A.5: Layout of the Willunga network used in field tests

ters: 100 mm (80% of the total length), 150 mm (10% of the total length) and 250 mm (10% of the total length). The majority of pipes are asbestos-cement (AC) pipes. The steady-state pressure varies betwen 20 and 80 m throughout the network.

Burst detection and location - network. Network burst detection and location tests were performed on the full-scale of the test network, i.e. no further division of the network was used. Since most of the pipes were AC pipes, the wave speed value was estimated for one of the dead-end AC branches and adopted to the rest of the network. The wave speed of the pipe was estimated from the measured travel time of the wave between two transducers that were connected to fire hydrants. Syncronisation of pressure measurements at two points is discussed later in this appendix. The estimated wave speed value was 1 120 m/s, which was in a good agreement with the theoretical wave speed of 1 100 m/s. Since the whole Willunga network was divided into two pressure zones by permanently closing isolation valves, a number of loops were discontinued. Thus, the test network had only two loops. The GIS map of the network is not available, but the layout of the network model is shown in Figure A.5.

Figure A.6: Connected fire hydrant cap with incorporated transducer.

Fire hydrants were used to connect pressure transducers and a burst generator during the tests. Fire hydrants are common elements of a water distribution network, usually located around 100 m apart. A fire hydrant plug comprises a valve chamber, which allows a standpipe or hose connection to be made. Special fire hydrant caps incorporating pressure transducers were produced for pressure measurements. A transducer is placed in such way that its face is exposed to the flow stream in the pipe beneath the fire hydrant plug. This setup allowed measuring the pressure within the pipe. Figure A.6 shows a connected pressure sensor plug. Each transducer was connected to a measurement system that will be discussed later in this appendix.

To simulate a pipe burst, a sudden opening of the discharge through the fire plug was used. A solenoid valve (Figure A.7) was used as the burst genera-

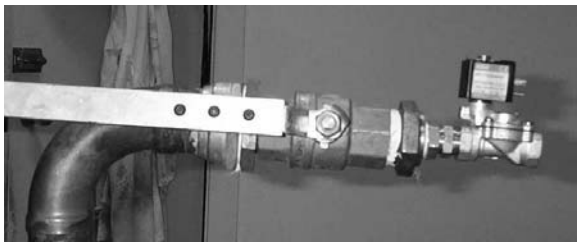

Figure A.7: Solenoid valve connected to the standpipe

Figure A.8: Experimental burst

tor. The internal diameter of the solenoid valve was 10 mm and the lumped discharge parameter $C_d A_0$ was equal to 5.4978×10^{-5} m^2. The valve was attached to the end of a standpipe that was connected to a fire hydrant plug. Figure A.8 shows the actual generated burst.

During the network burst tests, three pressure measurement stations were deployed at different locations within the network. The stations were kept in the same position for the whole length of testing. The burst generator was moved around the network to artificially generate bursts at different locations. Thus, the whole experimental setup can be divided into four stations - three measurement points and one mobile generator station. Radio communication was used between the stations. Pressure measurements at all the stations were synchronised in time, as discussed in more detail later in this appendix. Radio trigger was used to start all three measurements simultaneously and the burst generator was opened after the measurements were started. As already mentioned, this procedure was used to mimic the real situation where pressure is monitored continuously and the time of the burst is not known in advance.

Burst detection and location - a branch of a network. The pipeline burst detection and location algorithm (Chapter 6) was also validated on a single dead-end branch of the network. Tests were performed on a selected ductile iron concrete lined (DICL) branch of the Willunga network that was

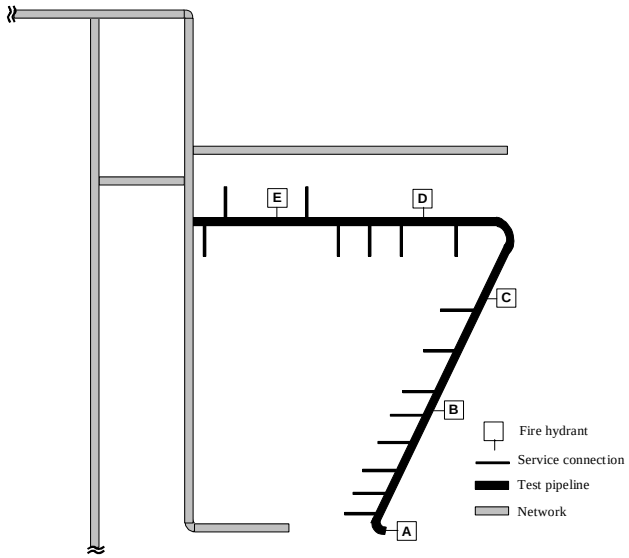

Figure A.9: Layout of the test branch

356.53 m long and had a diameter of 100 mm. The branch had a dead-end as one boundary and was connected to the rest of the network by a tee-junction at the other end, as indicated in Figure A.5. A more detailed schematic view of the test branch is shown in Figure A.9. Five fire hydrants are located at equal intervals along the length of the pipeline. A total of 15 service connections with diameters between 15 and 25 mm were connected to the branch. The estimated wave speed value for the pipe was 1 150 m/s.

Burst tests were performed using the same burst generator, pressure measurement equipment and the same procedure as in the network. During all network and branch burst tests, the distribution network was fully operational, i.e. no pipes or service connections were isolated. Tests were conducted during the day and the network had a normal water consumption pattern.

Pipeline tests

Several sets of tests were conducted on transmission pipelines. Two parallel mild steel concrete lined (MSCL) water transmission pipelines that are a part of the larger transmission system in South Australia were selected for testing.

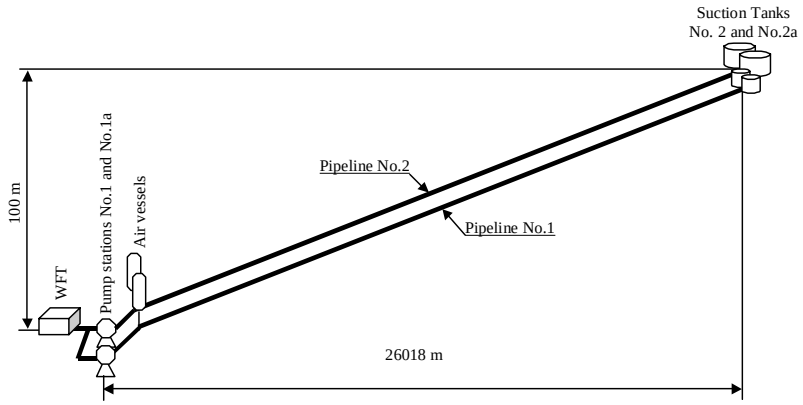

Figure A.10: Layout of the transmission pipeline system

The pipelines run in parallel from the water filtration plant (WFP) to the pair of tanks as shown in Figure A.10. The length of each pipeline is $26\,018$ m. Pipeline No.1 has a diameter of 750 mm and Pipeline No.2 has a diameter of $1\,050$ mm.

Pipeline No.2 has a uniform wall thickness of 7.94 mm along its whole length and the estimated wave speed value was 1100 m/s. The wall thickness of pipeline No.1 varies along the length. Starting from the upstream end at the WFP, the first 22% of the pipeline length has a wall thickness of 7.94 mm, the next 23% has the wall thickness equal to 6.35 mm and the remaining length of the pipeline (55%) has the wall thickness of 4.76 mm. There are two short sections (10 m each) of 7.94 mm pipe in the 6.35 mm part of the pipeline and a 100 m long section of 6.35 mm pipe in a 4.76 mm part of the pipeline. Changes in the wall thickness made the wave speed measurement process more complicated. However, using a number of different measurement locations, the wave speed values were estimated to be $1\,100$ m/s, $1\,030$ m/s and 950 m/s for the pipeline segments with wall thicknesses of 7.94 mm, 6.35 mm and 4.76 mm, respectively.

Leak detection and location - transmission pipeline. A pressure transient for leak detection and location tests (Chapter 5) was generated using the custom-built transient generator shown in Figure A.11. A $1/4$ turn ball valve with a diameter of 75 mm is closed by a spring that is released using a

Figure A.11: Transient generator

launching device, which can be triggered mechanically or actuated remotely using a power supply. The transient generator was designed to be mounted on a scour side-discharge valve. Different size nozzles can be attached on the generator to control the discharge flow rate and the size of the generated transient. The closing time of the generator was estimated to be 10 ms.

Since fire plug air valve (FPAV) connections are distributed at even distances along the length of the transmission pipeline, pressure transducers were connected to the pipeline in the same way as for the network tests. The transducer was mounted into a special cap and connected to the FPAV connection. A leak was simulated by opening the FPAV or as a discharge through the standpipe. An example of an artificially generated leak is shown in Figure A.13.

Burst detection and location - transmission pipeline. Burst detection and location tests (Chapter 6) were performed using the same setup as for the leak tests. A burst was simulated by opening the transient generator (Figure A.11) manually. In that way, different burst opening times could be simulated. Generator nozzles were used to adjust the size of the burst. Manual opening of the valve attached to the end of a standpipe, which was connected to a fire plug was also used to simulate the burst. To recreate a realistic burst situation, pressure measurements were started before the opening of the generator. In that way, a continuous pressure monitoring situation was simulated, where the burst time is unknown prior to the event.

Figure A.12: Pressure transducer mounted on the fire hydrant plug

Figure A.13: Artificially generated leak

Figure A.14: Valve operation

Condition assessment - transmission pipeline. The procedure of tests for pipe condition assessment is similar to the one for leak detection and location. A transient was generated using the transient generator mounted on a scour valve and the pressure was measured using a single measurement station located close to the generator. During one test, the condition of a 2 km long pipeline section was assessed. To test another section of the pipeline, both transient generation and pressure monitoring stations had to be moved.

Inline valve testing - transmission pipeline. For inline valve testing (Chapter 12), inline gate valves were closed following the normal procedure (Figure A.14) and the transient was generated using the same generator as for the leak and condition assessment tests. A single pressure measurement was set up by connecting the transducer to the fire plug. The measurement and generation points were placed between the downstream boundary of the pipeline and the valve that was tested.

A.4 Synchronization of measurements

The wave speed value for a pipe was obtained from the measurement of the wave travel time between two measurement points placed at different locations along the pipeline. Such an experiment requires synchronization of the two pressure measurements. For the network branch tests, this synchronisation was achieved by connecting two measurement stations to a common

cable and sending a voltage trigger before starting a test. The voltage change reaches both stations simultaneously in less than one millisecond and the data acquisition program was modified to record the voltage signal. In this way, the error of synchronisation was limited to one sampling period.

Continuous burst monitoring tests in the network situation also required measurements at different stations to be synchronised. However, the same synchronisation principle used for the wave speed estimation could not be employed, since the distances between measurement stations were longer. Thus, an alternative wireless approach had to be developed. A radio triggering system was developed in the instrumentation laboratory of the School of Civil and Environmental Engineering at the University of Adelaide, Australia. Synchronisation units were built to convert a short audio signal transmitted through the radio into a voltage step that was used as an external trigger for the data acquisition process. An audio signal of a pre-defined frequency was generated using a specially built beeper. The signal was transmitted using a "master" radio. Receiver radios at all measurement stations were connected to the trigger units that were monitoring for a trigger signal. Once received, the trigger signal was converted to a voltage step that, in turn, acted as an external trigger for the data acquisition program.

The same system was used to estimate wave speed values of the transmission pipelines. Precise synchronisation of pressure measurements was observed for a distance of up to 4 km between measurement stations.

A.5 Development of the measurement system

The laboratory measurement system has been described in Section A.2. The measurement system that was used for the field testing consisted of three pressure measurement stations. All three stations had the same function and structure. Figure A.15 shows a measurement station that is set up for testing. A transducer is connected to a connector block (6) that transfers a measured signal to a data acquisition unit (4). The transducer is powered using two 12 V batteries (3). The data acquisition unit is connected to a PC (8) that has data acquisition software installed on it. That software is used to control the process of data acquisition and to store the data on a hard disc drive (HDD) of the PC. The PC and the data acquisition unit are powered from a 12 V car

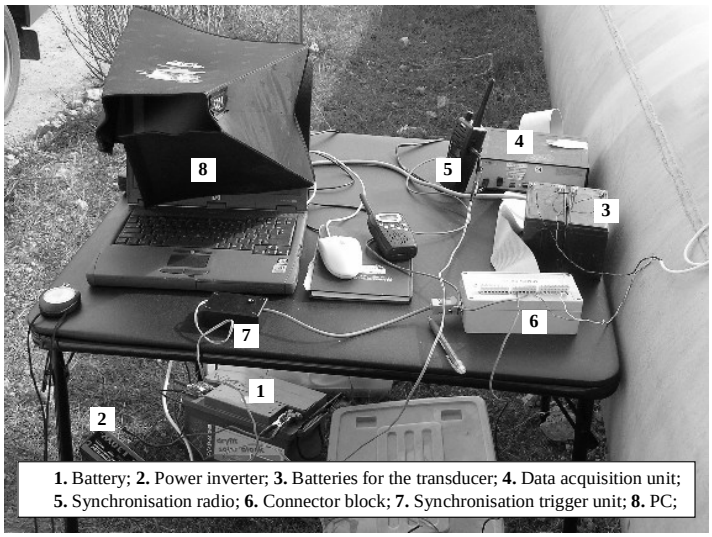

Figure A.15: Setup of the measurement station

battery (1) through a power inverter (2). Finally a synchronisation radio (5) is connected to a trigger unit (7) to generate an external trigger for the data acquisition program.

The measurement system that was used for testing was continuously developed and modified by engineers at the instrumentation laboratory at the School of Civil and Environmental Enguneering, the University of Adelaide, Australia. A feedback from field tests was used to improve the measurement system. Table A.2 describes different setups of the measurement system.

Setup 1 represents the laboratory measurement system, described in Section A.2, and is shown for comparison. Setups 2-4 correspond to different stages in the development process of the field measurement system. It has to be noted that the maximum sampling frequency of different setups is not declared in Table A.2 since it was much higher than the sampling frequency used during the testing. The setup of the measurement system for different types of tests was presented in Table A.1. For some tests, two or more setups were used. There were two reasons for that - first, some tests were conducted at two or more different occasions and, second, in some tests two or more

System setup	A/D card	Transducer range (kPa)	Amplifier gain	Measurement resolution (kPa)	DAQ software
1	12 bit	0-600	100	0.146	Visual Designer™
2	12 bit	0-1500	100	0.366	Visual Designer™
3	12 bit	0-1500	100-1500	0.366-0.025	Visual Designer™
4	16 bit	0-1500	100-1500	0.0229 - 0.001525	LabVIEW™

Table A.2: Parameters of different setups of the measurement system

measurement points were used simultaneously with different setups of the measurement system.

As it is shown in Table A.2, during the process of development, the resolution of pressure measurements was increased 240 times (from 0.366 to 0.001525 kPa). Such an increase was achieved by replacing the 12 bit data acquisition unit with a higher-resolution one (16 bit) and implementing a variable-gain amplification. A variable-gain amplifier enabled a reduction of the measured pressure range of up to 15 times. Discrete values of the amplifier gain were used, corresponding the pressure range reduction of 1, 2.5, 5, 7.5, 10, and 15 times. An offset mechanism was implemented to define the middle point of the measured pressure range. Depending on the selected gain, a certain range of the pressure around the offset value was amplified to the size of the full span of the amplifier's output.

Measurement noise was a problem in the early stage of testing. However, using earth stakes and shielding of the equipment, a considerable reduction in the measurement noise level was achieved. Because of the noise reduction and the increase in resolution, each new setup of the measurement system offers completely different precision of pressure measurements.

The latest version of the data acquisition unit (No. 4 in Table A.2) is shown in Figure A.16. Having a relatively small size (length=280 mm; width=200 mm; height=76 mm), this integrated device includes batteries, a variable-gain amplifier, a data acquisition card and a radio synchronisation unit.

The measurement system is being further developed at the University of Adelaide and it is planned to include a GPS-based synchronisation unit and data logger.

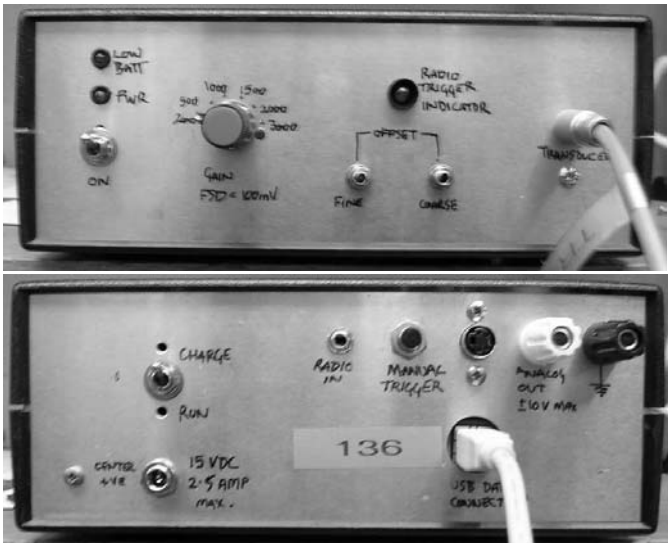

Figure A.16: Front and back panels of the data acquisition unit

Appendix B

Fluid transient modelling

In this appendix, the details of a computer simulation model based on the Method of Characteristics for modelling transients in pipelines and pipe networks is presented.

B.1 Introduction

A number of commercial software packages for transient simulation in water distribution pipelines and networks are available on the market. The use of these tools for research purposes is limited. The main restriction is the fact that no changes can be made in the source code, which means that modification of existing and implementation of new elements (such as boundary conditions or unsteady friction models) is prohibited. Therefore, as a part of the work described in this thesis, a hydraulic transient model was implemented.

B.2 Model implementation

The Method of Characteristics (MOC) is used for solving governing unsteady flow equations. The computer code is written in C++ programming language. The transient model is integrated with EPANET steady state hydraulic solver (Rossman; 2000), which is employed for simulating steady state flow in the network to establish the initial flow conditions for the tran-

sient simulation. Another important feature is the graphic user interface offered by EPANET. A network model is created and modified in a quick and convenient way. The model input files from most of the commercial software packages are compatible with EPANET.

Governing equations

Unsteady state flow in a closed conduit can be described by equations derived from the principles of conservation of mass and linear-momentum. The detailed derivation of governing equations is not demonstrated in this section, but can be found in Wylie (1983). The following simplified form of the continuity and motion equations is most commonly used

$$\frac{\partial H}{\partial t} + V\frac{\partial H}{\partial x} + \frac{a^2}{gA}\frac{\partial Q}{\partial x} = 0 \tag{B.1}$$

$$\frac{1}{gA}\frac{\partial Q}{\partial t} + \frac{V}{gA}\frac{\partial Q}{\partial x} + \frac{\partial H}{\partial x} + \frac{fQ|Q|}{2gDA^2} = 0 \tag{B.2}$$

where:

H	=	hydraulic head
Q	=	volumetric flow rate
V	=	mean velocity of the flow
g	=	gravitational acceleration
x	=	distance along the pipe
t	=	time
a	=	wave speed in a conduit
f	=	friction factor
D	=	pipe diameter
A	=	cross-sectional area

A number of assumptions were made while deriving the governing unsteady Equations B.1 and B.2:

- Liquid flow is one-dimensional and homogenous. Total hydraulic head does not change in the axial direction. Density is constant in the axial direction. Velocity is assumed to be uniform and the average value is used.

- The pipe is horizontal and full at all times.
- Both pipe and fluid are assumed to deform according to linear elasticity.
- Friction is evaluated using the Darcy-Weisbach equation. Unsteady friction loss is assumed to be equal to steady flow friction loss.

Wave speed in a conduit

In Equation B.1, the wave speed or celerity, a, is introduced. The wave speed specifies the speed of the pressure disturbance propagation through the fluid in the pipeline. When performing transient analysis, a generalised formula (Wylie and Streeter; 1993) for the wave speed in a thin walled ($D/e > 25$) elastic conduit is

$$a = \sqrt{\frac{\frac{K}{\rho}}{1 + \frac{K}{E}\frac{D}{e}\phi}} \tag{B.3}$$

where: K = bulk modulus of elasticity of the fluid
e = pipe wall thickness
E = Young's modulus of elasticity of the conduit walls
ρ = fluid density
ϕ = parameter depending on the pipe anchoring

For the case when a pipe is anchored against longitudinal movement throughout its length, $\phi = 1 - \mu^2$, where μ is the Poisson's ratio of the pipe material.

Method of characteristics

The Method of Characteristics is currently one of the most popular techniques for solving governing unsteady state equations. The technique is simple and computationally efficient. It is based on the transformation of partial differential equations into ordinary differential equations that apply

along specific lines called characteristics. MOC has an extremely flexible solution scheme, which allows fast implementation of models for networks, boundary conditions and non-pipe elements. The discontinuities, such as a fast valve closure, are also handled by MOC.

The governing unsteady pipe flow equations are rewritten as:

$$L_1 = \frac{\partial H}{\partial t} + V\frac{\partial H}{\partial x} + \frac{a^2}{gA}\frac{\partial Q}{\partial x} = 0 \tag{B.4}$$

$$L_2 = \frac{1}{gA}\frac{\partial Q}{\partial t} + \frac{V}{gA}\frac{\partial Q}{\partial x} + \frac{\partial H}{\partial x} + \frac{fQ|Q|}{2gDA^2} = 0 \tag{B.5}$$

Using the multiplier λ, a linear combination of Equations B.4 and B.5 is derived as:

$$\begin{aligned}\lambda L_1 + L_2 = {} & \frac{1}{gA}\left[\frac{\partial Q}{\partial t} + \left(V + \lambda a^2\right)\frac{\partial Q}{\partial x}\right] + \\ & \lambda\left[\frac{\partial H}{\partial t} + \left(V + \frac{1}{\lambda}\right)\frac{\partial H}{\partial x}\right] + \frac{fQ|Q|}{2gDA^2} = 0\end{aligned} \tag{B.6}$$

The bracketed terms are reduced to form the directional derivatives of Q

$$\frac{dQ}{dt} = \frac{\partial Q}{\partial t} + \frac{dx}{dt}\frac{\partial Q}{\partial x}$$

and H

$$\frac{dH}{dt} = \frac{\partial H}{\partial t} + \frac{dx}{dt}\frac{\partial H}{\partial x}$$

by introducing

$$\frac{dx}{dt} = V + \lambda a^2 = V + \frac{1}{\lambda} \tag{B.7}$$

Equation B.6 then becomes the ordinary differential equation

$$\frac{1}{gA}\frac{dQ}{dt} + \lambda\frac{dH}{dt} + \frac{fQ|Q|}{2gDA^2} = 0 \tag{B.8}$$

The equality in Equation B.7 leads to

$$\lambda = \pm\frac{1}{a} \tag{B.9}$$

which, when substituted back into Equation B.7, yields

$$\frac{dx}{dt} = V \pm a \tag{B.10}$$

Equation B.10 represents the propagation velocity of a disturbance in a pipe. In water pipes the wave speed is typically three orders of magnitude larger than the velocity of flow. Thus, the flow velocity can be neglected. Equation B.10 then becomes

$$\frac{dx}{dt} = \pm a \tag{B.11}$$

Equation B.11 defines two straight lines, called characteristics, along which the variables are differentiated. The characteristic associated with positive a is referred to as the C^+ characteristic, and the C^- characteristic is associated with negative a. Substituting corresponding values of λ into Equation B.8 leads to two pairs of equations which are grouped and identified as C^+ and C^- equations

$$C^+ : \quad \begin{cases} \dfrac{a}{gA}\dfrac{dQ}{dt} + \dfrac{dH}{dt} + \dfrac{fQ|Q|a}{2gDA^2} = 0 \\ \dfrac{dx}{dt} = +a \end{cases} \tag{B.12}$$

$$C^- : \quad \begin{cases} \dfrac{a}{gA}\dfrac{dQ}{dt} - \dfrac{dH}{dt} + \dfrac{fQ|Q|a}{2gDA^2} = 0 \\ \dfrac{dx}{dt} = -a \end{cases} \tag{B.13}$$

Equations B.12 and B.13 are called compatibility equations and are used to solve for points in the xt plane as shown in Figure B.1.

The solution of compatibility equations is achieved by integration along the characteristics

$$C^+ : \quad \frac{a}{gA}\int_A^P dQ + \int_A^P dH + \frac{fa}{2gDA^2}\int_A^P Q|Q|dt = 0 \tag{B.14}$$

$$C^- : \quad \frac{a}{gA}\int_B^P dQ - \int_B^P dH + \frac{fa}{2gDA^2}\int_B^P Q|Q|dt = 0 \tag{B.15}$$

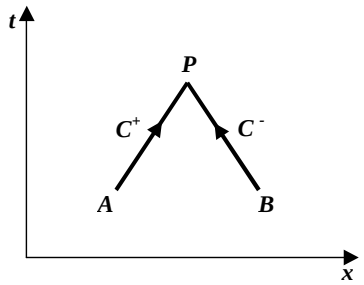

Figure B.1: Characteristics in the xt plane

The equations are integrated using an approximation of the friction term (the third term on the left hand side), which restricts results to a small increment in time Δt and space $\Delta x = a\Delta t$:

$$C^+ : \frac{a}{gA}(Q_P - Q_A) + (H_P - H_A) + \frac{f\Delta x}{2gDA^2}Q_{AP}|Q_{AP}| = 0 \quad \text{(B.16)}$$

$$C^- : \frac{a}{gA}(Q_P - Q_B) - (H_P - H_B) + \frac{f\Delta x}{2gDA^2}Q_{BP}|Q_{BP}| = 0 \quad \text{(B.17)}$$

where Q_{AP} and Q_{BP} represent the "average" flow along the characteristics during time Δt. Integration of the friction term requires an approximation of the behavior of the flow between end points of characteristics. As suggested by Arfaie et al. (1993), a linear approximation is used. The flow at one end of the characteristics is used in one Q-term and the flow at the other end in the other Q-term, which gives:

$$C^+ : \frac{a}{gA}(Q_P - Q_A) + (H_P - H_A) + \frac{f\Delta x}{2gDA^2}Q_P|Q_A| = 0 \quad \text{(B.18)}$$

$$C^- : \frac{a}{gA}(Q_P - Q_B) - (H_P - H_B) + \frac{f\Delta x}{2gDA^2}Q_P|Q_B| = 0 \quad \text{(B.19)}$$

Research has shown that steady state friction approximations do not generate a sufficient level of damping when compared to experimental results. The introduction of an unsteady friction term causes extra damping and a better fit with experimental data. The implementation of unsteady friction is presented in Section B.3.

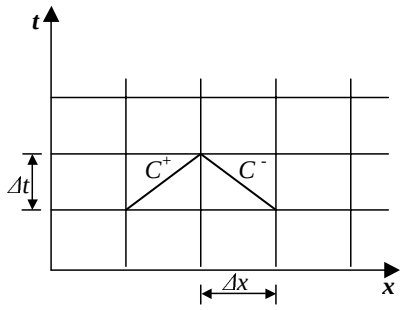

Figure B.2: xt plane with characteristics grid

The simultaneous solution of two compatibility equations yields the conditions at a particular time and position in the xt plane designated by point P (Figure B.1), given that the conditions at a previous time step are known (points A and B). The grid can be formed of small units (Figure B.2). This grid is called the characteristics grid.

Two forms of characteristics grid can be used for solving unsteady flow equations - diamond grid or rectangular grid (Figure B.3). A diamond grid is implemented in the described solver. This choice was based on the fact that, when simulating fast events using rectangular grid scheme, a phenomenon called grid separation introduces an error. Using diamond grid means that the solution at a particular point along the pipeline is obtained every second iteration.

The explicit MOC solution technique is used to solve the characteristics equations. This implies that compatibility equations can be solved explicitly and one at a time. By solving for H_P, Equations B.18 and B.19 can be simplified, as:

$$C^+ : \; H_P = C_P - BQ_P \tag{B.20}$$

$$C^- : \; H_P = C_M + BQ_P \tag{B.21}$$

where C_P and C_M are constants that depend on the known conditions at the

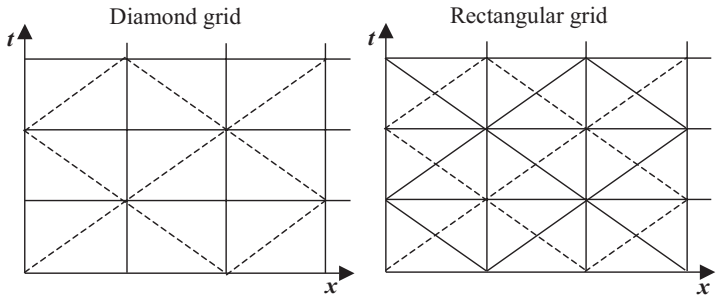

Figure B.3: Diamond and rectangular grid systems

previous time step

$$C^+ : \ C_P = H_A + Q_A(B - R|Q_A|) \tag{B.22}$$

$$C^- : \ C_M = H_B - Q_B(B - R|Q_B|) \tag{B.23}$$

B is a function of the physical properties of the pipeline, often called the pipeline characteristic impedance

$$B = \frac{a}{gA} \tag{B.24}$$

and R is the pipeline resistance coefficient

$$R = \frac{f\Delta x}{2gDA^2} \tag{B.25}$$

By first eliminating Q_P in Equations B.20 and B.21, H_P is found

$$H_P = \frac{C_P + C_M}{2} \tag{B.26}$$

Q_P can then be calculated directly from either Equation B.20 or B.21. At either end of the single pipe only one of the compatibility equations is available (Figure B.4). An auxiliary condition is needed in each case that specifies Q_P, H_P, or some relation between them. That is, the auxiliary equation must convey information on the behavior of the boundary of the pipeline. The boundary conditions for a number of the most common boundaries are defined in literature. Later in this section, the boundary equations for leakage and burst are given special attention, since these boundaries are of the highest significance for the presented research.

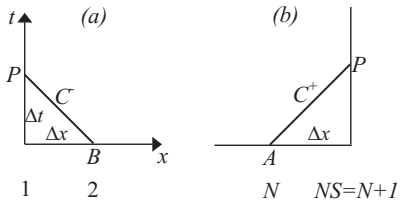

Figure B.4: Characteristics at boundaries

Nodal leakage boundary

A most convenient way of simulating the leakage is assigning it to the nodal points of the characteristic grid. The leaking node is then solved using two compatibility equations (from adjacent pipes) and an orifice equation that describes the leak. The orifice equation has the following form:

$$Q_L = C_d A_0 \sqrt{2gH_L} \tag{B.27}$$

where: Q_L = flow through the orifice
C_d = orifice discharge coefficient
A_0 = cross-section area of the orifice
H_L = hydraulic head at the leak

The continuity of mass must be applied for the node with a leak. A mass-balance equation represents the sum of the flows entering (positive) and exiting (negative) the node. This sum is equal to zero:

$$Q_u - Q_d - Q_L = 0 \tag{B.28}$$

where Q_u and Q_d are the upstream and downstream flows, respectively, and are derived from the compatibility equations

$$C^+ \quad : \qquad Q_u = \frac{C_{P,u} - H_L}{B_u} \tag{B.29}$$

$$C^- \quad : \qquad Q_d = \frac{H_L - C_{M,d}}{B_d} \tag{B.30}$$

By substituting the orifice equation and the compatibility equations into Equation B.28, the hydraulic head can be determined using a quadratic formula

$$H_i = a - b\sqrt{H_i} \tag{B.31}$$

$$\text{where:} \quad a = \frac{C_P B_M + C_M B_P}{B_M + B_P}$$

$$b = C_d A_0 \sqrt{2g} \frac{B_P B_M}{B_P + B_M}$$

After the head at the leaking node is obtained, flows Q_u and Q_d can be calculated from Equations B.29 and B.30, respectively.

In Equation B.27, the leak is defined by the cross-sectional area of the orifice, A_0, and the discharge coefficient C_d. The value of C_d depends on the geometrical shape of the orifice. In practise, a lumped leak coefficient $C_d A_0$ is often used to define the leak size.

Burst boundary

The burst is simulated at the nodal points of the characteristic grid. The head and flow values at the burst point are calculated using the same expressions as those used for the leak case (Equation B.31). The burst has the same discharge characteristics as the leak and the size of the burst is defined using the lumped leak coefficient $C_d A_0$. The only difference between the burst and leak simulations is that the burst event itself (a burst opening) has to be simulated. In the case of a leak, $C_d A_0$ has a constant value during the simulation. However, the burst opening is simulated using a variable lumped leak coefficient. Before the burst has occurred, $C_d A_0$ is equal to zero. After the burst opening $C_d A_0$ is proportional to the defined size of the burst. Since it is not realistic that the burst reaches its defined size instantly, $C_d A_0$ cannot be changed from zero to the defined value within one time step of MOC solver. To simulate a longer burst opening, the leak coefficient is increased linearly from zero to the final value over a certain period of time. This time is equal to the defined burst opening duration. Such an implementation allows the simulation of bursts with different opening times.

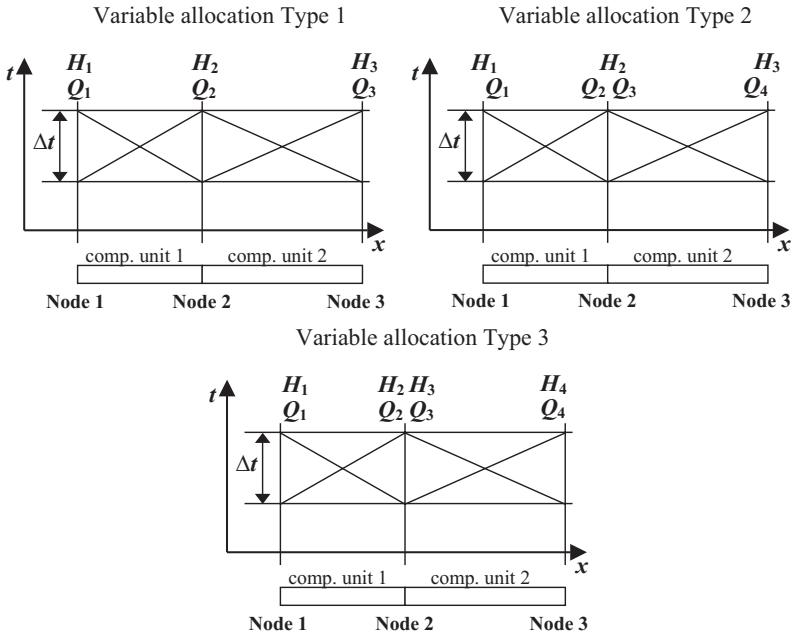

Figure B.5: Computational units - variable allocation types

Solving transients in pipe networks

The Method of Characteristics can be used to simulate transients in pipe networks. When the system contains more than one pipeline, the interior sections of each pipeline are treated independently of other parts in the system at each instant in time. The end conditions for each pipe must interface with adjoining pipes or with other boundary elements. The elements around the node, having characteristic length Δx, are called computational units. Head and flow variables are allocated to computational units. Three types of variable allocation are illustrated in Figure B.5. The choice of variable allocation type depends on the problem to be solved. For networks containing leakage, losses at junctions or valves, variable allocation Type 3 is applicable.

The explicit MOC solution at a junction is demonstrated using the example junction (Figure B.6) consisting of three pipes (or computational units). The

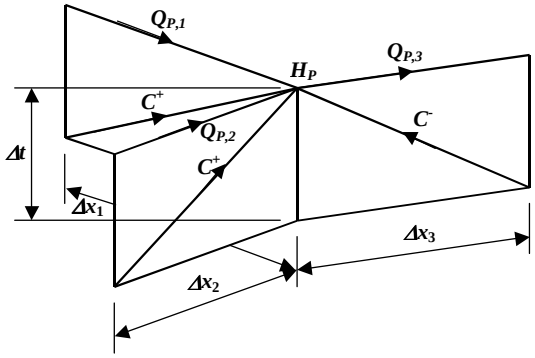

Figure B.6: Characteristic lines at a junction.

positive x-direction for pipes 1 and 2 is defined into the junction and the positive x-direction for pipe 3 is defined out of the junction. Two conditions are applied – the continuity of flows at the junction and the common hydraulic head at the junction. The characteristic equations are used to obtain the values for the head at the junction and flows in each of the pipes. A continuity equation at the junction is

$$\sum Q_P = Q_{P,1} + Q_{P,2} - Q_{P,3} = 0 \tag{B.32}$$

The compatibility equation for each pipe can be written as follows:

$$Q_{P,1} = \frac{C_{P,1} - H_P}{B_1} \tag{B.33}$$

$$Q_{P,2} = \frac{C_{P,2} - H_P}{B_2} \tag{B.34}$$

$$Q_{P,3} = \frac{C_{M,3} - H_P}{B_3} \tag{B.35}$$

Substituting the compatibility equations into continuity equation (Equation B.32) gives the solution for the common head

$$H_P = \frac{\dfrac{C_{P,1}}{B_1} + \dfrac{C_{P,2}}{B_2} + \dfrac{C_{M,3}}{B_3}}{\dfrac{1}{B_1} + \dfrac{1}{B_2} + \dfrac{1}{B_3}} \tag{B.36}$$

The flows can be determined from Equations B.33-B.35.

The choice of time step value

Determination of the adequate time step value for hydraulic transient simulation is an important procedure. A compromise between computational speed and accuracy has to be reached. Too small time step can require excessive computation, without any significant improvement, compared to the optimal one. Too great time step can mislead the interpretation of the results.

Limits of time step value. Computational time for simulation is a major factor that has to be considered when setting a lower limit for time step value. Every computer application includes certain limitations in terms of dynamic and static memory, which implies that the simulation time can be extensive, especially considering applications where a great number of repetitions is required. The simulation time is proportional to the total number of iterations that have to be carried out. The total number of iterations depends on the number of computation points in the system and the number of time steps in the simulation. The number of computational points is calculated from

$$N_{total} = \sum_{i=1}^{i=np} N_i \tag{B.37}$$

where np is the number of pipes in the network. If T_s is the duration of the physical process that has to be simulated, the number of iterations that have to be carried out in the simulation is equal to $T_s/\Delta t$ multiplied by N_{total}. Based on the maximum acceptable number of iterations the lower limit of the time step value, Δt_{min}, is chosen. However, numerical implementation of the MOC algorithm introduces additional restrictions on time step value selection. These restrictions are discussed in the following subsection.

Time step in MOC. The challenge of selecting a suitable time step arises from the nature of MOC. There are two conflicting constraints that have to be fulfilled: (1) if a system of two or more pipes is simulated, it is necessary that the time increment is equal for all pipes; (2) The Courant's criterion has to be satisfied for each pipe in the system (Wylie and Streeter; 1993):

$$\Delta t \leq \frac{\Delta x_i}{a_i}, \qquad i = 1,\ np \tag{B.38}$$

Ideally, the ratio of the space step Δx and the time step Δt must be equal to the wave speed a and the Courant number $C_r = a\Delta t/\Delta x$ must be equal

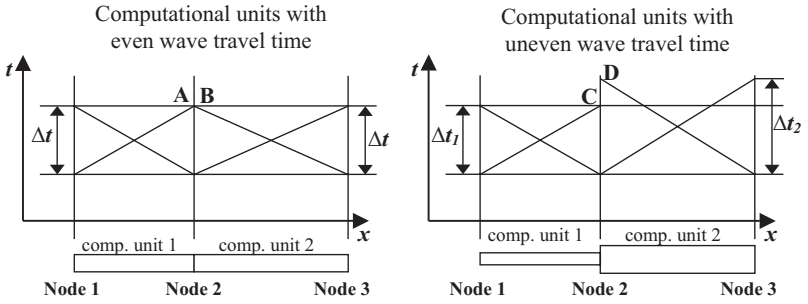

Figure B.7: Characteristics lines for adjacent computational units with even and uneven wave travel times

to one. Thus, the optimal time step value for a pipe can be determined as follows:

$$\Delta t_i = \frac{L_i}{a_i N_i} \tag{B.39}$$

where L_i is the pipe length. When a diamond grid of MOC is implemented, the number of sections in the ith pipe N_i must be an even integer. The smallest even integer is 2. Thus, as suggested in Vugdelija et al. (2000), the Courant's criterion for a particular pipe can be defined as:

$$\Delta t \leq \frac{L_i}{2a_i}, \qquad i = 1,\ np \tag{B.40}$$

Both the length and the wave speed are the individual characteristics of a pipe. Thus, for a network transient simulation, the upper time step limit is:

$$\Delta t \leq min\left(\frac{L_i}{2a_i}\right), \qquad i = 1,\ np \tag{B.41}$$

To have a common time step value for all pipes and to satisfy the Courant criterion, the wave travel time $a\Delta x$ has to be the same for a computational unit in any pipe of the network. This is almost impossible in a real network. Different pipe lengths and wave speeds usually cause different wave travel times. Additionally, as already mentioned, the condition that the number of sections in the ith pipe, N_i, is an even integer needs to be satisfied for MOC. In general, any value of Δt is likely to produce a different non-integer value

of N_i for each of the pipes. Thus, N_i has to be rounded to the closest even integer:

$$N_i = 2\ int\left(\frac{L_i}{2a_i\Delta t}\right), \qquad i = 1,\ np \tag{B.42}$$

Figure B.7 shows the characteristics lines for two adjacent computation units with equal and unequal wave travel times. In the case of an uneven wave travel time (right plot in Figure B.7), the ends of the two characteristics lines do not meet at the same time. In order to solve the compatibility equations, an interpolation between points C and D must be introduced. Two alternatives for this can be found in the literature. The first possibility is to adjust one of the pipe properties (usually the wave speed), forcing the number of reaches to be an even integer and making the Courant number equal to one. The second way is to allow the Courant number to be less than one and to interpolate between known grid points.

Spaceline and timeline interpolation. Both spaceline and timeline interpolation schemes (see Figure B.8) use interpolation between grid points to obtain values of the dependent variables at the foot of the characteristics lines. Since the physical parameters of the system and the values of the dependent variables at the adjacent nodes are known, it seems to be a simple matter to produce a good estimate. However, as noted in Ghidaoui et al. (1998); Greco and Carravetta (1999); Karney and Ghidaoui (1997), the function value at the foot of the characteristics can seldom be determined with certainty using this interpolation procedure. It is therefore suggested that the wave speed adjustment approach be used if the required wave speed correction is smaller than a certain value, e.g. 15%.

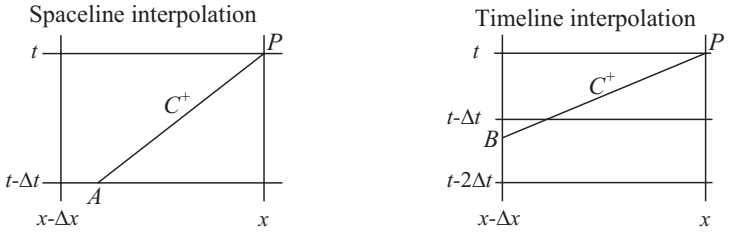

Figure B.8: Spaceline (left) and timeline (right) interpolation schemes

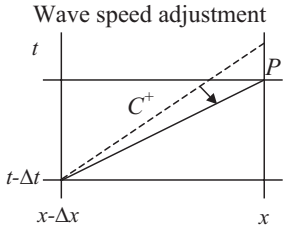

Figure B.9: Wave speed adjustment

Wave speed adjustment. The wave speed adjustment interpolation scheme (see Figure B.9) is based on the adjustment of the wave speed values to equalise the numerical wave travel times of adjacent computational units. According to Ghidaoui et al. (1998), there are three main advantages of the wave speed adjustment over spaceline and timeline interpolation: (1) it preserves the physical shape of the wave; (2) it is partly justified by the uncertainty associated with wave celerity; and (3) the proportional change in wave speed is smaller than the associated degree of interpolation required by the previous interpolation schemes. Despite that, large wave speed adjustment modifies the wave travel time and distorts the timing of wave interactions, which can be crucial for particular transient model applications, such as leakage detection. The error introduced by the round-up of N_i can be compensated by the correction of the wave speed a_i (Wylie and Streeter; 1993; Stapers; 2002):

$$\Delta t = \frac{L_i}{a_i(1 \pm \psi_i)N_i} \tag{B.43}$$

Least squares approximation can be used to determine Δt such that the sum of squares of the wave speed adjustments ψ_i is minimal. Equation B.43 can be rewritten as:

$$y = \begin{pmatrix} 1 \pm \psi_1 \\ 1 \pm \psi_2 \\ \vdots \\ 1 \pm \psi_J \end{pmatrix} = \begin{pmatrix} \dfrac{L_1}{a_1 N_1} \\ \dfrac{L_2}{a_2 N_2} \\ \vdots \\ \dfrac{L_J}{a_J N_J} \end{pmatrix} \left(\frac{1}{\Delta t}\right) = \Phi\Theta \tag{B.44}$$

where J is the total number of pipes in the network. An error vector is introduced as $e = y - y_m$, where y_m is a column vector $[J \times 1]$ of ones. The minimization of $\|\psi\|^2$ is achieved by solving the "normal" equation (Åström and Wittenmark; 1997):

$$\Theta = \left(\Phi^T \Phi\right)^{-1} \Phi^T y_m \tag{B.45}$$

The optimal Δt is given by $\Delta t = 1/\Theta$.

B.3 Unsteady friction

The traditional approach to incorporate frictional effects into the governing unsteady equations for pipe flow has been to approximate them with steady state friction relationships. Further research on the topic has shown that steady state approximations are only partially correct and that the non-uniform flow velocity profile plays an important role in the damping. The extra frictional dissipation caused by fluid acceleration is referred to as unsteady friction. A number of models for unsteady friction can be found in the literature. The unsteady friction implementation in the MOC scheme presented in this chapter is based on the Zielke's unsteady friction model (Zielke; 1968). The model uses weighted histories of past flows to determine the instantaneous shear stress. The expressions that describe laminar unsteady friction can be formulated for the MOC using a diamond grid. Figure B.10 shows the grid with specified time intervals. The headloss at point $P_{i,k}$ can be expressed as the sum of steady and unsteady parts

$$h_{i,k} = \bar{h_{i,k}} + h'_{i,k} \tag{B.46}$$

$$\bar{h_{i,k}} = \frac{32\nu}{gD^2} V_{i,k} \tag{B.47}$$

$$\begin{aligned} h'_{i,k} = \frac{16\nu}{gD^2} &\left[(V_{i,k} - V_{i,k-2})W(\Delta t) + (V_{i,k-2} - V_{i,k-4})W(3\Delta t)\right. \\ &\left. + \cdots + (V_{i,2} - V_{i,0})W((k-1)\Delta t)\right] \end{aligned} \tag{B.48}$$

where ν is the kinematic viscosity. The weight W is a function of the dimensionless time used to limit the influence of past velocity changes. The expression for calculating W is dependent on the flow regime defined by the

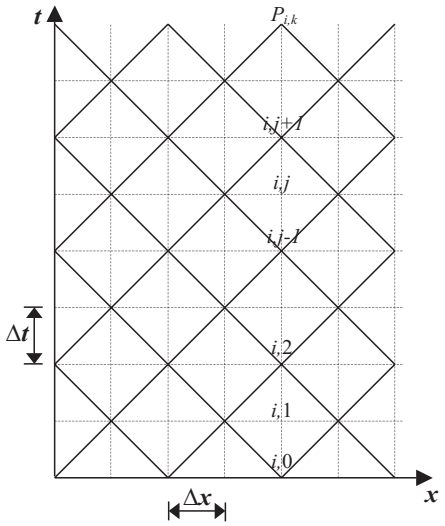

Figure B.10: Grid of characteristics for specified time intervals

dimensionless Reynolds number

$$Re = \frac{DV}{\nu} \tag{B.49}$$

Three different cases of flow regime are defined:

- Laminar smooth-walled flow. For the laminar flow:

$$Re < 2000 \tag{B.50}$$

- Turbulent smooth-walled flow:

$$Re > 2000 \tag{B.51}$$

- Fully rough-walled flow. The following relationship defines a fully rough-walled flow:

$$Re > \frac{200D}{r\sqrt{f}} \tag{B.52}$$

  where r is the pipe roughness height and f is a friction factor.

Laminar smooth-walled flow. The Zielke formulation (Zielke; 1968) is used to calculate the weighting function for a laminar smooth-walled flow. The weights W are a function of the dimensionless time τ

$$\tau = \frac{4\nu}{D^2}t \tag{B.53}$$

$W(\tau)$ approaches zero for $\tau \to \infty$ and can be calculated from the following series

$$\begin{aligned} \text{For } \tau &> 0.02 \\ W(\tau) &= e^{-26.3744\tau} + e^{-70.8493\tau} + e^{-135.0198\tau} + \\ &\quad e^{-218.9216\tau} + e^{-322.5544\tau} \end{aligned} \tag{B.54}$$

$$\begin{aligned} \text{For } \tau &\leq 0.02 \\ W(\tau) &= 0.282095\tau^{-\frac{1}{2}} - 1.250000 + 1.057855\tau^{\frac{1}{2}} + 0.937500\tau + \\ &\quad 0.396696\tau^{\frac{3}{2}} - 0.351563\tau^2 \end{aligned} \tag{B.55}$$

Turbulent smooth-walled flow. For turbulent smooth-walled flow, the weigh ing function representation from Vardy and Brown (1996) is used, where

$$W(\tau) = \frac{A}{\sqrt{\tau}}e^{-\tau/C} \tag{B.56}$$

$$A = \frac{1}{2\sqrt{\pi}} \tag{B.57}$$

$$C = \frac{7.41}{Re^{\kappa}} \tag{B.58}$$

$$\kappa = \log_{10}(14.3/Re^{0.05}) \tag{B.59}$$

Fully rough-walled flow. In Vardy and Brown (2003), the model for the weighting function in a rough-walled pipe flow is derived as:

$$W(\tau) = \frac{A}{\sqrt{\tau}}e^{-\tau/C} \tag{B.60}$$

$$A = 0.0103\sqrt{Re}\left(\frac{r}{D}\right)^{0.39} \tag{B.61}$$

$$\frac{1}{C} = 0.352Re\left(\frac{r}{D}\right)^{0.41} \tag{B.62}$$

Once the appropriate weighting function value is calculated, the headloss at the characteristic point is derived from Equations B.46 and B.48.

Appendix C

Pressure wave transmission and reflection coefficients

When a transient pressure wave interacts with a junction of two or more pipes, a certain part of the wave is transmitted through the junction and the rest of the wave is reflected. The wave transmission and reflection coefficients can be derived using the compatibility equations from the Method of Characteristics (Wylie and Streeter; 1993). The continuity equation for the junction before the wave reaches it (time $t - \Delta t$) is:

$$Q_{01} = Q_{02} + Q_{03} \tag{C.1}$$

where Q_{01}, Q_{02} and Q_{03} are the flows in pipes 1, 2 and 3 before the arrival of the wave. The continuity equation for the junction after the wave has reached it (time $t + \Delta t$) is:

$$Q_{J1} = Q_{J2} + Q_{J3} \tag{C.2}$$

where Q_{J1}, Q_{J2} and Q_{J3} are the flows in pipes 1, 2 and 3 after the wave has reached the junction. The head at the junction H_0 is common for all the pipes. Assuming that the pressure wave enters the junction from pipe 1, the head in pipe 1 is increased from H_0 to H_W. The corresponding flow Q_W can be calculated using the C^-compatibility equation (Equation B.19 in Appendix B) with neglected friction term:

$$H_w = H_0 + B_1(Q_w - Q_{01}) \tag{C.3}$$

and is equal to:

$$Q_w = Q_{01} + \frac{1}{B_2}(H_w - H_0) \tag{C.4}$$

where B_1 and B_2 are characteristic impedances of pipes 1 and 2, respectively. For any pipe, B can be calculated using the following expression:

$$B = \frac{a}{gA} \tag{C.5}$$

where: a = wave speed of the pipe
g = gravitational constant
A = cross-sectional area of the pipe

When the pressure wave reaches a junction, the conditions at that junction are described by the following compatibility equations:

$$H_j = H_W - B_1(Q_{J1} - Q_W) \tag{C.6}$$
$$H_j = H_0 + B_2(Q_{J2} - Q_{02}) \tag{C.7}$$
$$H_j = H_0 + B_3(Q_{J3} - Q_{03}) \tag{C.8}$$

Substituting Equation C.4 into Equation C.6 and rearranging Equations C.7 and C.8 results in:

$$Q_{J1} - Q_{01} = \frac{1}{B_1}(2H_w - H_0 - H_J) \tag{C.9}$$
$$Q_{J2} - Q_{02} = \frac{1}{B_2}(H_J - H_0) \tag{C.10}$$
$$Q_{J3} - Q_{03} = \frac{1}{B_3}(H_J - H_0) \tag{C.11}$$

Subtraction of Equation C.1 from Equation C.2 gives:

$$(Q_{J1} - Q_{01}) = (Q_{J2} - Q_{02}) + (Q_{J3} - Q_{03}) \tag{C.12}$$

Finally, substituting Equations C.9, C.10 and C.11 into Equation C.12 and rearranging the equation gives the expression for a wave transmission coefficient:

$$T = \frac{H_w - H_0}{H_J - H_0} = \frac{\frac{2}{B_1}}{\frac{1}{B_1} + \frac{1}{B_2} + \frac{1}{B_3}} \tag{C.13}$$

If a general junction n of p pipes is considered, the wave transmission coefficient T_n, in the case when the wave is approaching from pipe 1, is equal to:

$$T_n = \frac{(H_J - H_0)}{(H_W - H_0)} = \frac{\frac{2}{B_1}}{\sum_{k=1}^{p} \frac{1}{B_k}} \tag{C.14}$$

By substituting Equation C.5 into Equation C.14, the following expression is obtained:

$$T_n = \frac{\frac{2A_1}{a_1}}{\sum_{k=1}^{p} \frac{A_k}{a_k}} \tag{C.15}$$

Thus, the transmission coefficient for a junction depends on the properties of the pipes connected to it. The part of the transient wave that is not transmitted, is reflected. The reflection coefficient is defined as:

$$P_n = \frac{(H_J - H_W)}{(H_W - H_0)} = T_n - 1 \tag{C.16}$$

Equation C.15 is valid for any junction connecting two or more pipes. It can also be applied to situations when pipes with different diameters or wave speeds are connected in series. In the same manner, the transmission and reflection coefficients for the most common boundaries can be derived.

Reservoir A reservoir can be treated as a pipe with $A \to \infty$. This results in $T = 0$ and $P = -1$. In other words, the wave is reflected with the same magnitude and opposite sign, which means that the initial pressure is restored after reflection.

Dead-end Flow is equal to zero at the dead-end of a pipe. Thus, $T = 0$ and by solving the characteristic equations the reflection coefficient $P = 1$ is derived. The reflected wave has the same magnitude and same sign, which means that the head is amplified at the dead-end. The same reasoning is valid for a negative transient wave – it is further reduced at the boundary.

Appendix D

Calculation of burst size

In 1897, Joukowsky found a special solution of the governing unsteady pipe flow equations for the case of instantaneous valve closure. He formulated the expression, named the Joukowsky pressure rise formula, which related the change in velocity to the resulting change in pressure. The convective terms and frictional resistance are neglected and the pipe is assumed to be horizontal. The pressure rise formula can be applied only when the change in velocity is faster than the time it takes for the burst-induced wave to reach the induction point after reflection from the boundary. For closure of a valve at the downstream end of a pipeline, a change in velocity ΔV must occur in less that $2L/a$ seconds, where L is the length of the pipeline and a is the wavespeed of the pipeline. The Joukowsky rise in head is calculated from the following formula:

$$\Delta H = -\frac{a}{g}\Delta V \tag{D.1}$$

By substituting velocity with flow ($V = QA$) Equation D.1 becomes

$$\Delta H = -\frac{a}{gA}\Delta Q \tag{D.2}$$

As already noted, this relation is valid for instantaneous downstream valve closure. This means that the transient wave initiated by a sudden pressure rise will be travelling in one direction (upstream from the valve). In the case of a burst event somewhere along the pipe, the sudden change in flow (velocity) is caused by a side discharge through the burst orifice and is equal to the

burst flow Q_B. The impedance of pipe sections immediately upstream and downstream of the burst is equal. Therefore, the upstream and downstream flows after the burst occurs are:

$$Q_u = Q_0 + \frac{1}{2}Q_B \tag{D.3}$$

$$Q_u = Q_0 - \frac{1}{2}Q_B \tag{D.4}$$

respectively. It is important to realise that the Joukowsky formula was derived for a pressure wave propagating upstream. Applying Equation D.2 at any point upstream from the burst gives:

$$\Delta H_{Bu} = -\frac{a}{gA}\left[Q_0 - (Q_0 + \frac{1}{2}Q_B)\right] \tag{D.5}$$

and, after rearranging:

$$\Delta H_{Bu} = -\frac{aQ_B}{2gA} \tag{D.6}$$

The same analysis can be applied for the wave propagating downstream. In this case, the Joukowsky formula has the following form:

$$\Delta H = \frac{a}{gA}\Delta Q \tag{D.7}$$

Applying the above equation at any point downstream from the burst gives:

$$\Delta H_{Bd} = \frac{a}{gA}\left[Q_0 - (Q_0 - \frac{1}{2}Q_B)\right] \tag{D.8}$$

and, after rearrangement:

$$\Delta H_{Bd} = -\frac{aQ_B}{2gA} \tag{D.9}$$

From Equations D.6 and D.9 it is clear that $\Delta H_{Bu} = \Delta H_{Bd}$. This means that negative pressure waves of equal magnitude, ΔH_B, travel in opposite directions away from the burst point:

$$\Delta H_B = -\frac{aQ_B}{2gA} \tag{D.10}$$

The burst flow can be calculated using the orifice equation:

$$Q_B = C_d A_0 \sqrt{2gH_B} \tag{D.11}$$

where $C_d A_0$ is a lumped discharge parameter describing the size of the burst and H_B is the head at the burst point. Solving Equation D.10 for burst flow Q_B gives:

$$Q_B = -\frac{2gA}{a}\Delta H_B \tag{D.12}$$

After substituting Equation D.12 into Equation D.11 the expression for the burst size calculation is derived:

$$C_d A_0 = -\frac{A\Delta H_B \sqrt{2g}}{a\sqrt{H_B}} \tag{D.13}$$

Considering that a burst orifice discharge Q_B will always be positive and pressure change ΔH_B will always be negative (from Equation D.10) Equation D.13 can be rewritten as:

$$C_d A_0 = \frac{A|\Delta H_B|\sqrt{2g}}{a\sqrt{H_B}} \tag{D.14}$$

ΔH_B is the magnitude of the burst-induced pressure wave (from the pressure measurement). The head at the burst point H_B can be found by subtracting ΔH_B from the initial head value H_0:

$$H_B = H_0 - \Delta H_B \tag{D.15}$$

Equation D.13 does not provide the exact size of the burst due to the neglection of frictional effects. However, it still provides a reasonable estimate, which can be used to evaluate the severity of the burst.

Appendix E

Calculation of leak size

If the transient wave is generated by the sudden closure of an inline valve, the size of the generated wave, ΔH, will be proportional to the change of flow through the valve, ΔQ. The relationship between ΔH and ΔQ for a frictionless case is described by the Joukovsky pressure rise formula (see Appendix D):

$$\Delta H = -\frac{a}{gA}\Delta Q \tag{E.1}$$

where a is the wave speed of the pipe, g is the gravitational constant and A is the cross-sectional area of the pipe. Since the closure of the valve is considered, ΔQ in Equation E.1 will always be negative and therefore Equation E.1 can be rewritten:

$$\Delta H = \frac{a}{gA}\left|\Delta Q\right| \tag{E.2}$$

If the transient wave is generated by the sudden closure of the side-discharge, Eq.E.2 becomes:

$$\Delta H = \frac{1}{2}\frac{a}{gA}\left|\Delta Q\right| \tag{E.3}$$

If the leak is present somewhere along the pipe, the size of the leak can be expressed as a lumped leak orifice parameter $C_d A_o$. For steady-state pressure conditions, the flow through the leak orifice Q_L can be calculated:

$$Q_L = C_d A_o \sqrt{2gH_0} \tag{E.4}$$

where H_0 is the steady-state head at the leak point. When the generated transient wave reaches the leak point, the leak flow is increased due to increased pressure. The increase of the leak flow ΔQ_L, in turn, will cause a decrease of the pressure head ΔH_L that can be calculated using the Joukowsky formula:

$$\Delta H_L = -\frac{1}{2}\frac{a}{gA}\Delta Q_L \tag{E.5}$$

In other words, when the generated pressure wave reaches the leak point, a part if it with size ΔH_L is reflected and the remaining wave ($\Delta H - \Delta H_L$) continues to travel along the pipe in the initial direction.

The flow through the leak orifice after the wave has passed the leak point can be calculated:

$$Q_L + \Delta Q_L = C_d A_o \sqrt{2g(H_0 + \Delta H - \Delta H_L)} \tag{E.6}$$

The size of the reflection from the leak point ΔH_L and the magnitude of the generated wave ΔH can be identified in the measured pressure trace. Equation E.5 can then be rearranged to calculate the change in the leak flow ΔQ_L:

$$\Delta Q_L = -\frac{2gA}{a}\Delta H_L \tag{E.7}$$

Since ΔH_L will always be negative, ΔQ_L will always be positive. Thus, Equation E.6 can be rewritten:

$$\Delta Q_L = \frac{2gA}{a}\left|\Delta H_L\right| \tag{E.8}$$

By introducing Equations E.4 and E.8 into Equation E.6, the expression for the lumped leak orifice parameter $C_d A_o$ can be derived:

$$C_d A_o = \frac{2gA\ \left|\Delta H_L\right|}{a\sqrt{2gH_0}\left(\sqrt{1 + \dfrac{\Delta H}{H_0} - \dfrac{\left|\Delta H_L\right|}{H_0}} - 1\right)} \tag{E.9}$$

Equation E.9 does not provide the exact size of the leak due to the neglected frictional effects. However, it still provides a reasonable estimate, which can be used to evaluate the severity of the leak.

Bibliography

Andersen, J. H. and Powell, R. S. (2000). Implicit state-estimation technique for water networks monitoring, *Urban Water* **2**(2): 123–130.

Andersen, J. H., Powell, R. S. and Marsh, J. F. (2001). Constrained state estimation with applications in water distribution network monitoring, *International Journal of Systems Science* **32**(6): 807–816.

Anon (1997). Intelligent pigs now inspect pipelines down to 200 mm diameter, *NDT and E International* **30**(1): 41.

Arfaie, M., Suwan, K. and Anderson, A. (1993). Stability and accuracy of pipe friction approximations in method of characteristics solutions for waterhammer, *Mathematical Engineering in Industry* **1**(4): 265–281.

Åström, K. and Wittenmark, B. (1997). *Computer-Controlled Systems: theory and design*, 3rd edn, Prentice-Hall, Engelwood Cliffs, New Jersey, USA.

Atherton, D. (1989). Magnetic inspection is key to ensuring safe pipelines, *Oil and Gas Journal* **87**(32): 52–31.

Atherton, D. (1995). Remote field eddy current inspection, *IEEE Transactions on Magnetics* **31**(6): 4142–4147.

Atkinson, K., Whiter, J. T., Smith, P. A. and Mulheron, M. (2002). Failure of small diameter cast iron pipes, *Urban Water* **4**(3): 263–271.

Babbar, V. and Clapham, L. (2003). Residual magnetic flux leakage: A possible tool for studying pipeline defects, *Journal of Nondestructive Evaluation* **22**(4): 117–125.

Babovic, V., Drécourt, J.-P., Keijzer, M. and Hansen, P. (2002). A data mining approach to modelling of water supply assets, *Urban Water* **4**(4): 401–414.

Barán, B., von Lücken, C. and Sotelo, A. (2005). Multi-objective pump scheduling optimisation using evolutionary strategies, *Advances in Engineering Software* **36**(1): 39–48.

Basseville, M. and Nikiforov, I. (1993). *Detection of Abrupt Changes: Theory and Applications*, Prentice-Hall, Englewood Cliffs, New Jersey, USA.

Beckwith, S. and Wong, K. (1995). A genetic algorithm approach for electric pump scheduling in water supply systems, *IEEE International Conference on Evolutionary Computation* **1**: 21–26.

Bell, W. (1993). Experience of GIS in the water industry (geographic IS), *IEE Colloquium on Experience in the Use of Geographic Information Systems in the Electricity Supply Industry*, Vol. 6, pp. 1–3.

Benkherouf, A. and Allidina, A. (1988). Leak detection and location in gas pipelines, *IEE Proceedings D - Control Theory and Applications* **135**(2): 142–148.

Bernoulli, D. (1738). *Hydrodynamica*, Argentorati.

Beushausen, R., Tornow, S., Borchers, H., Murphy, K. and Zhang, J. (2004). Transient leak detection in crude oil pipelines, *International Pipeline Conference 2004*, Calgary, Canada, October 4-8, 2004.

Bose, J. R. and Olson, M. K. (1993). Taps's leak detection seeks greater precision, *Oil & Gas Journal* **91**(14): 43–48.

Bougadis, J., Adamowski, K. and Diduch, R. (2005). Short-term municipal water demand forecasting, *Hydrological Processes* **19**(1): 137–148.

Brodetsky, I. and Savic, M. (1993). Leak monitoring system for gas pipelines, *1993 IEEE International Conference on Acoustics, Speech, and Signal Processing*, Vol. 3, Minneapolis, Minnesota, USA, April 27-30, 1993, pp. 17–20.

Brunone, B. (1999). Transient test-based technique for leak detection in outfall pipes, *Journal of Water Resources Planning and Management* **125**(5): 302–306.

Brunone, B. and Ferrante, M. (2001). Detecting leaks in pressurised pipes by means of transients, *Journal of Hydraulic Research, IAHR* **39**(5): 539–547.

Buchberger, S. G. and Nadimpalli, G. (2004). Leak estimation in water distribution systems by statistical analysis of flow readings, *Journal of Water Resources Planning and Management* **130**(4): 321–329.

Bush, C. A. and Uber, J. G. (1998). Sampling design methods for water distribution model calibration, *Journal of Water Resources Planning and Management* **124**(6): 334–344.

Caputo, A. C. and Pelagagge, P. M. (2002). An inverse approach for piping networks monitoring, *Journal of Loss Prevention in the Process Industries* **15**(6): 497–505.

Chastain-Howley, A. (2005). Transmission main leakage: how to reduce the risk of a catastrophic failure, *Leakage 2005*, Halifax, Canada, September 12-14, 2005.

Covas, D., Graham, N., Maksimovic, C., Ramos, H., Kapelan, Z., Savic, D. and Walters, G. (2003). An assessment of the application of inverse transient analysis for leak detection: Part II - collection and application of experimental data, *International Conference on Advances in Water Supply Management, CCWI '03*, Vol. CD, Imperial College London, UK, September 15-17, 2003, pp. 79–87.

Covas, D., Ramos, H., Brunone, B. and Young, A. (2004). Leak detection in water trunk mains using transient pressure signals: Field tests in Scottish Water, *9th International Conference on Pressure Surges*, Vol. 1, BHR Group, Chester, UK, March 24-26, 2004, pp. 185–198.

Covas, D., Ramos, H., Young, A., Graham, I. and Maksimovic, C. (2005). Uncertainties of leak detection by means of hydraulic transients from the lab to the field, *International Conference on Water Management for*

the 21st Century, CCWI'05, Vol. 2, 5-7 September, 2005, Exeter, UK, pp. 143–148.

Covas, D., Stoianov, I., Butler, D., Maksimovic, C., Graham, N. and Ramos, H. (2001). Leak detection in pipeline systems by inverse transient analysis - from theory to practice, *in* B. Ulanicki, B. Coulback and J. Rance (eds), *Water Software Systems: Theory and Applications*, Vol. 1, Research Studies Press Ltd., Baldock, Hertfordshire, England, pp. 3–16.

Cowan, G. (1975). Digital processing adds accuracy to TDR, *Microwaves* pp. 47– 51.

Davis, D. N. (2000). Agent-based decision-support framework for water supply infrastructure rehabilitation and development, *Computers, Environment and Urban Systems* **24**(3): 173–190.

Demma, A., Cawley, P., Lowe, M., Roosenbrand, A. G. and Pavlakovic, B. (2004). The reflection of guided waves from notches in pipes: a guide for interpreting corrosion measurements, *NDT and E International* **37**(3): 167–180.

Diab, Y. G. (1995). Mechanical method to evaluate safety factors in buried pipes, *Journal of Transportation Engineering* **121**(1): 94–101.

Duran, O., Althoefer, K. and Seneviratne, L. (2003). Pipe inspection using a laser-based transducer and automated analysis techniques, *Mechatronics, IEEE/ASME Transactions on* **8**(3): 401–409.

Eiswirth, M., Heske, C., Burn, L. and DeSilva, D. (2001). New methods for water pipeline asssessment, *IWA 2nd World Water Congress*, Berlin, Germany, October 15-19, 2001.

Emara-Shabaik, H., Khulief, Y. and Hussaini, I. (2002). A non-linear multiple-model state estimation scheme for pipeline leak detection and isolation, *Proceedings of the Institution of Mechanical Engineers, Part I: Journal of Systems and Control Engineering* **216**(6): 497–512.

Engelhardt, M. O., Skipworth, P. J., Savic, D. A., Saul, A. J. and Walters, G. A. (2000). Rehabilitation strategies for water distribution networks: a literature review with a UK perspective, *Urban Water* **2**(2): 153–170.

Engelhardt, M., Skipworth, P., Savic, D., Cashman, A., Walters, G. and Saul, A. (2002). Determining maintenance requirements of a water distribution network using whole life costing, *Journal of Quality in Maintenance Engineering* **8**(2): 152–164.

EUREAU (2001). Losses from water distribution networks, *Position Paper EU1-01-A66(5)*, EUREAU, European Union of National Associations of Water Suppliers and Waste Water Services.

Ferrante, M. and Brunone, B. (2003a). Pipe system diagnosis and leak detection by unsteady-state tests. 1. Harmonic analysis, *Advances in Water Resources* **26**: 95–105.

Ferrante, M. and Brunone, B. (2003b). Pipe system diagnosis and leak detection by unsteady-state tests. 2. Wavelet analysis, *Advances in Water Resources* **26**: 107–116.

Fleming, K. N. and Lydell, B. O. (2004). Database development and uncertainty treatment for estimating pipe failure rates and rupture frequencies, *Reliability Engineering and System Safety* **86**(3): 227–246.

Fukushima, K., Maeshima, R., Kinoshita, A., Shiraishi, H. and Koshijima, I. (2000). Gas pipeline leak detection system using the online simulation method, *Computers and Chemical Engineering* **24**: 453–456.

Gao, Y., Brennan, M. J., Joseph, P. F., Muggleton, J. M. and Hunaidi, O. (2004). A model of the correlation function of leak noise in buried plastic pipes, *Journal of Sound and Vibration* **277**(1-2): 133–148.

Ghidaoui, M., Karney, B. and McInnis, D. (1998). Energy estimates for discretization errors in water hammer problems, *Journal of Hydraulic Engineering, ASCE* **124**(4): 384–393.

Greco, M. and Carravetta, A. (1999). Water hammer in branched networks, 28^{th} *IAHR congress*, Graz, Austria, August 22-27, 1999.

Grimaud, A. and Pascal, O. (1991). Monitoring system detects small leaks, *Water Engineering & Management* **138**(1): 14–16.

Guercio, R., Magini, R. and Pallavicini, I. (2001). Instantaneous residential water demand as stochastic point process, *First International Conference on Water Resources Management*, Halkidiki, Greece, September 24 - 26, 2001.

Hadzilacos, T., Kalles, D., Preston, N., Melbourne, P., Camarinopoulos, L., Eimermacher, M., Kallidromitis, V., Frondistou-Yannas, S. and Saegrov, S. (2000). Utilnets: a water mains rehabilitation decision-support system, *Computers, Environment and Urban Systems* **24**(3): 215–232.

Halhal, D. and Savic, D. A. (1999). Scheduling of water distribution system rehabilitation using structured messy genetic algorithms., *Evolutionary Computation* **7**(3): 311–330.

Harding, R. (1976). Use pulse instead of CW signals, *Electrical Design* **11**: 60–67.

Haugland, S. (1996). Fundamental analysis of the remote-field eddy-current effect, *IEEE Transactions on Magnetics* **32**(4-part-2): 3195–3211.

Heim, P. (1979). Conducting a leak detection search, *Journal of the American Water Works Association* **71**(2): 66–69.

Heitbrink, W. A., Earnest, G. S., Mickelsen, R. L., Mead, K. R. and D'Arcy, J. B. (1999). Evaluation of leakage from a metal machining center using tracer gas methods: A case study, *American Industrial Hygiene Association Journal* **60**(6): 785–788.

Hu, Y. and Hubble, D. (2005). Failure conditions of asbestos cement water mains in regina, *Canadian Society of Civil Engineering (CSCE) 33rd Annual Conference*, Toronto, Ontario, Canada, June 2-4, 2005.

Hudak, P. F., Sadler, B. and Hunter, B. A. (1998). Analyzing underground water-pipe breaks in residual soils, *Water Engineering & Management* **145**(12): 15–20.

Huebler, J. (2000). Leak detection and measurement facts, Gas Utility Manager Online Magazine, http://www.gasindustries.com.

Hunaidi, O. and Chu, W. (1999). Acoustical characteristics of leak signals in plastic water distribution pipes, *Applied Acoustics* **58**(3): 235–254.

Hunaidi, O. and Wang, A. (2004). Acoustic methods for locating leaks in municipal water pipe networks, *International Conference on Water Demand Management*, Dead Sea, Jordan, May 30 - June 3, 2004, pp. 1–14.

Hunaidi, O., Cho, W., Wang, A. and Guan, W. (2000). Leak detection methods for plastic water distribution pipes, *Journal of the American Water Works Association* **92**(2): 82–94.

Hyun, S.-Y., Jo, Y.-S., Oh, H.-C. and Kirn, S.-Y. (2003). An experimental study on a ground-penetrating radar for detecting water-leaks in buried water transfer pipes, *Antennas, Propagation and EM Theory, 2003* pp. 596–599.

Ivetic, M. and Savic, D. (2003). Practical implications of using induced transients for leak detection, *3rd World Water Forum*, Kyoto, Japan, March 16-23, 2003.

Jönsson, L. (1995). Hydraulic transients as a monitoring device, *Technical report*, Dept. of Water Resources Engineering, University of Lund, Lund, Sweden.

Jönsson, L. (2001). Interaction of a hydraulic transient with a leak in a pipe flow, 14^{th} *Australasian Fluid Mechanics Conference*, Adelaide University, Adelaide, Australia, December 10-14, 2001.

Jönsson, L. and Larson, M. (1992). Leak detection through hydraulic transient analysis, *in* B. Coulbeck and E. Evans (eds), *Pipeline Systems*, Kluwer Academic Publishers, pp. 273–286.

Kapelan, Z., Savic, D. and Walters, G. (2003a). A hybrid inverse transient model for leakage detection and roughness calibration in pipe networks, *Journal of Hydraulic Research, IAHR* **41**(5): 481–492.

Kapelan, Z., Savic, D. and Walters, G. (2003b). Multiobjective sampling design for water distribution model calibration, *Journal of Water Resources Planning and Management* **129**(6): 466–479.

Kapelan, Z., Savic, D., Walters, G., Covas, D., Graham, I. and Maksimovic, C. (2003c). An assessment of the application of inverse transient analysis

for leak detection: Part I - theoretical considerations, *International Conference on Advances in Water Supply Management, CCWI '03*, Vol. CD, Imperial College London, UK, 15-17 September, 2003, pp. 71–78.

Karney, B. and Ghidaoui, M. (1997). Flexible discretization algorithm for fixed-grid moc in pipelines, *Journal of Hydraulic Engineering, ASCE* **123**(11): 1004–1011.

Khan, A., Widdop, P., Day, A., Wood, A., Mounce, S. and Machell, J. (2002). Low-cost failure sensor design and development for water pipeline distribution systems, *Water Science and Technology* **45**(4-5): 207–216.

Khomsi, D., Walters, G. A., Thorley, R. D. and Ouazar, D. (1996). Reliability tester for water-distribution networks, *Journal of Computing in Civil Engineering* **10**(1): 10–19.

Kiuchi, T. (1993). A leak localization method of pipeline by means of fluid transient model, *Journal of Energy Resources Technology, ASME* **115**: 162–167.

Kleiner, Y. (2001). Scheduling inspection and renewal of large infrastructure assets, *Journal of Infrastructure Systems* **7**(4): 136–143.

Kleiner, Y., Adams, B. and Rogers, J. (2001). Water distribution network renewal planning, *Journal of Computing in Civil Engineering* **15**(1): 15–26.

Kleiner, Y. and Rajani, B. (2001). Comprehensive review of structural deterioration of water mains: statistical models, *Urban Water* **3**(3): 131–150.

Lambert, A. (1994). Accounting for losses: The bursts and background concept, *Water and Environmental Management: Journal of the Chartered Institution of Water and Environmental Management* **8**(2): 205–214.

Lambert, A. (2003). Assessing non-revenue water and its components: a practical approach, *Water 21. Magazine of the International Water Association* (August 2003): 50–51.

Lambert, A. and Hirner, W. (2000). Losses from water supply systems: standard terminology and recommended performance measures, *The blue pages*, IWA, London, UK.

Lang, L. (1992). Water's new world., *Civil Engineering* **62**(6): 48–51.

Lange, K. G. (2005). Signal analysis revolutionizes leakage detection, *Leakage 2005*, Halifax, Canada, September 12-14, 2005.

Lee, P. J., Vitkovsky, J. P., Lambert, M. F., Simpson, A. R. and Liggett, J. A. (2005). Frequency domain analysis for detecting pipeline leaks, *Journal of Hydraulic Engineering* **131**(7): 596–604.

Lei, J. and Saegrov, S. (1998). Statistical approach for describing failures and lifetimes of water mains, *Water Science and Technology* **38**(6): 209–217.

Licciardi, S. V. (1998). Quantification and location of leaks by internal inspection, *Tunnelling and Underground Space Technology* **13**(2): 5–16.

Liggett, J. and Chen, L.-C. (1994). Inverse transient analysis in pipe networks, *Journal of Hydraulic Engineering* **120**(8): 934–955.

Lima, P. C. R. and Neto, S. J. A. (1995). Foam pigs solve pipe cleaning problems offshore Brazil, *Oil & Gas Journal* **93**(40): 64–68.

Liou, J. (1994). Mass imbalance error of waterhammer equations and leak detection, *Journal of Fluids Engineering, ASME* **116**(1): 103–108.

Liou, J. (1998). Pipeline leak detection by impulse response extraction, *Journal of Fluids Engineering, ASME* **120**(4): 833–838.

Liou, J. and Tian, J. (1995). Leak detection - transient flow simulation approaches, *Journal of Energy Resources Technology* **117**(3): 243–248.

Liou, J. C. P. (1996). Leak detection by mass balance effective for Norman Wells line, *Oil & Gas Journal* **94**(17): 69–73.

Lowe, M. J. S., Alleyne, D. N. and Cawley, P. (1998). Defect detection in pipes using guided waves, *Ultrasonics* **36**(1-5): 147–154.

Luong, H. T. and Nagarur, N. N. (2005). Optimal maintenance policy and fund allocation in water distribution networks, *Journal of Water Resources Planning and Management* **131**(4): 299–306.

Luong, T. H. and Fujiwara, O. (2002). Fund allocation model for pipe repair maintenance in water distribution networks, *European Journal of Operational Research* **136**(2): 403–421.

Mackle, G., Savic, G. and Walters, G. (1995). Application of genetic algorithms to pump scheduling for water supply, *First International Conference on Genetic Algorithms in Engineering Systems: Innovations and Applications, GALESIA*, Sheffield, UK, 12 - 14 September, 1995, pp. 400–405.

Mactaggart, R. H. and Myers, R. M. (2000). PC-based leak detection, *Technical report*, Simulations division of TCEnet Inc.

Makar, J. (2000). A preliminary analysis of failures in gray cast iron water pipes, *Engineering Failure Analysis* **7**(1): 43–53.

Makar, J. and Kleiner, Y. (2000). Maintaining water pipeline integrity, *AWWA Infrastructure Conference and Exibition*, Baltimore, Maryland, USA, March 12-15, 2000.

Makar, J., Desnoyers, R. and McDonald, S. (2001). Failure modes and mechanisms in gray cast iron pipe, *Underground Infrastructure Research; Municipal, Industrial and Environmental Applications*, Kitchener, Ontario, Canada, June 10-13, 2001, pp. 1–10.

McInnis, D. and Karney, B. W. (1995). Transients in distribution networks: Field tests and demand models, *Journal of Hydraulic Engineering* **121**(3): 218–231.

Mergelas, B. and Henrich, G. (2005). Leak locating method for precommissioned transmission pipelines: North American case studies, *Leakage 2005*, Halifax, Canada, September 12-14, 2005.

Mergelas, B., Xiangjie, K., Roy, D. and Balliew, J. (2005). Using a combination of condition based asset management techniques to manage a water transmission system, *ASCE Pipeline 2005*, Houston, Texas, USA, August 21-24, 2005.

Misiunas, D. (2001a). Drinking water quality. Literature study on water distribution systems, *Technical report TEIE-7169*, Dept. of Industrial Electrical Engineering and Automation, Lund University, Lund, Sweden.

Misiunas, D. (2001b). Dynamic behaviour of a pump/pipeline system. Literature study on water distribution systems, *Technical report TEIE-7166*, Dept. of Industrial Electrical Engineering and Automation, Lund University, Lund, Sweden.

Misiunas, D. (2001c). Leakage control. Literature study on water distribution systems, *Technical report TEIE-7167*, Dept. of Industrial Electrical Engineering and Automation, Lund University, Lund, Sweden.

Misiunas, D. (2001d). Water storage. Literature study on water distribution systems, *Technical report TEIE-7168*, Dept. of Industrial Electrical Engineering and Automation, Lund University, Lund, Sweden.

Misiunas, D., Lambert, M., Simpson, A. and Olsson, G. (2005a). Burst detection and location in water distribution networks, *3rd International Conference on Efficient Use and Management of Water*, Santiago, Chile, March 15-17, 2005, pp. 464–471.

Misiunas, D., Lambert, M., Simpson, A. and Olsson, G. (2005b). Burst detection and location in water transmission pipelines, *World Water and Environmental Resources Congress*, May 15-19, 2005, Anchorage, Alaska, USA.

Misiunas, D., Lambert, M., Simpson, A. and Olsson, G. (2005c). Condition assessment of water transmission pipelines using hydraulic transients, *International Conference on Water Management for the 21st Century, CCWI'05*, Vol. 1, 5-7 September 2005, Exeter, UK, pp. 269–274.

Misiunas, D., Simpson, A., Lambert, M. and Olsson, G. (2005d). Hydraulic transients for diagnosis of inline valves in water transmission pipelines, *International Conference on Water Management for the 21st Century, CCWI'05*, Vol. 1, 5-7 September 2005, Exeter, UK, pp. 293–298.

Misiunas, D., Vitkovsky, J., Olsson, G., Simpson, A. and Lambert, M. (2005e). Pipeline break detection using the transient monitoring, *Journal of Water Resources Planning and Management* **131**(4): 316–325.

Misiunas, D., Vitkovsky, J. P., Olsson, G., Simpson, A. and Lambert, M. (2005f). Failure monitoring in water distribution networks, *Proc.* 2^{nd} *IWA*

Conference on Instrumentation, Control and Automation, Busan, Korea, May 29 - June 2, 2005, pp. 631–639.

Misiunas, D., Vítkovský, J., Olsson, G., Simpson, A. and Lambert, M. (2003). Pipeline burst detection and location using a continuous monitoring technique, *International Conference on Advances in Water Supply Management, CCWI'03*, Vol. CD, Imperial College London, UK, September 15-17, 2003, pp. 89–96.

Misiunas, D., Vítkovský, J., Olsson, G., Simpson, A. and Lambert, M. (2004). Burst detection and location in pipe networks using a continuous monitoring technique, *9th International Conference on Pressure Surges*, Vol. 1, Chester, UK, March 24-26 ,2004, pp. 225–238.

Mounce, S. R., Khan, A., Wood, A. S., Day, A. J., Widdop, P. D. and Machell, J. (2003). Sensor-fusion of hydraulic data for burst detection and location in a treated water distribution system, *Information Fusion* (4): 217–229.

Mpesha, W., Chaudhry, M. and Gassman, S. (2002). Leak detection in pipes by frequency response method using a step excitation, *Journal of Hydraulic Research, IAHR* **40**(1): 55–62.

Mpesha, W., Gassman, S. and Chaudhry, M. (2001). Leak detection in pipes by frequency response method, *Journal of Hydraulic Engineering, ASCE* **127**(2): 134–147.

Mukherjee, J. and Narasimhan, S. (1996). Leak detection in networks of pipelines by the generalized likelihood ratio method, *Industrial & Engineering Chemistry Research, ASC* **35**: 1886–1893.

Murigendrappa, S. M., Maiti, S. K. and Srirangarajan, H. R. (2004a). Experimental and theoretical study on crack detection in pipes filled with fluid, *Journal of Sound and Vibration* **270**(4-5): 1013–1032.

Murigendrappa, S. M., Maiti, S. K. and Srirangarajan, H. R. (2004b). Frequency-based experimental and theoretical identification of multiple cracks in straight pipes filled with fluid, *NDT and E International* **37**(6): 431–438.

Nagar, A. and Powell, R. (2002). LFT/SDP approach to the uncertainty analysis for state estimation of water distribution systems, *Control Theory and Applications, IEE Proceedings D* **149**(2): 137–142.

Nakhkash, M. and Mahmood-Zadeh, M. (2004). Water leak detection using ground penetrating radar, *Proceedings of the Tenth International Conference on Ground Penetrating Radar, GPR 2004*, Delft, The Netherlands, June 21-24, 2004, pp. 525–528.

NRC (1995). Water mains break data on different pipe materials for 1992 and 1993, *Technical Report A-7019.1*, National Research Council Canada.

O'day, D. (1982). Organizing and analyzing leak and break data for making main replacement decisions, *Journal of American Water Works Association* **74**(11): 588–594.

Page, E. (1954). Continuous inspection schemes, *Biometrika* **41**: 100–115.

Pelletier, G., Milhot, A. and Villeneuve, J.-P. (2003). Modeling water pipe breaks - three case studies, *Journal of Water Resources Planning and Management* **129**(2): 115–123.

Pilcher, R. (2003). Leak detection practices and techniques: a practical approach, *Water 21. Magazine of the International Water Association* (December 2003): 44–45.

Poulakis, Z., Valougeorgis, C. and Papadimitriou, C. (2003). Leakage detection in water pipe networks using a bayesian probabilistic framework, *Probabilistic Engineering Mechanics* (18): 315–327.

Pudar, R. and Liggett, J. (1992). Leaks in pipe networks, *Journal of Hydraulic Engineering, ASCE* **118**(7): 1031–1046.

Rajani, B. and Kleiner, Y. (2001). Comprehensive review of structural deterioration of water mains: physically based models, *Urban Water* **3**(3): 151–164.

Rajani, B. and Kleiner, Y. (2004). Non-destructive inspection techniques to determine structural distress indicators in water mains, *Evaluation and Control of Water Loss in Urban Water Networks*, Valencia, Spain, June 21-25, 2004, pp. 1–20.

Rajani, B. and Tesfamariam, S. (2004). Uncoupled axial, flexural, and circunferential pipe-soil interaction analyses of partially supported jointed water mains, *Canadian Geotechnical Journal* **41**: 997–1010.

Rajtar, J. and Muthiah, R. (1997). Pipeline leak detection system for oil and gas flowlines, *Journal of Manufacturing Science and Engineering, Transactions of the ASME* **19**(1): 105–109.

Report26 (1980). Leakage control policy and practice, *Technical report*, UK Water Authorities Association.

Robinson, D. (1998). Identification and sizing of defects in metallic pipes by remote field eddy current inspection, *Tunnelling and Underground Space Technology* **13**(2): 17–28.

Robison, R. (1995). High-speed impact echo, *Civil Engineering* **65**(6): 61.

Rossman, L. (2000). EPANET users manual, *Technical report*, Risk Reduction Engineering Laboratory, Cincinnati: EPA, USA.

Saegrov, S. and Schilling, W. (2004). Computer aided rehabilitation of water networks (CARE-W), *IWA World Water Congress*, Marrakech, Morocco, September 19-24, 2004.

Saegrov, S., Melo Baptista, J., Conroy, P., Herz, R., Legauffre, P., Moss, G., Oddevald, J., Rajani, B. and Schiatti, M. (1999). Rehabilitation of water networks: Survey of research needs and on-going efforts, *Urban Water* **1**(1): 15–22.

Samoilov, B. V. (1998). In-line inspection, repairs used on aging Russian product lines, *Oil & Gas Journal* **96**(47): 42–46.

Sánchez, E. H., Ibáñez, J. C. and Cubillo, F. (2005). Testing applicability and cost effectiveness of permanent acoustic leakage monitoring for loss management in Madrid distribution network, *Leakage 2005*, Halifax, Canada, September 12-14, 2005.

Savic, D. A. and Walters, G. A. (1999). Hydroinformatics, data mining and maintenance of UK water networks, *Anti-Corrosion Methods and Materials* **46**(6): 415–425.

Savic, D. A., Walters, G. A. and Knezevic, J. (1995a). Optimal opportunistic maintenance policy using genetic algorithms, 1: formulation, *Journal of Quality in Maintenance Engineering* **1**(2): 34–49.

Savic, D. A., Walters, G. A. and Knezevic, J. (1995b). Optimal, opportunistic maintenance policy using genetic algorithms, 2: analysis, *Journal of Quality in Maintenance Engineering* **1**(3): 25–34.

Savic, D., Walters, G., Ashcroft, P. G. and Arscott, A. (1997). Hydroinformatics technology and maintenance of UK water networks, *Journal of Quality in Maintenance Engineering* **3**(4): 289–301.

Schlattman, D. T. (1991). Pressure analysis improves lines' leak-detection capabilities, *Oil & Gas Journal* **89**(52): 98–102.

Shinozuka, M. (1999). On-line damage identification of water delivery systems, 13^{th} *ASCE Engineering Mechanics Conference*, Baltimore, MD, USA, June 13-16, 1999.

Silva, R., Buiatti, C., Cruz, S. and Pereira, J. (1996). Pressure wave behaviour and leak detection in pipelines, *Computers & Chemical Engineering* **20**(6): S491–S496.

Simpson, A., Dandy, G. and Murphy, L. (1994). Genetic algorithms compared to other techniques for pipeline optimisation, *Journal of Water Resources Planning and Management, ASCE* **120**(4): 423–443.

Sinha, S. K., Fieguth, P. W. and Polak, M. A. (2003). Computer vision techniques for automatic structural assessment of underground pipes, *Computer-Aided Civil and Infrastructure Engineering* **18**(2): 95–112.

Skalak, R. (1956). An extension of the theory of water hammer, *Transactions of the ASME* **78**: 105–116.

Slaats, P., Mesman, G., Rosenthal, L. and Brink, H. (2004). Tools to monitor corrosion of cement-containing water mains, *Water Science and Technology* **49**(2): 33–39.

Sokolov, S. Y. (1935). Ultrasonic methods of detecting internal flaws in metal articles, *Zavodskaya Laboratoriya* **4**: 1468–1473.

Stampolidis, A., Soupios, P., Vallianatos, F. and Tsokas, G. (2003). Detection of leaks in buried plastic water distribution pipes in urban places - a case study, *Proceedings of the 2nd International Workshop on Advanced Ground Penetrating Radar*, Delft, The Netherlands, May 14-16, 2003, pp. 120–124.

Stapers, R. J. J. (2002). Urban water distribution. leak detection and model calibration in complex pipe networks, *Technical report TEIE-7170*, Dept. of Industrial Electrical Engineering and Automation, Lund University, Lund, Sweden.

Stephens, M., Lambert, M. F., Simpson, A. R., Vitkovsky, J. P. and Nixon, J. B. (2005). Using field measured transient responses in a water distribution system to assess valve status and network topology, *in* R. Walton (ed.), *World Water Congress 2005*, Vol. 173, ASCE, p. 54.

Stephens, M., Lambert, M., Simpson, A., Vitkovsky, J. and Nixon, J. (2004). Field tests for leakage, air pocket, and discrete blockage detection using inverse transient analysis in water distribution pipes, *in* G. Sehlke, D. F. Hayes and D. K. Stevens (eds), *World Water and Environmental Congress 2004*, Vol. 138-147, ASCE, p. 474.

Strommen, R. D., Horn, H. and Wold, K. R. (1993). New technique monitors pipeline corrosion, cracking, *Oil & Gas Journal* **91**(52): 88–93.

Threlfall, R. (1999). Using transient models of liquid pipelines, *Advanced Process Control Applications for Industry Workshop, 1999. IEEE Industry Applications Society* pp. 39–44.

Travers, F. A. (1997). Acoustic monitoring of prestressed concrete pipe, *Construction and Building Materials* **11**(3): 175–188.

Tripartite Group (2002). Leakage target setting for water companies. summary report, *Technical report*, Tripartite Group.

Unwin, D., Boxall, J. and Saul, A. (2003). Data mining and relationship analysis of water distribution system databases for improved understanding of operations performance, *International Conference on Advances in Water Supply Management, CCWI'03*, Vol. CD, Imperial College London, UK, September 15-17, 2003, pp. 51–58.

van der Kleij, F. C. and Stephenson, M. J. (2002). Acoustic logging, the Bristol water experience, *Leakage Management - A Practical Approach*, Lemesos, Cyprus, November 20-22, 2002.

Vardy, A. and Brown, J. (1996). On turbulent, unsteady, smooth-pipe friction, 7^{th} *International Conference on Pressure Surges and Transients in Pipelines and Open Channels*, BHR Group, Harrogate, UK, pp. 289–311.

Vardy, A. and Brown, J. (2003). Transient turbulent friction in fully-rough pipe flows, *Journal of Sound and Vibration*. In press.

Verde, C. (2001). Multi-leak detection and isolation in fluid pipelines, *Control Engineering Practice* **9**(6): 673–682.

Verde, C. (2005). Accommodation of multi-leak location in a pipeline, *Control Engineering Practice* **13**(8): 1071–1078.

Vítkovský, J., Liggett, J., Simpson, A. and Lambert, M. (2003). Optimal measurement site locations for inverse transient analysis in pipe networks, *Journal of Water Resources Planning and Management* **129**(6): 480–492.

Vítkovský, J. P., Simpson, A. R. and Lambert, M. F. (2000). Leak detection and calibration using transients and genetic algorithms, *Journal of Water Resources Planning and Management* **126**(4): 262–265.

Vítkovský, J., Simpson, A., Lambert, M. and Wang, X. (2001). An experimental verification of the inverse transient technique, *6th Conference on Hydraulics in Civil Engineering*, I.E.Aust., Hobart, Australia, November 28-30, 2001, pp. 373–380.

Vugdelija, M., Stojanovic, Z. and Stojanovic, Z. (2000). Determination of a time step interval in hydraulic systems transients simulation, *Advances in Engineering Software* **31**(2): 143–148.

Walski, T. (1983). Technique for calibrating network models, *Journal of Water Resources Planning and Management, ASCE* **109**(4): 360–372.

Walski, T. (1986). Case study: Pipe network model calibration issues, *Journal of Water Resources Planning and Management, ASCE* **112**(2): 238–249.

Wang, G., Dong, D. and Fang, C. (1993). Leak detection for transport pipelines based on autoregressive modeling, *IEEE Transactions on Instrumentation and Measurement* **42**(1): 68–71.

Wang, J. and Atrens, A. (2004). Analysis of service stress corrosion cracking in a natural gas transmission pipeline, active or dormant?, *Engineering Failure Analysis* **11**(1): 3–18.

Wang, X.-J., Lambert, M., Simpson, A., Liggett, J. and Vítkovský, J. (2002). Leak detection in pipeline systems using the damping of fluid transients, *Journal of Hydraulic Engineering, ASCE* **128**(7): 697–711.

Weil, G. and Graf, R. (1996). Infrared thermography based pipeline leak detection, *NDT and E International* **29**(6): 396.

Weil, G., Graf, R. and Forister, L. (1994). Remote sensing pipeline rehabilitation methodologies based upon the utilisation of infrared thermography, *in* W. Macaitis (ed.), *Urban Rehabilitation Programs and Techniques*, ASCE, pp. 173–181.

Weimer, D. (2001). Water loss management and techniques, *Technical report*, DVGW, The German Technical and Scientific Association for Gas and Water.

Whaley, R. S., Nicolas, R. E. and Reet, J. V. (1992). A tutorial on software based leak detection methods, *Technical report*, Pipeline Simulation Interest Group.

Wylie, E. (1983). The mircocomputer and pipeline transients, *Journal of Hydraulic Engineering, ASCE* **109**(12): 1723–1739.

Wylie, E. and Streeter, V. (1993). *Fluid Transients in Systems*, Prentice-Hall Inc., Englewood Cliffs, New Jersey, USA.

Young, J. G. (1979). Why we need non-destructive testing of welded constructions, *Philosophical Transactions for the Royal Society of London. Series A, Mathematical and Physical Sciences* **292**(1390): 201–205.

Zhang, J. (2001). Statistical pipeline leak detection for all operating conditions, *Pipeline & Gas Journal* pp. 42–45.

Zielke, W. (1968). Frequency-dependent friction in transient pipe flow, *Journal of Basic Engineering, Trans. ASME Series D* **90**: 109–115.